

EXAMINATION OF INTERACTIONS BETWEEN FERROUS
METALS AND THE ARCHAEOLOGICAL BURIAL
ENVIRONMENT AT A SEVENTEENTH-CENTURY
PLANTATION SITE

CENTRE FOR NEWFOUNDLAND STUDIES

**TOTAL OF 10 PAGES ONLY
MAY BE XEROXED**

(Without Author's Permission)

CATHY MATHIAS

INFORMATION TO USERS

This manuscript has been reproduced from the microfilm master. UMI films the text directly from the original or copy submitted. Thus, some thesis and dissertation copies are in typewriter face, while others may be from any type of computer printer.

The quality of this reproduction is dependent upon the quality of the copy submitted. Broken or indistinct print, colored or poor quality illustrations and photographs, print bleedthrough, substandard margins, and improper alignment can adversely affect reproduction.

In the unlikely event that the author did not send UMI a complete manuscript and there are missing pages, these will be noted. Also, if unauthorized copyright material had to be removed, a note will indicate the deletion.

Oversize materials (e.g., maps, drawings, charts) are reproduced by sectioning the original, beginning at the upper left-hand corner and continuing from left to right in equal sections with small overlaps.

Photographs included in the original manuscript have been reproduced xerographically in this copy. Higher quality 6" x 9" black and white photographic prints are available for any photographs or illustrations appearing in this copy for an additional charge. Contact UMI directly to order.

**Bell & Howell Information and Learning
300 North Zeeb Road, Ann Arbor, MI 48106-1346 USA
800-521-0600**

UMI[®]

NOTE TO USERS

This reproduction is the best copy available.

UMI



**National Library
of Canada**

**Acquisitions and
Bibliographic Services**

**395 Wellington Street
Ottawa ON K1A 0N4
Canada**

**Bibliothèque nationale
du Canada**

**Acquisitions et
services bibliographiques**

**395, rue Wellington
Ottawa ON K1A 0N4
Canada**

Your file Votre référence

Our file Notre référence

The author has granted a non-exclusive licence allowing the National Library of Canada to reproduce, loan, distribute or sell copies of this thesis in microform, paper or electronic formats.

The author retains ownership of the copyright in this thesis. Neither the thesis nor substantial extracts from it may be printed or otherwise reproduced without the author's permission.

L'auteur a accordé une licence non exclusive permettant à la Bibliothèque nationale du Canada de reproduire, prêter, distribuer ou vendre des copies de cette thèse sous la forme de microfiche/film, de reproduction sur papier ou sur format électronique.

L'auteur conserve la propriété du droit d'auteur qui protège cette thèse. Ni la thèse ni des extraits substantiels de celle-ci ne doivent être imprimés ou autrement reproduits sans son autorisation.

0-612-42481-2

Canada

**EXAMINATION OF INTERACTIONS BETWEEN FERROUS METALS
AND THE ARCHAEOLOGICAL BURIAL ENVIRONMENT
AT A SEVENTEENTH-CENTURY PLANTATION SITE**

by

Cathy Mathias, B.Sc., Dip. Art Conservation

A thesis submitted to the
School of Graduate Studies
in partial fulfilment of the
requirements for the degree of
Master of Science

Department of Earth Science
Memorial University of Newfoundland
St. John's, Newfoundland

June 1998

ABSTRACT

Few data exist on the burial environment condition and its affect on archaeological artifacts. Dowman (1970) introduced the need for archaeologists to incorporate the conservation of artifacts and analysis of soils into their field work. Fortunately the need for field conservation has been accepted by most institutes supporting archaeological research. Unfortunately extensive soil analysis has not been generally accepted as a means to understand better what has occurred to the buried artifact over time. The past few decades have seen Canadian and international archaeological sites excavated without soil data to aid the conservator in the stabilization of artifacts. During the years since Dowman's publication both archaeology and conservation methods have changed as technology advances and our understanding of past material culture grows. However our understanding of the burial environment has not grown at the same pace. Because of this void in data pertaining to the burial environment it is important that a concise survey of the techniques used for soil analyses be assessed. This thesis, in part, provides a guide to methods and techniques which can be used for assessment of burial conditions.

This thesis focuses on a seventeenth-century plantation site located at Ferryland, Newfoundland. This investigation centres on gaining a better understanding of the interaction between ferrous metals and the archaeological burial environment, whether or

not predictions of iron condition can be made based on soil analyses alone and evaluating the methods and techniques used to characterize the soils and iron.

Analyses of soil samples involved chemical analysis by XRF, ICP-MS, soil solution ion activity by pH and conductivity meters. Corrosion rates were measured using a potentiostat, identification of mineralogy was performed using XRD, particle sizes were estimated by sieving, organic content was measured by weight loss after digestion and soil colour was evaluated using a Munsell colour chart. Iron preservation was determined qualitatively based on magnetic attraction and physical appearance. Analyses of individual iron nail samples, representing strata of varying depth and horizontal distribution, were performed using reflected light, transmitted light and electron microscopy to describe the metal, radiographic techniques to measure the metal loss and XRD for mineral identification of the exterior corrosion layer (corrosion halo). Colour of corrosion halos was measured using a Munsell colour chart. Chemical analysis of slag samples was performed using XRF.

The results show that variations in iron preservation is linked to soil porosity, pH, conductivity, corrosion rate, Cl, SiO₂ and P₂O₅ concentrations. Variation in soil colour, particle size distribution and element composition are linked to both the natural environment and the presence of the seventeenth-century colonists. The best preserved iron was excavated from soil with the following conditions; 43% gravel, 53% sand, 3%

clay, pH of 4.9, conductivity of 24.9 micromhos, corrosion rate of 0.09 mmpy, organic wt% of 12.7%, 54.8 wt % of SiO_2 , 2.5 wt% of P_2O_5 , Cl concentration of 3,858 ppb for soil solutions and a Cl concentration of 417 ppm for soil samples. This soil was removed from events representing seventeenth-century occupation and subsequent destruction. Thus the bulk of the iron from the Ferryland site is found in soil which offers good conditions for preservation.

An extensive survey of iron and soil can therefore provide general information about the corrosive nature of the soil and identify areas of occupation and industry. Examining the soil environment, however, involves lengthy chemical processing and instrumental analysis. It was hoped that one analytical technique, in this case the corrosion rate analysis, might provide the basic information necessary for predicting iron condition. However, this was not realized. Given the heterogeneous nature of the archaeological burial environment several techniques must be used to describe the soil effectively. Of the methods and techniques used, those which show the greatest promise for future work include: element mapping using an electron microprobe and the elemental and chemical analysis using XRF and ICP-MS techniques. These methods of analysis examine the elemental compositions of iron and soil. Also the method for radiographic analysis used in this thesis, if adopted by other conservation laboratories, could facilitate a standardization of iron condition terminology for conservators. Thus this thesis provides a framework for future research in the field of archaeological conservation.

ACKNOWLEDGEMENTS

In every sense this thesis was interdisciplinary from both the research end to supervision and technical support. Many difficult hurdles were encountered over the past five years from equipment malfunctions to convincing granting organizations to fund projects outside of their mandate. These challenges were in part because of the interdisciplinary nature of this thesis and because of this I have learned so much more about all aspects of academic research. I must therefore begin by thanking Memorial University's Department of Graduate Studies and the Department of Earth Sciences for accepting a thesis proposal which was just different.

More specifically I would like to thank Dr. Roger Mason, my primary supervisor, for his endless encouragement, patience and guidance. I would also like to thank Dr. James Tuck, my supervisor for the archaeological side of this thesis, for his support. Dr. Lyndsie Selwyn of the Canadian Conservation Institute provided valued comments on the content and structuring of the thesis for which I am grateful. I thank Dr. Robert Hopkins who provided the initial instruction for the soil corrosion rate analysis and the Department of Engineering for sharing instrumentation and technical support. Special thanks to the editorial committees of the IIC (The International Institute for Conservation) and CAC (Canadian Association for Conservation of Cultural Property) whose comments helped guide and direct the research of this thesis. I would also like to thank Elizabeth

Dowman and Judy Logan who have influenced my approach to archaeological conservation. I would like to thank Dr. Arthur King and Sean O'Driscoll who provided information and field support with respect to the geology of Ferryland.

Within the Department of Earth Science many individuals, both faculty, staff and students, have either provided guidance or support and for this I am grateful. Special thanks must be extended to; Dr. Abid, Dr. Longerich, Dr. Wadleigh, Maggy Piranian, Pam King, Jeff Saunders, Mike Tubrett and Darren Smith.

Members of the Archaeology Unit also provided much support. Ellen Foulkes and Patricia Donnelly were helpful in providing artifact documentation information and extended endless support and encouragement. Dr. Pastore and Dr. Jerkic also provided support. Barry Gaulton, Amanda Crompton, Doug Nixon and Matthew Carter provided both editorial comments and helped with the archaeological interpretation.

I would like to thank family and friends for their encouragement, with special thanks to Doug Nixon and Steve Mathias.

Financial support for this thesis was provided by ISER, the Smallwood Foundation and EG & G Instruments Inc. for which I am indebted.

Finally, I would like to thank the people of Ferryland who welcomed, into their community, an archaeology team from Memorial University and who have generously shared with us their rich history.

TABLE OF CONTENTS

Abstract	ii
Acknowledgements	v
Table of Contents	viii
List of Tables	xii
List of Figures	xiv
List of Plates	xv
List of Abbreviations	xvi
 Chapter 1: Introduction	 1
 Chapter 2: Archaeological Conservation and Corrosion of Ferrous Metals	 5
2.1 Background on Conservation	5
2.1.1 Previous Work	6
2.2 Ferrous Metals and Conservation	7
2.3 Soil Properties and Corrosion	8
2.4 Corrosion Products Associated with Ferrous Metals	10
2.5 Description of the Corrosion of Ferrous Metals in a Terrestrial Burial ..	14
2.5.1 Role of Chloride	16
2.5.2 Explanation for Physical Damage to Archaeological Iron	17
2.5.3 Akaganeite	19
2.6 Previous Work on the Ferryland Site - Soil Properties/Artifact Condition	20
 Chapter 3: Study Area	 21
3.1 Choice of Study Area	21
3.2 Local Geography	23
3.3 Local Geology	23
3.4 Local Environment	26
3.5 Seventeenth Century Occupation at Ferryland	26
3.6 The Ferryland Project	28
3.7 Background on the Archaeology	30
3.7.1 Description of Area B	31
3.7.2 Description of Area C	31
3.7.3 Description of Area D	33

Chapter 4: Study Samples	35
4.1 Choice of Materials for Study	35
4.1.1 Metal Samples for Scientific Analyses	35
4.2 Purpose for Condition Survey of Nails	36
4.2.1 Sectioning for Analysis	37
4.2.2 Nail Terminology	37
4.3 Soil Sampling	39
4.4 Slag Sampling	39
4.5 Wrought Iron	40
4.5.1 Metallographic Structure for Iron/Carbon Steels	41
4.5.2 Impurities in the Wrought Iron	43
 Chapter 5: Methods and Techniques	 44
5.1 Qualitative Methods	44
5.1.1 Methodology used for the Artifact Survey	44
5.1.2 Munsell Colour Chart	44
5.2 Quantitative Methods for Soils	45
5.2.1 Particle Size Distribution	45
5.2.2 Organic Component of Soil Samples	46
5.3 Qualitative Analyses for Quantitative Methods	46
5.3.1 Radiography of Nails	46
5.3.2 Preparation of Thin-sections for Microscopic Identification	47
5.3.3 Reflected and Transmitted Light Microscope Analysis	47
5.4 Instrumental Methods	47
5.4.1 XRF Analysis for Soils and Slags	48
5.4.2 XRD Analysis for Soils, Clays and Nail Corrosion Halos	49
5.4.3 ICP-MS Analysis for Soil Solutions	50
5.4.4 Conductivity Measurements for Soil Solutions	51
5.4.5 pH Measurements	53
5.4.6 Electron Microprobe Analysis	53
5.4.7 Elemental Concentrations	54
5.5 Instrumental Methods for Monitoring Corrosion Rates	54
5.5.1 Background for Corrosion Rate Measurements	55
5.5.2 Background for Polarization Methods to Measure Corrosion	58
5.5.3 System set-up for Corrosion Rate Measurements	60
5.5.4 Derivation of Corrosion Rate	65

Chapter 6: Physicochemical Characteristics of Soil	68
6.1 Introduction	68
6.2 Particle Size Distribution	68
6.3 Soil pH, Conductivity, Corrosion Rate and Organic Wt%	72
6.4 Elemental Analysis for Soils	79
6.5 Chemical Analysis for Soil Solutions	85
6.6 Munsell Colour Separation of soils	87
6.7 Soil Mineralogy	92
6.7.1 Identification of Clay Minerals	92
6.8 Discussion	99
6.8.1 Particle Size Distribution	102
6.8.2 Soil pH, Conductivity, Corrosion Rate and Cl Concentration	103
6.8.3 Organic Component	108
6.8.4 Soil Colour	110
6.8.5 Soil Mineralogy	110
6.8.6 Elemental and Chemical Analysis for Soils and Soil Solution	111
 Chapter 7: Characterization of Excavated Iron Nail and Slag Samples	 114
7.1 Introduction	114
7.2 Survey of Nails	114
7.2.1 Pre-storage and Post-storage Nail Condition	116
7.2.2 Post-storage Condition Survey of Nails by Event	117
7.3 Interior Nail Condition	119
7.3.1 Metallography of Nails	119
7.3.2 Grouping of Nails Based on Metallographic Observations	121
7.3.3 Chemical Analysis of Iron Nail Shaft Cross-sections	132
7.3.4 Element Maps of Iron Nail Shaft Cross-sections	136
7.3.5 Radiography of Nails	143
7.3.6 Thickness of Iron Core and Corrosion Halo	147
7.4 Corrosion Halos	150
7.4.1 Munsell Colour for Corrosion Halos	150
7.4.2 Mineralogy of Nail Corrosion Halos	153
7.4.3 Corrosion Halo Mineralogy and Colour	155
7.5 Visual Examination of the 35 Nails	155
7.6 Characterization of Slag by Chemical Analysis	162
7.7 Summary	164
7.7.1 Artifact Survey	164
7.7.2 Nail Description	165
7.7.3 X-radiography of Nails	165
7.7.4 Munsell Colour	167

7.7.5	Mineralogy of Nail Corrosion Halos	
7.8	Slag	168
Chapter 8: Discussion of Burial Environment Implications for Iron Nails		169
8.1	Introduction	169
8.2	Summary of the Iron Nail Condition	169
8.3	Summary of Soil Conditions for the Ferryland Archaeological Site	172
8.4	Model for the corrosion Reaction of the Ferryland Iron Nail Samples	179
8.5	Ferryland Nail Deterioration Model and Turgoose Model: A Comparison	187
8.6	Methods of Analysis	188
8.7	The Burial Environment as an Alternate Repository for Storage	190
8.8	Future Work	191
8.8.1	Samples	191
8.8.2	Instrumentation	192
REFERENCES CITED		194
APPENDIX 5a		230
APPENDIX 5b		232
APPENDIX 6a		234
APPENDIX 6b		238
APPENDIX 6c		247
APPENDIX 7a		256
APPENDIX 7b		263
APPENDIX 7c		268
APPENDIX 7d		289
APPENDIX 7e		351
APPENDIX 7f		372
APPENDIX 7g		375

LIST OF TABLES

Table 2.4	Iron Corrosion Products	11
Table 4.2.2	Nail Type Descriptions in Pennyweight	39
Table 5.2.1	System of Texture Grade (in mm)	46
Table 5.4.2	Diffractionmeter Operating Conditions For XRD Analysis	50
Table 5.4.3	ICP-MS Operating Conditions	52
Table 5.5.3	Potentiostat Model 273a Operating Conditions	64
Table 6.1	Soil Samples from Areas B, C and D	69
Table 6.2a	Particle Size Distribution for Soil Samples from Occupation/Destruction Events	70
Table 6.2b	Particle Size Distribution for Soil Samples from Fill/Building Events and Subsoil	71
Table 6.3a	Comparison of soil pH, Conductivity, Corrosion Rate, Organic wt% and Cl Concentration for soil from Occupation/Destruction Events	73
Table 6.3b	Comparison of soil pH, Conductivity, Corrosion Rate, Organic wt% and Cl Concentration for soil from Fill/Building Events	74
Table 6.4e	Inorganic and Organic Components of Soil from Areas B, C and D	80
Table 6.4j	Comparison of Soil from Area B, C and D Based on SiO ₂ Concentrations	85
Table 6.5i	Chlorine Concentrations for Soil Solutions and Dry Soils	86
Table 6.5j	Chemical Species for Soil and Soil Solutions from Occupation/Destruction and Fill/Building Events	88
Table 6.6a	Colour of Soil from Occupation/Destruction Events	89
Table 6.6b	Colour of Soil from Fill/Building Events	90
Table 6.7a	Mineralogy of Soil from Occupation/Destruction Events	93
Table 6.7b	Mineralogy of Soil from Fill/Building Events and Subsoil	94
Table 6.7.1	Clay Mineralogy for the Ferryland Archaeological Site	98
Table 6.8a	Soil Description by Archaeology and Soil Chemistry Area B	100
Table 6.8b	Soil Description by Archaeology and Soil Chemistry Area C	101
Table 6.8c	Soil Description by Archaeology and Soil Chemistry Area D	102
Table 6.8.1	Soil with Particle Size Distribution Different from Mean	104
Table 6.8.2	Comparison of Potentially Damaging Soil Parameters for Buried Iron	107
Table 6.8.3	Predicted Iron Condition Based on Soil Condition	109
Table 6.8.6	Summary of Predicted Iron Condition	113
Table 7.2.1	Pre-storage and Post-storage Nail Condition	117
Table 7.2.2a	Post-storage Nail Condition for Selected Events	118
Table 7.2.2b	Nails from Occupation/Destruction and Fill/Building Events	120
Table 7.3.1	Carbon Content for Sample 115772 - Element % by Stoichiometry	121
Table 7.3.2a	Condition Classifications for Nail Thin-Sections	129

Table 7.3.2b	Metallographic Groups; Areas B, C and D; Nails from Occupation/Destruction	130
Table 7.3.2c	Metallographic Groups; Areas B, C and D; Nails from Fill/Building ..	131
Table 7.3.3a	Chemical Analysis of Iron Nail Cross-Sections	133
Table 7.3.3g	Chemical Analysis of Corrosion Halo Matrix	134
Table 7.3.3h	Averaged Values of Chemical Compositions for Corrosion Halos by Area	135
Table 7.3.3i	Chemical Analyses of Iron	135
Table 7.3.3j	Chemical Analysis of Iron/Corrosion Halo Interface	136
Table 7.3.4a	Chemical Variation for Nail Shaft Cross-Sections (excluding mineral inclusions)	138
Table 7.3.4b	Element Distribution Based on Element Mapping for Nails from Occupation/Destruction Events	139
Table 7.3.4c	Element Distribution Based on Element Mapping for Nails from Fill/Building Events	140
Table 7.3.6a	Iron Core vs Corrosion Halo for Nail Type	148
Table 7.3.6b	Iron Core vs Corrosion Halo for Metallographic Groups	149
Table 7.4.1a	Colour of Nail Corrosion Halos; Nails from Occupation/Destruction Events	151
Table 7.4.1b	Colour of Nail Corrosion Halos; Nails from Fill/Building Events	152
Table 7.4.1c	Colour of Nail Corrosion Halos by Metallographic Groups	153
Table 7.4.2	Mineralogy of Corrosion Halo for Areas B, C and D	154
Table 7.5a	Nail Condition by Visual Examination; Nails from Occupation/Destruction Events	159
Table 7.5b	Nail Condition by Visual Examination; Nails from Fill/Building Events	160
Table 7.5c	Nail Condition by Visual Examination for 35 Nails	161
Table 7.5d	Nail Condition vs Size	163
Table 8.2	Summary of Iron Nail Condition Excavated from the Ferryland Site ..	170
Table 8.3a	Optimum Burial Environment for Iron Nails from the Ferryland Archaeology Site	175
Table 8.3b	Range in Burial Environment Condition for the Ferryland Archaeology Site	176
Table 8.4a	Chemical Composition at Corrosion Halo and Iron/Corrosion Interface	180
Table 8.4b	% Distribution of Condition Classifications for Nail Thin-Sections ...	185
Table 8.4c	Mineral Identification of Corrosion Halo	186
Table 8.4d	Summary of Corrosion Halo Colour	187

LIST OF FIGURES

Figure 2.1.	Model for the corrosion of Archaeological iron by Turgoose (1982) . . .	18
Figure 3.1.	Location of Ferryland	22
Figure 3.2.	Sketch shows the site location with respect to land around Ferryland . .	24
Figure 3.3	Sketch map shows excavation areas at Ferryland	29
Figure 3.4.	Typical soil profiles for Areas B, C and D	34
Figure 4.1.	Complete iron nail with corrosion halo	38
Figure 4.2.	Iron-carbon phase diagram	42
Figure 5.1.	Graph shows E_{corr} and its relationship to half-cell electrode potentials and Tafel regions	59
Figure 5.2.	Corrosion flask used in corrosion rate experiments	61
Figure 5.3.	Holder for working electrode	62
Figure 6.4.	Soil profiles showing variation in soil pH and conductivity	77
Figure 6.5.	Soil profiles showing variation in soil corrosion rate and organic wt% .	78
Figure 6.6.	Soil profiles showing variation in soil SiO_2 and P_2O_5	83
Figure 6.7.	Soil profiles showing variation in soil Fe_2O_3 and Cl concentration. . . .	84
Figure 6.8.	Soil profiles showing variation in soil colour.. . . .	91
Figure 6.9.	Representative XRD spectra for soil samples from Area B	95
Figure 6.10.	Representative XRD spectra for soil samples from Area C	96
Figure 6.11.	Representative XRD spectra for soil samples from Area D	97
Figure 7.1.	Cross-section of iron nail shaft	115
Figure 7.5.	Description of G-1 metallographic group. The photograph is of nail sample 128304 (x 1.5)	123
Figure 7.6.	Description of G-2 metallographic group. The photograph is of nail sample 94788 (x 1.5)	124
Figure 7.7	Description of G-3 metallographic group. The photograph is of nail sample 128290 (x 10) showing single and multi-phase iron at the iron corrosion interface	125
Figure 7.8a.	Description of G-4 metallographic group. The photograph is of nail sample 115294 (x 10) showing single phase iron	126
Figure 7.8b.	Description of G-4 metallographic group. The photograph is of nail sample 94737 (x 10) showing multi-phase iron	127
Figure 7.9.	Description of G-5 metallographic group. The photograph is of nail sample 115772 (x 50) showing metal structure for single phase iron . .	128
Figure 7.10.	Models showing iron and chlorine distribution for nails from the Ferryland site	137
Figure 7.11.	Distribution of chlorine at iron/corrosion interface for nails 128193 (x 65) and 99060 (x50)	141

Figure 7.12.	Distribution of chlorine and iron at the iron/corrosion interface for nails 94759 (x 50) and 115521 (x 60)	142
Figure 7.13.	Schematic drawing showing location for size measurements	144
Figure 7.14.	Interpretation of x-ray grey levels	146
Figure 7.15.	Spectra for Area B nail 115811 with chromite identified	156
Figure 7.16.	Spectra for Area C nail 128304 with goethite and akaganeite identified	157
Figure 7.17.	Spectra for Area B nail 115811 with cacoxenite identified	158
Figure 8.1.	Schematic drawing showing iron nail condition with reference to soil profiles	171
Figure 8.2.	Line graphs showing nail condition for Areas B and C	173
Figure 8.3.	Line graph showing iron nail condition for Area D	174
Figure 8.4.	Line graphs showing Cl concentration versus corrosion rate for soils from Areas B and C	178
Figure 8.5.	Line graph showing Cl concentration versus corrosion rate for soil from Area D	179
Figure 8.6	Schematic drawing showing iron and chlorine distribution for nails from the Ferryland site	181
Figure 8.7	Iron/corrosion halo interface for nail sample 128193 (x 10)	182
Figure 8.8	Possible mechanism for the course of deterioration of the Ferryland iron nails	184

LIST OF PLATES

Plate 1.	Glacial till deposit of the Ferryland "Downs"	27
Plate 2.	Flooding of Area C, Ferryland archaeological site	32

LIST OF ABBREVIATIONS

The following abbreviations are used in this thesis.

Li ⁶ :	lithium	Ce:	cerium
Li ⁷ :	lithium	Hg:	mercury
Be:	beryllium	Tl:	thallium
B:	boron	Pb:	lead
C:	carbon	Bi:	bismuth
N:	nitrogen	U:	uranium
Mg:	magnesium	Sc:	scandium
Al:	aluminum	MgO:	magnesium oxide
Si:	silicon	Al ₂ O ₃ :	aluminum oxide
P:	phosphorous	P ₂ O ₅ :	phosphorous pentoxide
S:	sulfur	K ₂ O:	potassium oxide
Cl:	chlorine	CaO:	calcium oxide
Ca ⁴² :	calcium	TiO ₂ :	titanium oxide
Ca ⁴³ :	calcium	MnO ₂ :	manganese oxide
Ti:	titanium	Na ₂ O:	sodium oxide
Ga:	gallium	Cd:	cadmium
Y:	yttrium	Sb:	antimony
Zr:	zirconium	I:	iodine
Nb:	niobium	Cs:	cesium
Ba:	barium	Ba:	barium
Th:	thorium	La:	lanthanum
V:	vanadium	Mo:	molybdenum
Cr ⁵² :	chromium	Ag:	silver
Cr ⁵³ :	chromium	d:	pennyweight = measure of nail size
Fe ⁵⁴ :	iron	2d:	1" nail
Fe ⁵⁶ :	iron	6d:	2" nail
Fe ⁵⁷ :	iron	10d:	3" nail
Mn:	manganese	20d:	4" nail
Co:	cobalt	40d:	5" nail
Ni:	nickel	G:	% of iron corrosion
Cu:	copper	G-1:	80-100% corrosion
Zn:	zinc	G-2:	60-80% corrosion
As:	arsenic	G-3:	40-60% corrosion
Br:	bromine	G-4:	20-40% corrosion
Se:	selenium	G-5:	0-20% corrosion
Rb:	rubidium		
Sr:	strontium		

Abbreviations used for Mineral Identifications.

Mineral	abbreviation	PDF number	formula
akaganeite	ak	34-1266	$\beta\text{-FeO(OH)}$
albite	alb	10-0393	$\text{NaAlSi}_3\text{O}_8$
cacoxenite	cac	14-0331	$\text{Fe}_4(\text{PO}_4)_3(\text{OH})_3 \cdot 12\text{H}_2\text{O}$
chromite	chr	34-0140	FeCr_2O_4
goethite	goe	29-0713	$\alpha\text{-FeO(OH)}$
graphite	gr	25-0284	C
hematite	hm	33-0664	$\alpha\text{-Fe}_2\text{O}_3$
illite	il	26-0911	$\text{K}_{1.5-1.0}\text{Al}_4[\text{Si}_{6.5-7.0}\text{Al}_{1.5-1.0}\text{O}_{20}](\text{OH})_4$
kaolinite	kao	29-1488	$\text{Al}_2[\text{Si}_2\text{O}_5](\text{OH})_4$
magnetite	mg	19-0629	Fe_3O_4
magnesioferrite	mf	36-0398	$\text{MgFe}_2^{3+}\text{O}_4$
muscovite	mus	06-0263	$\text{KAl}_2(\text{Si}_3\text{Al})\text{O}_{10}$
phlogopite	pht	16-0344	$\text{K}_2\text{Mg}_3[\text{Si}_6\text{Al}_2\text{O}_{20}](\text{OH})_4$
quartz	qtz	33-1161	SiO_2
sanidine	san	25-0618	$\text{K}[\text{AlSi}_3\text{O}_8]$
sepiolite	sep	29-0863	$(\text{Mg,Fe})_4\text{Si}_6\text{O}_{15}(\text{OH})_2 \cdot 6\text{H}_2\text{O}$
smectite	sm	29-1490	$(1/2\text{Ca,Na})_{0.7}(\text{Mg,Fe,Al})_6$ $[(\text{Si,Al})_8\text{O}_{20}](\text{OH})_4 \cdot n\text{H}_2\text{O}$
vermiculite	verm	34-0166	$(\text{Mg,Ca})_{0.6-0.9}(\text{Mg,Fe}^{3+},\text{Al})_6$ $[(\text{Si,Al})_8\text{O}_{20}](\text{OH})_4 \cdot n\text{H}_2\text{O}$

PDF=powder diffraction files

CHAPTER 1: INTRODUCTION

The deterioration of terrestrial buried archaeological iron is generally referred to as an electrochemical corrosion process occurring because of an aggressive soil environment. Electrochemical corrosion in an aggressive environment such as a chloride rich soil/soil solution results in a reduction of the original metal with much of the physical shape of the object being replaced by a corrosion product.

The stimulus for this study is the need to stabilize archaeological artifacts as archaeological research relies in part on artifacts to interpret past cultures. These objects, having interacted with the burial environment, generally require stabilization once removed from this environment so that they will survive to be studied.

Before the extent of deterioration can be predicted for a given iron artifact in a terrestrial burial environment, both the metal composition and soil environment (inorganic/organic composition and electrolytic solution) must be understood. Often conservators have the opportunity to examine the condition of artifacts only after excavation. This results in little being known about the reactions occurring during burial. The complex nature of soils suggests that several parameters (pH, conductivity, corrosion rate, organic concentration, element concentration and mineralogy) are variable in time, geographical location and depth. How this variation in soil composition effects the

composition of buried iron is not well understood.

The purpose of this study is to focus on the electrochemical/chemical processes occurring to buried iron in an attempt to understand how these processes might be influenced by variation in soil composition. A large part of this thesis investigates the value of using a wide range of analytical techniques to identify soils which are corrosive to buried iron. Of interest is a potentiodynamic technique used to evaluate the corrosion rate of ferrous metal in soil solutions.

The choice of this thesis topic was stimulated by the fact that the author currently heads the Archaeological Conservation Laboratory for Memorial University of Newfoundland's Archaeology Unit and more specifically the Ferryland Archaeological Project. To date, the Ferryland Project has produced approximately 60,000 iron artifacts providing many opportunities to view artifact condition at the time of excavation and after treatment. Also, the author has participated in iron treatment research projects (Costain 1985; Selwyn and Logan 1993). This first-hand research and treatment of archaeological artifacts provides the background information for this thesis.

This thesis is divided into eight chapters. Chapter One provides an overview of current issues of concern to the profession of archaeological conservation with specific reference to the corrosion rate of ferrous metals in a terrestrial burial environment. A

background description of archaeological conservation, electrochemical deterioration of iron artifacts and the role of the burial matrix are presented in Chapter Two. Chapter Two also contains a brief introduction to corrosion rate measurement techniques. The location, regional geology and specimens selected for analyses are described in Chapters Three and Four. Chapter Five introduces the multi-survey qualitative and quantitative analytical techniques. The results from the soil analyses are described in Chapter Six. Chapter Seven includes the results pertaining to the characterization of nail samples. The results of measurements for the soils and iron nails are compared and discussed in Chapter Eight. The large sample size and numerous investigative techniques used for this thesis have resulted in a fairly large database. Within the text, only representative or distinctive samples are included. The bulk of the data such as chemical analysis for soil solutions, element concentrations for soil samples and image data are included here as appendices.

The appendices are numbered according to the chapter to which they belong. There are three sections of appendices. Appendix Five includes procedures for processing the organic and clay components of soil samples. Appendix Six includes maps showing soil sample locations, the chemical analysis tables for soil solutions and element concentration tables for soil samples. Appendix Seven includes maps showing locations for nail samples, sketches of nail cross-sections showing metal phases and corrosion products, tables for element analysis of nail cross-sections with sketches

showing points for analysis, element maps produced from the electron microprobe, photographs of nail x-radiographs and chemical analysis for slag samples.

CHAPTER 2: ARCHAEOLOGICAL CONSERVATION AND CORROSION OF FERROUS METALS

2.1 Background on Conservation

Within a Canadian context, the act of conserving/restoring artifacts began in 1639 at the Ursuline Convent in Quebec City (Hartin 1990). By the nineteenth century the profession had matured to a point where restorers routinely collaborated with scientists, expanding their knowledge of materials and the processes of deterioration (Brommelle 1956).

Public awareness of the importance of conservation practices was probably not realized until the 1960s to 1970s (Stolow 1972). It was at this time that the National Historic Sites Division of Parks Canada began a conservation program to facilitate the care and maintenance of both historic and archaeological sites.

The incompleteness of the archaeological record demands the many techniques and methods of both archaeology and conservation (Deetz 1977:8). At the first level is the excavation, which enables the archaeologist to gain maximum information from the material buried beneath the earth. Objects are then described according to space, time and form (Deetz 1993:172). The conservator becomes a key player in this interpretive process as it is her/his job to identify and stabilize the material culture of the past. The

role of the conservator today is viewed as being distinct from that of the restorer of the past, who often altered the object in an attempt to remove the deteriorating effects of time. Conservators, by contrast, aim only to stabilize the artifact so that it will survive for future generations (Cronyn 1990:1). It is the conservator's ethical responsibility to maintain the historic and aesthetic integrity of the objects being treated. The artifact is stabilized only to the point that it can be studied and viewed.

Because archaeological remains have generally changed both physically and chemically, the act of stabilization becomes a challenge. Rarely can preventive conservation measures alone ensure the preservation of artifacts. The deleterious effects of time produce varying artifact conditions and therefore conservation measures must address a wide range of possible damage. We must choose treatments which will be sympathetic to and effective on the artifact. An understanding of the reactions occurring between objects and treatment solution must be realized for all treatments. However we must first understand the changes that have occurred to the artifact during use, burial and in the post-excavation environment. Thus the twentieth/twenty first-century conservator must also understand something of the surficial environmental/geological process(es).

2.1.1 Previous Work

Elizabeth Dowman (1970) introduced the use of soil analysis for the conservator to a general archaeological audience in her book *Conservation in Field Archaeology*.

Unfortunately, either because of the expense, or the fact that much of the archaeology today is of a rescue nature (e.g. that construction demands that the "old things" be removed as quickly as possible), extensive soil analysis is rarely undertaken.

2.2 Ferrous Metals and Conservation

Throughout the historic archaeological record iron has been used to manufacture everything from a nail to a gun lock (Noël Hume 1970:124, 235, 252, 267, 274; Holmstrom 1904:9; Gaynor 1993:314). Because this was a multi-purpose material, it also represents one of the larger artifact groups from sites of the fourteenth to nineteenth centuries (Light and Unglik 1987:18; Pogue 1993:377). Thus, for the conservator the sheer number of artifacts makes their conservation difficult. Iron reacts readily with many of the components comprising most burial environments (Jones 1992:74; Gaynor 1993:312), making it one of the most problematic materials in an archaeological collection. Research on treatments for excavated iron artifacts has been the focus for many conservators and conservation scientists for the last few decades (Argo 1981; MacLeod 1981; Gilberg and Seeley 1981; Rinuy and Schwerzer 1982; Turgoose 1982, 1985; Carpenter 1986; Scoot and Seeley 1987; MacLeod 1989; Logan 1989; Carpenter and MacLeod 1993; Hjelm and Hansen et al. 1993; MacLeod et al. 1994; MacLeod 1996). Understanding what happens while the artifact is buried and being able to predict its condition upon excavation is the next logical direction for the profession.

2.3 Soil Properties and Corrosion

No single soil property can be related to its corrosive properties. It is the combination of properties such as pH, conductivity, ion concentrations, particle size and mineral composition that gives a soil its characteristic corrosive quality (Harris and Eyre 1994:79). Understanding the complete nature of soil structure would take into account particle size distribution, organic matter, moisture, gases, mineral phases and living organisms. Possibly the greatest influences on corrosive properties of a given soil come from the clay mineral phases present, pore spaces (which allow for water and gases to diffuse), water, oxygen, pH and conductivity (Harris and Eyre 1994:79).

Clays affect the physical and chemical properties of soils such as plasticity, cation exchange capacity (CEC) and moisture content (Harris and Eyre 1994; Qui and Zhu 1993; Bell 1993). A smectite clay, for example, having a high CEC (Moore and Reynolds 1989) may release potassium and magnesium to the pore solution. The potassium and magnesium in the clay may be replaced with other ions present in the pore solution. This same clay type may absorb water, swell and produce plastic properties in the soil (Hundal 1993; Eberl et al. 1993; Pollastro 1993; Schroeder 1993). A clay which is this reactive also has the potential to be corrosive to iron metal (Jones 1992:383). Kaolinite clay, having a lower CEC and generally being less reactive than smectite, will be less corrosive to iron metal (Harris and Eyre 1994:76; Moore and Reynolds 1989; Mathias 1996; Dowman 1970; Cronyn 1990).

Pore spaces within a soil may contain either water or gas (Varela et al. 1993). For a soil with a high clay concentration, the pore spaces will be small and therefore have a lower capacity for diffusion (Jones 1992:383). For a moist soil, with small pore spaces pockets of water stagnation can develop which can be detrimental to trapped metals. A sandy soil will have large pore spaces and therefore greater diffusion rate allowing for good drainage and better iron preservation (Mathias 1994).

The oxygen content of the upper layers of a soil will be similar to the fixed oxygen content of the atmosphere. Because oxygen concentration is generally perceived to decrease with depth (as does biological activity and water content) we would also expect the corrosion reactions which are oxygen dependent to change with depth (Harris and Eyre 1994; Jones 1992; Varela et al. 1993).

Water in a soil will contribute to the concentration of soil electrolytes (a solution of dissociated constituents resulting in free ions). The cations commonly present in the soil solution are potassium, magnesium and calcium. The abundant anions of the soil solution are chloride, iodide and bromide (Harris and Eyre 1994).

Conductivity (the capacity to transmit electricity) of a soil is an important factor as this can be rate-controlling for the reactions occurring in a given soil. These electrolytes (usually chloride ions), which serve as paths for electric (ionic) current, will

maintain the corrosive activity of a soil. Ionic currents can also be carried using sulphate (SO_4^{2-}) ions, often found associated with archaeological burial environments (Turgoose 1989). Of the above-mentioned ions, the chloride ion has a greater mobility and therefore will predominantly carry the ionic current. However in environments where the sulphate to chloride ion ratio is high, sulphate will carry the ionic current (Turgoose 1989). In general, studies of the electrochemical mechanisms of corrosion indicate that a highly conductive soil will also have a high corrosion rate (Harris and Eyre 1994:75; Miller et al. 1981).

The soil pH value (pH defines the activity of the hydrogen ion for a specific solution), though not directly related to corrosion rates (Ramanoff 1957), can accelerate the corrosive processes. Soils with a pH of 4.0 and lower will cause rapid corrosion of bare metals (Cronyn 1990). Few soils, however, exhibit such low pH values with the exception of peat bogs or areas where acidic plant materials have accumulated. Soils generally range from pH 5.0 to pH 8.0 (Harris and Eyre 1994:79) though the heterogeneous nature of soils will allow for pockets with higher acidity (Mathias 1996).

2.4 Corrosion Products Associated with Ferrous Metals

Conservators and corrosion engineers agree that land site burial of iron results in the alteration products of iron oxyhydroxides, iron oxides, iron chloride, iron carbonate, iron sulphate and iron phosphate (Table 2.4).

Table 2.4
Iron Corrosion Products

CHEMICAL FORMULA	NAME	OCCURRENCE	REFERENCES
$\alpha\text{-FeOOH}$ or $\alpha\text{-Fe}_2\text{O}_3\cdot\text{H}_2\text{O}$	goethite	<ul style="list-style-type: none"> - almost every soil type and climate region - typically formed under oxidizing conditions 	<p style="text-align: right;">Argo 1981 Argyropoulos 1995,1996 Binnie et al. 1992 Cox and Lyon 1994 Gettens 1963 Mathias 1993,1994 Misawa 1973 North and Pearson 1975 Rinuy 1982 Shima and Yabuki 1979 Taylor et al. 1977 Yamashita et al. 1994 Zucchi et al. 1977</p>
$\gamma\text{-FeOOH}$ or $\gamma\text{-Fe}_2\text{O}_3\cdot\text{H}_2\text{O}$	lepidocrocite	<ul style="list-style-type: none"> - often associated with goethite in soil - hydromorphic soil where Fe^{2+} in soil is generated by oxygen deficiency - common to gleys and pseudogleys which have a high clay content 	<p style="text-align: right;">Argo 1981 Argyropoulos 1996 Binnie et al. 1992 Gilberg and Seeley 1981 Mathias 1993, 1994 Misawa 1973 Refait and Genin 1993 Rinuy 1982 Schlesinger 1991 Shima and Yabuki 1979 Taylor et al. 1977 Yamashita et al.1994 Zucchi et al. 1977</p>

Table 2.4 continued

CHEMICAL FORMULA	NAME	OCCURRENCE	REFERENCES
Fe_3O_4	magnetite	- reducing conditions	Argo 1981 Argyropoulos 1995, 1996 Binnie et al. 1992 Cox and Lyon 1994 Gettens 1963 Mathias 1993, 1994 North 1976 Pearson 1972 Shima and Yabuki 1979 Turgoose 1989 Zucchi et al. 1977
$\alpha\text{Fe}_2\text{O}_3$	hematite	- associated with goethite in reddish soils oxidizing environment	Argo 1981 Binnie et al. 1992
$\beta\text{-FeOOH}$ or $\beta\text{-Fe}_2\text{O}_3 \cdot \text{H}_2\text{O}$	akaganeite	- chloride-containing environment	Argo 1981 Argyropoulos 1996 MacKay 1962 Misawa 1973 Shima and Yabuki 1979 Turgoose 1989 Zucchi et al. 1977
FeCl_2	lawrencite	- chloride-containing environment; high Cl^- concentration occurs - maritime terrestrial environment underwater environment	Lehmann and Nosek 1978 Nosek 1978 North 1982
FeCl_3	molysite	- same as for Lawrencite	Lehmann and Nosek 1978 Nosek 1978 North 1982

Table 2.4 continued

CHEMICAL FORMULA	NAME	OCCURRENCE	REFERENCES
$\text{Fe}_3(\text{PO}_4)_2 \cdot 8\text{H}_2\text{O}$	vivianite	- wet clay soils	Booth 1962 Farrer et al. 1953 Gettens 1963 Mathias 1993
FeS	pyrrhotite	- anaerobic environment	North 1976
$\text{KFe}_2(\text{SO}_4)_2(\text{OH})_3$ $\text{NaFe}_2(\text{SO}_4)_2(\text{OH})_3$	jarosite	- occurs in oxidizing environment containing sulfates	Zucchi et al. 1977
FeCr_2O_4	chromite	- gravel rich soil	Mathias 1993, 1994
FeCO_3	siderite or chalybite	- with clay minerals in iron concretions under reducing conditions	North 1976

Although the structure of these corrosion layers is not well understood, this is rapidly becoming an area of interest to corrosion engineers (Yamashita et al. 1994). These structures are also of importance in artifact conservation. Unfortunately more work is needed in this area (Turgoose 1982, 1989; MacLeod 1981; North 1982; Argo 1981; Gilberg and Seeley 1981).

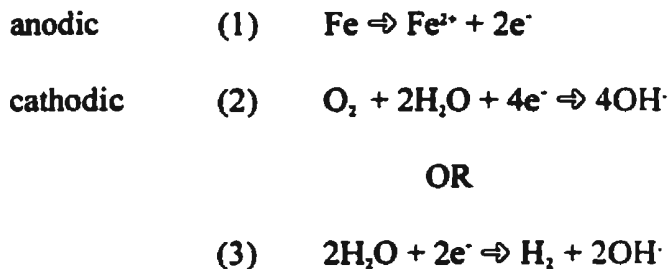
2.5 Description of the Corrosion of Ferrous Metals in a Terrestrial Burial

For the purpose of conservation, a metal can undergo two types of corrosion: dry or aqueous (Cronyn 1990:166). During use an artifact will likely experience dry corrosion as the fresh metal surface reacts with oxygen, producing a metal oxide. This oxide film or patina, as it is sometimes called, often serves to protect the metal. Patinas are therefore considered to be a passive corrosion layer. Aqueous corrosive processes are considered active and deteriorating. Of greater concern to the conservator therefore are the aqueous corrosion processes, particularly because most burial environments contain moisture.

Corrosion of ferrous metals is thermodynamically possible for all burial environments, however, chemical kinetics may exert an influence on the reaction products that are actually developed (Jones 1992:74). Corrosion in aqueous systems involving iron, which is the main concern for the conservation of the Ferryland assemblage (Mathias 1993), is governed primarily by electrochemical reactions.

Electrochemical reactions involve the exchange of electrons between chemical species.

The rate of electron flow to or from the reacting metal is a measure of the corrosion/reaction rate (Jones 1992:75). In this case corrosion of an iron artifact can be expressed by three half-reactions:



Because of the heterogeneity of soils the potential for iron to corrode is further enhanced. Different microenvironments may react on different parts of the same metal surface resulting in spatially different electrochemical potentials at the same metal/environment interface (Harris and Eyre 1994:75). This results in areas on the metal which are predominantly cathodic or predominantly anodic. The electrical circuit is completed by electronic movement in the metal and ionic movement in the soil solution (Turgoose 1982). Thus differences in aeration, pH or salt content will result in a corrosion cell, as just described, and hence the deterioration of the iron.

Understanding the contents of the corrosion layers involves a study of the reactions occurring during burial, at the time of excavation and during storage in the

ambient environment. One of the species commonly identified on archaeological iron is an iron oxyhydroxide called goethite (α -FeOOH) (Table 2.4). It is believed that this phase is produced by the oxidation of the anodically produced ferrous ions of equation (1) in the presence of chloride ions. Rapid oxidation rates result in formation of β -FeOOH while a slower oxidation rate may result in γ -FeOOH and Fe_3O_4 (Misawa et al. 1971; Detournay et al. 1976). Sulphate solutions may produce α -FeOOH, γ -FeOOH or Fe_3O_4 (Misawa et al. 1971). Essentially the above describes what would develop early in the burial history of an artifact. Over time, however, the aqueous solution appears to convert all forms of iron oxyhydroxide to an α -FeOOH (Turgoose 1982). Upon excavation, the artifact is once again exposed to rapid oxidation and it appears that β -FeOOH and γ -FeOOH are produced. Many authors have identified these phases on excavated artifacts (Zucchi et al. 1977; Lehman and Nosek 1978; North and Pearson 1975; Birchenall and Meussner 1977:45; Argo 1981; Gilberg and Seeley 1981).

2.5.1 Role of Chloride

Though it is a common belief that chlorides are primarily responsible for the corrosion of archaeological iron (Cronyn 1990; Organ 1977; Limbrey 1975; Dowman 1970; Zucchi et al. 1977:104; Pourbaix 1975:674; North and Pearson 1978; Gilberg and Seeley 1981; Scott and Seeley 1987; Refait and Genin 1993) and that excavated iron not receiving treatment will fall apart because of chlorides in the pores of metal and corrosion layers, it has been difficult to pinpoint their physical state within archaeological iron

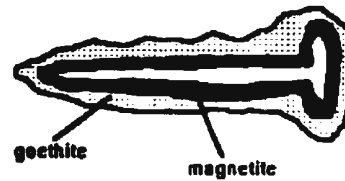
artifacts. The chlorides could be present as a solid chloride-rich component of the corrosion product, adsorbed on the surface of a corrosion product or in solution within the pores of the corrosion product. Evidence suggests that the latter is more likely the case (Parfitt and Russell 1977; North and Pearson 1977; Turgoose 1982).

2.5.2 Possible Explanation for Physical Damage to Archaeological Iron

Turgoose (1982) proposed the following model for the corrosion of archaeological iron (Figure 2.1). Though somewhat dated, conservation scientists are coming back to this model as a possible explanation of deterioration of iron (Selwyn, personal communication).

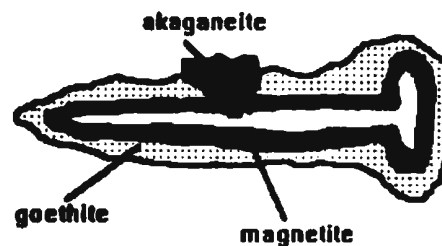
The cracking and spalling of untreated excavated archaeological iron was initially attributed to the presence of chloride ions in the form of β - iron oxyhydroxide (Zucchi et al. 1977), ferric chloride (Organ 1977; North and Pearson 1978; Smith 1977; Nosek 1978), iron oxychloride (Rinuy and Schwerzer 1982; North and Pearson 1975) and ferrous chloride (Nosek 1978). Turgoose (1982) suggested that the oxidation of the ferrous ions, resulting in precipitation of the β -FeOOH, caused the physical damage to the artifact by occupying a greater volume than that of the ferrous ions in solution. He provided supporting evidence by observing that ferric chloride formed secondary to the iron oxyhydroxide. He explained this observation with the following scenario:

Structure of Corrosion Products at the Time of Excavation



Solution within pores of corrosion deposit = ferrous ions (Fe^{2+}) and chloride ions (Cl^-).

After Excavation - Deterioration of Iron



crystallization of $\beta\text{-FeOOH}$ - akaganeite (results from ferrous ions being oxidized)



if pH sufficiently acidic to produce ferric ions (Fe^{3+}) reaction (5) can proceed.

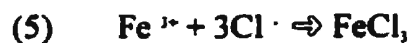


Fig 2.1 Model for the Corrosion of Archaeological Iron (after Turgoose, 1982).

Should reaction (4) occur at a distance from the metal surface, such that the hydrogen ions will not be consumed by reaction with metal, the pH value will decrease and the solubility of the FeOOH will become significant. This adds ferric ions to solution and these can react with the chloride ions to produce ferric chloride. Thus, the ferric chloride phase is produced after the FeOOH precipitation imparts physical damage to the artifact (Turgoose 1982). Regardless, the presence of chloride ions (if water is present to allow for dissociation) will increase the rate of reaction (4) by increasing the conductivity of the electrolytic solution (Jones 1994; Singley 1988; Pourbaix 1977:2).

2.5.3 Akaganeite - β -FeOOH

Conservators working with archaeological iron generally agree that the break-up of this material in the post-excavation environment is because of the presence of akaganeite (Logan and Selwyn, personal communication; Gilberg and Seeley 1981; Turgoose 1982; Selwyn and Logan 1993; Zucchi et al. 1977; Scott and Seeley 1987). Akaganeite has been identified as a reddish-brown powdery deposit (Turgoose 1982) or as “fuzzy” orange crystals (Selwyn and Logan 1993). Visual description of the mineral may vary, but all authors associate akaganeite with actively corroding areas around a surface crack (Zucchi et al. 1977; Selwyn and Logan 1993; Turgoose 1982). Though chloride ions are not essential for the formation of akaganeite, experiments show that the bulk of absorbed chloride ion is taken up in its structure (Gilberg and Seeley 1981). Scott and Seeley (1987) suggest that chloride ions are also probably present in microcracks and

chemisorbed on iron oxide and iron hydroxide surfaces. If akaganeite has the greatest concentration of chloride ions compared to other iron oxyhydroxides (goethite and lepidocrocite) then it also would have the greatest potential to accelerate/promote corrosion processes upon the release of Cl ions (Turgoose 1982). Confusion in the identification of this mineral phase may arise because it is a product of the initial stage of ferrous ion oxidation upon excavation (reaction 4). For archaeological field conservation laboratories, where iron is stored in aqueous solutions prior to analysis (thus preventing extensive oxidation), the presence of this phase may not be detected.

2.6. Previous Work on the Ferryland Site - Soil Properties and Artifact Condition

The Ferryland site soil matrix has been described as a wet soil environment with areas ranging from clay to silica rich. The site's close proximity to sea water introduces chloride rich salts to the soil (Mathias 1996). Previous artifact condition observations indicate that iron not receiving treatment will fall apart in the ambient environment because of chlorides in the soil solution (Dowman 1979:14; Rinuy and Schwerzer 1982; Turgoose 1982; Cronyn 1990:195; North and Pearson 1977; Organ 1977; Blackshaw 1982; Knight 1982; Argyropoulos 1996; Selwyn et al. 1993). This information provided the basis for the soil characterization used for the corrosion rate analyses for this study.

CHAPTER 3: STUDY AREA

3.1 Choice of Study Area

The province of Newfoundland is as unique culturally as it is geographically. Cultures as old as 9,000 years to the seventeenth-century European colonists have settled here and built their lives on the once-rich fishing resources of the Atlantic.

The bedrock varies from ocean floor and mantle rock of the Bay of Islands, to the continental margins of Humber Arm region to the Archean granitic basement rock of Red Bay, Labrador. Such diverse rock formations have resulted in soils with varying physical, chemical and mineralogical properties. Working with artifacts from this broad spectrum of burial environments, one realizes that this diversity explains to some extent the variation in artifact condition. However, differences in soil properties and artifact condition are usually not observed within one archaeological area. The Ferryland archaeological site, located approximately 80km south of St. John's on the Avalon Peninsula, is unusual in exhibiting both variation in burial environment and artifact condition (Figure 3.1). This makes Ferryland ideal for a study of the present type and was therefore chosen as the study area. In addition, approximately 500,000 artifacts had been excavated over the past five years of excavation affording many samples for scientific research purposes.

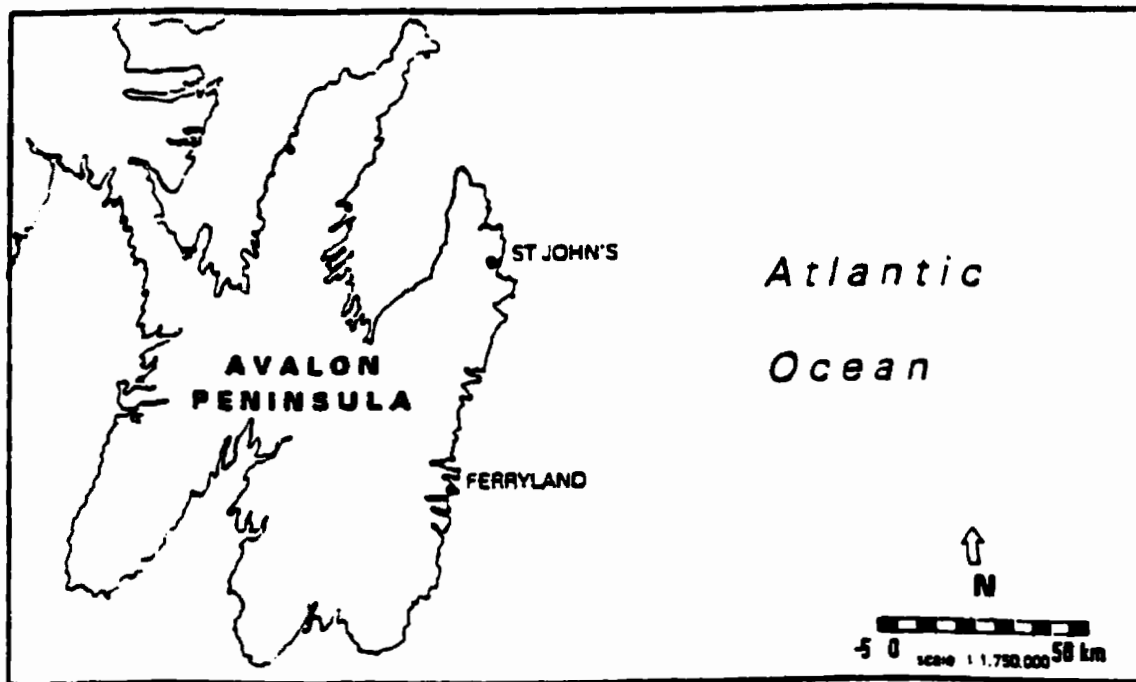
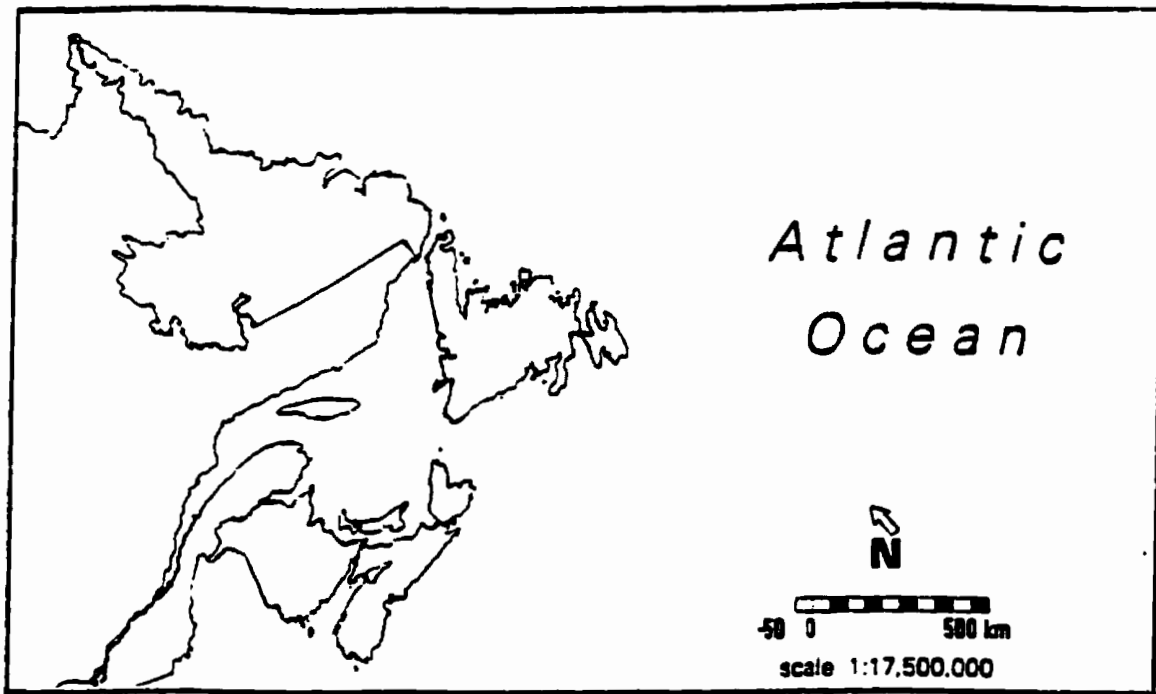


Figure 3.1 Location of Ferryland.

3.2 Local Geography

The seventeenth-century archaeological site at Ferryland is located on an arm of land that extends into the Atlantic Ocean at latitude 52°53'45"N and longitude 47°01'00"W. Figure 3.2 shows the site location. Just behind the highway running through the community, the land rises to 80 metres above sea level. This area is referred to as "the Gaze". The "Ferryland Head" located to the east of the site has an elevation of 41 metres above sea level. The section of land connecting the Ferryland "Pool" area to the community or "the Gaze" is a tombolo beach. The Ferryland site is one of the lowest elevated areas of the community, affording easy access to the ocean-going trade and fishing operations.

3.3 Local Geology

Once an object has been discarded or lost to the terrestrial burial environment it begins to react attempting to attain a state of chemical equilibrium. The interpretation of any corrosion product must therefore include an investigation of the country rock and soil matrix into which these artifacts fall.

The rocks of Eastern Newfoundland, which form part of the Avalon zone, are of Late Precambrian to Early Paleozoic age. Flanking the Appalachian orogen these rocks are fairly well exposed and have been described by many authors (Rose 1952; McCartney 1967; Williams et al. 1974, 1995; King 1989). The rocks comprise a sequence of Late

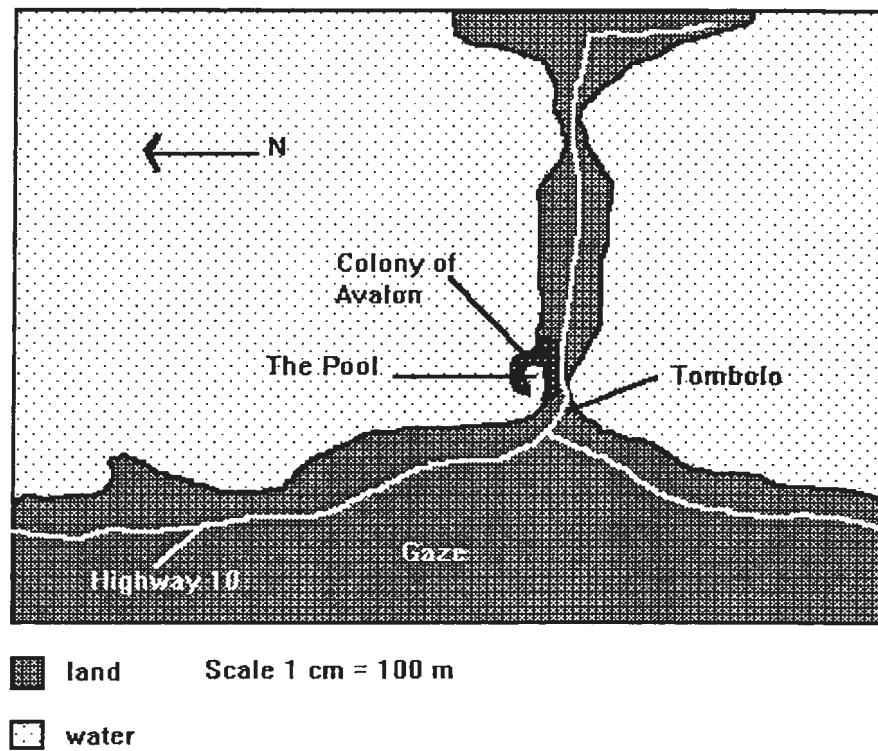


Figure 3.2 Sketch shows the site location (Colony of Avalon) with respect to land around Ferryland.

Precambrian volcanic and sedimentary rocks, which subsequently were intruded by a granitoid pluton of Late Precambrian age and unconformably overlain by sediments of Lower Paleozoic age.

The local geology of the Ferryland area consists of rock formations of the Conception, Signal Hill and St. John's Groups (King 1990). The Renew's Head Formation, belonging to the St. John's group, lies directly below the Ferryland archaeological excavations. This formation consists of interbedded gray/black shale and thin buff/rusty weathering sandstone. Seaward of this area, the bedrock consists of thickly bedded greenish-grey sandstone, siltstone and tuff of the Gibbet Hill Formation and the red sandstone of the Ferryland Head Formation. The Fermeuse Formation, Trepassey Formation, Mistaken Point Formation and Drook Formation, all located on the landward side of the site, consist of gray black shale with laminae of siltstone and sandstone, gray tuffaceous siltstone and argillaceous sandstone, interbedded greenish grey and reddish purple tuffaceous siltstone, shale and sandstone and yellow-green siliceous siltstone and sandstone, respectively (King 1990).

The Avalon Peninsula was glaciated throughout the Wisconsin Period (13000yr BP) (Hodych et al. 1989). The till material of the "Downs" (located to the west of the archaeological site) was derived from local bedrock to the east of the site probably as far away as 10 kilometres (King, personal communication). The till is dominated by

sedimentary material of the Renew Head and Fermeuse formations with a small component of the Harbour Main Volcanics (Plate 1). The seventeenth-century colonists altered the original terrain of the Ferryland "Pool" area by filling the original topography using the glacial till material of the Ferryland "Downs" (Tuck 1993).

3.4 Local Environment

The climate of Ferryland is controlled by proximity to the Atlantic ocean. The total mean annual precipitation of the area is 100 to 165 cm (Heringa 1981). From this we can confidently assume there to be a high water to artifact ratio. The average July temperatures range from 13 to 16°C. Winter temperatures range from -4 to -2°C for the months of December to February. According to Heringa (1981) the main trees of the Avalon peninsula are balsam fir, black spruce, white spruce, tamarack, white and yellow birch and alder. The local soils have been described as being coarse to medium coarse texture, stony, acid to extremely acid and wet (Heringa 1981).

3.5 Seventeenth Century Occupation at Ferryland

In 1621 George Calvert (later the first Lord Baltimore) sent Captain Edward Wynne and a group of West Country and Welsh settlers to Ferryland with the intention of establishing permanent settlement (Wynne 1622). Historical documents indicate that these first colonists constructed a mansion house, brew house, salt works, forge, hen house, kitchen, fishing stores and dwellings (Pope 1986:19). Lord Baltimore visited his



Plate 1. Glacial till deposit of the Ferryland "Downs".

colony in the summer of 1627 and returned with his family in 1628 (Tuck 1996). Perhaps because the climate was not suitable for the Baltimores, they left one year after their arrival. However, archaeological evidence indicates that the colony continued after their departure (Tuck 1993). Sir David Kirke, who was granted Newfoundland in 1637, assumed responsibility for Ferryland (Pope 1986). The Dutch attacked the area in 1673 inflicting a great deal of damage on several plantations, especially Ferryland (Lovelace 1673). The area recovered from this attack but after the French captured the settlement in 1696, activities at the site appear to have been greatly reduced.

3.6 The Ferryland Project

The present Ferryland Project, under the direction of Dr. James Tuck began excavation in July of 1992. Tuck (1985, 1986, 1992) has established that the area of excavation which surrounds the present day "Ferryland Pool" dates to the seventeenth century. The site itself is believed to cover an area of approximately 30,000 m². To date about 1000 m² have been excavated and designated as Areas A, B, C, D, E, F and G (Figure 3.3). The areas under investigation for this study include Area B which is a house, Area C which is the waterfront with a working area, cesspit and cow barn and Area D which is a house.

Although the seventeenth century is the focus of this study, the area has been occupied since the sixteenth century when the Beothuck natives and seasonal fisherman

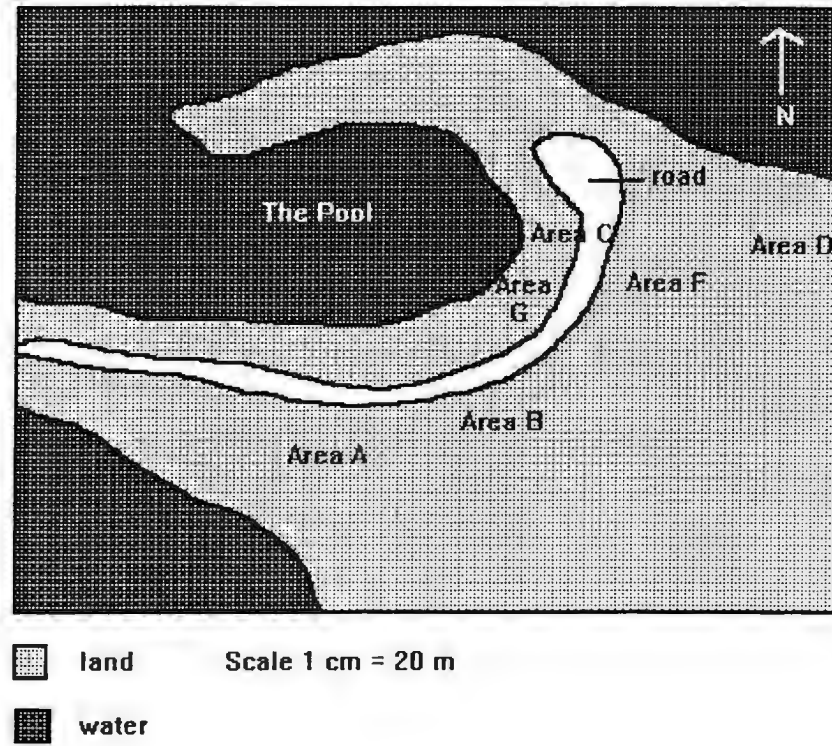


Figure 3.3 Sketch map shows excavation areas at Ferryland.

from several European countries visited. Excavation has provided evidence of eighteenth- nineteenth- and twentieth- century inhabitants as well (Tuck 1993). Areas B, C and D have not been built upon or disturbed significantly since the seventeenth century. Areas B and C had been used as gardens during the twentieth century. Thus the upper 10 - 20 cm of the stratigraphic column represents a "mixed" or disturbed component. Although chemical fertilizers had not been used, in most years dead fish remains (capelin) were spread over the gardens (Mrs. Elizabeth Costello, personal communication).

3.7 Background on the Archaeology

The archaeological stratigraphy for the seventeenth-century Ferryland Archaeology site is described using an event system (Tuck 1985, 1986, 1992; Pope 1986, 1993). Each event describes a different layer or lens in the site. Area A was excavated in search of the "palisado", or exterior fence (Pope 1993), but unfortunately only nails, tobacco pipes, a few ceramics and glass were found (Tuck 1985). Area B was identified as a forge, probably the one built by Captain Wynne in 1622 (Tuck 1985; Carter 1997). Area C is a portion of the waterfront. Area D, located to the east of Area C, represents a late seventeenth-century dwelling. Area E, located up the slope from Area C, provided evidence for several different occupations and activities including defensive works and a tavern (Tuck 1993). Area F has yielded much in terms of high quality domestic artifacts. It seems possible that the mansion house will be located in this area. Area G appears to

be a continuation of Area C. Common to all areas was the use of local slate (as a roofing material) and building stone (for walls) for the construction of the plantation.

3.7.1 Description of Area B

The Area B house was in use in the late seventeenth-century around the same time that the Area D house was occupied (Tuck, personal communication). A fireplace, cobble stone hearth and stone wall foundation represent the structural remains of the house. The events of interest as they were used for the thesis experiments were: 133, 134, 138, 143, 145, 177 and 178. Events 134 and 143 represent fill deposited by the colonists. This material was obtained from the local glacial till.

3.7.2 Description of Area C

Area C (Plate 2) is located closest to the sea, for the areas of excavation. Note that because of its close proximity to the sea, Area C floods each spring. Along the northern boundary of Area C is a seawall which defines the seventeenth-century pool edge. Several well-laid stone walls were uncovered with the excavation of Area C. The structure features both flagstone and cobblestone floors (Tuck 1993). This structure probably represents some sort of outbuilding or barn (Gaulton 1997). A drain from the cobblestone floor leads into the cesspit.



Plate 2. Flooding of Area C, Ferryland archaeological site.

Samples for the project were taken from the cesspit and surrounding sections of Area C. Of interest to the study, as they were used for experiments, were events 0, 16, 19, 22, 55 and 195. Sections of Area C were deliberately filled to provide a level surface. Events 8, 22 and 55 represent fill events.

3.7.3 Description of Area D

Area D is located along the “Downs” and further from the Pool than Areas B or C. It represents a dwelling, probably dating to the latter part of the seventeenth century, as evidenced by artifactual remains. A fireplace, cobble stone hearth and some burnt boards (possibly floor or wall boards) are all that remains of this structure. There is no evidence of stone wall construction thus implying that the structure was made of wood. The structure was burnt in the French raid of 1696 (Tuck 1993). It should be noted that Area D does not appear to have been filled or levelled off by the seventeenth-century inhabitants. The events of interest, as they were used for the experiments to follow, were 62, 63, 88, 96 and 141. Figure 3.4 shows typical soil profiles for Areas B, C and D.

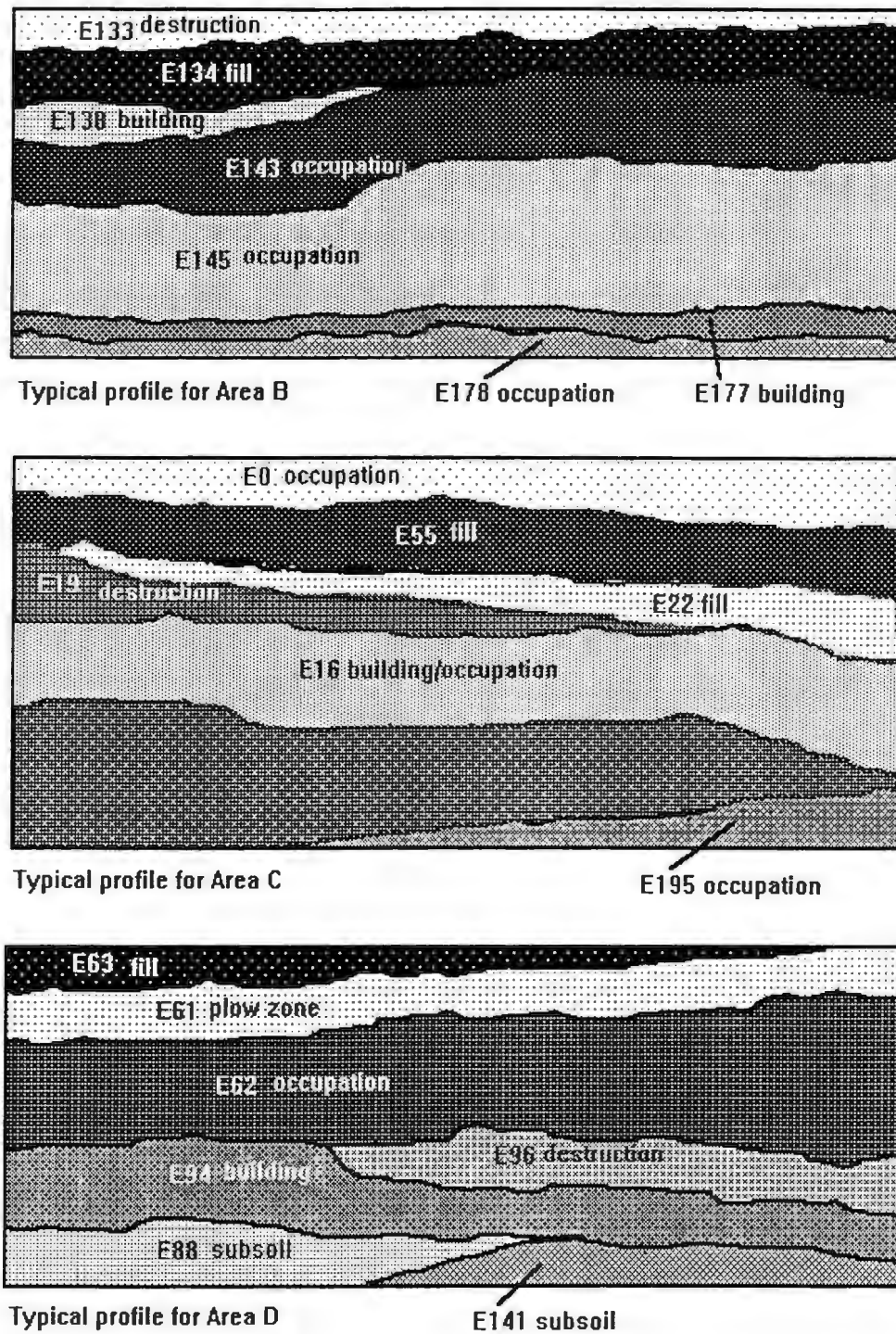


Figure 3.4 Typical soil profiles for Areas B, C and D.

CHAPTER 4: STUDY SAMPLES

4.1 Choice of Materials for Study

A total of 6,961 iron nail samples from Areas B, C and D were selected for a visual survey of condition. From this group 35 nails were selected for detailed analyses. A representative wrought iron nail section, free of corrosion and included chlorides, was used for all of the corrosion rate experiments. 25 soil samples were collected representing areas which contained iron nails. 46 iron slag samples from Areas B and C were collected.

Sampling of soil, slag and nails was dictated by the areas undergoing excavation for the 1994/1995 field seasons. Two areas representing dwellings (Area D and the house associated with the Area B forge) were chosen for the study. This type of feature usually offers the most interesting and largest quantity of artifactual remains making the "dynamics" of deterioration of interest to the conservator. The exposed sections of Area C were also sampled. Because Area C provided no evidence of human domestic occupation it would provide a contrast to Areas B and D.

4.1.1 Metal Samples for Scientific Analyses

Unlike most samples used for scientific purposes, archaeological artifacts generally cannot be destroyed. Exceptions to this rule are made, however, if for example

the selected samples are part of a large collection of similar objects with little museum display potential. Excavated materials of this province are protected by the Historic Resources Act (1985).

At the Ferryland site wrought iron nail fragments were most suited for analytical purposes. These samples which are numerous (approximately 14,000 specimens to date) afforded sampling for scientific examination. Moreover, wrought iron nail samples share a common manufacturing technology and they do not receive chemical treatment for conservation. Upon excavation these samples were air-dried and stored in a controlled environment. All samples were documented to include site location, visual artifact condition assessment, an artifact tracing, measurement of length, width and thickness and an x-radiographic assessment.

4.2 Purpose for Condition Survey of Nails

The condition survey of 6,961 nails assessed iron condition following the approximate 350 years of burial. Iron condition was assessed as good or bad. This condition survey allowed for the identification of trends within samples. For detailed analyses nails were separated based on their condition. For example, if all the nails from Area B were in good condition and nails from Areas C and D were in poor condition, the nails for the detailed study would be sorted accordingly and tested in two groups.

4.2.1 Sectioning for Analysis

For the purpose of analysis, apart from the condition survey, the nail shaft was the focus of study. Also note that the nail once manufactured would react to the air forming an iron oxide layer on its surface (Jones 1992). Archaeological evidence indicates that most nails recovered had been driven into wood in the construction of buildings. Therefore, nail samples could react with both cellulose and oxygen prior to burial.

4.2.2 Nail Terminology

Figure 4.1 shows a complete nail with a head, shaft and point. The nail also has a thick corrosion halo surrounding the iron core. For the purpose of this study reference to any component of the corrosion layer will be referred to as a “corrosion halo” and reference to the metal component of the nail will be as an “iron core”. For the purpose of this thesis nails will be described by type in pennyweight (d) which was the measurement of the seventeenth century (Bodey 1983:31; Edwards 1993:43). Table 4.2.2 presents the range of nail types found at the Ferryland site.

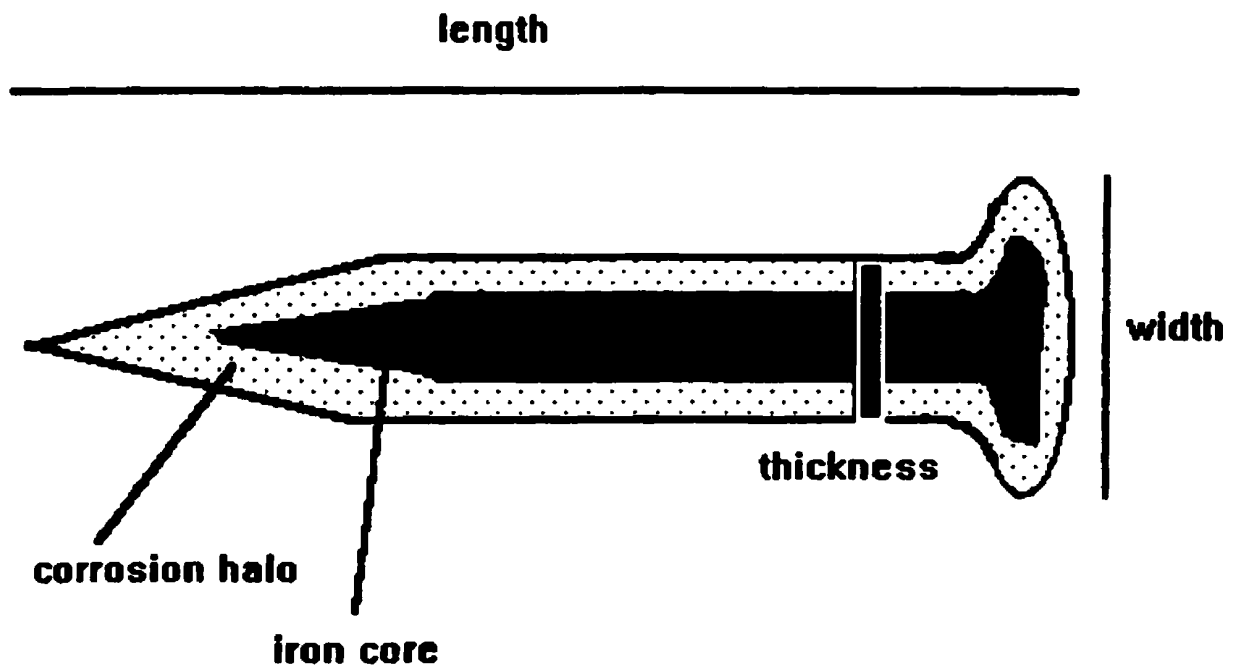


Figure 4.1 Complete iron nail with corrosion halo.

Table 4.2.2
Nail Type Descriptions in Pennyweight

Pennyweight (d)	Length (mm)
8d	64
10d	76
16d	90
20d	102
30d	115
40d	127

4.3 Soil Sampling

Because concentrations of chloride were to be analysed, crew members used sterile polyethylene plastic bags for collection and avoided hand contact. Both culture and fill layers were collected for analysis, although few to no nail samples existed for the fill sections. The soil samples were air dried. All laboratory analyses (unless otherwise stated) were performed on particles of less than 1.25 mm size obtained using a dry sieve. Sieving of soil samples to the 1.25 mm size removed stones. Stones in soil samples would interfere with the corrosion rate analyses.

4.4 Slag Sampling

Slag samples were randomly selected from Areas B and C each of which had a

slag heap. The slag of Area B represented the forge (Tuck 1996). It was uncertain if the slag from Area C had been dumped in that location after the Area B slag heap was full. Determination of a similar composition of the Area B and C slag would provide evidence that the Area B forge was the only one in operation for the Colony of Avalon. Also this would indicate a similar composition for the nails given that slag is the by-product of nail manufacturing. Because nail samples could not be processed for chemical analysis, as it would be totally destructive and required a larger sample size than an individual nail provided, it was decided to substitute slag for nails.

4.5 Wrought Iron

The manufacturing technique used to produce seventeenth-century nails will be described to explain the metal phases and textures. Wrought iron was the raw material used for manufacture (Noël Hume 1970:253; Gaynor 1993:312). The term wrought iron essentially describes the pure iron prepared from pig iron (pig iron is produced when iron ore is reduced by fusion in a blast furnace) (Sinha 1989). Wrought iron has a fibrous structure appearance, is strong, bends and forges easily (Unglik 1987:70; Rostoker and Dvorak 1990). It melts at about 1500°C (Parkinson 1967:4; Holmstrom 1904:50; Meilach 1977:65). It is probably the oldest commercially available form of ferrous metal produced (Unglik 1987:91; Higgins 1973; Parkinson 1967:4; Deetz 1993:68; Hodges 1964:80).

4.5.1 Metallographic Structure for Iron/Carbon Steels

Wrought iron consists of an α -ferrite phase with a carbon content of 0.1% (by weight) or less (Higgins 1973; Parkinson 1967:4; Rostoker and Dvorak 1990). Because this metal can exhibit a heterogeneous composition, sections can exist with a carbon content greater than the 0.1% (Rostoker and Dvorak 1990). The “pure” α -ferrite composition of the metal can be altered by variation in heat treatment and carbon content during manufacture (Higgins 1973). Figure 4.2 describes the iron-carbon phase diagram. Pure ferrite exists for a fairly narrow carbon range but remains stable for a wide temperature range. Ferrite can exist, however, with other phases such as pearlite, cementite and austenite. These other phases differ from ferrite by having a greater carbon content. Because the transformation of metallic phases is essentially controlled by diffusion in the solid state this allows for the preservation of various phases outside of their stability range through heat treatment, undercooling and quenching (fast cooling in water or oil) (Alexander and Street 1979:64). The blacksmith therefore had much more control over his material because of the “flexibility” of the metallic structure than the potter using crystalline clays. Thus when looking at the metallic structure of archaeological iron one must consider the raw material, forge environment, manufacturing techniques and possible burial environment alterations.

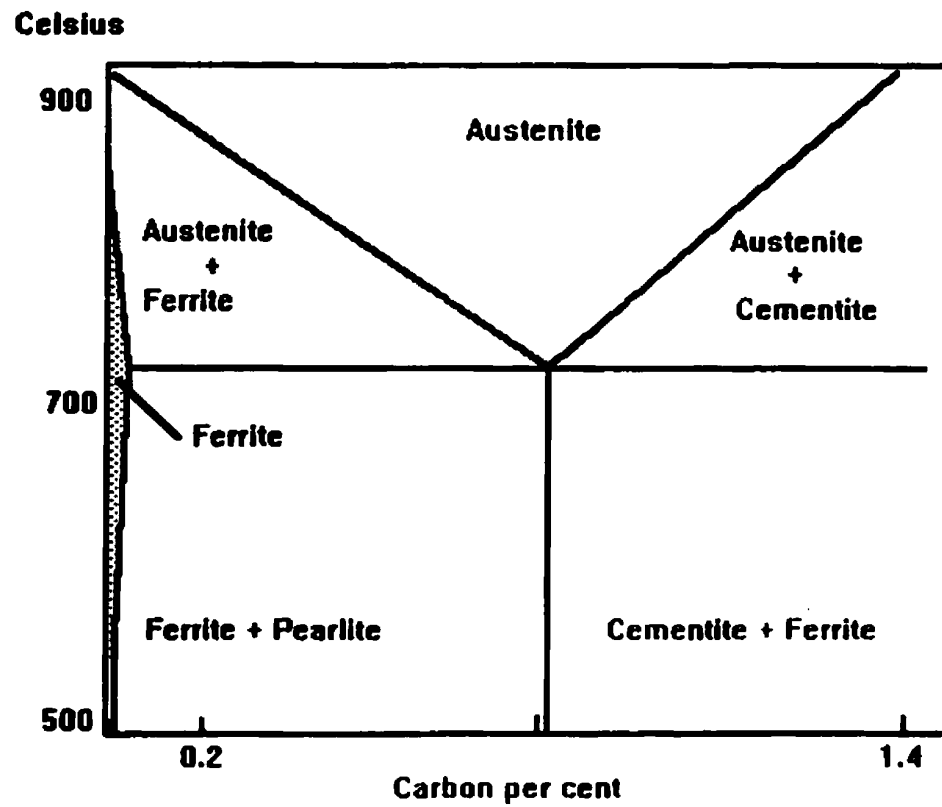


Figure 4.2 Iron-carbon phase diagram (after Higgins 1973).

4.5.2 Impurities in the Wrought Iron

The iron ore deposit could contain many impurities including silicates, carbonates and oxides (Scott 1989:8; Hodges 1964:81). These were generally considered undesirable by-products and were removed when possible, usually at the bloomery. Any remaining impurities could be removed by the blacksmith as a slag by-product of working the nail. Slag can generally be described as a mixture of noncombustible material in the coal/charcoal matrix (Weygers 1974:11). Some of the slag was incorporated into the final product as inclusions. During the working of the iron, slag inclusions would be stretched and thinned and transformed from a liquid to crystalline state (Alexander and Street 1979:72; Unglik 1987:66; Rostoker and Dvorak 1990; Scott 1989:8). Carter (1997) has determined that the source of heat for the Ferryland forge was probably charcoal and coal, introducing carbon, phosphorous and sulphur to the iron. Slag found at the site could provide information as to the identity of these impurities in the Ferryland manufactured iron artifacts (Frurip et al. 1983:3).

CHAPTER 5: METHODS AND TECHNIQUES

5.1 Qualitative Methods

5.1.1 Methodology Used for the Artifact Survey

The survey of iron nail fragments involved 1,718 specimens from Area B, 3,599 from Area C and 1,644 from Area D. The condition of each nail was documented upon excavation (pre-storage condition) and before drying as nail fragments were measured and traced. Condition was assessed based on attraction to a magnet. Three categories were used: lots of iron (strong magnetic attraction), some iron (weak magnetic attraction) and no iron (no magnetic attraction). Artifacts were individually stored in polypropylene zip lock bags with the corners removed to allow for air circulation. Persons handling ferrous metals wore latex gloves to prevent chloride contamination. Area B nails were stored for 12 months. Area C nails were stored for 2-7 months and Area D nails for 5-8 months. Conditions of storage were 17 to 21 °C and relative humidity in the range of 50-60% (summer) and 29-42% (winter). Condition was recorded again after storage (post-storage condition). Artifact condition was then recorded as “stable” (no change) or “cracked” (implying that change had occurred to the artifact).

5.1.2 Munsell Colour Chart

The colour of 25 soil samples, 35 corrosion halo samples and 46 slag samples was compared to a Munsell Soil Colour Chart (1992) consisting of 251 standard colour chips.

Colour comparisons were performed on air-dried soil and, for the nails and slag, powdered samples. The Munsell system describes colour by hue, value and chroma. The hue describes the colour in relation to red, yellow, green, blue and purple. Value describes the lightness of the colour and chroma represents the strength of the colour. The nomenclature used by the system employs both a colour name and notation. The order given to the Munsell notation is hue, value and chroma (e.g. a designation of 7.5YR 4/2 translates to 7.5 YR hue, 4 for value and a 2 chroma).

5.2 Quantitative Methods for Soils

5.2.1 Particle Size Distribution

Particle-size analysis provides a basis for soil texture classification that is not greatly modified by cultivation or human occupation (Sheldrick and Wang 1993:499; Day 1965:546). Sieving was used to separate the air-dried soil by particle size. Soil samples were initially hand-picked to remove roots, twigs and leaves then passed through sieves of mesh size: 2 mm, 1.25 mm and .063 mm sieves. Because concentrations of chloride were to be analysed, sterile polyethylene plastic bags were used to contain samples and persons handling soils wore latex gloves. Table 5.2.1 describes the system of texture grades in this study (based on the Canadian Soil Survey Committee (CSSC) System) (McKeague 1978). After removal of gravel and stones the remaining sand, silt and clay fractions were used to measure organic concentration, pH, conductivity, corrosion rate, element concentrations and mineralogy.

Table 5.2.1
System of Texture Grade (in mm)

Gravel	Coarse sand	Coarse to fine sand	silt/clay
>2	2-1.25	1.25-0.063	<0.063

5.2.2 Organic Component of Soil Samples

The abundance of organic matter was determined only for those soils with an associated nail sample. The organic component of the less than 2 mm size fraction was measured as a weight loss after digestion with hydrogen peroxide (Appendix 5a).

5.3 Qualitative Analyses for Quantitative Methods

Prior to performing instrumental analyses, radiographic and reflected and transmitted light microscopic analyses were performed on nail samples.

5.3.1 Radiography of Nails

Photographs were taken using a Phillips Super 70 radiography machine under two sets of conditions. Settings of 55kV/5mA provided x-rays of wavelength 0.45Å; settings of 80kV/4mA provided x-rays of wavelength 0.38Å. The former were used to image artifact exteriors and the latter to image the interiors. Exposure time was 1/120 sec for both settings. Images were produced on Ultra-vision G (Dupont) x-ray film.

5.3.2 Preparation of Thin-sections for Microscopic Identification

Nail shaft sections were found to be fairly consistent in terms of condition and were chosen for sectioning. Section locations were chosen to have a representative corrosion halo. Nails were impregnated with Epo-Kwick Epoxy hardener and resin, then cut perpendicular to their length using a water-cooled diamond saw. Sections were polished to a thickness of $30\mu\text{m}$. Polishing was performed with 1.0 and $0.3\mu\text{m}$ alumina, followed by ultrasonic cleaning and sealing in plastic (to exclude air).

5.3.3 Reflected and Transmitted Light Microscope Analysis of Nail Thin-Sections

A metallographic analysis of the iron core and an examination of the corrosion halo was conducted to characterize mineral(s) and metal phase(s). Initial transmitted light and reflected microscopy was performed on un-etched samples immediately after thin section preparation. Results were recorded using sketches and photographs. This allowed for a characterization of metal phase(s), inclusions, and the nature of the metal/corrosion interface and corrosion halos.

5.4 Instrumental Methods

Most of the instrumental techniques applied are those used in geochemical and mineralogical analysis. The technique employed for the corrosion rate measurements was adapted from similar applications used in engineering science. Corrosion rate, inductively coupled plasma-mass spectrometry (ICP-MS) and x-ray fluorescence (XRF)

analyses were performed specifically for those samples with an associated nail sample.

5.4.1 XRF Analysis for Soils and Slag

Soil and slag samples were analyzed for 30 elements (Na, Mg, Al, Si, P, S, Cl, K, Ca, Se, Ti, V, Cr, Mn, Fe, Ne, Cu, Zn, Ga, As, Rb, Sr, Y, Zr, Nb, Ba, Ce, Pb, Th and U) using a Fisons/ARL model 8420 sequential wavelength dispersive x-ray spectrometer. Samples were prepared as pressed pellets using BRP-5933 Bakelite phenolic resin (Longerich 1995).

The standard laboratory data acquisition protocol for geological samples was employed for the soils (Longerich et al. 1993). Slag samples were calibrated using an internal standard and an iron ore standard (Lincolnshire Iron Ore deposit - Bureau of Analysed Samples, Ltd. No. 301). The internal standard was produced by mixing powder from all 46 Ferryland slag samples. Two pressed pellets, produced from the powder, were then analyzed. The XRF analyses were repeated, on the two pellets, to test for consistent results.

Detection limits range from 100 ppm for the light major elements such as Na and Mg down to 0.6 to 0.7 ppm for the less abundant elements of Rb, Y and Nb (Longerich 1995).

5.4.2 XRD Analysis for Soils, Clays and Nail Corrosion Halos

Bulk soil samples, extracted clay phases and corrosion halos were investigated to identify mineral phases. Samples were ground to a fine powder and mounted on a glass slide for analysis.

For clay identification, a less than 1.25 mm soil fraction was processed to separate the clay fraction from the soil using the combined methodology of Jackson (1964) and Moore and Reynolds (1989). Appendix 5b describes the procedure for the clay mineral separation. Slides of the clay fraction were prepared by depositing a clay suspension in water from a 5cc syringe drop-wise onto a glass slide. The slides were then allowed to air dry. After recording the XRD spectra, these slides were exposed to ethylene glycol vapour for a 12 hour period at 60°C. The glycol treatment distinguishes illite from smectite clay phases as smectite expands on glycolation and gives a different XRD spectra. Slides were also exposed to glycerine as this will distinguish vermiculite from illite and smectite. Vermiculite expands when exposed to glycerine. Glycerine was applied to the slides by syringe until saturated and the slides were then air-dried. Corrosion halos were removed from the iron surface using a scalpel, then ground to a fine powder for mounting.

X-ray diffractograms were obtained using a Rigaku RU-200 diffractometer using $\text{CuK}\alpha$ radiation at 40kV and 100mA with a diffracted beam monochromator engaged.

Other details of operating conditions are given in Table 5.4.2.

Table 5.4.2
Diffractometer Operating Conditions for XRD Analysis

Sample	Scan Speed	Start angle	Stop angle	scan mode	goniometer axis	divergence slit width	receiving slit width
clay	10°/min	5°2 θ	70°2 θ	continuous	2 θ / θ	1°	0.15°
soil	5°/min	10°2 θ	70°2 θ	continuous	2 θ / θ	1°	0.15°
corrosion	5°/min	10°2 θ	70°2 θ	continuous	2 θ / θ	1°	0.15°

Identification of crystalline components was carried out using the XRD pattern-processing programme JADE (1991) and the International Centre for Diffraction Data (ICDD) and Powder Diffraction Files (PDF). Difficulties in interpreting patterns were encountered because of the heterogenous nature of the samples. Categories of identification were used which included: good pattern - 80% of peaks matching PDF (X or ✓), fair pattern - 50% of peaks matching PDF (?) and poor pattern - 40% of peaks matching PDF (??).

5.4.3 ICP-MS Analysis for Soil Solutions

Inductively coupled plasma-mass spectrometry (ICP-MS) analyses were performed on soil solutions prepared using a 1:10 soil to water ratio. The solution was stirred vigorously and allowed to stabilize for approximately 30 minutes before filtration

through a Millipore filter system (Whatman 0.45 μm cellulose nitrate membrane filter paper) and washed with 10% HCl. The filter paper was placed in a refluxing test tube. Five ml of concentrated HNO_3 were added to dissolve the filter paper. Concentrated HCl was added to dissolve all precipitate. The solution was then diluted to 100 g with deionized water.

Solutions were analyzed for 41 elements (Li, Be, B, C, N, Mg, Al, Si, P, S, Cl, Ca, Ti, V, Cr, Fe, Mn, Co, Ni, Cu, Zn, As, Br, Se, Rb, Sr, Mo, Ag, Cd, Sn, Sb, I, Cs, Ba, La, Ce, Hg, Tl, Pb, Bi and U). The instrument employed was an ELAN model 250 (SCIEX, Thornhill, Ontario, Canada). Modifications to the instrument are described by Longerich et al. (1986, 1987) and Jackson et al. (1990). Operating conditions are presented in Table 5.4.3.

5.4.4 Conductivity Measurements for Soil Solutions

A solution was prepared using a 1:10 volume ratio of soil to solution. This was stirred vigorously and allowed to stabilize for approximately 30 minutes prior to making the measurements, for which a Fisher Scientific Conductivity Meter, Model number 09-327, was used.

Table 5.4.3
ICP-MS Operating Conditions

Inductively coupled plasma:	
forward power	1,200 W
reflected power	<5 W
Argon gas flows:	
plasma (outer)	13 l min. ⁻¹
auxiliary (intermediate)	1 l min. ⁻¹
nebulizer (inner)	1 l min. ⁻¹
sampling distance (load coil to sampler aperture)	21 mm
sample uptake rate	0.64 ml min. ⁻¹
internal standard uptake rate	0.36 ml min. ⁻¹
Typical ion lens settings:	(digipot):
B lens (barrel)	95
P lens (plate)	4
E-1 lens (Einzel)	70
S-2 lens (stop)	0
Data acquisition parameters:	
measurement mode	multichannel
dwelt time	50 ms
integration time	15 s/mass
wash time	240 s
sample equilibration time	90 s

5.4.5 pH Measurements

Soil pH was measured in the laboratory using 1:2 soil-to-water and soil-to-0.01 M CaCl_2 solutions by volume. The latter demonstrates the buffering capacity of the soil. The CaCl_2 solution forces all of the hydrogen ions into solution as they are displaced by calcium. Thus the value obtained has a lower value than it would with water if the soil contains a phase capable of absorbing hydrogen ions (Rempel et al. 1996). Fisher Scientific Model 910 pH meter and electrode Model 13-620-285 were used for the experiments. The meter was calibrated prior to each measurement using Fisher Scientific pH 4 and 7 standards.

5.4.6 Electron Microprobe Analysis

A Cameca SX50 electron microprobe was used to map element distribution in iron nail sections using a beam current of 20nA, an accelerating voltage of 15 kV and a magnification of 1000X. Elements S, P, Cl, Fe, and Si were detected using Energy Dispersive Spectrometry (EDS). Chlorine was monitored using Wavelength Dispersive Spectrometry (WDS). The calibration standard used for the WDS analyses was tugtupite. The crystals employed were TAP and PET. A dwell time of 5 milliseconds was used to produce a 256^2 pixel map (equal to area of 2mm^2). Data were reduced using ZAF corrections.

5.4.7 Elemental Concentrations

Iron nails representative of each area of the site were analyzed to identify element concentrations in the corrosion halo and nail core. Additional samples were examined to identify mineral inclusions in the corrosion halo and carbon concentrations in metal phases. The following elements were analysed using EDS: S, P, Al, Si, Fe, Ca, K, Mg and Mn. WDS was used to measure Na, Cl and C concentrations. These elements were calibrated using albite, tugtupite and siderite standards. Crystals used for the study were TAP and PET. A current of 10 nA and an accelerating voltage of 15kV was employed. Data were reduced using ZAF corrections. All samples were analysed using the K α line.

5.5 Instrumental Methods for Monitoring Corrosion Rates

Other analytical techniques (pH, conductivity, XRD, ICP-MS and XRF) used for soil characterization in this thesis have been extensively tested (ASTM D1125, ASTM G51-77, Longerich 1995, Moore and Reynolds 1989; Taylor et al. 1977). Though corrosion rate measurements are used to interpret soil condition the application used in this thesis has not yet been tested. Therefore the following descriptions of the corrosion rate measurements are included both to justify why corrosion rate measurements were included and to demonstrate the importance of this soil parameter to the understanding of iron deterioration.

Corrosion scientists have developed a variety of techniques for evaluating

corrosion rates (Rocchini 1994). For a uniform corrosive process or localized attack either electrochemical techniques or method of weight loss can be used (Stern 1958; Jones 1992:24). The latter method uses coupons (uniform rectangular pieces of the metal under investigation) which have been exposed to a known environment. However, the analyses are time-consuming, provide only average values, and are valid only when the metal's mechanical properties and resistance to localized attacks are considered (Feitler 1970; Binnie, personal communication). Electrochemical methods allow for rapid calculation and are therefore preferred (Rocchini 1994).

5.5.1 Background for Corrosion Rate Measurements

Electrochemical reactions involve the transfer of electrons between an anode and a cathode (Pourbaix 1977:3). Current, I - units in amperes, is a measure of the electron flow to and from a given metal surface. Faraday's Law describes the proportionality between current and the reacted mass (m).

$$(1) \quad m = \frac{Ita}{nF}$$

F = Faraday's constant

n = number of electrons transferred

a = atomic weight

t = time

If equation (1) is divided by unit area, A , and time, t , an equation for corrosion rate (r) is obtained.

$$(2) \quad r = \frac{m}{tA} = \frac{i}{nF}$$

i = current density, I/A amps/unit area

Equation (2) shows the relationship between mass loss per unit time per unit area and current density. Because current can be measured precisely to very low values, it allows sensitive electrochemical measurements of corrosion rate (Jones 1992:75).

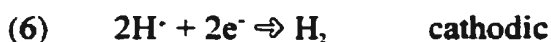
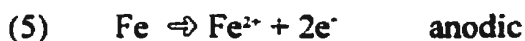
The fundamental thermodynamic parameter for an electrochemical reaction is the half-cell electrode potential (Richardson and McSwen 1989; Jones 1992:75). For example, iron in an aqueous solution of hydrochloric acid would produce the following reaction:



This reaction involves a change in free energy, as would any chemical reaction. If we write reaction (3) as a simple ionic reaction for metal it becomes:



Reaction (4) can be broken down into half-cell electrochemical reactions:



The free energy change (ΔG) is related to the electrochemical potential (E), at equilibrium by the equation:

$$(7) \quad \Delta G = -nFE$$

Half-cell reactions (5) and (6) have specific free energy changes. The sum of their corresponding half-cell electrode potentials e_a (for the anodic reaction) and e_c (for the cathodic reaction) is:

$$(8) \quad E = e_a + e_c$$

Changes to an electrochemical system are described in terms of electrochemical polarization, arising from the potential change ($E - e$) from the half-cell electrode potential at equilibrium as electrons are supplied to the cathodic half-cell or removed from the anodic half-cell. The term overpotential is often used to describe this build-up or depletion of electrons. For anodic overpotential (or activation polarization as it is sometimes called) polarization is positive and for cathodic overpotential polarization is negative (Jones 1992:80).

The overpotential (η) and current density (i_a , i_c for anodic and cathodic half-cell reactions, respectively) are related by:

$$(9) \quad \text{anodic polarization} \quad \eta_a = \beta_a \log i_a / i_o$$

$$(10) \quad \text{cathodic polarization} \quad \eta_c = \beta_c \log i_c / i_o$$

β_a and β_c are the Tafel constants (for activation polarization) for the half-cell reactions.
 i_o = total current exchanged between cathode and anode.

For many reactions, both anodic and cathodic half-cell reactions occur simultaneously. Each will have separate half-cell electrode potentials and exchange current densities. For them to coexist on the same electrically conductive surface each half-cell electrode potential must polarize to a common value. This common value is known as the corrosion potential (steady-state corrosion potential) or E_{corr} , the “mixed potential” (Shreir 1993:20:3-6). Its relationship to the half-cell electrode potentials and Tafel region is shown graphically in Figure 5.1.

5.5.2 Background for Polarization Methods to Measure Corrosion Rate

The mixed potential theory allows an electrochemical means to calculate corrosion rates. There are two methods of measurement of E_{corr} : Tafel extrapolation and polarization resistance (Jones 1992:94). The easiest is Tafel extrapolation for determining i_{corr} (Jones 1992:94). The second method is preferred, however, as it requires only a few minutes to determine corrosion rate, is sensitive and does not require increased temperatures to accelerate reactions. It is also non-destructive (Jones 1992:143). This is the method used in this study.

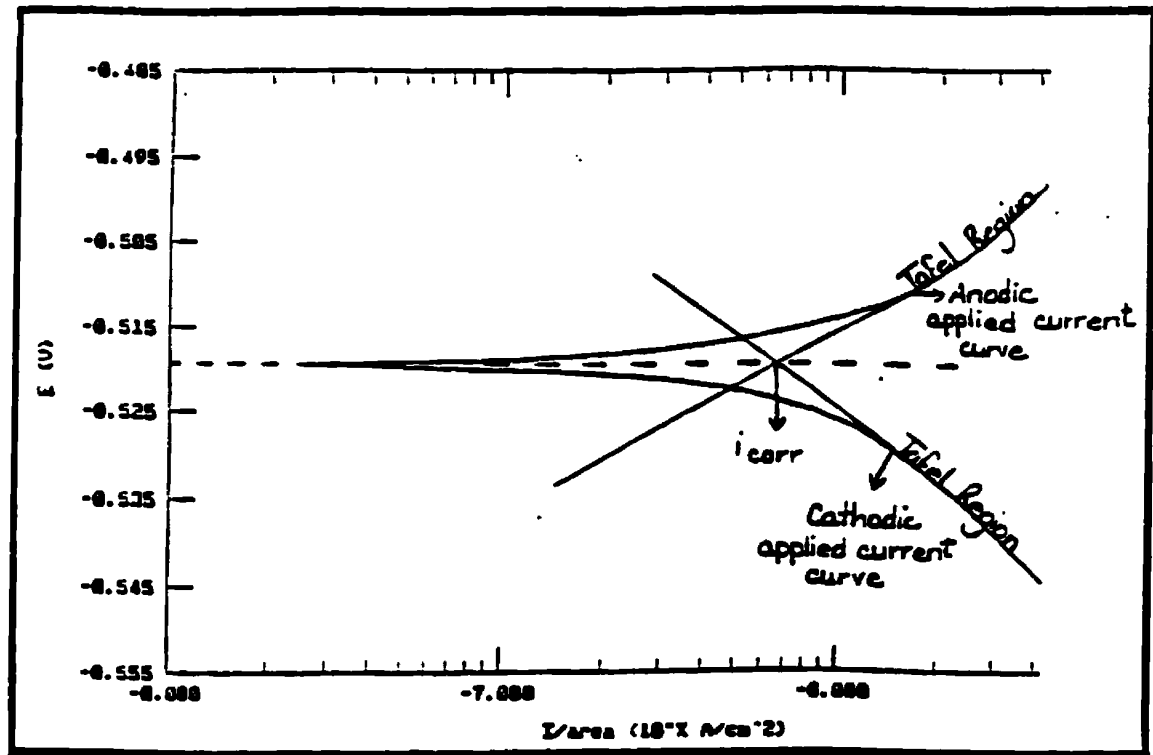


Figure 5.1 Graph shows E_{corr} and its relationship to half-cell electrode potentials and Tafel regions.

5.5.3 System set-up for Corrosion Rate Measurements

Corrosion rates of soil samples were measured using an EG & G Applied Research Potentiostat Model 273A with SoftCorr II corrosion measurement software. Initial research has shown a correlation between soil corrosion rate and artifact condition (Mathias 1996). The specimen used for corrosion testing was a single iron nail. This was used for each experiment. Though randomly selected, the nail was in excellent condition, and had been treated with an aqueous 1% NaOH solution for 1 year to remove chlorides. The working electrode was constructed using a section (2mm thickness) sliced from the shaft of the iron nail. Because the nail cross-section was small, a corrosion flask (EG & G model K047) was used for the corrosion cell (Figure 5.2). Figure 5.3 shows the holder and assembling procedure for the working electrode suitable for the corrosion cell. The iron surface was cleaned after each experiment using silicon carbide and diamond papers down to 600 grit, followed by rinsing with deionized water and solvent drying using acetone.

For all experiments the cell was set-up as in Figure 5.2. A reference electrode (saturated calomel electrode - SCE Ag/AgCl/1M KCl) (model number SL0032 for Ag/AgCl section and model number RDE0022 for KCl section) was placed within 1 mm of the working electrode and carbon rods provided the cathode. A soil solution (described below) served as an electrolyte.

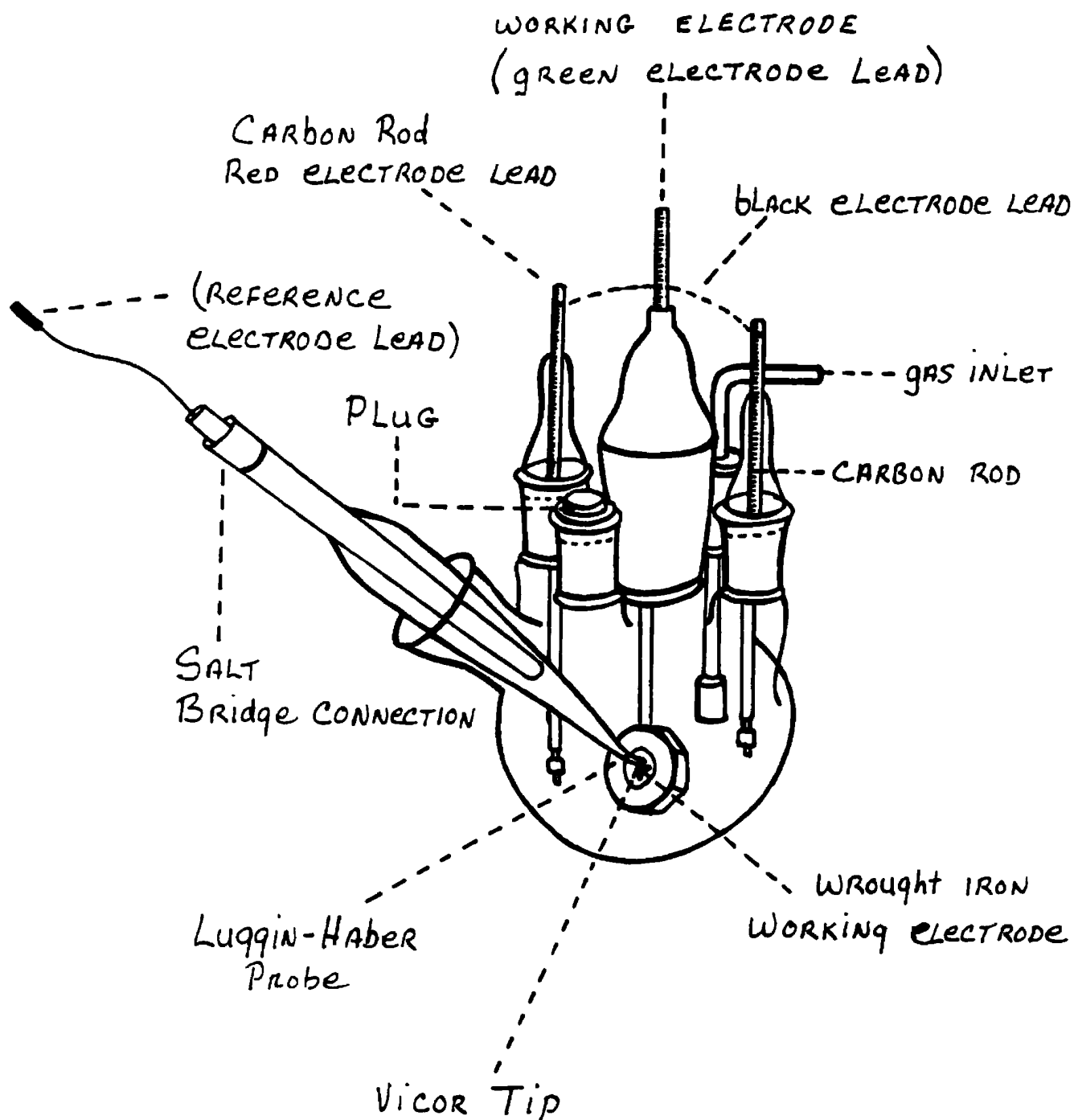


Figure 5.2 Corrosion flask used in corrosion rate experiments.

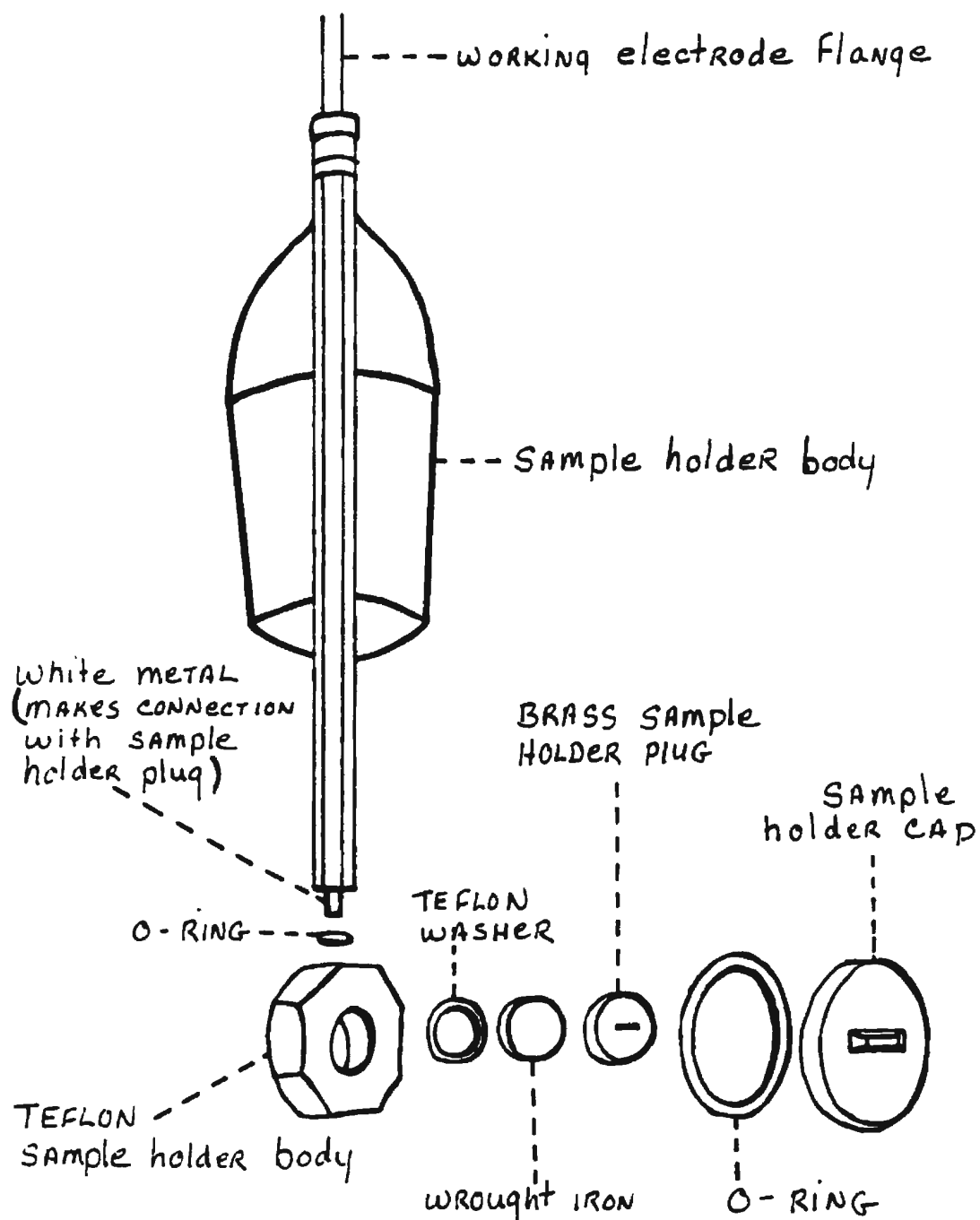


Figure 5.3 Holder for working electrode.

For a working electrode in contact with a soil solution, the electrode potential is the corrosion potential of the metal in the soil solution relative to the reference electrode. The soil solution in contact with the metal and the solution of the reference electrode must be connected by a salt bridge which has no diffusion potential. In this study, a Vycor tip and a saturated potassium chloride solution in a Luggin-Haber probe provided the salt bridge.

Soil solutions were prepared using a 1:10 soil to water ratio. The solution was stirred vigorously and allowed to stabilize for 30 minutes before being sieved through a 0.5 mm mesh to remove large stones (which damage the cell). The solution was poured into the cell. Dissolved oxygen is responsible for an increased rate of many corrosion related phenomena. Therefore, the cell was purged with nitrogen gas for 20 minutes (Robert Hopkins and Creig Monahan, personal communication). After purging, the cell was monitored using a Fluke Digital Multimeter model 8010A to determine the point of stabilization. When the voltage was stable the cell was connected to the potentiostat.

The electrical connection from the cell to potentiostat may be specific to the Model 273A potentiostat, therefore, check colour codes if using other models. The working electrode flange made contact with a brass holder plug which connected to the sample (Figure 5.3). The reference electrode lead was plugged into the reference electrode jack on the electrometer thus completing the connection from cell to

potentiostat. Table 5.5.3 presents the operating conditions. For these experiments the cell was cleaned after each run as was the working electrode. The working electrode was not re-weighed after each run nor was there any temperature control for the cell.

Table 5.5.3
Potentiostat Model 273A Operating Conditions

condition time	CT - pass	s
condition potential	CP - pass	V
initial delay	ID - pass	s
scan rate	SR	0.3333 mV/s
scan increment	SI	1.0000 mV
line sync.	LS	no
rise time	RT	high stability
working electrode	WE	solid
sample area	AR	0.7225 cm ²
density	DE	6.825 g/ml
initial potential	IP	specific to sample
final potential	FP	specific to sample
current range	CR	auto
step time	ST	3.000 s
IR mode	IR	none
filter	FL	off
reference electrode	RE - user	0.000 V
equivalent weight of iron	EW	27.92 g

With the cell connected and the system stabilized, a rough measurement of the free corrosion potential is obtained using the computer (Soft Corr II software). The free

corrosion potential was used to set limits and operating conditions. The cell is polarized to values ± 0.025 V on either side of this initial potential. The computer collects the data and a plot similar to Figure 5.1 is obtained. The measured current density (which is obtained as the intersection of tangents to the anodic applied current curve and the cathodic applied current curve) intersects the X axis at the value for E_{corr} .

5.5.4 Derivation of Corrosion Rate

Many researchers (Stern and Geary 1957; Simmons 1955; Skold and Larsen 1957) have contributed to the development of polarization methods for measuring corrosion rates. A synthesis has resulted in the acceptance of the inverse relationship between the slope at the origin of the polarization curve and the corrosion rate. This method of determining corrosion rates has become known as the polarization resistance method. The common method for measuring polarization resistance is the “potentiostatic” or “potentiodynamic” technique employed for this project. This method was selected because of its simplicity. When a controlled overvoltage is applied to the corroding electrode, the applied current density (I_{app}) is directly proportional to the corrosion rate as current density (I_{corr}).

$$(11) \quad R_p = \Delta\epsilon / \Delta I_{\text{app}} = \beta / I_{\text{corr}}$$

R_p = polarization resistance

$\Delta\epsilon$ = change in overvoltage

β = proportionality constant

It is therefore possible to obtain the corrosion rate directly from readings of applied

voltage versus measured current (when β is known). When a potentiodynamic scan is applied, the current will follow the controlled overvoltage and the polarization resistance curve can be plotted automatically (Figure 5.1).

The method used by the SoftCorr II software package to determine corrosion rate is related to the theoretical approach of Stern and Geary (1957). This approach assumes that a typical corroding system involves only 2 electrochemical reactions - oxidation and reduction. Equation (12) is that proposed by Stern and Geary.

$$(12) I(E) = I_{\text{corr}} [10^{(E-E_{\text{corr}})\beta_a} - 10^{(E_{\text{corr}}-E)\beta_c}]$$

where I = net or total current flowing at specific applied potential (E),

E_{corr} = open circuit potential for the system,

β_a = Tafel proportionality constant for anodic reaction,

β_c = Tafel proportionality constant for cathodic reaction.

When the applied potential (E) is equal to E_{corr} , equation (12) predicts that the current density (I) will equal zero. If the applied potential (E) is close to the open circuit potential (E_{corr}) equation (11) can be simplified to relate E to I :

$$(13) I = 2.3 I_{\text{corr}} (\beta_a + \beta_c) (E - E_{\text{corr}}) / (\beta_a \beta_c)$$

Equation (13) predicts that current density (I) will be linearly related to applied potential (E) when potentials are close to open circuit potential (E_{corr}). The slope E/I is called the polarization resistance.

$$(14) \text{Polarization resistance (Rp)} = \beta_a \beta_c / [2.3 I_{\text{corr}} (\beta_a + \beta_c)]$$

For this study, the Quickcalc and Parcalc Tafel analyses (Model 352/252 SoftCorrII user's

guide, 1992) were employed to calculate corrosion rates. Quickcalc relies on the linear least-squares treatment of selected points to calculate the results. It performs three linear least squares analyses of the data to obtain values for E_{corr} , I_{corr} , β_a and β_c . Parcalc uses all the data to perform a nonlinear least-squares fit. Once I_{corr} is obtained a corrosion rate can be determined using the equation:

$$(15) \text{ Corrosion rate} = C (EW/d) (I_{\text{corr}}/A)$$

EW = equivalent weight of sample in grams

A = sample area (cm²)

d = density g/ml

C = conversion constant = 3.268×10^3 for corrosion rate in millimetres per year (mmpy).

CHAPTER 6: PHYSICOCHEMICAL CHARACTERISTICS OF THE FERRYLAND SOIL

6.1 Introduction

Table 6.1 contains a brief description of the soil samples used for the study and a list of the associated nails. Appendices 6a-c contain Figures 6.1, 6.2 and 6.3 which show soil sample location for areas of excavation, the results for the chemical analysis for soil solutions and element concentrations for soil samples.

6.2 Particle Size Distribution

Tables 6.2a and b show the particle size distribution for soil samples from Areas B, C and D. Results shown in Table 6.2a represent occupation and destruction events, those in Table 6.2b represent filling and building events. The data correspond to gravel loamy sand on the classification scheme of Clarke (1971:45). These results support the field observation and historic records indicating that the area was filled or levelled off by the colonists from the glacial till deposit of the Downs (Tuck 1996). Percent standard deviations are 20% and 10% for the soil from the occupation/destruction and fill/building events, respectively, indicating greater variation between samples from occupation/destruction events. Standard errors are small and identical for soil from both event groups indicating little variation of sampling distribution around the sample mean.

Table 6.1
Soil Samples from Areas B, C and D

Area	Sample	Event	Event Description	Co-ordinate	Depth (cm)	Associated Nail
B	B-1	133	destruction	E3N0	54	106289
B	B-2	134	fill	E0N6	38-69	115811
B	B-3	134	fill	E3N3	55	115294
B	B-4	134	fill	E3N2	57-68	97546
B	B-5	134	fill	W1N7	59	115470, 115772*
B	B-6	138	building	E3N3	85-120	115521
B	B-7	143	occupation	E2N7	72-80	120161
B	B-8	145	occupation	E2N5	75-97	120531
B	B-9	177	building	E2N6	80-85	120340
B	B-10	178	occupation	E3N6	95-110	120389*
C	C-11	0	occupation	E89N29	0-30	128193*
C	C-12	55	fill	E88N29	46-53	128190*, 128192*
C	C-13	19	destruction	E88N29	53-57	128189*
C	C-14	22	fill	E89N35	57	128195*
C	C-15	16	building/occupation	E88N36	85	128304*
C	C-16	195	occupation	E88N29	89-121	128290*
D	D-17	62	occupation	E137N8	28-40	94158, 94160
D	D-18	62	occupation	E138N8	28-40	94120, 94121, 94123
D	D-19	62	occupation	E147N8	28-40	94742, 94743*, 94745, 94785 94786, 94787, 94788,
D	D-20	62	occupation	E135N7	30	94758, 94759
D	D-21	62	occupation	E149N9	34-38	87872
D	D-22	63	fill	E148N12	16-26	94737*
D	D-23	96	destruction	E148N12	53	99060
D	D-24	88	subsoil	E141S11	32	N/A
D	D-25	141	subsoil	E147N8	62	N/A

(*) nail sample does not have identical co-ordinates to soil sample
(N/A) - artifacts not found in the soil

Table 6.2a
Particle Size Distribution for Soil Samples
from occupation/destruction events

occupation/destruction events								
Sample	Sample Size (g)	Event	Co-ordinate	Depth (cm)	Particle Size (wt %)			
					>2mm (gravel)	2mm- 1.25mm (sand)	1.25mm- 63 μ m (sand)	<63 μ m (silt/ clay)
B-1	603	133	E3N0	54	64	2	31	3
B-7	360	143	E2N7	72-80	48	7	34	1
B-8	253	145	E2N5	75-97	44	9	44	3
B-10	391	178	E3N6	95-110	56	15	26	3
C-11	1446	0	E89N29	0-30	50	12	35	3
C-13	491	19	E88N29	53-57	33	17	46	4
C-16	659	195	E88N29	89-121	39	20	38	3
D-17	412	62	E137N8	28-40	37	16	40	7
D-18	348	62	E138N8	28-40	37	13	45	5
D-19	553	62	E147N8	28-40	53	21	23	3
D-20	502	62	E135N7	30	45	13	38	4
D-21	357	62	E149N9	34-38	41	13	39	7
D-23	574	96	E148N12	53	40	13	46	1
Mean	535				45	14	37	4
Standard deviation					9	5	7	2
Standard error					2	1	2	1

Table 6.2b
Particle Size Distribution for Soil Samples
from fill/building events and subsoil

fill/building events								
Sample	Sample Size (g)	Event	Co-ordinate	Depth (cm)	Particle Size (wt%)			
					>2mm (gravel)	2mm- 1.25mm (sand)	1.25mm- 63 μ m (sand)	<63 μ m (silt/ clay)
B-2	659	134	E0N6	38-69	50	15	33	2
B-3	452	134	E3N3	55	48	18	30	4
B-4	200	134	E3N2	57-68	53	21	25	1
B-5	778	134	WIN7	59	2*	5*	90*	3*
B-6	857	138	E3N3	85-120	54	10	28	8
B-9	406	177	E2N6	80-85	50	18	29	3
C-12	707	55	E88N29	46-53	47	14	36	3
C-14	687	22	E89N35	57	49	12	33	6
C-15	789	16	E88N36	85	44	13	40	3
D-22	352	63	E148N12	16-26	38	9	47	6
Mean	589				48	14	33	4
Standard deviation					5	4	7	2
Standard error					2	1	2	1
subsoils								
D-24	591	88	E141S11	32	63	6	23	8
D-25	617	141	E147N8	62	36	17	46	1

*value not included in mean or standard deviation for fill/building events

Soil samples D-25 and D-24, representing subsoil or soil free of artifactual remains, are located below the Area D house and outside of the Area D house, respectively. Sample D-25 has a particle size distribution similar to the soils representing occupation of the house. Sample D-24, however, has a greater gravel component, lower sand component and larger clay fraction compared to other soil samples related to human occupation.

6.3 Soil pH, Conductivity, Corrosion Rate and Organic wt%

Tables 6.3a and b contain measurements of soil pH, conductivity, corrosion rate, organic wt% and Cl concentrations. The Cl concentrations will be discussed later in the chapter. These data representing occupation/destruction and fill/building events are sorted by increasing pH for water solutions. The averaged soil pH is similar for both the occupation/destruction and fill/building events. Soil from occupation/destruction events in Areas C and D becomes more acidic with depth. Other soil samples indicate that the remaining areas of excavation have soil profiles which become more alkaline with depth. Events 195, 133, 19 and 62 (sample D-20) are more acidic than the other soils. Events 178, 145 and 62 (D-17,18 and 19) are more alkaline than the other soils. Events 178, 145 and 62 (D-17,18 and 19) are more alkaline than the other soils.

With the standard deviations, soil samples from occupation/destruction and fill/building events do not exhibit large differences in soil pH for H₂O and CaCl₂ solutions

Table 6.3a
Comparison of soil pH, conductivity, corrosion rate, organic wt% and Cl concentration
for soil from occupation/destruction events

occupation/destruction events										
Sample	Event	Co-ordinate	Depth (cm)	pH		Conductance (micromhos)	Corrosion Rate (mmpy) Quickcalc	Organic wt%	Cl concentration for soil (ppm)	Cl concentration for soil solutions (ppb)
				H ₂ O	CaCO ₃					
C-16	195	E88N29	89-121	4.37	3.55	29.9	0.11	19.2	1446	16432
B-1	133	E3N0	54	4.41	3.81	37.7	0.10	10.0	351	2952
D-20	62	E135N7	30	4.71	3.85	16.8	0.06	6.0	70	957
C-13	19	E88N29	53-57	4.73	3.64	29.4	0.06	29.8	373	5066
D-23	96	E148N12	53	4.90	4.07	8.7	0.08	8.6	110	13436
D-21	62	E149N9	34-38	4.94	3.98	8.1	-----	6.0	282	-----
B-7	143	E2N7	72-80	4.97	4.07	43.3	0.06	25.0	378	2348
C-11	0	E89N29	0-30	5.04	3.70	26.0	0.09	17.0	667	4939
D-19	62	E147N8	28-40	5.24	4.35	18.4	0.07	5.4	206	618
D-17	62	E137N8	28-40	5.34	4.16	7.7	0.11	5.9	393	1056
D-18	62	E138N8	28-40	5.40	4.51	10.6	0.07	6.0	129	514
B-8	145	E2N5	75-97	5.63	4.61	13.6	0.11	2.0	427	1038
B-10	178	E3N6	95-110	5.74	4.23	29.9	0.05	5.6	359	1063
Mean				5.03	4.04	21.5	0.08	11.3	399	4202
Standard Deviation				0.43	0.33	11.9	0.02	8.7	352	5290
Standard error				0.12	0.09	3.3	0.01	2.4	67	1527

Table 6.3b
Comparison of soil pH, conductivity, corrosion rate, organic wt% and Cl concentration
for soil from fill/building events

fill/building events										
Sample	Event	Co-ordinate	Depth (cm)	pH		Conductance (micromhos)	Corrosion Rate (mmpy) Quickcalc	Organic wt%	Cl concentration for soil (ppm)	Cl concentration for soil solutions (ppb)
				H ₂ O	CaCl ₂					
B-4	134	E3N2	57-68	3.81	3.45	35.0	0.06	10.6	313	1074
B-2	134	E0N6	38-69	3.99	3.66	52.2	0.07	6.9	217	1780
D-22	63	E148N12	16-26	4.04	3.56	52.8	0.22	8.0	368	5630
B-5	134	W1N7	59	4.45	3.61	11.2	0.03	1.8	100	635
C-12	55	E88N29	46-53	4.45	3.53	28.6	0.14	12.1	593	6788
B-3	134	E3N3	55	4.70	3.97	20.0	0.02	17.8	209	1691
C-14	22	E89N35	57	4.93	4.16	73.3	0.12	15.2	784	33109
B-9	177	E2N6	80-85	4.96	3.96	14.7	0.06	4.1	382	2240
B-6	138	E3N3	85-120	4.99	3.98	15.2	0.09	2.0	157	1871
C-15	16	E88N36	85	5.60	4.42	29.6	0.08	29.4	462	10049
Mean				4.61	3.85	33.3	0.09	10.8	358	6487
Standard deviation				0.58	0.32	20.3	0.06	8.4	211	9834
Standard error				0.18	0.10	6.42	0.02	2.7	67	3110
subsoils										
D-24	88	E141S11	32	4.82	3.54	10.4	0.12	5.9	<1.0	773
D-25	141	E147N8	62	5.91	4.75	5.7	0.09	2.0	28	476

(Table 6.3a and b). The greatest difference is observed for soil from occupation/destruction events. Soil pH for CaCl_2 solutions has similar % standard deviations and errors for both event groups. Percent standard deviation and error for soil pH (H_2O) is greater for soil from fill/building events indicating variation between samples and variation in sampling distribution around the sample mean.

Soil conductivity for occupation/destruction events is lower than for fill/building events, however there is much overlap. Soil samples decrease in soil conductivity with depth for Areas B and D. With exception of sample C-14, soil conductivity is uniform for the events from Area C. Soil conductivity is lowest for samples from Area D. Samples B-7 (event 143), C-14 (event 22) and D-22 (event 63) have the highest soil conductivity for the site.

The soils from the two event groups have similar averaged corrosion rates, although the standard deviation indicates significant variation in corrosion rate between individual soil samples. Percent standard deviation is greatest for the soil from fill/building events indicating greater variation between samples. Percent standard error for this group is also higher suggesting greater variation in sample distribution about the mean. Soil from fill/building events also has greater percent standard deviation and standard errors for soil conductivity. The most corrosive soils are from events 55 and 63, both located near the surface. The least corrosive soils are from events 96, 62, 16, 19,

143 and 134.

The organic soil component for all soils from Areas B, C and D represents approximately 10% of the soil by weight. The weights for individual soil samples before digestion range from 3.7 to 5.8 g and weight changes after digestion range from 0.1 to 1.7 g. The organic soil fraction from the occupation/destruction events and the fill/building events is similar. The % standard deviations for soil from both the occupation/destruction and fill/building events is 77% of the mean organic weight % indicating similarly high variability within each data set. Standard error for soils from occupation/destruction and fill/building events is similar indicating variability of sampling distribution around the sample mean is equal. Soil samples from Areas C and D show an increase in organic concentration for samples with depth. Organic weight % for soil from Area B fluctuates with depth. Soil from Area C has a higher concentration of organic matter than soil from Areas B and D.

Figures 6.4 and 6.5 are schematic drawings of soil profiles showing variation in soil pH, conductivity, corrosion rate and organic wt%. A visual examination of these profiles indicates that some correlations between pH, conductivity, corrosion rate and organic content exists. For example, an acidic soil pH correlates with high soil conductivity and high organic wt%. This is true for events 143, 22, 19 and 195. Note that these events have a low soil corrosion rate. Also soil from events 145, 178, 16 and

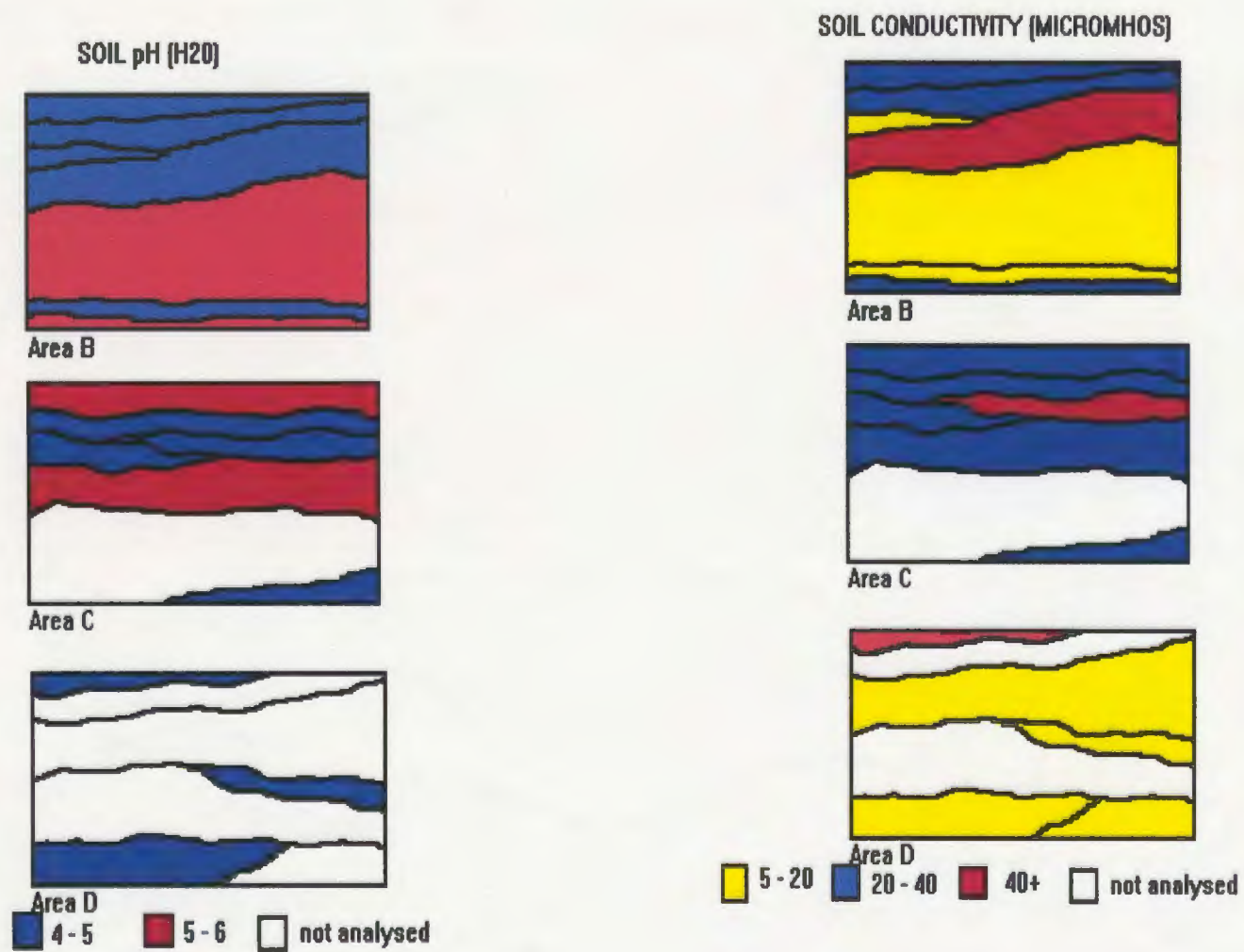


Figure 6.4 Soil profiles showing variation in soil pH and conductivity.

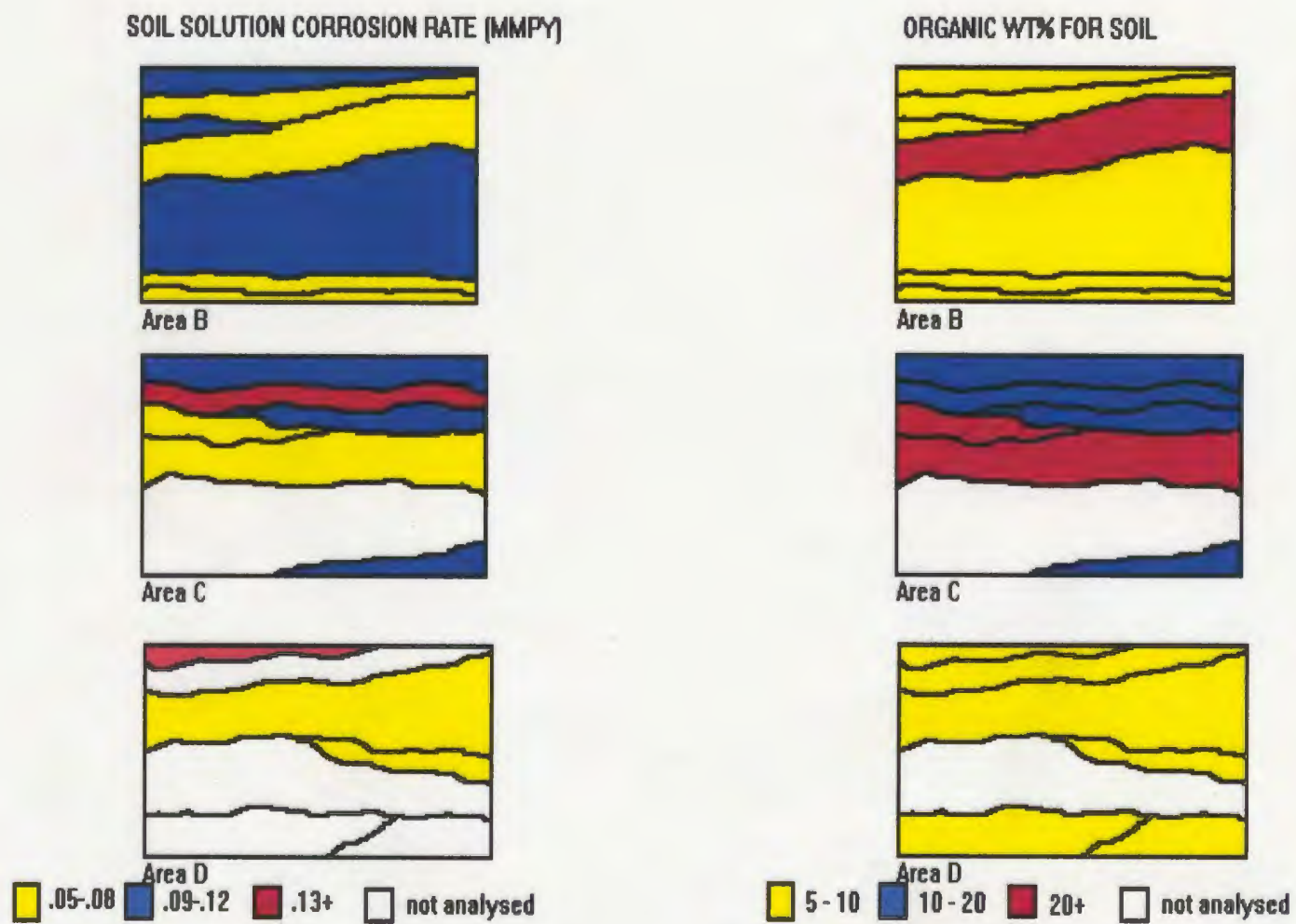


Figure 6.5 Soil profiles showing variation in soil corrosion rate and organic wt%.

62 are more alkaline, and have the lowest soil corrosion rates. Soil from events 55 (Area C) and 63 (Area D) have the highest corrosion rates.

Soil from Area C has the highest conductivity, has the highest corrosion rate and organic wt%. With exception of soil from event 63, soil from Area D is less conductive and has the lowest corrosion rate and organic wt% than soils from Areas B and C.

Subsoils, represented by event 88 and 141, are less conductive, have lower corrosion rates and organic wt% than most of the other soil samples.

6.4 Elemental Analyses for Soils

Tables 6.4a-d (Appendix 6b) contain the elemental analyses for soil samples from the occupation/destruction and fill/building events in Areas B, C and D. Element concentrations at or below detection limits and for which analysis has no significance will not be discussed. Table 6.4e presents averaged totals of weight %, standard deviation, % standard deviation, standard error and % standard error for soils grouped by area and events. Note that averaged totals for element wt% are closer to 100% if the measured organic component is added back. For the inorganic soil component, differences in % standard deviation and % standard error are lower when samples are grouped by area and will therefore be discussed by area. For the organic soil component differences in % standard deviation and % standard error are lower when samples are grouped according to the archaeological stratigraphic location (event) and will be discussed by event.

Table 6.4e
Inorganic + Organic Components of Soil from Areas B, C and D

Inorganic			
Measurement	Area B	Area C	Area D
Mean total wt%	83.6	83.5	90.8
Standard deviation	3.8	2.6	4.4
% Standard deviation	4.5	3.1	4.9
Standard error	1.2	1.1	1.5
% Standard error	1.4	1.3	1.6
Organic			
Mean total wt%	8.6	20.5	6.0
Standard deviation	7.6	7.5	1.8
% Standard deviation	89.0	36.0	31.0
Standard error	2.4	3.0	0.6
% Standard error	28.0	36.0	10.0
Inorganic + Organic			
Total wt%	92.2	104.0	96.7
Inorganic			
	occupation/destruction	fill/building	
Mean total wt%	86.0	84.9	
Standard deviation	5.8	3.0	
% Standard deviation	6.7	3.5	
Standard error	1.6	1.0	
% Standard error	1.8	1.1	
Organic			
Mean total wt%	11.3	10.8	
Standard deviation	8.7	8.4	
% Standard deviation	77.0	78.0	
Standard error	2.4	2.7	
% Standard error	21.0	25.0	
Inorganic + Organic			
Total wt%	97.3	95.7	

From a geological perspective, elements are divided into 3 groups based on their abundance. Major elements each constitute more than 1.0% of a rock, minor elements represent from 1.0 to 0.1%, while trace element concentration represents less than 0.1% of the rock (Philpotts 1990:88). The seven major oxides which are found in the Ferryland soil are; SiO_2 , Al_2O_3 , FeO (Fe_2O_3), MgO , CaO , Na_2O and K_2O (Tables 6.4a-d). Overall the data revealed a consistency for elements probably representing a soil mineralogy dominated by quartz, feldspar, clay and mica. XRD analyses to follow confirm this observation.

Tables 6.4f and g (Appendix 6b) contain data showing concentrations of S, Cr, Fe_2O_3 , Cu, Pb and Zn which are probably derived from buried artifacts. Concentrations of S, Cr, Fe_2O_3 , Cu, Pb and Zn are consistently greater than detection limits (19 ppm, 7 ppm, 0.006wt%, 4 ppm, 4 ppm and 4 ppm, respectively). Table 6.4h (Appendix 6b) shows that concentrations of Cu, Zn, Pb, Cr, S and Ba were highest for events representing occupation and therefore containing artifacts. Large % standard deviations indicate variation between events. Sample D-23, event 96 of Area D has greater concentration of S, Zn, Pb, Cr, S and Ba. Concentrations of Cu, Zn, Pb, Cr, S and Ba were lower for subsoils. Subsoil D-25, located below the Area D house, had higher concentrations of the metals than subsoil D-24, located outside of the house, probably because of a leaching effect from the soils above. Table 6.4h (Appendix 6b) also contains data showing concentrations of elements derived from the environment. Percent standard deviation for

soils from both occupation/destruction and fill/building events are lowest for concentrations of SiO_2 , Rb, Sr, Ba and Ce. Concentrations of SiO_2 decrease with occupation while chlorine concentrations increase with occupation. Table 6.4i (Appendix 6b) contains data showing that the concentrations for Cu, Pb, Cr and S were highest for Area B. Figures 6.6 and 6.7 show schematic drawings of typical soil profiles showing variation in soil SiO_2 , Fe_2O_3 , P_2O_5 , and Cl concentrations.

Concentrations of SiO_2 , Fe_2O_3 , P_2O_5 , and Cl were examined to identify relationships between them as they represent both environment and occupation and are ubiquitous throughout the site. Overall Area D soil samples had a higher SiO_2 concentration and lower Cl, Fe_2O_3 , and P_2O_5 concentration than Areas B and C. Soil from Area C had a similar SiO_2 concentration and the highest Cl concentration compared to other soils. Table 6.4j summarizes the relationship between SiO_2 , Fe_2O_3 , P_2O_5 , and Cl concentrations for soil from Areas B, C and D. Note that if SiO_2 concentrations are high, concentrations of Fe_2O_3 , P_2O_5 , and Cl are generally low and vice versa. The exception to this is soil from Area C which has a high Cl concentration regardless of other soil parameters. For soil from all three areas P_2O_5 concentrations were highest for soil associated with human occupation and high soil organic concentration.

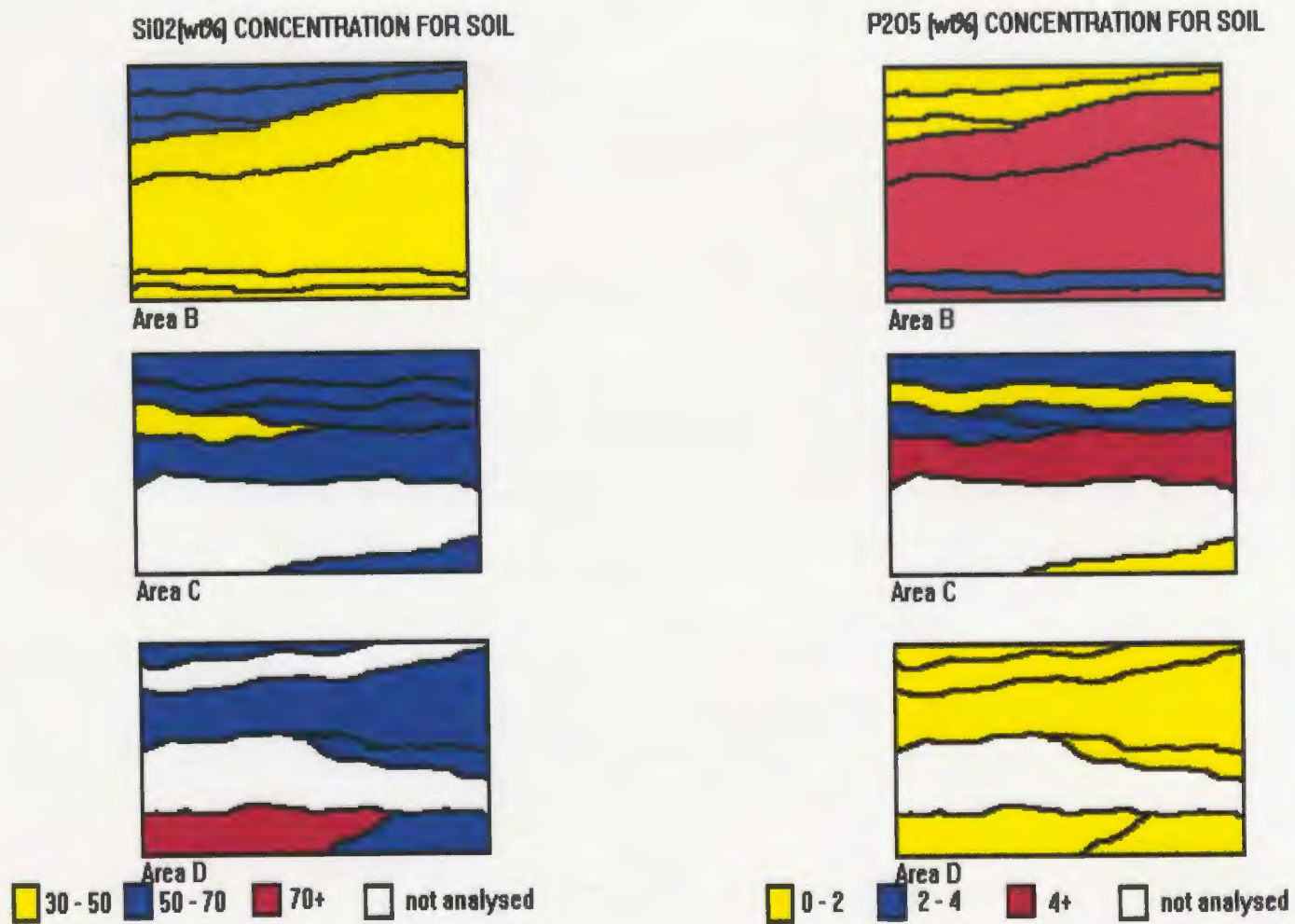


Figure 6.7 Soil profiles showing variation in soil SiO₂ and P₂O₅.

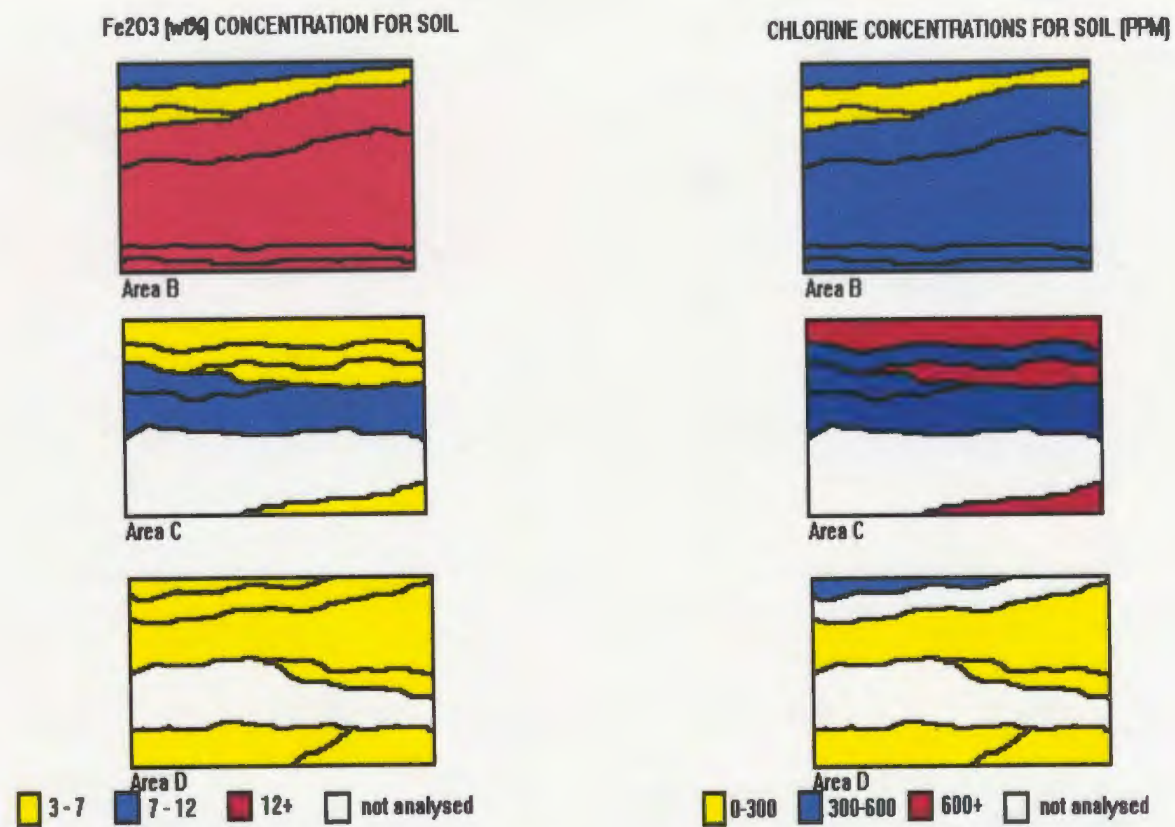


Figure 6.8 Soil profiles showing variation in soil Fe₂O₃ and chlorine concentrations.

Table 6.4j
Comparison of Soil from Area B, C and D based on SiO₂ Concentrations

Area	SiO ₂ (wt%)	Fe ₂ O ₃ (wt%)	P ₂ O ₅ (wt%)	Cl (ppm)
B	↓	↑	↑	↑
C	↑	↓	↓	↑
D	↑	↓	↓	↓

6.5 Chemical Analysis for Soil Solutions

Tables 6.5a-h (Appendix 6c) contain the chemical analysis for soil solutions from occupation/destruction and fill/building events of Areas B, C and D. Results for sample D-21, Area D event 62, differ from other analyses and, as yet, there is no explanation for this variation. Therefore sample D-21 is not included in the statistical analyses of the data. This analysis is included to provide information about the corrosive potential of the soil solution. The observed standard deviations indicate variation between soil samples from different events. This variation suggests a heterogeneous mixture of soluble species.

Variation in Cl concentration between the soil solutions from the different areas is similar to that for dry soil samples. Table 6.5i contains data showing chlorine concentrations for soil and soil solutions. Figure 6.7 shows that Cl concentrations for

Table 6.5i
Chlorine concentration for soil solutions and dry soils

occupation/destruction					
Sample	Event	Depth (cm)	soil solution (ppb)	soil (ppm)	soil (ppb)
D-18	62	28-40	514	129	0.1
D-19	62	28-40	618	206	0.2
D-20	62	30	957	70	0.1
B-8	145	75-97	1038	427	0.4
D-17	62	28-40	1056	393	0.4
B-10	178	95-110	1063	359	0.4
B-7	143	72-80	2348	378	0.4
B-1	133	54	2952	351	0.4
C-11	0	0-30	4939	667	0.7
C-13	19	53-57	5066	373	0.4
D-23	96	53	13436	110	0.1
C-16	195	89-121	16432	1446	1.5
D-21	62	34-38		282	0.3
fill/building					
B-5	134	59	635	100	0.1
B-4	134	57-68	1074	313	0.3
B-3	134	55	1691	209	0.2
B-2	134	38-69	1780	217	0.2
B-6	138	85-120	1871	157	0.2
B-9	177	80-85	2240	382	0.4
D-22	63	16-26	5630	368	0.4
C-12	55	46-53	6788	593	0.6
C-15	16	85	10049	462	0.5
C-14	22	57	33109	784	0.8
subsoils					
D-24	88	32	773	<LD	0.8
D-25	141	62	476	28	0.5

soil solutions are highest for Area C and lowest for Area D. Table 6.5j compares, as a ratio, concentrations of Cl, Cu, Zn, Pb and Ba between soil and soil solutions from occupation/destruction and fill/building events. Concentration of Zn, Pb and Ba are greater for both soil and soil solutions from occupation/destruction events.

Concentrations of Cl are greater for soil solutions from fill/building events.

Concentrations of Cl and Cu are greater for soil from occupation/destruction events.

Overall there appears to be a greater percent of soluble chlorine in the soil, however the experimental method was not designed to allow for precise interpretation of the soluble soil fraction. It is sufficient to know that an increase in chlorine concentration will occur in the presence of water.

6.6 Munsell Colour Separation of Soils

The colour data are presented in Tables 6.6a and b. Figure 6.8 is a schematic drawing of soil profiles showing variation in soil colour. The soils from Areas B, C and D range in colour from dark grey to brown to yellowish brown. The subsoils are pale to dark yellowish brown. Soils from the occupation/destruction events are generally dark in colour. Soils from the fill/building events are generally light in colour. Dark colours correspond to higher concentrations of either or all of organic matter, Fe_2O_3 and P_2O_5 , for example soil from events 143 (Area B), 16 (Area C) and 19 (Area C). Soils having a dark yellowish brown colour had lower concentrations of Fe_2O_3 and P_2O_5 , for example event 145 (Area B). Soils from events 88 and 141,

Table 6.5j
Chemical Species for Soil and Soil Solutions
from occupation/destruction and fill/building events

Soil Solutions					
Chemical Species	occupation/ destruction events (mean concentration - ppb)	fill/building events (mean concentration- ppb)	ratio o/d to f/b	subsoil (D-24)	subsoil (D-25)
Cl	3169	6487	1:2.1	773	476
Cu	11	12	1:1.1	<6.20	6.63
Zn	72	32	2.3:1	8.04	<7.32
Pb	6	5	1.2:1	1.62	0.68
Ba	20	13	1.5:1	1.25	0.41
Soil					
Cl	0.399	0.358	1.1:1	<LD	0.028
Cu	0.151	0.091	1.7:1	0.005	0.023
Zn	0.153	0.118	1.3:1	0.012	0.073
Pb	1.110	0.814	1.4:1	0.089	0.048
Ba	0.770	0.109	7.1:1	0.459	0.555

representing subsoils, are dark yellowish brown and pale brown, respectively. These soils have high silicate concentrations and low iron and phosphate concentrations. Soil from events 62, 63 and 96 of Area D also have low concentrations of iron and phosphate but higher silicate concentrations. Soil colour for soil from events 62, 63 and 96 is greyish brown to dark grey indicating other properties in the soil such as

Table 6.6a
Colour of Soil
from occupation/destruction events

occupation/destruction events							
Sample	Event	Co- ordinate	Depth (cm)	Colour	Hue	Value	Chroma
B-8	145	E2N5	75-97	dark yellowish brown	10YR	4	4
B-10	178	E3N6	95-110	dark yellowish brown	10YR	4	4
D-19	62	E147N8	28-40	pale brown	10YR	6	3
D-21	62	E149N9	34-38	pale brown	10YR	6	3
C-11	0	E89N29	0-30	brown	7.5YR	4	3
B-1	133	E3N0	54	brown	7.5YR	4	2
D-20	62	E135N7	30	brown	10YR	5	3
C-16	195	E88N29	89-121	dark brown	10YR	3	3
B-7	143	E2N7	72-80	very dark brown	10YR	2	2
D-17	62	E137N8	28-40	greyish brown	2.5Y	5	2
D-18	62	E138N8	28-40	greyish brown	10YR	5	2
C-13	19	E88N29	53-57	darkish greyish brown	10YR	3	2
D-23	96	E148N12	53	dark grey	10YR	4	1

Table 6.6b
Colour of Soil
from fill/building events

fill/building events							
Sample	Event	Co- ordinate	Depth (cm)	Colour	Hue	Value	Chroma
B-3	134	E3N3	55	yellowish brown	10YR	5	4
C-12	55	E88N29	46-53	dark yellowish brown	10YR	4	4
B-6	138	E3N3	85-120	pale brown	10YR	6	3
B-2	134	E0N6	38-69	brown	10YR	5	3
B-4	134	E3N2	57-68	brown	7.5YR	5	4
B-5	134	WIN7	59	brown	10YR	5	3
C-14	22	E89N35	57	brown	10YR	4	3
B-9	177	E2N6	80-85	greyish brown	10YR	5	2
D-22	63	E148N12	16-26	greyish brown	2.5Y	5	2
C-15	16	E88N36	85	dark greyish brown	10YR	3	2
subsoils							
D-24	88	E141S11	32	dark yellowish brown	10YR	4	4
D-25	141	E147N8	62	pale brown	10YR	6	3

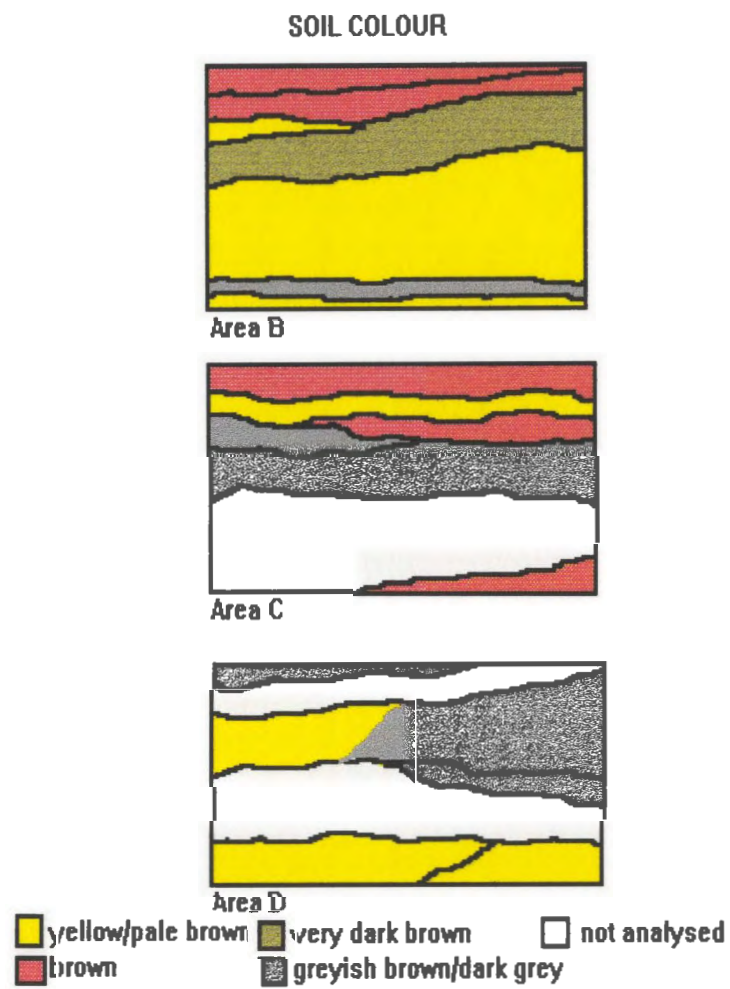


Figure 6.8 Soil profiles showing variation in soil colour.

carbon from the destruction of the area have influenced soil colour.

6.7 Soil Mineralogy

Tables 6.7a and b contain the mineral identifications for soil samples from the occupation/destruction and fill/building events. Figures 6.9, 6.10 and 6.11 show representative XRD spectra for soil samples from the occupation/destruction and fill/building events. The XRD spectra obtained for soil samples can be obtained from author by request. The interpretation of the XRD patterns indicate that the soil mineralogy for the subsoil consists of quartz (SiO_2), albite ($\text{NaAlSi}_3\text{O}_8$) and phlogopite. Soil from occupation/destruction events consists of quartz, albite, sepiolite and phlogopite. Soils B-1, C-11, D-18, D-19, D-21 and D-23 also contained muscovite. Soil samples C-13, C-16, B-7 and D-20 contained illite. Soil from fill/building events contained quartz, albite, sepiolite and phlogopite. Samples B-9, B-5 and C-15 contained illite. Samples B-5 and C-15 contained graphite. The former sample is from an area next to the seventeenth-century forge, the latter represents building rubble after destruction.

6.7.1 Identification of Clay Minerals

Samples from Area D selected for the analysis represent the seventeenth-century occupation plus the subsoil. The soil consisted of a mixture of quartz, illite and kaolinite. Samples were further tested for smectite by glycolating. Vermiculite

Table 6.7a
Mineralogy of Soil
from occupation/destruction events

occupation/destruction events											
Sample	Event	Co- ordinate	Depth (cm)	qtz	alb	san	mus	sep	phl	il	gr
B-1	133	E3N0	54	X	?		X	X	X		
C-11	0	E89N29	0-30	X	X		X	X	X		
D-18	62	E138N8	28-40	X	X		X	X	X		
D-19	62	E147N8	28-40	X	X		X	X	X		
D-21	62	E149N9	34-38	X	X		X	X	X		
D-23	96	E148N12	53	X	X		X	X	X		
D-17	62	E137N8	28-40	X	X			X	X		
B-8	145	E2N5	75-97	X	?			X	X		
B-10	178	E3N6	95-110	X	?			X			
C-13	19	E88N29	53-57	X	X			X		X	
C-16	195	E88N29	89-121	X	X			X		X	
B-7	143	E2N7	72-80	X	X					X	X
D-20	62	E135N7	30	X		X	X	X	X	X	

? = 50% of peaks match PDF

Table 6.7b
Mineralogy of Soil
from fill/building events and subsoil

fill/building events									
Sample	Event	Co- ordinate	Depth (cm)	qtz	alb	sep	phl	il	gr
B-3	134	E3N3	55	X		X			
C-12	55	E88N29	46-53	X	X	X			
D-22	63	E148N12	16-26	X	X		X		
B-2	134	E0N6	38-69	X		X	?		
C-14	22	E89N35	57	X	X	?	X		
B-6	138	E3N3	85-120	X		X	X		
B-4	134	E3N2	57-68	X		X	X	?	
B-9	177	E2N6	80-85	X	X	X	X	X	
B-5	134	W1N7	59	X	?	X	X	X	X
C-15	16	E88N36	85	X	X	X	X	X	X
subsoils									
D-24	88	E141S11	32	X	X	X	X		
D-25	141	E147N8	62	X	X		X		

? = 50% of peaks match PDF

B-1

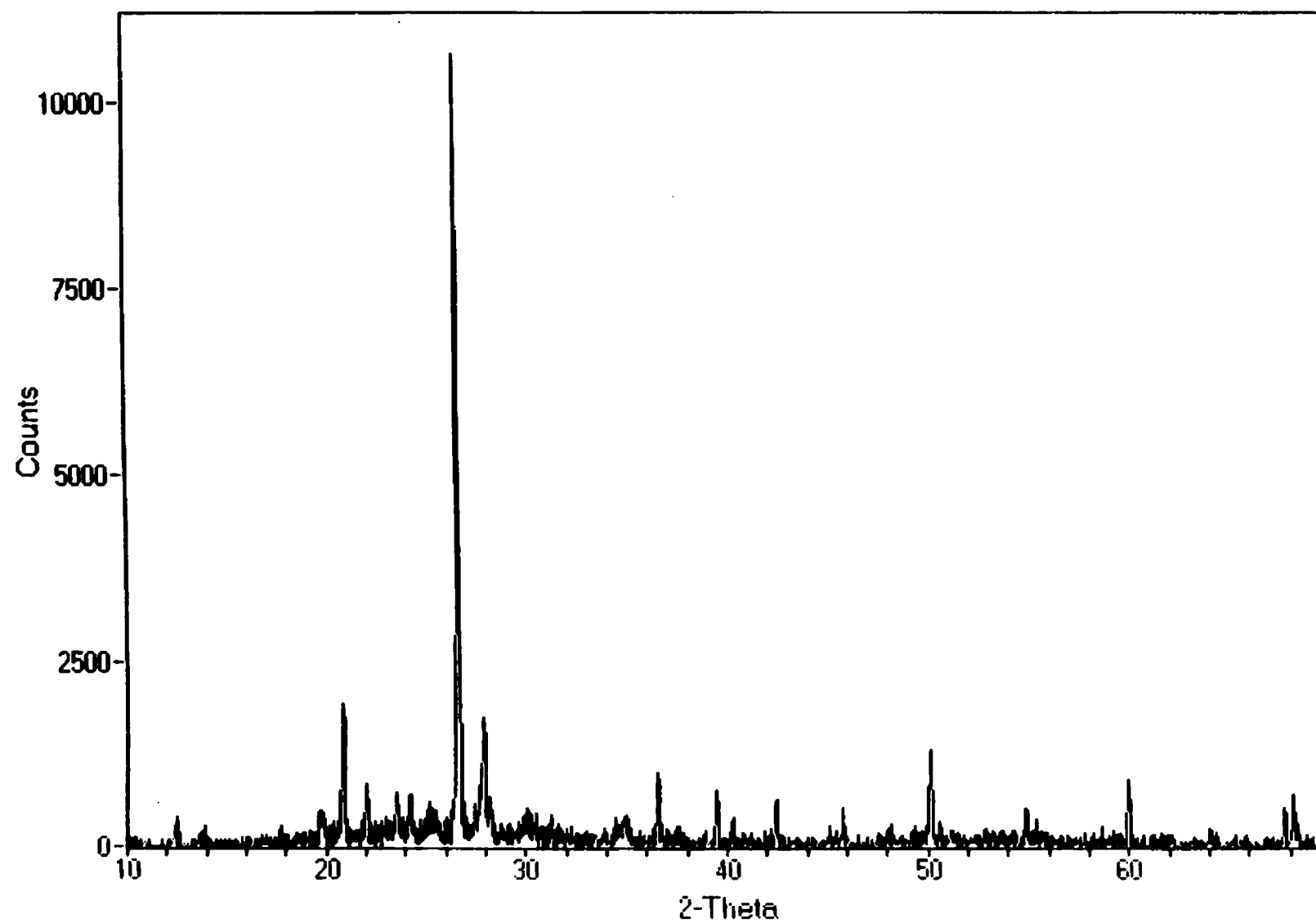


Figure 6.9 Representative XRD spectra for soil samples from Area B.

C- 14

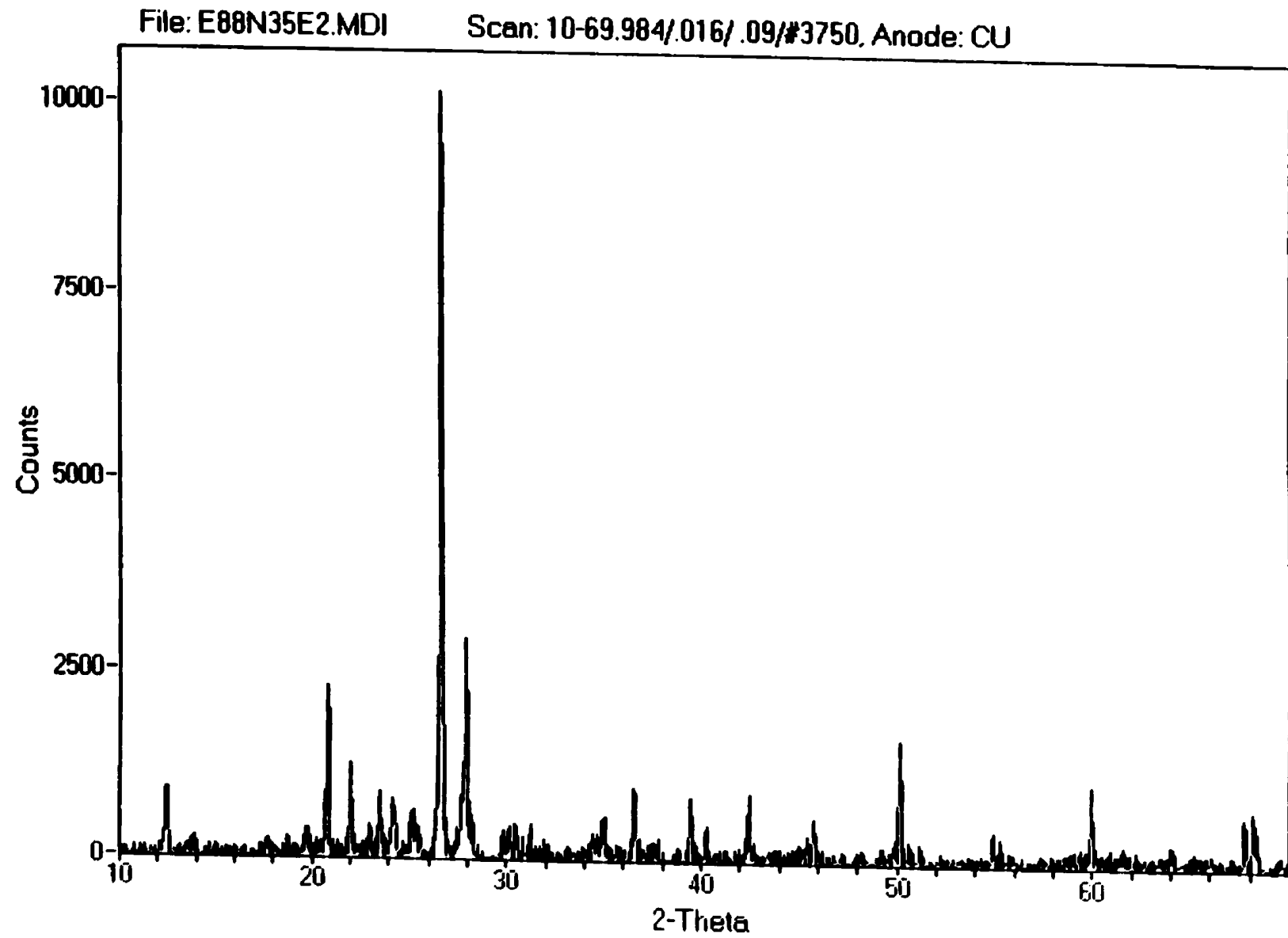


Figure 6.10 Representative XRD spectra for soil samples from Area C.

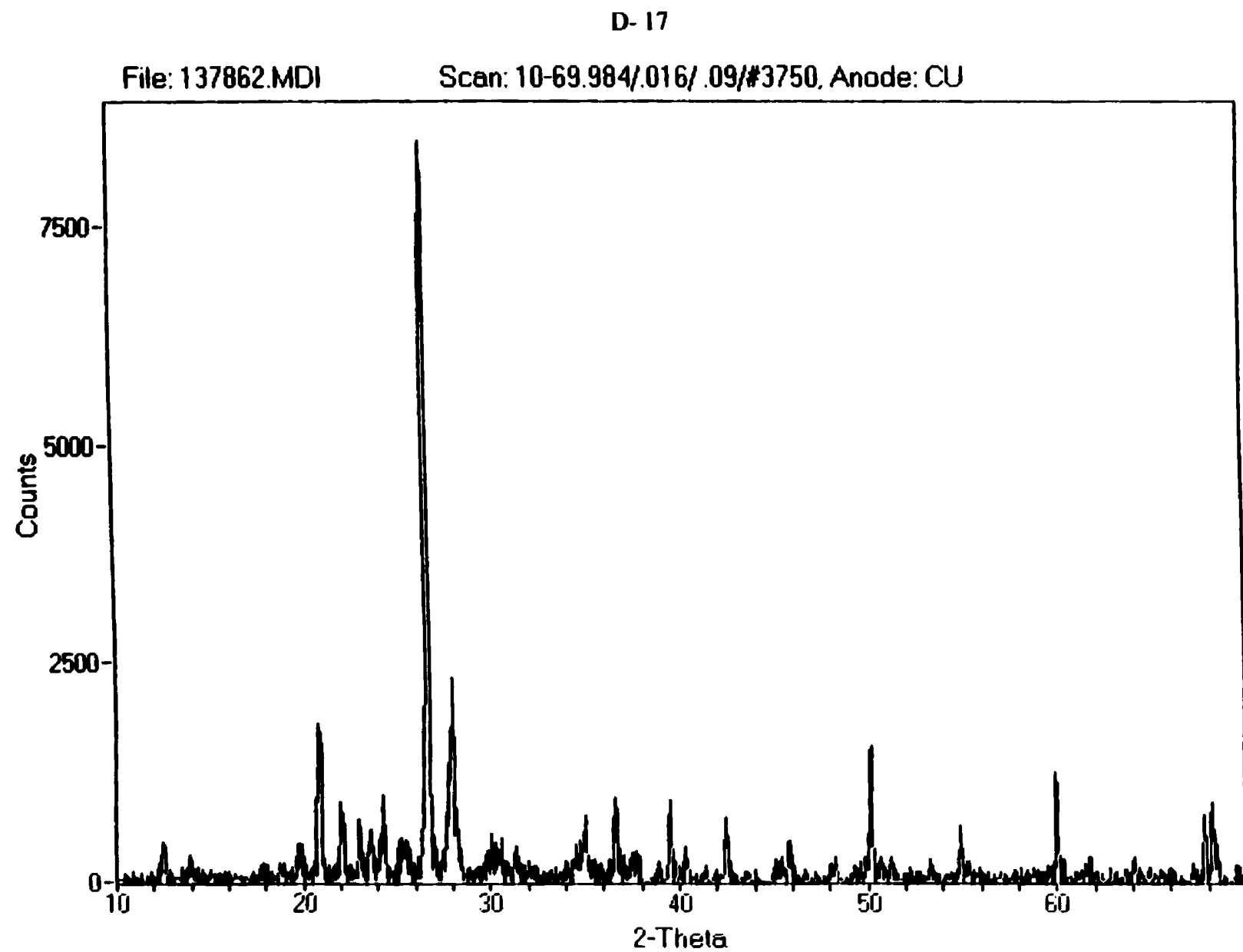


Figure 6.11 Representative XRD spectra for soil samples from Area D.

was sought using glycerine. Because of the fairly consistent results within each event it was decided to reduce the number of samples by using one representative sample (based on pH, colour and particle size) for each event. Table 6.7.1 presents the data. Event 62 generally had neither smectite nor vermiculite. Samples from events 88, 96 and 141 have some smectite but were dominated by illite. Moore and Reynolds (1989) and Deer et al. (1993:364) indicate that wide peaks would be associated with an illite/smectite phase. Given the narrow peaks from the Area D clay samples and experimental results one can say with confidence that the Area D soil and event 88 subsoil contain quartz, kaolinite and illite.

Table 6.7.1
Clay Mineralogy for the Ferryland Archaeological Site

Sample	Event	Co-ordinate	Depth (cm)	qtz	ll	sm	verm	mus	kao	sep
D-17	62	E137N8	28-40	X	X				X	
D-18	62	E138N8	28-40	X	X			X	X	
D-19	62	E147N8	28-40	X	X		X		X	
D-20	62	E135N7	30	X	X				X	
D-21	62	E149N9	34-38	X	X				X	
D-23	96	E148N12	53	X	X	X			X	
D-24	88	E141S11	32	X	X	X			X	X
D-25	141	E147N8	62	X	X	X		X	X	X

6.8 Discussion

Particle size and size distribution are major controls on a soil's capacity for fluid movement while a pH and conductivity measurement will indicate the ionic concentration of the soil. Soil colour separates a soil by the constituents from which it was derived. The organic concentrations for soil from an archaeological excavation is probably an indication of human/animal occupation. The elemental concentration of soils will help define the mineral composition. Soil solution chemistry will indicate what is available to react with buried artifactual remains. Tables 6.8a-c summarize these results and compare changes in soil characteristics to changes in archaeological events. Tables and Figures presented earlier in this chapter show there are no clear cut patterns in this data. When measurement and instrumental errors are accounted for, differences in soil composition are not significant. However, if true, then the burial environment is relatively homogenous and should impart a uniform effect of artifact condition. Therefore the results obtained in this chapter will be examined to predict iron condition based on soil condition. The soil assessment, with respect to the predicted iron condition, will be compared to the results of artifact analysis to follow in Chapter 7.

Some differences in soil from different events and areas of excavations did exist along with significant anomalies in the data. These will be discussed below with suggestions of other parameters which may affect artifact condition more significantly. For example, residence time of soil solutions may vary with soils from different events.

Table 6.8a
Soil Description by Archaeology and Soil Chemistry
Area B

Archaeology	Soil Chemistry
E133 - destruction	corrosive; silica rich soil
E134 - fill - artifacts date to 1640?	silica rich; high zinc concentration
E138 - possible cobble deposit	corrosive; silica rich
E143 - possibly same layer as E145, contains artifacts	chlorine, iron, lead, sulfur, copper, zinc and phosphate in soil; organic rich; highly conductive
E145 - artifacts, lots of nails, dates to mid 17 th century, post-dates forge	chlorine, iron, lead, calcium and phosphate rich; corrosive; organic poor; pH-5.63
E177 - sand/gravel floor, some artifacts, dates with E177	iron, copper, zinc and phosphate rich; organic poor
E178 - first occupation, contains artifacts	iron, calcium, sulfur and phosphate rich; pH-5.74

Table 6.8b
Soil Description by Archaeology and Soil Chemistry
Area C

Archaeology	Soil Chemistry
E0 - plow zone with mix of 17 th to 20 th century artifacts	silica and organic rich; pH-5.04
E55 - pebble fill	silica rich; corrosive
E22 - cobblestone fill	chlorine, sulfur and silica rich; highly conductive, corrosive
E19 - charcoal destruction layer - associated with second construction phase - destroyed in 1696	iron, phosphate and organic rich
E16 - represents the destruction and collapse of the waterfront storehouse built in 1620 and destroyed in 1673	iron, phosphate, sulfur, lead and silica rich; pH-5.60
E195 - secondary waste deposit of 17 th century artifacts dating to first half of century - not associated with Area C's occupation	silica and chlorine rich; corrosive; organic rich

Table 6.8c
Soil Description by Archaeology and Soil Chemistry
Area D

Archaeology	Soil Chemistry
E63 - fill - artifact assemblage dominated by 20 th century with some 17 th century objects	chlorine, zinc and sulfur rich; highly conductive; corrosive
E61 - plow zone - mix of 17 th to 20 th century artifacts	plow zone
E62 - 17 th century occupation - second half of 17 th century may not be associated with primary occupation	silica and barium rich soil; pH-5.12
E96 - charcoal layer, 1696 destruction	silica, arsenic, zinc and lead rich; higher organic concentration than E62
E88 - subsoil outside of 17 th century house	silica rich
E141 - subsoil below 17 th century fireplace	silica rich; pH-5.91

If residence time is accounted for some of the data may show better patterns.

6.8.1 Particle Size Distribution

The overall good state of preservation for ferrous metals upon excavation (pre-storage) from Ferryland can in part be attributed to the gravel loamy sand soil texture

which has provided good drainage of the site over the past 350 years of burial.

Distribution of gravel, sand and clay differ between the occupation/destruction and fill/building events with the latter having a larger gravel component. The overall larger particle size for soils from fill/building events would allow for better drainage and a lower soil solution residence time. Based on the above, the overall iron condition is predicted to be better for iron excavated from soil of fill/building events. However, within these broad event groups anomalies exist in particle size distribution which would be expected to produce different conditions for iron preservation. For example sample B-5 . event 134. has higher concentrations of fine particles than sample B-4 of event 134. Iron excavated from soil sample B-5 was in fair condition while that from soil sample B-4 was in good condition. In this case the larger particle size possibly allowed for better drainage and preservation of iron excavated from B-4 soil. In Table 6.8.1 soils with particle size distributions different from the means are listed and described. Based on the results of particle size distribution iron condition is predicted (Table 6.8.1).

6.8.2 Soil pH, Conductivity , Corrosion Rate and Cl Concentration

The soil pH, conductivity, corrosion rate and Cl concentration are all measurements of the activity of ions in soil solutions. These are the parameters generally attributed to the initiation and continuation of the iron corrosion process (Jones 1992; Turgoose 1989). These parameters will be discussed together for the purpose of identifying soils which could be aggressive to ferrous metal, but first a brief discussion of

Table 6.8.1
Soil with Particle Size Distribution Different from Mean

Area	Soil	Event	Gravel			Sand			Clay			Drainage	Iron Condition
			High	Low	Mean	High	Low	Mean	High	Low	Mean		
B	B-1	133	X				X			X		good	good
B	B-10	178	X				X			X		good	good
B	B-6	138	X				X		X			good/poor	fair
C	C-3	19		X		X					X	poor/good	fair
B	B-5	134		X		X				X		poor/good	fair
D	D-23	96		X		X				X		good/poor	fair
D	D-18	62		X		X					X	good/poor	fair
D	D-22	63		X		X			X			poor	poor
D	D-19	62	X				X				X	good	good
B	B-4	134	X				X			X		good	good
D	D-17	62		X		X			X			poor	poor
D	D-21	62		X				X	X			poor	poor
C	C-14	22			X			X	X			poor	poor
B	B-7	143			X			X		X		good	good

each parameter and its affect on iron condition will be included. In terms of iron nail condition, the averaged soil pH would not be expected to cause large variation in iron preservation. Because soil from Areas C and D are more acidic with depth, iron nail condition would be expected to worsen with depth. Events 195, 133, 19 and 62 (D-20) being the most acidic would be expected to cause more damage to iron nails. Events 178, 145 and 62 (D-17, 18, 19) being more alkaline would be expected to preserve the iron nails better than soil from other events.

Soil conductivity for occupation/destruction events is lower than for fill/building events, however there is much overlap. Percent standard deviations indicate variation in soil conductivity for samples in each of the event groups with soil from fill/building events having greater variation. Percent standard error is also greater for soil from fill/building events indicating greater variation around the sample mean. This variation between soils from different events would be expected to produce different iron nail condition. Soil from Area D has the lowest soil conductivity and, if based on condition, alone would be expected to preserve iron. Soil samples from events 143, 22 and 63 had the highest conductivity and would be expected to be damaging to iron.

Soils with the highest corrosion rates are from events 55 and 63 and would be expected to be damaging to iron. Soils with the lowest corrosion rates are from events 96, 62, 16, 19, 143 and 134 and would be expected to be passive for iron. These soils

with low corrosion rates all have a high artifact concentration. This may suggest that as the artifacts corrode, generally by oxidation processes, oxygen, hydrogen and chloride ions are consumed from the surrounding soil resulting in a less corrosive soil.

Chlorine concentrations for soil solutions are all well above the instrument level of detection. The highest Cl concentrations are for soils from Area C and events 63 and 96 (Area D). These soils would be expected to be damaging to iron. The lowest Cl concentrations are from soils from Area B and events 62 of Area D but because overall concentrations are high, these soils would also be expected to be damaging to iron. Table 6.8.2 compares measurements for pH, conductivity, corrosion rate and soil solution Cl concentration. Soils which are acidic, conductive, have a high corrosion rate and Cl concentration would be expected to be damaging to buried iron. From Table 6.8.2 no one soil sample matches the above, however, some soil samples have some of these characteristics. For example soil from events 63 and 22 are both acidic and conductive. Soil from event 63 also has a high corrosion rate and soil from event 22 is concentrated in Cl. Iron excavated from soils of events 63 and 22 would be expected to be fragile. Soils from events 145, 178 and 62 which are alkaline, have a low conductivity, corrosion rate, and Cl concentration would be expected to be passive to buried iron. When predicting iron condition based on soil solution pH, conductivity, corrosion rate and Cl concentration one must be aware that one parameter may have a greater affect on condition. Also if residence time for soil solutions from different events vary, this too

Table 6.8.2
Comparison of Potentially Damaging Soil Parameters for Buried Iron

Area	Event	pH		conductivity			corrosion rate			Cl concentration for soil solution			Iron condition		
		acidic	alkaline	high	low	mean	high	low	mean	high	low	mean	good	poor	good/poor
B	133	X		X					x		x				x
B	134	X				x		x			x		X		
B	138	X			x				x		x		X		
B	143	X		X				x			x				x
B	145		x		x				x		x		X		
B	177	X			x			x			x		X		
B	178		x			x		x			x		X		
C	0		x			x			x			x		x	
C	55	X				x	X					x		x	
C	22	X		X					x	X				x	
C	19	X				x		x				x			x
C	16		x			x		x		X				x	
C	195	X				x			x	X				x	
D	63	X		X			X					x		x	
D	62		x		x			x			x		X		
D	96	X			x			x		X				x	
D	88	X			x				x		x		X		
D	141		x		x				x		x		X		

will affect iron condition. For example soil from event 133 is acidic and conductive which could be damaging to iron, however the Cl concentration is low and drainage is good probably outweighing the former in terms of affect on iron reactions. Therefore, in this case, iron would be in better condition than that from soil of event 22.

6.8.3 Organic Component

Soil with a high organic concentration has been shown to be damaging to buried iron (Cronyn 1990), though the organic soil component is probably not the only parameter promoting corrosion (Mathias 1996). Organic content is highest for soil samples from events 143 (Area B), 19 and 16 (Area C), all representing or being associated with occupation. The cow barn, of Area C, identified by Gaulton (1977), probably contributed to the soil's high organic concentration. Based on previous observations of the Ferryland soil, the iron excavated from soil in these events would be fragile. Soil from Area D, including events associated with occupation, has the lowest organic content and it would be expected that iron excavated from this soil would be in good condition. However, given the reactive nature of the surficial geological environment, iron condition should not be predicted based on one soil parameter. Table 6.8.3 combines the predicted iron condition, based on the results of soil pH, conductivity, corrosion rate, Cl concentration, drainage and organic wt% for the Ferryland soils. Iron condition, based on the predicted results for each soil parameter, is estimated by percent.

Table 6.8.3
Predicted Iron Condition Based on Soil Condition

Area	Event	Iron Condition based on soil pH, conductivity, corrosion rate and Cl concentration			Iron Condition based on Drainage			Iron Condition based on organic wt%			Predicted iron condition (%)	
		good	poor	good/poor(g/p)	good	poor	g/p	good	poor	g/p	good	poor
B	133			x	X					x		67
B	134	X			X					x	67	
B	138	X					x	X			67	
B	143			x	X				x			67
B	145	X			X			X			100	
B	177	X			X			X			100	
B	178	X			X			X			100	
C	0		x		X				x			67
C	55		x		X					x		67
C	22		x			x			x			100
C	19			x			x		x			67
C	16		x		X				x			67
C	195		x		X				x			67
D	63		x			x		X				67
D	62	X			X			X				100
D	96		x				x	X				67
D	88	X			X			X				100
D	141	X			X			X				100

6.8.4 Soil Colour

Soil colour ranges from pale brown to yellowish brown to dark brown and grey for soils from Areas B, C and D. Soils from the occupation/destruction events are generally darker in colour than those from fill/building events. The soil colour can therefore be used to predict activities which occurred in the past, in this case living versus building activities. Though soil colour cannot be used to predict iron condition alone, it can provide information as to possible reactions over time. Soils from event 63 which are a grey colour are probably grey because other soil constituents have been leached out to the soils below. Thus soil from event 63 has experienced much water movement over time with short residence times and, therefore, iron was exposed to a continuous flow of oxygen rich water probably resulting in fragile iron. Soil from events 16 and 19 are also grey but rich in iron and phosphate thus eliminating leaching as cause for colour. In this case the grey colour represents a high carbon content resulting from structures being burned. Burning of artifactual remains has been noted to help preserve iron because of iron phase changes with increased temperature (Cronyn 1990). Therefore the soil colour of grey for event 16 and 19 would be an indicator that the iron condition would be stable.

6.8.5 Soil Mineralogy

Mineralogy for soil from Areas B, C and D is dominated by quartz and feldspar. The clay size fraction of the soil consisted of a mixture of quartz, illite and kaolinite. Of these

minerals, quartz is the least reactive and therefore soils with a high SiO_2 concentration would be relatively inert in relation to the buried iron. Kaolinite clay has the lowest cation exchange capacity (CEC) of the clays (Moore and Reynolds 1989). Illite also has a low CEC and therefore together with the kaolinite would be expected to contribute little to soil reactions.

6.8.6 Elemental and Chemical Analysis for Soils and Soil Solutions

The data show a consistency for elements representing a soil mineralogy dominated by quartz, feldspar, clay and mica. Concentrations for soils and soil solutions follow similar trends except for the concentrations of Cl which are discussed in Section 6.8.2. Variation of element concentration between events does exist for Areas B, C and D. For example, P_2O_5 , Cu, S, Pb and Zn concentrations are highest for soil from Areas B and C associated with artifact-rich events. The P_2O_5 is probably derived from human/animal excrement or fish processing activities while the Cu, S, Pb and Zn represent the tools and implements used by the seventeenth-century colonists. Area B soil exhibited the highest values for Ca, S, Pb, Cu, P_2O_5 , and Fe_2O_3 , either because this area is near the seventeenth-century forge or because it had a greater number of occupants or was occupied for a longer period than Areas C and D. Area C has the highest values for Cl probably because of its close proximity to the salt water. Soil from Area D has the highest concentrations for Na, Mg, K, Zn and SiO_2 and lowest concentration of P_2O_5 , Cu, Zn, S, Pb and Cl. The low concentration of metals for soil from Area D probably indicates that this house was occupied for the shortest period of time of those areas studied.

Examining results for soil element concentrations (Appendix 6b), concentrations for S, Pb, Cu, Zn and Fe_2O_3 are all higher than subsoils and probably represent artifacts buried in the soil. Quantification of these results is difficult because the varied activities of the seventeenth-century colonists would result in varying use and artifactual remains in the soil. However, the fact that the soil associated with occupation has greater concentrations of the above elements than subsoils indicates that some reactions have occurred between the soil matrix and the buried artifact. Though some of the soils appear stable/unreactive in the 1990s it does not preclude that they exhibited the same condition in 1648. Table 6.8.6 summarizes all soil parameters analysed and indicates the predicted iron condition which can be compared with the results obtained for iron condition in Chapter 7. Based on the data presented in Table 6.8.6 soil from events 62, 88 and 141 will provide the best iron preservation. Soil from events 145, 177 and 178 will provide the second-best iron preservation. Soil from events 134 and 138 will be more corrosive to iron nails than those above.

Table 6.8.6
Summary of Predicted Iron Condition

Area	Event	Predicted iron condition (%) based on soil pH, conductivity, corrosion rate, Cl concentration, drainage and organic wt%		Condition predicted based on soil colour			Condition predicted based on soil silicate concentration		
		good	poor	good	poor	g/p	good	poor	g/p
B	133	33	67			x			x
B	134	67	33			x			x
B	138	67	33			x			x
B	143	33	67		x			x	
B	145	100	0			x		x	
B	177	100	0			x		x	
B	178	100	0			x		x	
C	0	33	67		x				x
C	55	33	67			x			x
C	22	0	100		x				x
C	19	33	67	x				x	
C	16	33	67	x					x
C	195	33	67		x				x
D	63	33	67		x				x
D	62	100	0		x		x		
D	96	33	67	x			x		
D	88	100	0	x			x		
D	141	100	0	x			x		

g/p = good to poor condition

CHAPTER 7: CHARACTERIZATION OF EXCAVATED IRON NAIL AND SLAG SAMPLES

7.1 Introduction

The purpose of the research presented in this chapter is to gain a better understanding of the changes that occur to buried iron nails at the Ferryland site. Various techniques were used to analyse the element distribution for nail shaft cross-sections in an attempt to characterize ferrous metal alteration with time of burial.

7.2 Survey of Nails

A total of 6,961 iron nails were selected for a bulk condition survey. Samples were excavated from Areas B, C and D.

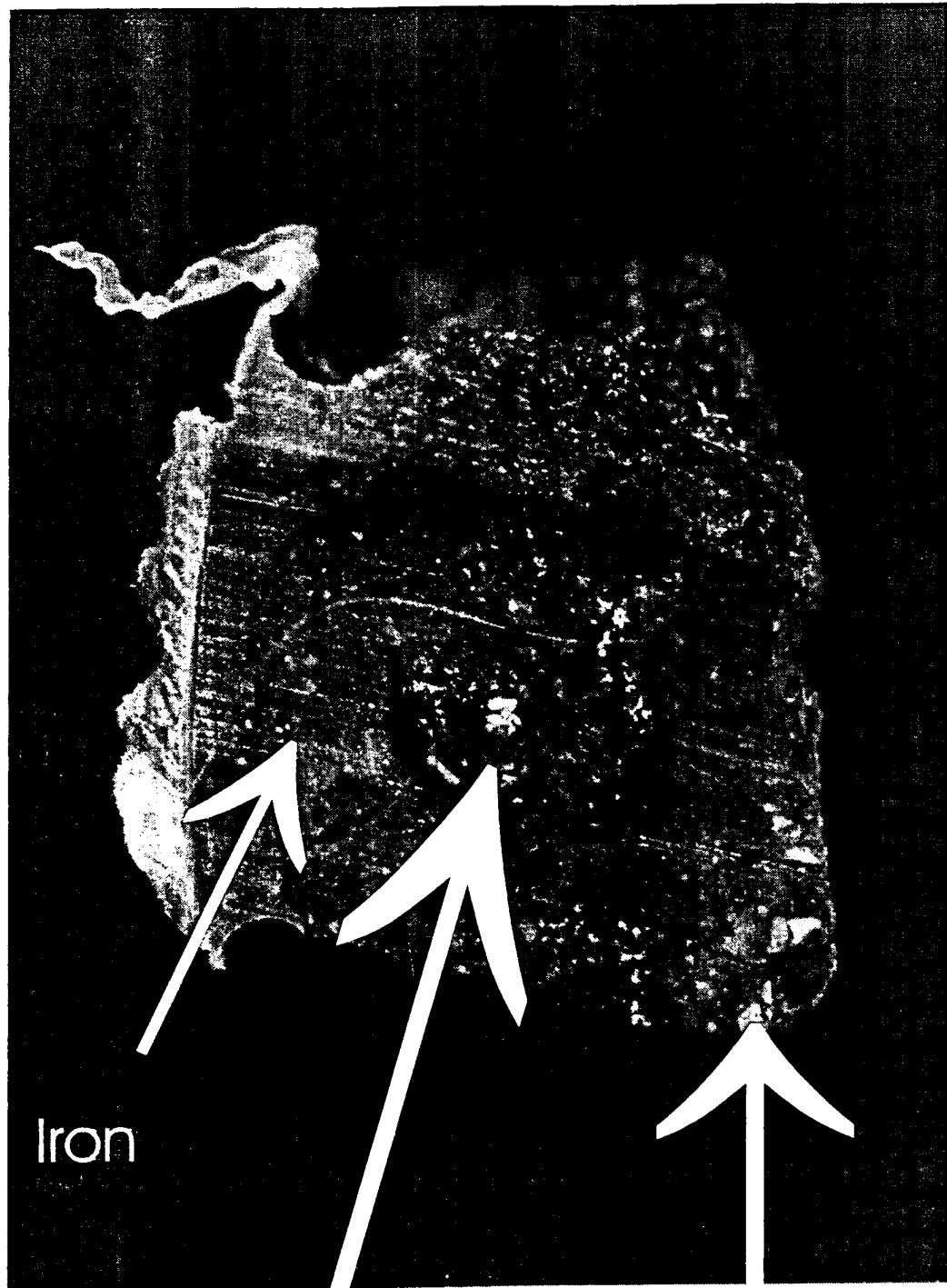
Buried iron nails change to obtain a steady state with the burial environment. When first excavated the “pre-storage” nail condition can help explain the burial reactions. Changes to the nail will continue in the “post-storage” environment if there is no intervention by a conservator to stabilize the nail. The “post-storage” condition reveals information about both the burial and storage environments. For example, iron that looks well-preserved upon excavation may experience cracking and spalling in the field laboratory. Such a change demonstrates that some component of the iron nail has reacted when exposed to humidity, oxygen or other elemental constituents in the storage environment. Figure 7.1 is an iron nail shaft cross-section which has reacted when

exposed to the post-storage environment evident by "bubbles" representing "active corrosion" or an area where iron chloride salts in the nail are reacting to humidity.

7.2.1 Pre-storage and Post-storage Nail Condition

Figures 7.2a, 7.3a and 7.4a show the location of the 6,961 nails surveyed (Appendix 7a). Figures 7.2b, 7.3 b and 7.4b show the location of nail samples used for detailed analysis (Appendix 7a). Table 7.2.1 presents the results of the pre-storage and post-storage condition survey. The majority of the nails were found to be in good condition during the pre-storage survey, though differences in condition existed between nails of different areas. For example, Area B had the highest number of nails in good condition, Areas C and D had the highest number of nails in fair condition and Area C had the highest number of totally mineralized nails.

For the post-storage survey, fewer nails fell in the good condition category than for the pre-storage survey. Numbers of nails in fair condition increased after storage. The number of nails having a totally mineralized condition was unchanged from the pre-storage survey. Area D had the most nails in good condition, and Area C had the most nails in both fair and mineralized condition. Nails from Area B experienced the greatest change as many of the nails previously in good condition were now in fair condition.



Active corrosion

Corrosion halo

Figure 7.1 Cross-section of an iron nail shaft.

Table 7.2.1
Pre-storage and Post-storage Nail Condition

Area	B	B	C	C	D	D
Time	pre-storage	post-storage	pre-storage	post-storage	pre-storage	post-storage
Good Condition (%)	93	49	76	41	80	55
Fair Condition (%)	6	50	18	53	17	42
Totally Mineralized (%)	1	1	6	6	3	3
Total Number of Nails	1718	1718	3599	3599	1644	1644

7.2.2 Post-storage Condition Survey of Nails by Event

The post-storage condition of nails from the events of interest for Areas B, C and D were also investigated. The results are summarized in Table 7.2.2a.

Nails from Area D were in the best condition. Nail condition for Areas B and C varied by event with some events having similar condition to those of Area D. 900 nails from Area B varied in condition by event from most to least stable as follows: 143>145>133>178>134>138>177. 2,003 nails from Area C varied in condition by event from most to least stable as follows: 19 and 195>22> 0 and 16> 22. 1,347 nails from Area D varied in condition by event from most to least stable as follows: 96>62>63. Nails from similar events had a similar condition regardless of the area of excavation.

Table 7.2.2a
Post-storage Nail Condition for Selected Events

Event	Condition - cracked (%)	Condition - stable (%)	Total Number of Nails
Area B			
133	50	50	4
134	57	43	214
138	64	36	17
143	41	59	430
145	42	58	148
177	67	33	12
178	55	45	75
Area C			
0	56	44	320
16	56	44	106
19	34	66	1328
22	40	60	5
55	78	22	92
195	34	66	152
Area D			
62	41	59	974
63	46	54	208
96	39	61	165

For example, events 145 and 62 both representing occupation had nails of similar condition after storage. The nails from the occupation and destruction events were in good condition while nails from the fill and building events were in poor condition. Based on the above, the 35 nails selected for further analysis were sorted by event. Nails from events representing occupation/destruction and expected to be in good condition formed one class. Nails from events representing fill/building and expected to be in poor condition formed the second class. Table 7.2.2b shows the division of the 35 nails into the two classes.

7.3 Interior Nail Condition

The 35 nails were randomly selected for further analysis from the 6,961 nails surveyed. Individual nails were described beginning at the interior iron core and extending to the corrosion halo.

7.3.1 Metallography of Nails

Initial transmitted and reflected light microscopic examination was performed on unetched samples immediately after thin-section preparation. This initial work allowed for a rough description of the extent of the corrosion for the nail samples.

Microscopic examination of texture, colour and grain boundaries indicated that at least three iron phases are present in some nails. The results of the reflected light

Table 7.2.2b
Nails from Occupation/Destruction and
Fill/Building Events

occupation/destruction				fill/building			
Area	Event	Co-ordinate	Nail	Area	Event	Co-ordinate	Nail
B	133	E3N0	106289	B	134	E0N6	115811
B	143	E2N7	120161	B	134	E3N2	97546
B	145	E2N5	120531	B	134	W1N7	115470
B	178	E2N6	120389	B	134	E3N3	115294
C	0	E89N30	128193	B	134	W1N6	115772
C	19	E88N32	128189	B	138	E3N3	115521
C	195	E89N30	128290	B	177	E2N6	120340
D	62	E135N7	94758	C	16	E89N31	128304
D	62	E135N7	94759	C	55	E89N31	128190
D	62	E137N8	94158	C	55	E88N32	128192
D	62	E137N8	94160	C	22	E88N30	128195
D	62	E138N8	94120	D	63	E147N4	94737
D	62	E138N8	94121				
D	62	E138N8	94123				
D	62	E146N8	94743				
D	62	E147N8	94742				
D	62	E147N8	94745				
D	62	E147N8	94785				
D	62	E147N8	94786				
D	62	E147N8	94787				
D	62	E147N8	94788				
D	62	E149N9	87872				
D	96	E148N12	99060				

microscopy indicated the presence of light, middle and dark grey metallic phases. Nail 115772 was examined for carbon concentration of the different hues of grey by electron microprobe analysis. Table 7.3.1 presents the results.

Table 7.3.1
Carbon Content for Sample 115772 - element % by stoichiometry

iron phase identified by colour	carbon concentration (%)	iron phase identification by carbon concentration (Higgins, 1973)
light grey	0.612 to 0.617	40% - ferrite 60% - pearlite
middle grey	0.707 to 0.753	20% - ferrite 80% - pearlite
dark grey	2.542	40% - cementite 60% - pearlite

The carbon concentration for the dark grey phase is high for archaeological wrought iron, however, researchers of historic metallography have observed wrought iron to have high carbon contents because of contamination either during smelting or forging procedures (Fell, personal communication 1996; Higgins 1973). Because further work is needed to clarify the identification of iron phases in the nails, they will be described only as having either single or multi-phase iron.

7.3.2 Grouping of Nails Based on Metallographic Observations

Nail thin-sections from Areas B, C and D were grouped according to the following classifications based on visual images of cross-sections recorded by sketches

and photographs: corroded centre with voids surrounded by multi-phase iron with a corrosion halo (group 1: G-1); corroded centre with voids surrounded by single-phase iron with a corrosion halo (group 2: G-2); multi-phase iron at centre surrounded by a corrosion halo (group 3: G-3); single-phase iron at centre surrounded by a multi-phase iron and a corrosion halo (group 4: G-4); single phase iron and a corrosion halo (group 5: G-5). The extent of internal nail corrosion varies with group 1 having most extensive and group 5 the least extensive corrosion. Appendix 7b contains sketches of each nail shaft cross-section. Figures 7.5 to 7.9 are photographs of a representative nail shaft cross-section from each group. Table 7.3.2a provides a summary of the nail samples for each area based on these groups. Most of the nails classify into G-1 and G-2 implying most nails from Ferryland experience internal iron corrosion. The second largest category of nails would be those with a 70 to 90% concentration of multi-phase iron. All nails had a corrosion halo.

In Table 7.3.2a it is noteworthy that Area C contains no G-4 samples. Area B had the greatest percentage of nails in G-2 and G-4 and Area C had the greatest percentage of nails in G-3.

Tables 7.3.2b and c summarize nail condition based on metallographic group for the occupation/destruction and fill/building events. Nails from Area D dominate the occupation/destruction event classification while nails from Areas B and C dominate the

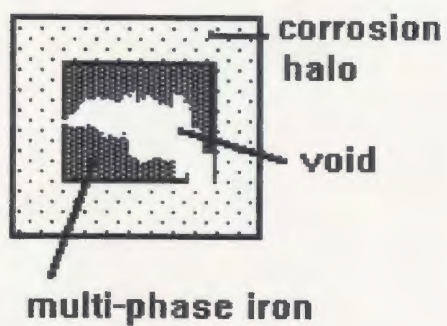


Figure 7.5 Description of G-1 metallographic group. The photograph is of nail sample 128304 (x 1.5).

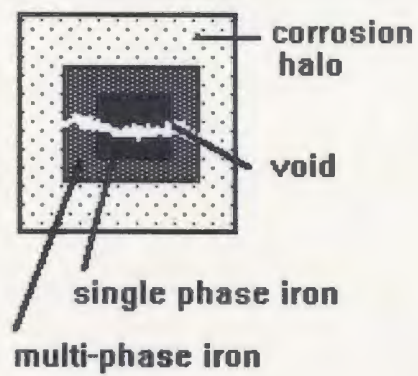


Figure 7.6 Description of G- 2 metallographic group. The photograph is of nail sample 94788 (x 1.5).

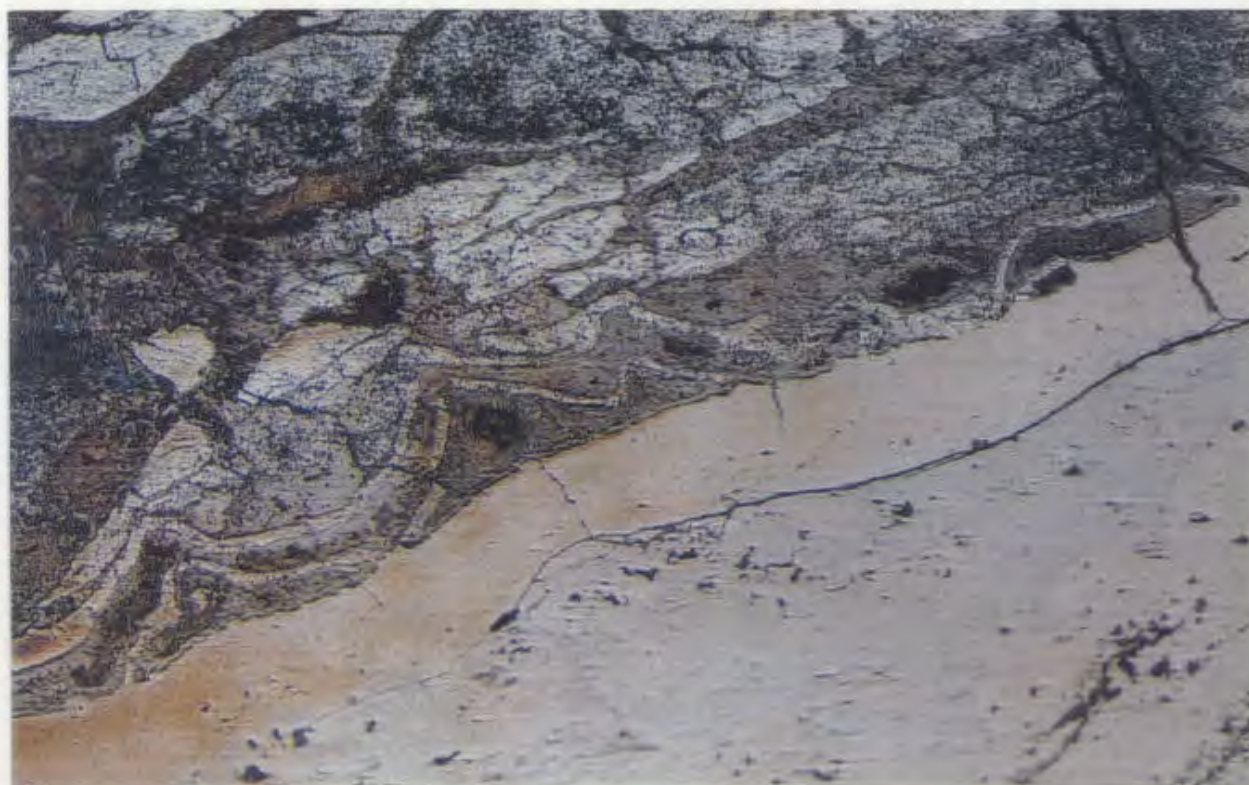
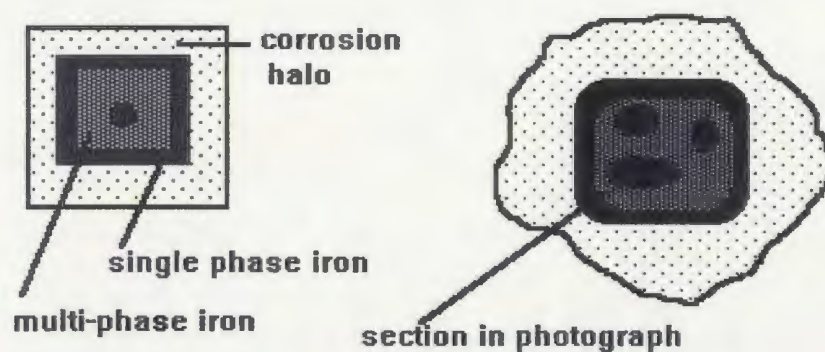


Figure 7.7 Description of G-3 metallographic group. The photograph is of nail sample 128290 (x 10) showing single and multi-phase iron at the iron corrosion interface.

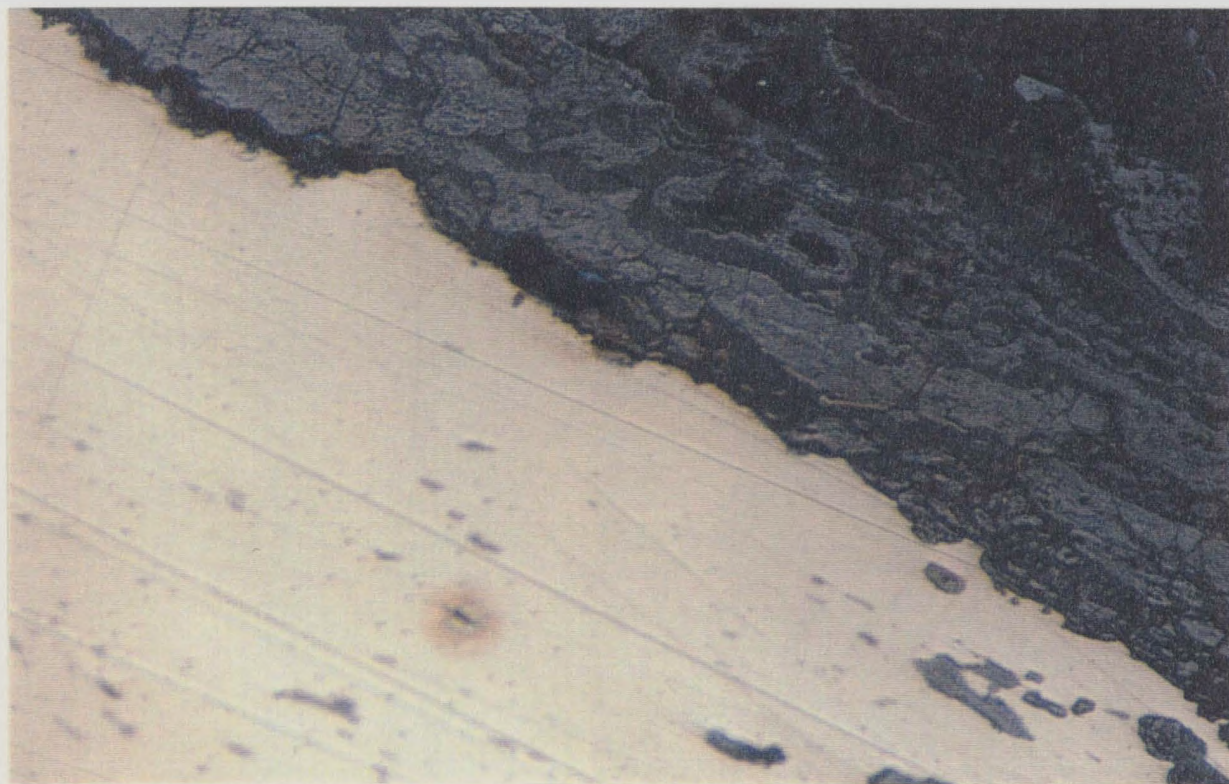
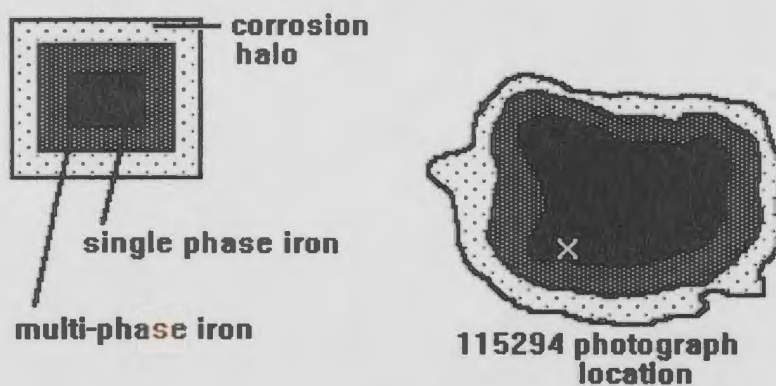


Figure 7.8a Description of G-4 metallographic group. The photograph is of nail sample 115294 (x10) showing single phase iron.

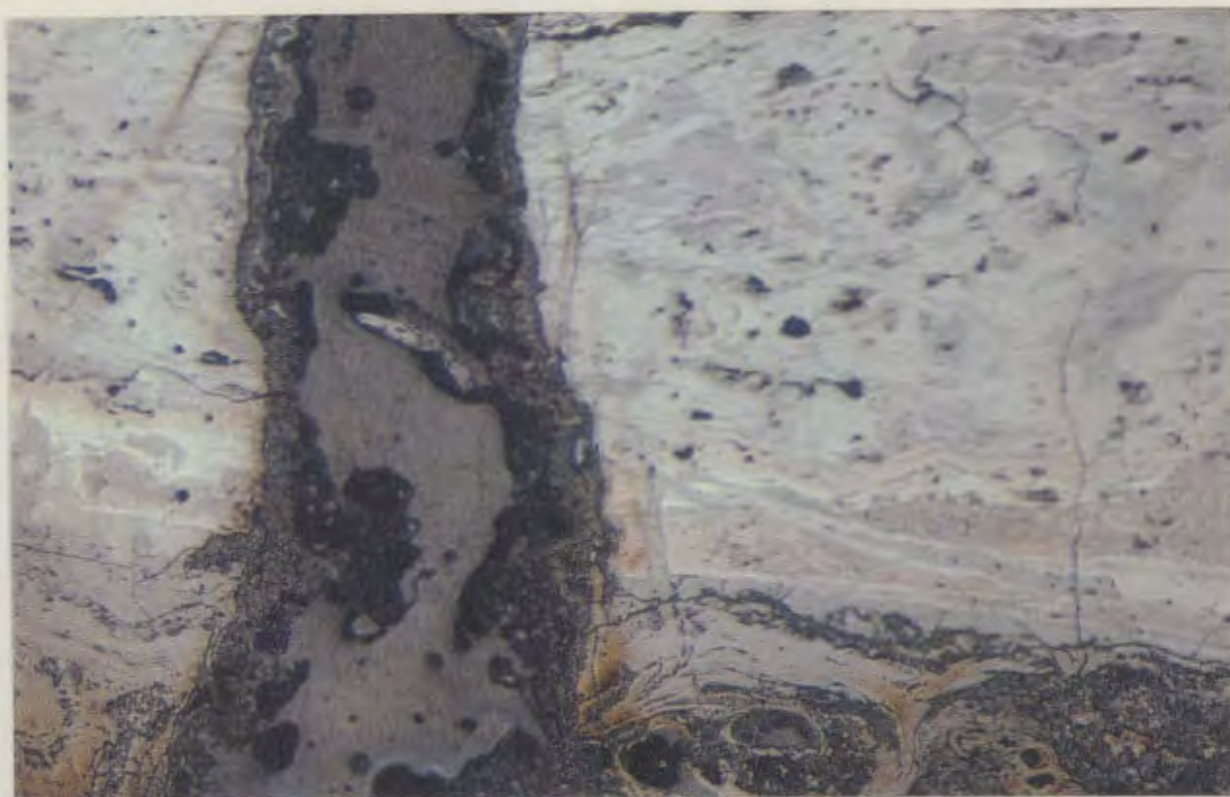
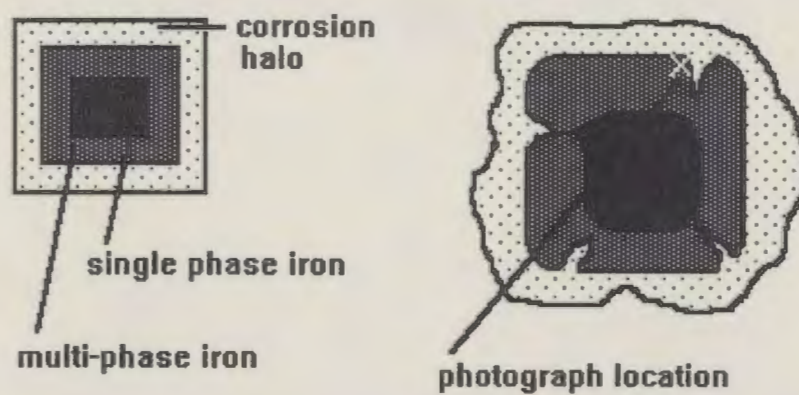


Figure 7.8b Description of G-4 metallographic group. The photograph is of nail sample 94737 (x10) showing multi-phase iron.

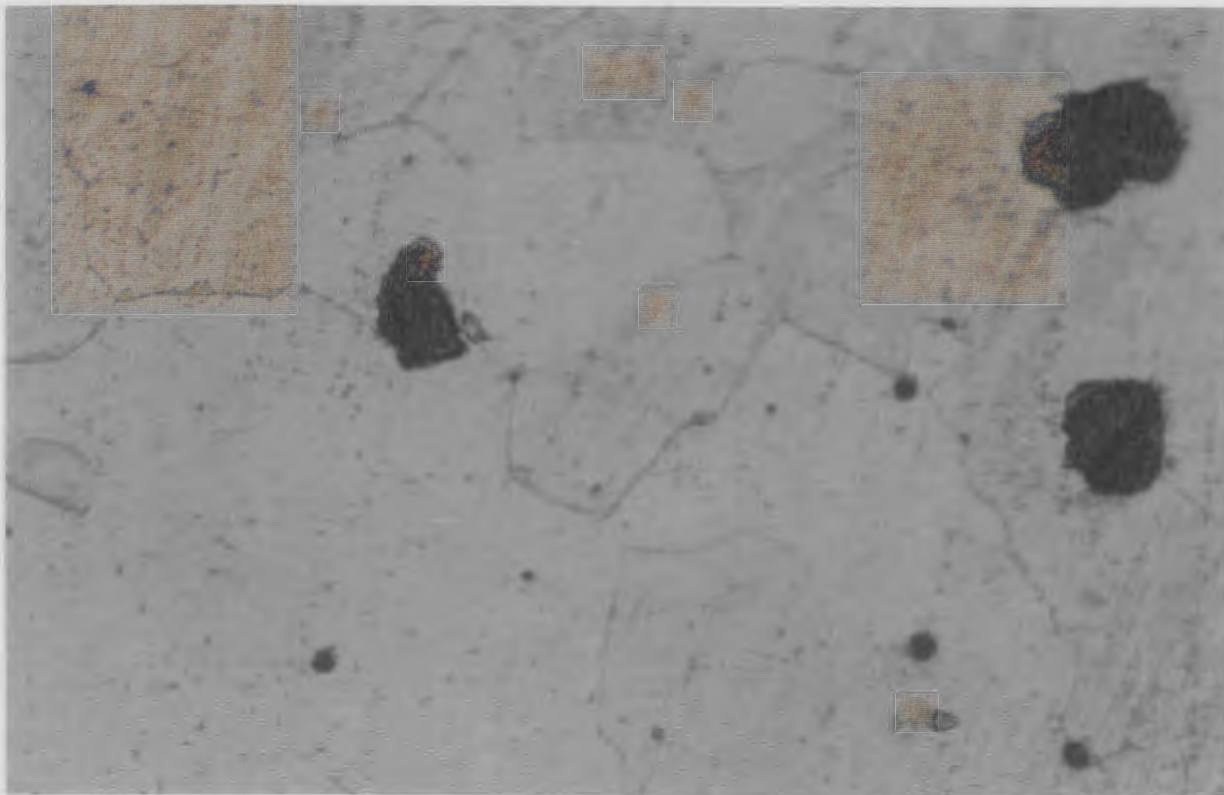
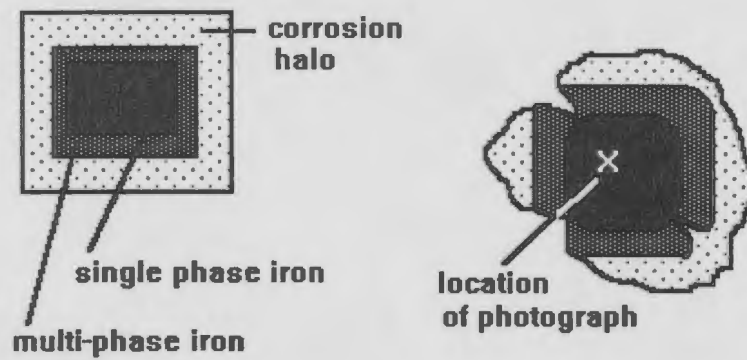


Figure 7.9 Description of G-5 metallographic group. The photograph is of nail sample 115772 (x50) showing metal structure for single phase iron.

Table 7.3.2a
Condition Classifications for Nail Thin-sections

Area	Group 1 centre void >20% of nail surrounded by multi-phase iron - corrosion halo	Group 2 centre void <25% of nail surrounded by single phase and multi-phase iron - corrosion halo	Group 3 single phase iron (10-30%), multi-phase iron (90-70%) - corrosion halo	Group 4 single phase iron (30-50%), multi-phase iron (70-50%) - corrosion halo	Group 5 single phase iron (60-90%), multi-phase iron (40-10%) - corrosion halo	Totals per Area
B	97546 115470 106289	115811 120531 120161	115521 120389	115294 120340	115772	11 nails
Distribution by %	27	37	9	18	9	100%
C	128304 128190	128193	128189 128290 128192		128195	7 nails
Distribution by %	29	14	43		14	100%
D	94787 94160 87872 94158 94743	94123 94785 94742 94120 94788 94121	94745 99060	94737 94759	94758 94786	17 nails
Distribution by %	29	35	12	12	12	100%

Table 7.3.2b
Metallographic Groups
Areas B, C and D
Nails from occupation/destruction

Area	Event	Co-ordinate	Nail sample	Metallographic Groups
D	62	E147N8	94787	G-1
D	62	E137N8	94160	G-1
D	62	E149N9	87872	G-1
B	133	E3N0	106289	G-1
D	62	E137N8	94158	G-1
D	62	E146N8	94743	G-1
D	62	E138N8	94121	G-2
D	62	E147N8	94788	G-2
B	145	E2N5	120531	G-2
D	62	E138N8	94120	G-2
B	143	E2N7	120161	G-2
D	62	E147N8	94742	G-2
D	62	E147N8	94785	G-2
C	0	E89N30	128193	G-2
D	62	E138N8	94123	G-2
C	195	E89N30	128290	G-3
D	62	E147N8	94745	G-3
B	178	E2N6	120389	G-3
D	96	E148N12	99060	G-3
C	19	E88N32	128189	G-3
D	62	E135N7	94759	G-4
D	62	E135N7	94758	G-5
D	62	E147N8	94786	G-5

Table 7.3.2c
Metallographic Groups
Areas B, C and D
Nails from fill/building

Area	Event	Co-ordinate	Nail sample	Metallo-graphic Group
C	55	E89N31	128190	G-1
C	16	E89N31	128304	G-1
B	134	E3N2	97546	G-1
B	134	W1N7	115470	G-1
B	134	E0N6	115811	G-2
B	138	E3N3	115521	G-2
C	55	E88N32	128192	G-3
B	134	E3N3	115294	G-4
B	177	E2N6	120340	G-4
D	63	E147N8	94737	G-4
B	134	W1N6	115772	G-5
C	22	E88N30	128195	G-5

fill/building event classification. 65% of the nails from an occupation/destruction belong to G-1 or G-2, indicating that most of the nail shaft cross-sections were corroded in the centre. The fill/building group had 50% of its nails with centre voids.

7.3.3 Chemical Analyses of Iron Nail Shaft Cross-sections

Chemical analyses of 5 nail shaft cross-sections describe mineral inclusions in corrosion halos, corrosion halo matrixes and iron/corrosion halo interfaces. A description of each of the 5 nails is presented in Table 7.3.3a. Tables 7.3.3b - f (Appendix 7c) summarize the results of the chemical analyses. Appendix 7c contains photographs with points used for analyses indicated. Concentrations for oxygen are not accurate, as instrumentation was not available for precision measurement. Mineral inclusions identified in the corrosion halo included quartz and feldspars. Grains 97546d and g were unidentified but possibly represent weathered feldspars or iron oxide/oxyhydroxide corrosion products. Concentrations for Ca, K, Mg, Mn and Na were highest for the analyses of mineral inclusions. Table 7.3.3g summarizes the corrosion halo matrix composition. Iron values vary from 13.09% to 54.18% with the higher concentrations being located at the exterior edge of the corrosion halo. The higher iron concentrations at the corrosion halo edge probably represent iron values for the soil. Chlorine concentrations were lowest for the corrosion halo. Table 7.3.3h presents averaged values of Fe, Cl, P and Si for corrosion halos from nails of Areas B, C and D. Different areas of excavation had nails with different corrosion halo compositions. Iron

Table 7.3.3a
Chemical Analysis of Iron Nail Cross-Sections

Nail	Area	Event	Event Description	Metallographic Group	Purpose
94759	D	62	occupation	G-4	identify changes in iron core and corrosion halo
128193	C	0	occupation	G-2	as above
120389	B	178	occupation	G-3	as above
115470	B	134	fill	G-1	identify inclusions in corrosion halo
97546	B	134	fill	G-1	as above

concentrations for the nails were different for all three areas. Area D nails had the highest iron concentrations. Chlorine and silicon concentrations were highest for Area B and lowest for Area C. Phosphorus concentrations were highest for Area C. Table 7.3.3i summarizes the results of analyses for the iron section of the nail. Chemical analyses of the iron indicated variation in Fe and Cl which was not specific to an area of excavation. The nail centre had the lowest concentrations of iron but highest of chlorine. Iron with a multi-phase composition had a lower Fe concentration than the single phase iron. Areas with a high iron concentration had a low chlorine concentration. Table 7.3.3j summarizes the chemical analyses for the iron/corrosion halo interface. Iron concentrations are for the most part lower than values for the nail but higher than the corrosion halo. Chlorine was identified for all samples analysed. Figure 7.10 presents models showing the iron and chlorine distributions for the iron nails studied.

Table 7.3.3g
Chemical Analysis of Corrosion Halo Matrix

Nail	Point	Area	Event	Metallo- graphic Group	Fe(%)	Cl(%)	P(%)	Si(%)	O(%)
115470	f	B	134	G-1	22.73	N/A	1.46	7.74	19.28
115470	g	B	134	G-1	19.82	N/A	1.35	9.77	24.55
115470	i	B	134	G-1	24.61	N/A	0.71	14.17	29.36
115470	j	B	134	G-1	35.3	N/A	1.34	12.53	28.86
115470	k	B	134	G-1	36.51	N/A	1.15	8.31	25.11
115470	l	B	134	G-1	27.57	N/A	0.6	2.3	43.74
115470	m	B	134	G-1	1.66	N/A	0	6.57	23.85
115470	n	B	134	G-1	33.95	N/A	0.77	7.1	23.09
128193	a	C	0	G-2	13.09	0.15	5.13	0	11.59
128193	b	C	0	G-2	54.18	0.07	2.22	0.25	18.96
128193	c	C	0	G-2	52.48	0.08	0.84	0.35	16.83
94759	a	D	62	G-4	52	0.04	3.02	2.53	23.29
94759	k	D	62	G-4	51.49	0.07	1.83	4.85	25.62
94759	m	D	62	G-4	43.18	0.2	1.56	7.47	27.25
120389	a	B	178	G-3	33.63	0.7	2.99	4.54	21
120389	c	B	178	G-3	38.12	0.6	1.92	3.85	18.5

N/A - not analyzed

Table 7.3.3h
Averaged Values of Chemical Composition for Corrosion Halos by Area

Area	Fe(%)	Cl(%)	P(%)	Si(%)
B	27.39±0.29	0.65±0.01	1.23±0.05	7.69±0.07
C	39.92±0.33	0.10±0.01	2.73±0.06	0.20±0.02
D	48.89±0.29	0.10±0.01	2.14±0.06	4.95±0.07

Table 7.3.3i
Chemical Analyses of Iron

Nail	Point	Area	Event	Metallo-graphic Group	Fe(%)	Cl(%)	P(%)	Si(%)	Q(%)
94759	f-centre nail	D	62	G-4	0.6	2.43	0	0.03	1.08
128193	f-centre nail	C	0	G-2	51.51	2.21	0.47	0.08	15.52
128193	g-centre nail	C	0	G-2	52.93	7.33	0.25	0.05	15.48
120389	l-centre nail	B	178	G-3	54.69	0.02	0.01	0.28	16.15
120389	k-multi-phase	B	178	G-3	48.67	0.03	3.43	3.61	23.79
128193	h-multi-phase	C	0	G-2	52.47	1.56	0.01	0.05	15.27
120389	h-multi-phase	B	178	G-3	59.03	0.09	0.56	0.15	18.02
128193	i-multi-phase	C	0	G-2	60.21	0.15	0.45	1.49	19.53
120389	g-multi-phase	B	178	G-3	64	0.03	0.33	0.24	19.03
128193	e-multi-phase	C	0	G-2	65.84	0.17	0.25	0.22	19.43
120389	j-multi-phase	B	178	G-3	69.6	0	0.02	0.4	20.4
94759	g-single phase	D	62	G-4	61.05	0.09	0	0.67	18.23
120389	e-single phase	B	178	G-3	68.4	0	0.32	0.29	20.33
120389	f-crack	B	178	G-3	60.5	0.04	0.53	0.48	18.77

Table 7.3.3j
Chemical Analysis of Iron/Corrosion Halo Interface

Nail	Point	Area	Event	Metallo-graphic Group	Fe(%)	Cl(%)	P(%)	Si(%)	O(%)
115470	p	B	134	G-1	46.17	N/A	2.11	0.7	17.29
128193	j	C	0	G-2	33.45	0.64	3.45	7.84	26.94
94759	c	D	62	G-4	67.79	0.13	0	0.11	19.5
94759	d	D	62	G-4	53.75	4.7	0	0.02	15.86
94759	h	D	62	G-4	43.93	0.03	0.77	10.46	26.9
94759	i	D	62	G-4	60.75	0.06	0.14	1	18.83
120389	d	B	178	G-3	43.22	0.02	0	0.12	13.85

N/A - not analysed

7.3.4 Element Maps of Iron Nail Shaft Cross-Sections

Section 7.3.3 identified areas of potential iron alteration and chloride concentration and provided a guide for elemental mapping. Electron microprobe element analyses for nails from Areas B, C and D were performed on cracks, iron/corrosion halo interfaces, areas surrounding voids in the iron, the iron core and corrosion halo. Microprobe operating conditions and standards for the analytical data are presented in Section 5.4.6. All samples were analyzed for S, P, Cl, Fe and Si. Randomly selected samples were also examined for carbon. Appendix 7d contains the pixel maps of the nail sections studied. Element maps for which the element was below the detection limit or where images were obscure are not included.

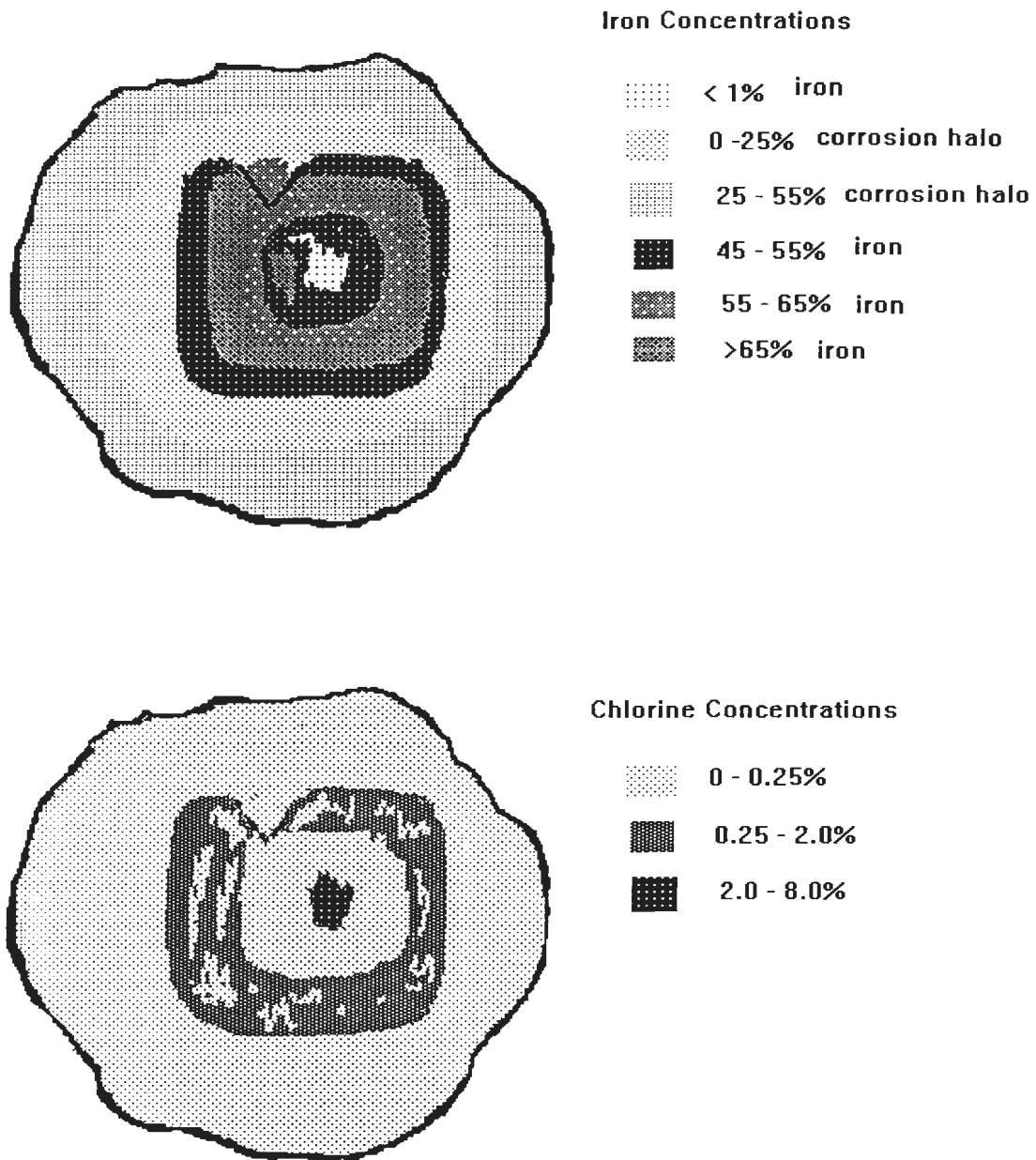


Figure 7.10 Models showing iron and chlorine distribution for nails from the Ferryland site.

Based on the analyses of the previous section, Table 7.3.4a summarizes the chemical analyses of the iron nail shaft cross-sections for Fe, Cl, P, S and Si. The element mapping supports the chemical data.

Table 7.3.4a
Chemical Variation for Nail Shaft Cross-sections (excluding mineral inclusions)

Nail section	Fe (%)	Cl (%)	P (%)	S (%)	Si (%)
nail centre	40	3	<1	<1	<1
iron	61	<1	<1	<1	1
iron/corrosion halo interface	50	1	1	<1	3
corrosion halo	34	<1	2	<1	6

Tables 7.3.4b and c present the results of the element mapping based on the presence/absence of the elements analyzed. In summary, Fe and P are identified throughout the nail cross-section. S is most abundant in the iron/corrosion interfaces. Si is common but least abundant in the iron section. Carbon was present in those samples analyzed which included iron/corrosion interfaces, iron and slag. Cl concentrations were lowest for the corrosion halos. Figures 7.11 and 7.12 show the distribution of chlorine and iron at the iron/corrosion interface for nails 128193, 99060, 94759 and 115521. Chlorine is concentrated along the interface for nails 129193 and 99060 usually at the iron surface. Nail 115521 however did not have a concentration of chlorine at the

Table 7.3.4b
Element Distribution based on Element Mapping
For Nails from Occupation/Destruction Events

Nail	Area	Event	location	C	Cl	Fe	P	S	Si
Centre of Nail									
120161	B	143	crack in iron	N/A	X	X	X	X	X
94787	D	62	iron near void	N/A		X	X	X	X
94787	D	62	iron near crack	N/A		X	X		X
94787	D	62	iron	N/A		X	X	X	X - slide
Iron									
106289	B	133	oxide layer	N/A		X	X		
94123	D	62	iron at grain boundaries	N/A	X	X	X		X
94123	D	62	multi-phase iron	N/A		X			
94123	D	62	crack in multi-phase iron	N/A	X	X	X	X	X
94785	D	62	iron around crack	N/A	X	X	X	X	X
94785	D	62	multi-phase iron	N/A	X	X			
87872	D	62	multi-phase iron	N/A	X	X	X		X
120161	B	143	edge of nail	N/A	X	X	X	X	X
120161	B	143	crack at edge of nail	N/A		X	X	X	X
120389	B	178	crack at edge of nail	N/A	X	X	X	X	X
Iron/Corrosion Halo Interface									
106289	B	133		N/A		X	X	X	X
120160	B	143		N/A		X	X	X	X
120161	B	143		N/A	X	X	X	X	X
99060	D	96		X	X	X	X	X	X
94759	D	62		X	X	X	X	X	N/A
128193	C	0		X	X	X	X	X	X
Corrosion Halo									
87872	D	62		N/A		X	X	X	X
94158	D	62		N/A		X	X		X
120161	B	143	corrosion halo edge	N/A		X	X		X
120161	B	143	corrosion halo edge	N/A		X	X	X	X
120161	B	143		N/A	X	X			

Table 7.3.4c
Element Distribution based on Element Mapping
For Nails from Fill/Building Events

Nail	Area	Event	location	C	Cl	Fe	P	S	Si
Centre of Nail									
115811	B	134		N/A		X			
97546	B	134	edge of void	N/A	X	X	X	X	X
97546	B	134	edge of void	N/A	X	X	X	X	X
Iron									
97546	B	134	crack	N/A	X	X	X	X	X
94737	D	63	crack	X	X	X	X	X	X
Iron/Corrosion Interface									
115521	B	138		X		X	X	X	X
Corrosion Halo									
97546	B	134	grain in corrosion halo	N/A		X	X		X
115470	B	134	crack	N/A	X	X	X	X	X
115470	B	134	wood in corrosion halo	N/A	X	X	X		X
Slag									
115294	B	134		X	X	X		X	X

N/A - not analyzed

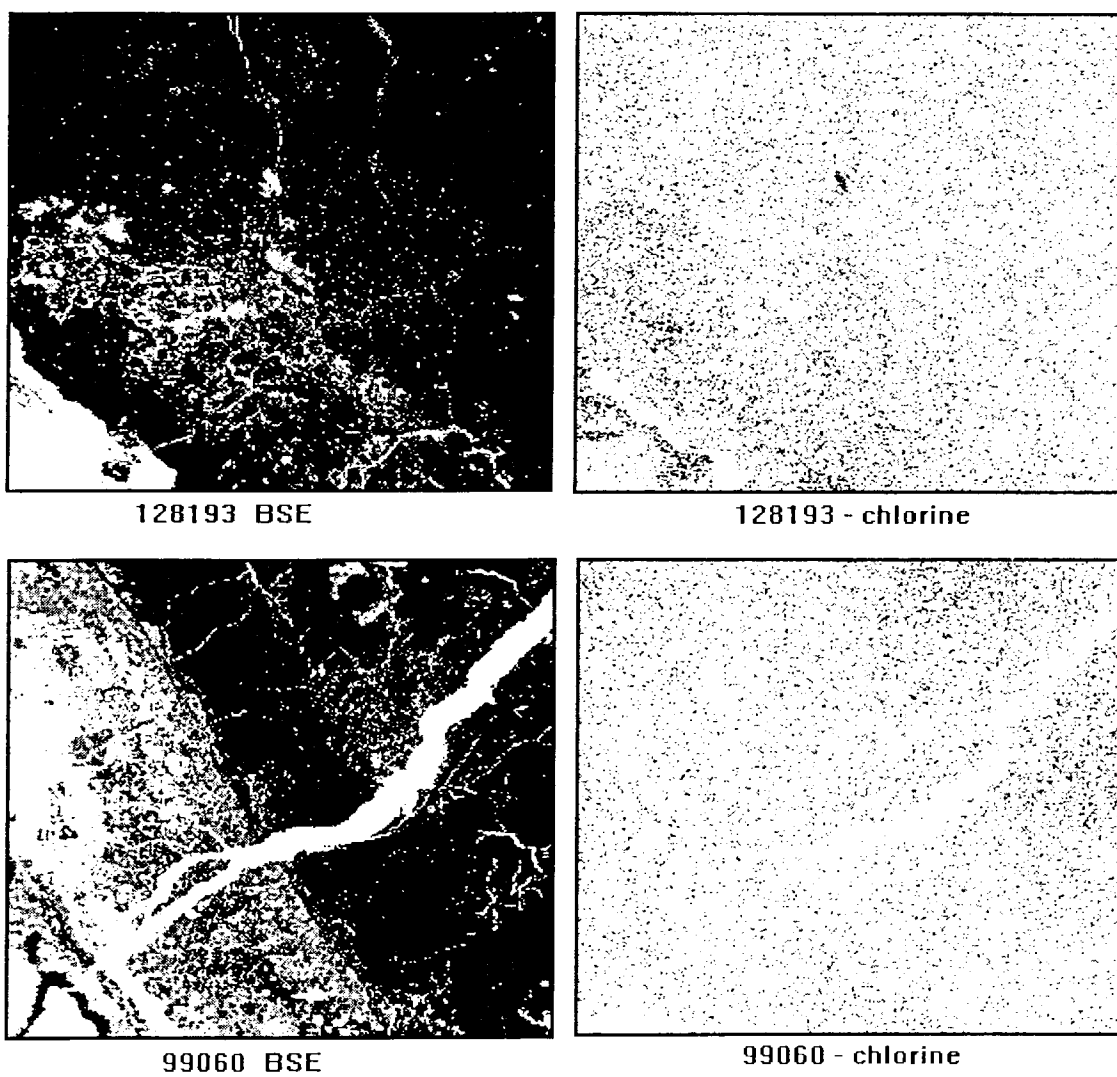


Figure 7.11 Distribution of chlorine at iron corrosion interface for nails 128193 (x 65) and 99060 (x 50).

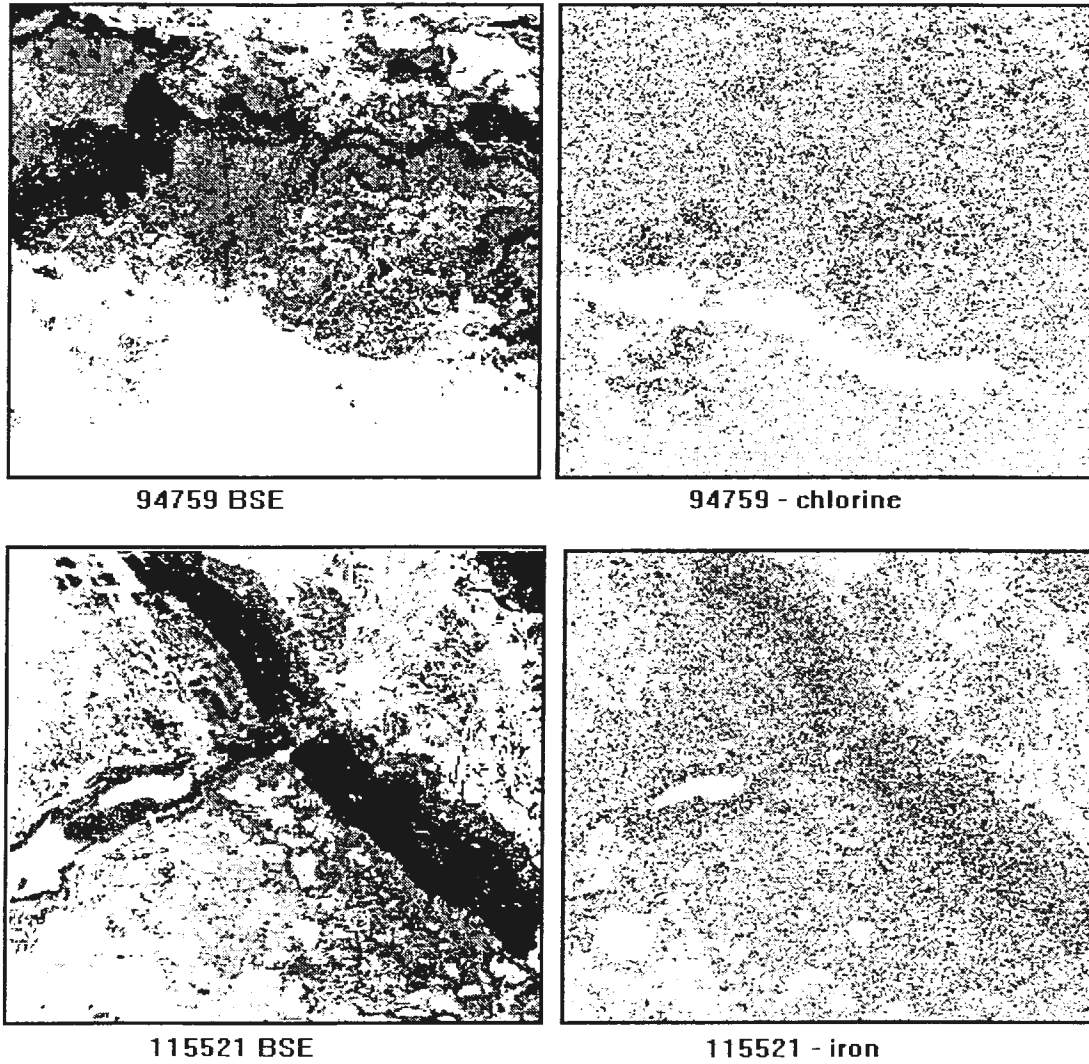


Figure 7.12 Distribution of chlorine and iron at the iron/corrosion interface for nails 94759 (x 50) and 115521 (x 60).

interface. For the nails studied, iron concentration is lower at the interface. Nail 128193 shows the uneven nature of the iron surface and iron particles being dispersed to the corrosion halo.

Nails of the occupation/destruction events and fill/building events differed only in element concentration of chlorine for the iron/corrosion interface and corrosion halo. Nails from the occupation/destruction events had chlorine concentrated along the iron/corrosion interface with very low concentrations in the corrosion halo. Nails from the fill/building events had chlorine concentrated in the corrosion halo but not at the iron/corrosion interface.

7.3.5 Radiography of Nails

Nail samples were radiographed to determine the amount of metal remaining. Appendix 7e contains the radiographed nail images. Metal loss was determined using the x-ray images and metallographic observations for nail shaft cross-sections. A calculation of metal loss based on change in length, width and thickness from the original size could be misleading because points and nail heads are prone to damage during use. The shaft cross-sections therefore provide a better measure of total internal metal loss and were used in this thesis. The radiographs produced using settings of 55kV/5mA and 80 kV/4mA provide information about exterior nail loss. Figure 7.13 shows the locations for size measurements on the nails. Original nail size was estimated from radiographs and

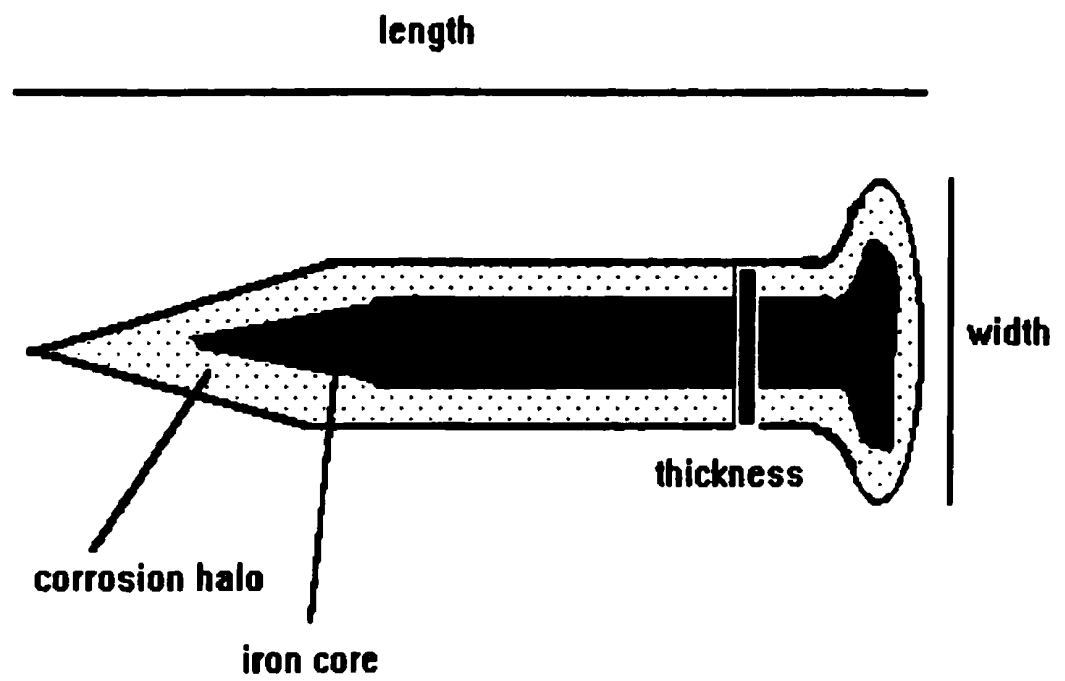


Figure 7.13 Schematic drawing showing locations for size measurements.

recorded as penny-weight (measurement used at time of manufacture). Figure 7.14 shows schematic drawings illustrating the interpretation of x-ray grey levels (reader is reminded that an x-ray is a negative print). Tables 7.3.5a, b, c and d summarize the change in nail size from the original/normal size (Appendix 7e). Tables 7.3.5e and f summarize estimates of total iron loss by metallographic groups (Appendix 7e).

Overall the small nails (8d and 10d) exhibited less deterioration for both length and width. The change in width or head of the nail was greatest for nails from the fill/building events. The change in core diameter is similar for nails from the occupation/destruction events. The 8d and 10d type nails from the fill/building events have a 41% decrease in core diameter while the 16d, 20d and 30d nails had a 27% decrease in core diameter. The total iron loss is greater for nails with a G-1 and 2 metallographic classification with the difference being that the G-1 and 2 nails are corroding internally and externally while the nails of the G-3, 4 and 5 groups are only corroding externally.

The magnet test for nail samples appearing in Tables 7.3.5e and f indicated that all but 2 samples had lots of iron. Samples 97546 and 128190 were recorded as partially mineralized using the magnet test. These samples both had an estimated iron loss of 90% or greater. Metal loss for samples recorded as having lots of iron ranged from 17 to 79%.

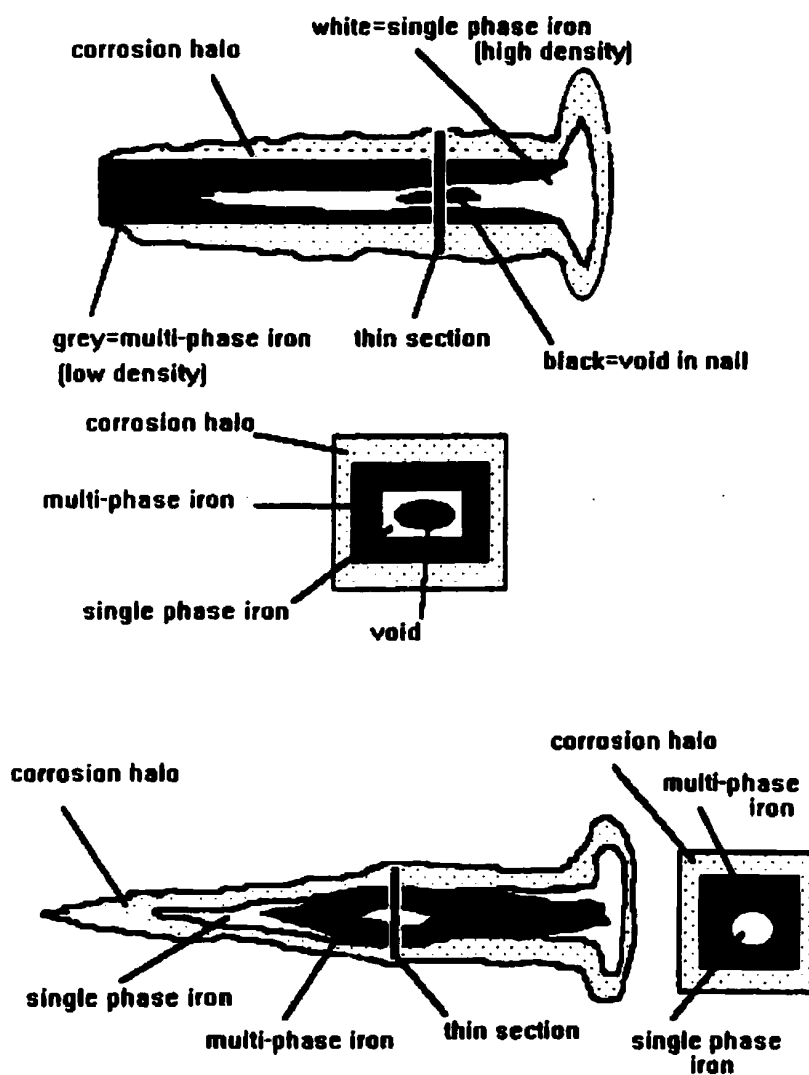


Figure 7.14 Interpretation of x-ray grey levels.

The magnet test for iron condition is useful only in separating nails with extensive metal alteration.

7.3.6 Thickness of Iron Core and Corrosion Halo

Table 7.3.6a summarizes comparisons of iron core thickness to corrosion halo thickness for different nail types. Nails from the occupation/destruction events had smaller iron core diameter than nails from fill/building events. Corrosion halo thickness was greater for nails from the occupation/destruction events. The iron core diameters and thickness of corrosion halos did not vary significantly by nail type. Table 7.3.6b summarizes comparisons of iron core thickness to corrosion halo thickness for different metallographic groups. The results are similar to that of Table 7.3.6a with nails from the occupation/destruction events having a smaller iron core diameter and greater corrosion halo thickness. The majority of nails from the metallographic groups G-2, 3 and 4 for occupation/ destruction events and G-1 and 3 for fill/building events have a thicker corrosion halo than iron core but the differentiation of thickness between iron core and corrosion halo is not great. Nails of the G-4 metallographic group for both event groups exhibit higher iron core:corrosion halo ratios than nails from other metallographic groups. For example, nail sample 94759 from an occupation/destruction event had an iron core to corrosion halo ratio of 28:72 while nails from fill/building events had a 69:31 iron core to corrosion halo ratio. For the G-4 nails, the nails from occupation/destruction events have a greater external metal loss and increase in corrosion halo than the nails from the fill/building events.

Table 7.3.6a
Iron Core vs Corrosion Halo
for Nail Type

occupation/destruction				
Nail type	thickness (mm)		% thickness	
	iron core	corrosion halo	iron core	corrosion halo
8d	5	7	42	58
10d	5	6	45	55
16d	5	10	33	67
20d	7	8	47	53
30d	7	6	54	46
40d	10	12	45	55
Averaged thickness	6.5	8	45	55
fill/building				
8d	4	4	50	50
10d	9	6	60	40
16d	6	7	46	54
20d	8	4	67	33
30d	7	6	54	46
Averaged thickness	6	5	55	45

Table 7.3.6b
Iron Core vs Corrosion Halo
for Metallographic Groups

occupation/destruction		
Metallographic Group	% thickness	
	iron core	corrosion halo
G-1	50	50
G-2	43	57
G-3	41	59
G-4	28	72
G-5	63	37
Average	45	55
fill/building		
G-1	43	57
G-2	50	50
G-3	44	56
G-4	69	31
G-5	50	50
Average	51	49

7.4 Corrosion Halos

Around each nail a halo of soil particles develops that is cemented together and to the nail surface by products of electrochemical oxidation/reduction. This corrosion halo represents the exterior nail changes occurring during burial.

7.4.1 Munsell Colour for Corrosion Halos

Tables 7.4.1 a and b present the data for colour analyses. Corrosion halo colour of nails from the occupation/destruction events had more nails with a 7.5YR hue while nails from the fill/building events had more corrosion halos with a 10YR hue. For nails from fill/building events, most of the corrosion halo had a level of 4 for both value and chroma. This was in contrast to the majority of nails from occupation/destruction events which had levels of 4 and 5 for value and 4 and 6 for chroma. Table 7.4.1c summarizes the averages of the colour analyses by metallographic group. Similar patterns as described above were observed. For example, nails from occupation/destruction events with a G-5 metallographic description had a 7.5YR hue for corrosion halo colour. This is in contrast to the nails from fill/building events belonging to metallographic group G-5 with a 10YR hue for corrosion halo.

Table 7.4.1a
Colour of Nail Corrosion Halos
Nails from occupation/destruction events

Metal-lographic Classification	Area	Event	Co-ordinate	Nail sample	Colour	Hue	Value	Chroma
G-3	C	19	E88N32	128189	light yellowish brown	10YR	6	4
G-2	C	0	E89N30	128193	yellowish brown	10YR	5	4
G-2	D	62	E138N8	94121	yellowish brown	10YR	5	8
G-3	C	195	E89N30	128290	yellowish brown	10YR	5	6
G-2	D	62	E138N8	94123	yellowish brown	10YR	5	6
G-2	D	62	E147N8	94788	dark yellowish brown	10YR	4	6
G-3	B	178	E2N6	120389	dark yellowish brown	10YR	4	4
G-1	D	62	E146N8	94743	dark yellowish brown	10YR	4	6
G-2	B	143	E2N7	120161	dark yellowish brown	10YR	4	4
G-1	B	133	E3N0	106289	brown	10YR	5	3
G-1	B	145	E2N75	120531	brown	10YR	5	3
G-2	D	96	E148N12	99060	brown	7.5YR	4	4
G-2	D	62	E138N8	94120	strong brown	7.5YR	5	6
G-1	D	62	E147N8	94745	strong brown	7.5YR	4	6
G-1	D	62	E137N8	94160	strong brown	7.5YR	4	6
G-1	D	62	E149N9	87872	strong brown	7.5YR	5	6
G-1	D	62	E137N8	94158	strong brown	7.5YR	4	6
G-2	D	62	E147N8	94742	strong brown	7.5YR	4	6
G-2	D	62	E147N8	94785	strong brown	7.5YR	5	6
G-4	D	62	E135N7	94759	strong brown	7.5YR	5	6
G-5	D	62	E135N7	94758	strong brown	7.5YR	5	6
G-1	D	62	E147N8	94787	dark brown	7.5YR	3	4
G-5	D	62	E147N8	94786	dark brown	7.5YR	3	4

Table 7.4.1b
Colour of Nail Corrosion Halos
Nails from fill/building events

Metal- Igraphic Classifi- cation	Area	Event	Co-ordinate	Nail sample	Colour	Hue	Value	Chroma
G-5	C	22	E88N30	128195	light yellowish brown	10YR	6	4
G-1	C	55	E89N31	128190	dark yellowish brown	10YR	4	4
G-2	B	134	E0N6	115811	dark yellowish brown	10YR	4	4
G-1	B	134	E3N2	97546	dark yellowish brown	10YR	4	4
G-3	C	55	E88N32	128192	dark yellowish brown	10YR	4	4
G-4	B	134	E3N3	115294	dark yellowish brown	10YR	4	4
G-5	B	134	W1N6	115772	dark yellowish brown	10YR	3	6
G-1	C	16	E89N31	128304	brown	7.5YR	4	4
G-1	B	134	W1N7	115470	brown	7.5YR	4	4
G-2	B	138	E3N3	115521	brown	7.5YR	4	4
G-4	B	177	E2N6	120340	brown	7.5YR	4	4
G-4	D	63	E147N8	94737	strong brown	7.5YR	4	6

Table 7.4.1c
Colour of Nail Corrosion Halos
by metallographic groups

occupation/destruction										
metallographic	Hue (%)		Value (%)				Chroma (%)			
group	7.5YR	10YR	3	4	5	6	3	4	6	8
G-1	63	37	12	50	38	0	25	12	63	0
G-2	44	56	0	44	56	0	0	33	56	11
G-3	0	100	0	33	33	33	0	67	37	0
G-4	100	0	0	0	100	0	0	0	100	0
G-5	100	0	50	0	50	0	0	50	50	0
Average	61	39	12	25	55	8	5	32	61	2
fill/building										
G-1	50	50	0	100	0	0	0	100	0	0
G-2	50	50	0	100	0	0	0	100	0	0
G-3	0	100	0	100	0	0	0	100	0	0
G-4	67	33	0	100	0	0	0	67	33	0
G-5	0	100	50	0	50	0	0	50	50	0
Average	33	67	10	80	10	0	0	83	17	0

7.4.2 Mineralogy of Nail Corrosion Halos

Table 7.4.2 presents the mineral identifications based on the sample XRD spectra. The XRD spectra for each nail can be obtained from the author by request. All corrosion halos for the 35 nails contained quartz. Feldspar was identified for 36% of Area B nails, 71% of Area C nails and 76% of Area D nails. The three areas differed in

Table 7.4.2
Mineralogy of Corrosion Halo for Areas B, C and D

Area	Metallographic Group	Sample	alb	san	cac	ll	hm	goe	ak	mg	mf	chr	mh	gr	sep	ph
B	G-2	115811			✓			?	?	✓		✓	✓			
B	G-1	120531														
B	G-2	115521					✓			✓		✓		✓		
B	G-4	115294					✓	?		✓		✓		✓	?	?
B	G-1	97546	✓					?	?	?					?	?
B	G-1	106289													?	
B	G-1	115470	✓												?	?
B	G-2	120161								✓	✓					
B	G-3	120389		✓	✓			✓	✓	✓						
B	G-4	120340						?		✓						
B	G-5	115772	✓		✓			✓	✓	✓				✓		
C	G-5	128195	✓		✓				✓						✓	✓
C	G-3	128192	✓		✓			?	?							
C	G-2	128193	✓		?				?							
C	G-1	128304			✓			✓	✓							
C	G-1	128190	✓		✓			??	??							
C	G-3	128290			✓			?	✓							
C	G-3	128189	✓		✓			??	??							
D	G-4	94759	✓			??									??	
D	G-5	94758	✓												??	
D	G-1	94160	✓												?	
D	G-2	94121	✓			?		?	??					✓	?	
D	G-1	94743	✓					✓							??	
D	G-2	94742		✓										✓	?	
D	G-2	94788	?											✓	✓	
D	G-1	94787		✓			✓			✓		✓		✓	✓	✓
D	G-5	94786		✓						✓		✓		✓	✓	?
D	G-1	94745	✓											✓	✓	
D	G-4	94737	✓			??								??	?	
D	G-2	99060	✓							??				??	✓	
D	G-1	94158	✓						??						?	
D	G-2	94120						?	??					✓	?	
D	G-2	94123				??			??					✓	?	
D	G-2	94785	✓											✓	✓	
D	G-1	87872	✓			?			??						?	?

? = 50% of peaks match PDF

?? = 40% of peaks match PDF

corrosion halo composition as 73% of Area B nails contained magnetite or chromite (Figure 7.15), 71% of Area C nails contained goethite and akaganeite (Figure 7.16) and/or cacoixentite (Figure 7.17) and 76% of Area D nails contained graphite and sepiolite.

7.4.3 Corrosion Halo Mineralogy and Colour

Tables 7.4.3a and b summarize the corrosion halo mineralogy sorted by colour (Appendix 7f). Sorting of nail corrosion halo samples by hue, the 7.5YR group had predominantly Area D nails while the 10YR group consisted of Area B and C nails. Most of the nail corrosion halos with a 7.5YR hue (brown) were from occupation/destruction events. Nail corrosion halos with a 10YR hue (yellowish brown) were represented from all events.

7.5 Visual Examination of the 35 Nails

Tables 7.5a and b summarize the visual examination of the 35 nails from the occupation/destruction and fill/building events. Nails of both the occupation/destruction or fill/building event classes had cracked in the post-storage environment and most had only a head and shaft remaining. Table 7.5c summarizes nail condition averages for fill/building and occupation/destruction events.

Stable nails represent 14% of the nail samples. Of the 14% group, 9% had a G-1 metallographic classification and 5% equally shared a G-2 and G-4 classification.

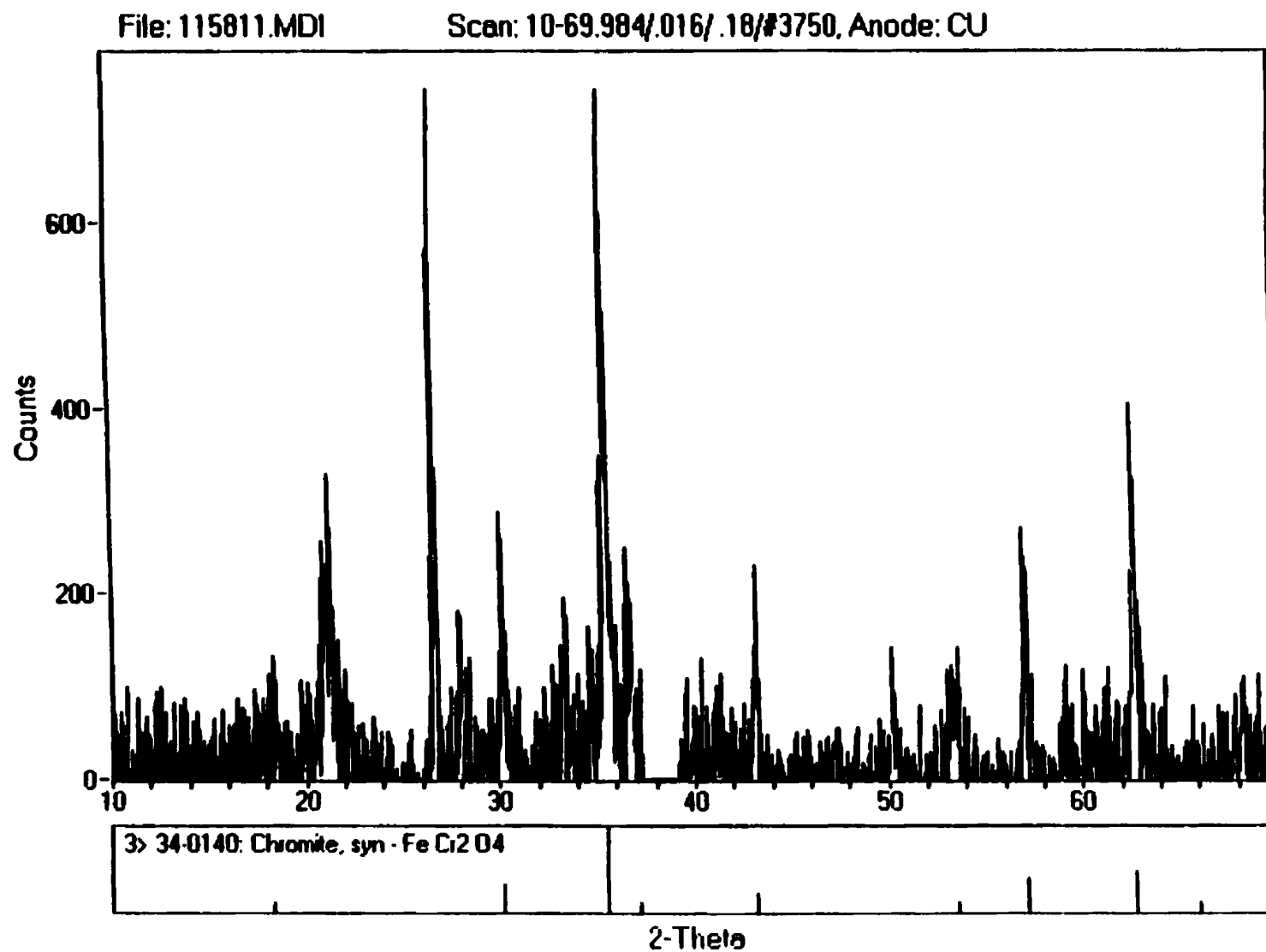


Figure 7.15 Spectra for Area B nail 115811 with chromite identified.

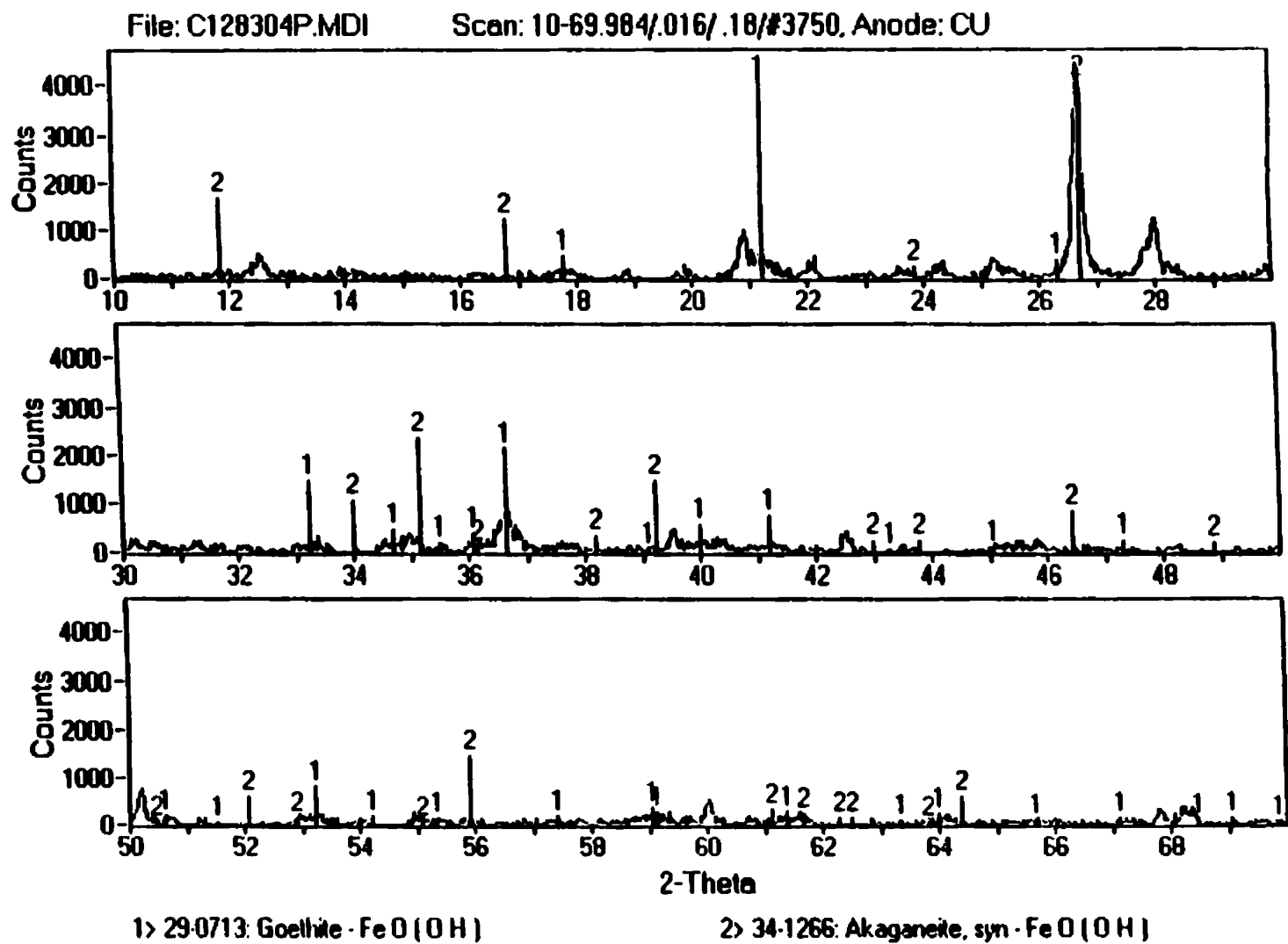


Figure 7.16 Spectra for Area C nail 128304 with goethite and akagenite identified.

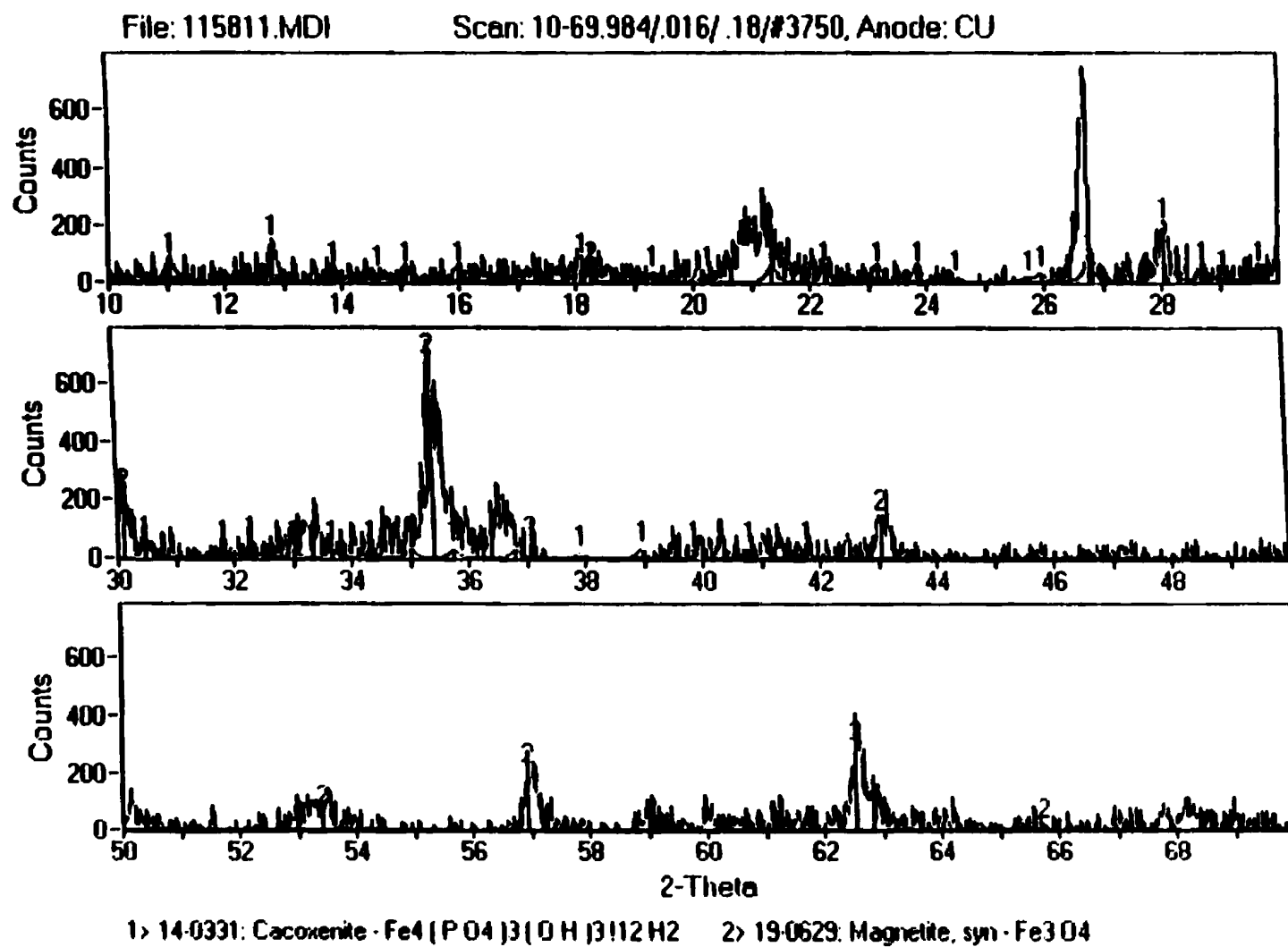


Figure 7.17 Spectra for Area B nail 115811 with cacoenite identified.

Table 7.5a
Nail Condition by Visual Examination
Nails from occupation/destruction events

Metal-lographic Classification	Area	Event	Co-ordinate	Nail sample	Condition	Description	Nail type
G-1	D	62	E149N9	87872	cracked	shaft	16d
G-1	B	133	E3N0	106289	stable	shaft	10d
G-2	D	62	E147N8	94785	cracked	shaft	8d
G-3	C	19	E88N32	128189	cracked	shaft	40d
G-2	D	62	E147N8	94788	cracked	head,shaft	10d
G-2	B	145	E2N5	120531	cracked	head,shaft	20d
G-2	D	62	E138N8	94120	cracked	head,shaft	10d
G-1	D	62	E147N8	94787	cracked	head,shaft	10d
G-3	D	62	E147N8	94745	cracked	head,shaft	8d
G-3	B	178	E2N6	120389	cracked	head,shaft	16d
G-2	C	0	E89N30	128193	cracked	head,shaft	8d
G-1	D	62	E137N8	94160	stable	head,shaft	8d
G-2	D	62	E138N8	94121	cracked	head,shaft	30d
G-3	C	195	E89N30	128290	cracked	head,shaft	10d
G-1	D	62	E137N8	94158	cracked	head,shaft	30d
G-1	D	62	E146N8	94743	cracked	head,shaft	16d
G-2	B	143	E2N7	120161	cracked	head,shaft	20d
G-2	D	62	E147N8	94742	cracked	head,shaft	10d
G-3	D	96	E148N12	99060	cracked	head,shaft	16d
G-2	D	62	E138N8	94123	stable	head,shaft	30d
G-4	D	62	E135N7	94759	cracked	head,shaft	16d
G-5	D	62	E135N7	94758	cracked	head,shaft	30d
G-5	D	62	E147N8	94786	cracked	head,shaft, point	10d

Table 7.5b
Nail Condition by Visual Examination
Nails from fill/building events

Metal-lographic Classification	Area	Event	Co-ordinate	Nail sample	Condition	Description	Nail type
G-4	B	177	E2N6	120340	stable	shaft	?
G-1	C	55	E89N31	128190	cracked	shaft	10d
G-2	B	134	E0N6	115811	cracked	shaft	16d
G-1	B	134	E3N2	97546	stable	shaft	20d
G-2	B	138	E3N3	115521	cracked	shaft	10d
G-5	B	134	W1N6	115772	cracked	shaft	30d
G-4	D	63	E147N8	94737	cracked	shaft	20d
G-1	C	16	E89N31	128304	cracked	head,shaft	10d
G-1	B	134	W1N7	115470	cracked	head,shaft	16d
G-3	C	55	E88N32	128192	cracked	head,shaft	10d
G-4	B	134	E3N3	115294	cracked	head,shaft	10d
G-5	C	22	E88N30	128195	cracked	head,shaft, point	8d

Table 7.5c
Nail Condition by Visual Examination
for 35 Nails

fill/building							
Metallo- graphic Group	Metal loss for nails (%)	Condition		Nail Description			
		stable (%)	cracked (%)	shaft	head, shaft	shaft, point	head, shaft, point
G-1	33	25	75	50	50	0	0
G-2	17		100	100	0	0	0
G-3	8	0	100	0	100	0	0
G-4	25	33	67	67	33	0	0
G-5	17	0	100	50	0	0	50
occupation/destruction							
G-1	26	33	67	33	67	0	0
G-2	39	11	89	11	89	0	0
G-3	22	0	100	20	80	0	0
G-4	4	0	100	0	100	0	0
G-5	9	0	100	0	50	0	50

The nails with a G-1 and G-2 classification had an averaged total estimated metal loss of 57% while that of the G-4 nail was 33%. Complete nails (head, shaft and point) were from G-1, G-3 and G-5 metallographic groups. Table 7.5d shows nail condition versus size. Overall the shaft of the nail was best-preserved and the point the least well-preserved. For the nails from fill/building (f/b) events generally only a shaft remained while nails from occupation/destruction (o/d) events had both heads and shafts. The shaft sections are represented by nails of all sizes. Most nails with a head and shaft are 10d to 16d in size. Most nails with a head, shaft and point are 8d to 10d in size.

7.6 Characterization of Slag by Chemical Analyses

X-ray fluorescence analysis were conducted on slag remains found at Areas B and C. Slag represents the by-product of forging and was used to provide some information regarding the original iron composition of the nails. Tables 7.6a-f summarize the results (Appendix 7g). Tables 7.6g and h present the mean, standard deviation and spread for the data (Appendix 7g). The chemical analyses for the slag from Areas B and C had a similar standard deviation indicating that slag composition was essentially the same for both areas. Slag composition varied somewhat with some samples having more Fe_2O_3 and others with a higher SiO_2 concentration. Concentrations of Cl also varied. As with the iron nail samples Cl is associated with areas of high Fe and low Si compositions for the slag.

Table 7.5d
Nail Condition vs Size

fill/building - distribution by %				
Nail type	shaft	head, shaft	head, shaft, point	total number of samples
8d	0	0	100	1
10d	33	75	0	5
16d	17	25	0	2
20d	33	0	0	2
30d	17	0	0	1
Total	58	33	9	11
occupation/destruction - distribution by %				
8d	25	17	0	4
10d	25	28	100	7
16d	25	22	0	5
20d	0	11	0	2
30d	0	22	0	4
40d	25	0	0	1
Total	17	78	5	23

7.7 Discussion

7.7.1 Artifact Survey

Generally this type of visual survey indicates whether or not reactions/crystallization processes are occurring internally. For example a nail upon excavation may appear stable but as evaporation in the ambient environment removes moisture salts crystallize and expand internally causing the surface to crack. Nails from Area D experienced the least change from pre- to post-storage indicating that low concentrations of chlorides were present in the nail. Results presented in Chapter 6 indicated that soil from Area D have the lowest concentration of Cl. Nails from Area C have the highest number of totally mineralized nails suggesting that Area C soil is the most reactive. The Cl concentration for soils from Area C is the highest for the soils from the site which supports this observation. Iron from Area B experienced the greatest change from pre- to post-storage. The iron from Area B had a high iron content and the soil did contain Cl. Thus, although the iron was in better condition, the Cl-rich electrolytic soil solution had more sites for reaction.

Nails separated by event showed that those from occupation/destruction events were in better condition than those of fill/building events. This probably indicates that soil from occupation/destruction events is less corrosive to ferrous metals.

From a conservation point of view, the greater the extent of mineralization within

an object the easier it will be to conserve because there is nothing left to react with the environment. Therefore nails from Area D with extensive mineralization, combined with the fact that they were buried in relatively inert soil, means that they will require little treatment time.

7.7.2 Nail Description

Based on nail metallography, 5 different groups exist for the Ferryland collection. Nails are described as having corroded centres with voids (>20% nail volume) surrounded by a multi-phase iron with a corrosion halo (G-1); corroded centres with voids (<25% nail volume) surrounded by single phase and multi-phase iron and a corrosion halo (G-2); single phase iron (10-30%), multi-phase iron (90-70%) surrounded by a corrosion halo (G-3); single phase iron (30-50%), multi-phase iron (70-50%) and a corrosion halo (G-4) and a single phase iron (60-90%), multi-phase iron (40-10%) with a corrosion halo (G-5). From the 35 nails studied more than half of the samples are corroding on both the interior nail surface and exterior nail surface. The corrosion halos with a lower chlorine concentration and high silicon concentration appear to be protecting the nail surface from corroding. Small cracks in the nails allow for fluid movement and chloride ion transfer to the nail centre which promotes the corrosion of this section.

7.7.3 X-radiography of Nails

X-radiography of artifacts indicate that artifacts of all areas show a range of

preservation from nails with very little iron to those with a high percent of iron.

Deterioration of nail heads is greatest for nails from fill/building events which could be a function of use or burial. The difference in deterioration between the length and width of the nails is probably a function of manufacture as the shaft and head were worked differently by the blacksmith. Change in nail length and width (head width) is less for smaller nails (8d and 10d). Change in core diameter is similar for most nails.

Differences in core diameter is observed for nails of fill/building events where condition appears size-dependent. Total metal loss is greatest for nails from the G-1 and 2 metal groups because both internal and external corrosion occur. Depth of deposit for these nail samples was less than those from G-3, 4 and 5. The increase in soil chloride ions and oxygen concentration for the soil nearer the surface are the probable catalysts for the internal corrosion process. Approximately half the nail samples of the G-1 and 2 groups are from Area D. This could be interpreted as either that the Area D nails were generally found in stratigraphic layers close to the surface or that the Area D nails were of a different composition. The results from the slag analyses, however, indicate that nail composition was uniform.

The range in preservation for all Areas illustrates the reactive electrochemical nature of the burial environment and that specific predictions of iron condition will be difficult. However, the fact that one Area had a greater degree of metal loss indicates that general predictions of iron condition may be possible. Because differences in

preservation were found to be size-dependent, predictions of iron condition must include background soil analyses and an understanding of the material culture of being excavated.

7.7.4 Munsell Colour

Colour of the corrosion halos correlates with mineral identification which probably reflects the soil at the site. The nails can best be divided by area of excavation based on the corrosion halo composition and colour. The bulk of the Area D samples exhibited a 7.5YR hue while samples of Areas B and C had a 10YR hue.

7.7.5 Mineralogy of Nail Corrosion Halos

All corrosion halos contained quartz which was derived from the surrounding soil. Feldspar was also ubiquitous but concentrated in nails from Areas C and D. The presence of quartz and feldspar being universal for all samples is probably because they are dominant mineral phases for the soil. Differences in corrosion halo composition are probably a function of the archaeological remains and the environment combined. The presence of magnetite and chromite in the corrosion halos of nails from Area B may be a result of the forging activities of the blacksmith. Akaganeite was identified in the corrosion halos for Area C nails probably because of the higher concentrations of Cl in the soil from Area C. Corrosion halo composition for the Area D nails consisted of graphite and sepiolite. In this case the former is probably present because the site was burned in the seventeenth-century while the latter has been incorporated into the

corrosion halo from the natural soil.

7.8 Slag

Chemical analysis showed a similarity in composition for Areas B and C slag.

This probably indicates that the nails produced shared a common chemical composition and that differences in the nails instead reflects the post-production environment (burial environment).

CHAPTER 8: DISCUSSION AND BURIAL ENVIRONMENT IMPLICATIONS FOR IRON NAILS

8.1 Introduction

In this chapter the iron nail condition is evaluated with respect to soil conditions in an attempt to identify relationships between artifact condition and environment. Also deductions regarding the reaction sequence for the deterioration of the iron nails are compared with those used in the model proposed by Turgoose (1982, 1995). Finally the value of this type of environmental assessment to the conservation of archaeological ferrous metal is discussed.

8.2 Summary of the Iron Nail Condition

Table 8.2 summarizes iron nail condition for samples excavated from the Ferryland archaeological site. Figure 8.1 shows typical profiles for Areas B, C and D with nail condition by event indicated. Note that nails excavated from soil of events adjacent one another do not necessarily have an equal condition. Also depth of deposit does not have a direct relationship with nail preservation. However, both Table 8.2 and Figure 8.1 show that nails excavated from soil representing concentrated human occupation are in better condition than nails excavated from events representing fill and building activities.

The soil from events 143, 145, 0, 19, 195, 63, 96 and sections of event 62

Table 8.2
Summary of Iron Nail Condition
Excavated from the Ferryland Site

Nail(s)	Event	Area	Soil Description	Area(s) of Iron Deterioration	Estimate of Total Iron Loss (%)
Nails in good condition					
120161	143	B	occupation	internal + external	30 - 40
120531	145	B	occupation	internal + external	20 - 30
128193	0	C	occupation	internal + external	20 - 30
128189	19	C	destruction	external	0 - 20
128290	195	C	occupation	external	20 - 30
94123,94745,94758	62	D	occupation	internal + external	20 - 40
94737	63	D	fill	external	20 - 30
99060	96	D	destruction	external	20 - 30
Nails in poor condition					
106289	133	B	destruction	internal + external	40 - 50
115811,115294 97546,115470 115772	134	B	fill	internal + external	40 - 50
115521	138	B	building	internal + external	40 - 50
120389	178	B	occupation	external	40 - 50
128190,128192	55	C	fill	external	55 - 93
128195	22	C	fill	external	40 - 50
128304	16	C	building/occupation	internal + external	75
87872,94120,94121 94158,94160,94742 94743,94758,94759 94786,94787,94788	62	D	occupation	internal + external	40 - 79

Iron Nail Condition

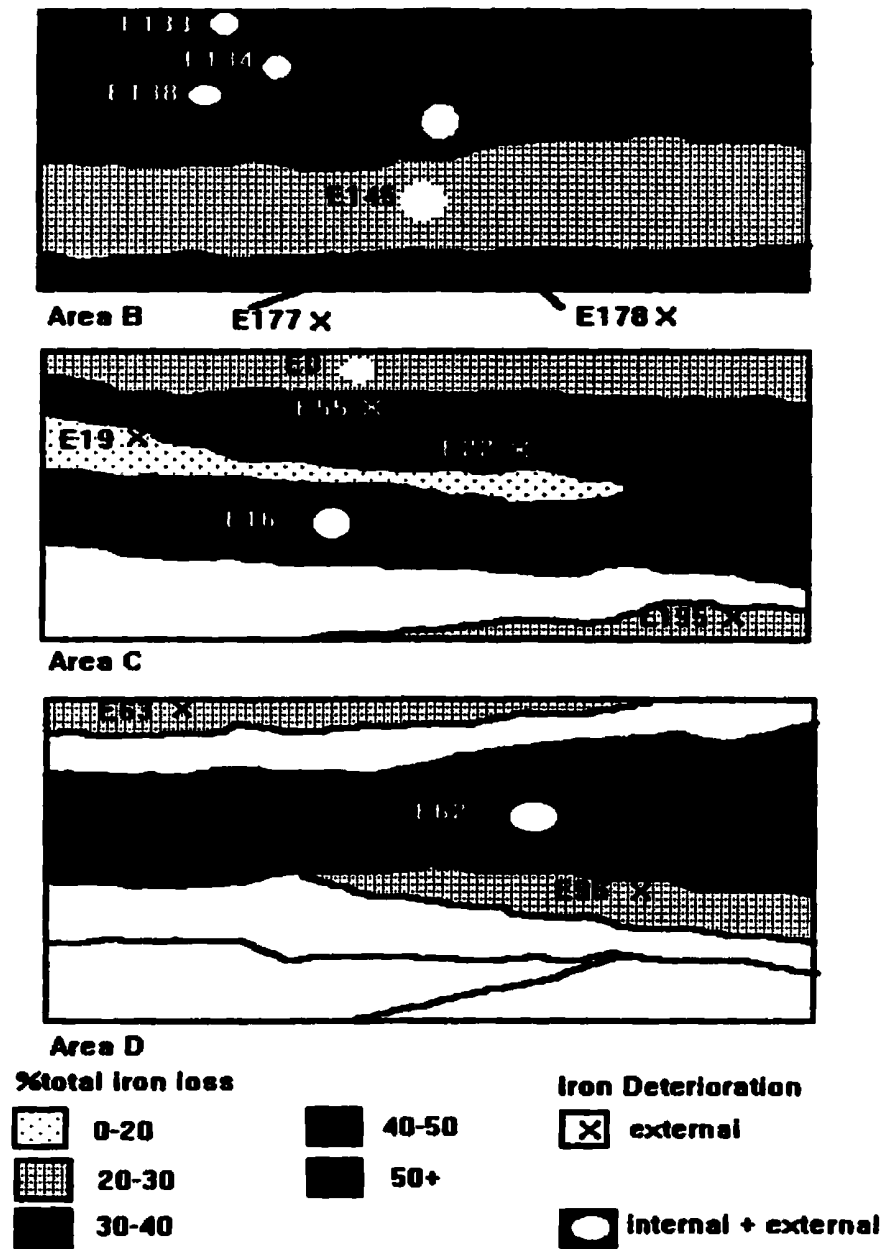


Figure 8.1 Schematic drawing showing iron nail condition with reference to soil profiles.

contained the best preserved nails. From the visual survey (Section 7.2.2), nails from events 143, 145, 19, 195, 22, 62, 63 and 96 are the most stable after being stored. For the suite of samples analysed in this thesis, both the visual and scientific surveys produced similar results.

Figures 8.2 and 3 show line graphs of iron nail condition by area of excavation. In the graphs nail size (d), metallographic condition (G), % core change or change in nail shaft and % total nail change or metal loss are compared. Overall larger nails have lower metal loss. For example nail 128189 from soil of event 19 is the largest nail representing Area C and has the lowest estimated metal loss. Most of the nails from soil of Areas C and D have a greater % of metal loss through the nail shaft cross-section. Most of the nails from soil of Area B exhibit metal loss in nail head and length.

8.3 Summary of Soil Conditions for the Ferryland Archaeological Site

Tables 8.3a and b summarize the optimum burial environment and the range in burial environment, respectively. The optimum soil conditions represent soil conditions surrounding the good condition nails (Section 8.2). Generally the best conditions for iron preservation are mid-range for the overall site soil conditions.

From the soil descriptions a soil texture of gravel loamy sand implies good drainage, preventing extended contact between artifact and soil solution. This would be a

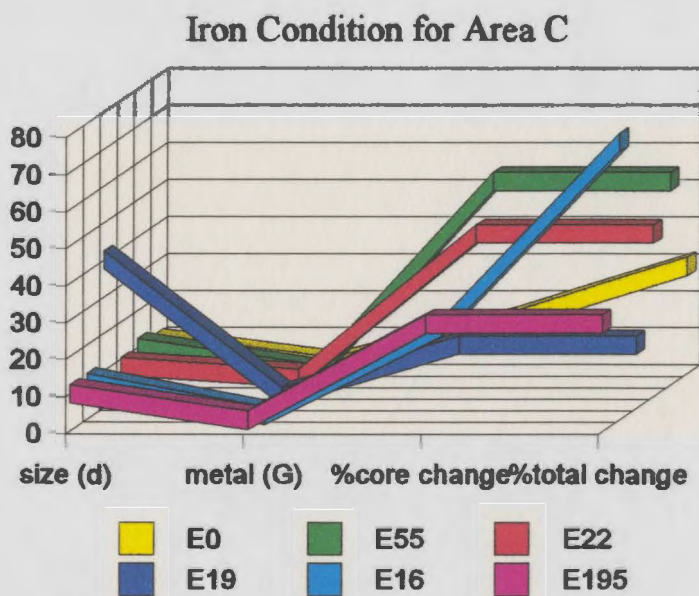
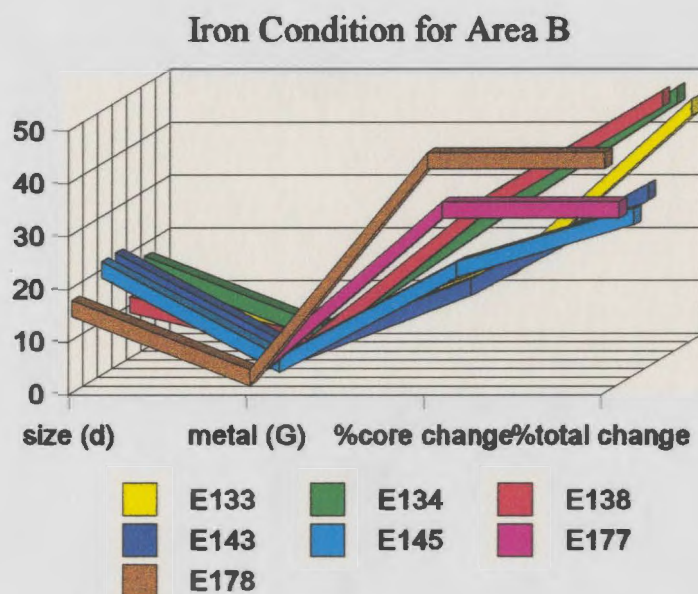


Figure 8.2 Line graphs showing iron nail condition for Areas B and C.
 d = nail size by pennyweight (see abbreviations section)
 G = measure of corrosion (%) (see abbreviations section)

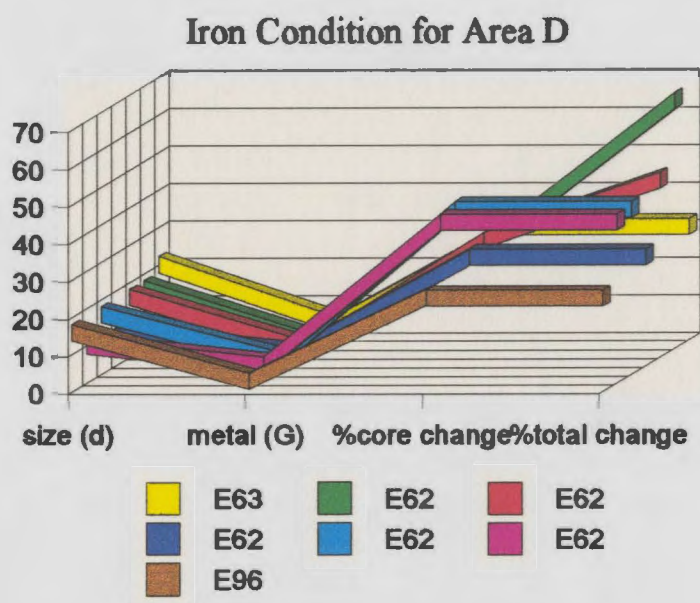


Figure 8.3 Line graph showing iron nail condition for Area D.

better environment for iron preservation than a moisture-rich impervious soil (Cronyn 1990; Dowman 1970; Mathias 1996).

The pH values for Ferryland varied between 3.5 and 5.8. Differences in soil pH for water versus CaCO_3 solutions indicates a variation in hydrogen ion exchange capacity for the soil from different events.

Soil mineralogy and soil element concentration indicate a relatively homogeneous soil matrix with some variation in Cl and metal element concentration by events within

Table 8.3a
Optimum Burial Environment for Iron Nails
from the Ferryland Archaeology Site

	Particle size distribution (%)			pH		Conductivity (micromhos)	Corrosion Rate (mmpy)	organic wt %	Fe ₂ O ₃ wt %	SiO ₂ wt%	Cl (ppb) for soil solution	Cl (ppm) for soil	P ₂ O ₅ wt %
	gravel	sand	clay	H ₂ O	CaCO ₃								
Mean	42.7	53.0	3.3	4.9	4.0	24.9	0.09	12.7	8.7	54.8	3,858	417	2.5
St. dv.	6.4	7.1	1.6	0.5	0.4	14.4	0.05	9.4	4.0	8.6	4,855	404	1.2
St.cr.	2.0	2.2	0.5	0.2	0.1	4.6	0.02	3.0	1.3	2.7	1,535	128	0.4

St.dv.=standard deviation

St.cr.= standard

Table 8.3b
Range in Burial Environment Condition for the Ferryland Archaeology Site

	Particle size distribution (%)			pH		Conductivity (micromhos)	Corrosion Rate (mmpy)	organic wt %	Fe ₂ O ₃ wt %	SiO ₂ wt%	Cl (ppb) for soil solution	Cl (ppm) for soil	P ₂ O ₅ wt %
	gravel	sand	clay	H ₂ O	CaCO ₃								
Range	37-64	33-58	1-7	3.81-5.74	3.55-4.23	7.7-73.3	0.02-0.22	2-30	2-18	39-68	500-33,000	70-1500	1-5.5
Occupation/destruction													
mean	45	50	4	5.03	4.04	21.5	0.08	11.3	8.70	54.7	3,169	399	2.59
St.dv.	9	9	2	0.43	0.33	11.9	0.02	8.7	3.78	8.4	4,470	352	1.40
Fill/building													
mean	48	48	4	4.61	3.85	33.3	0.09	10.8	7.35	56.0	6,487	358	2.22
St.dv.	5	5	2	0.58	0.32	20.3	0.06	8.4	2.51	5.8	9,834	211	1.05

St.dv.=standard deviation

different areas. The chemical analyses of soil solutions indicates variation for soil samples from different events with the Cl and transition metal concentrations being the most distinct. Chlorine variation, reflecting the salt spray, pore water and sea water penetration within the stratigraphic column, defined areas of good/poor preservation within the site and correlated with the artifact descriptions. Figures 8.4 and 5 present line graphs of Cl concentration and corrosion rate for soil from Areas B, C and D. Soil from events 88 and 141 representing subsoil exhibited the lower Cl concentration and corrosion rates. The soil from event 195 has the highest Cl concentrations but soil solution corrosion rate is lower than that for soils of event 55 and 22. Iron excavated from event 195 soil was generally in better condition than that from events 55 and 22. The greatest spread for soil solution corrosion rate occurs for soil from Area D with soil from event 63 having the highest corrosion rate. Cl concentration for this soil is the highest for soil from Area D. Iron condition for the event 63 soil, however, is good. This observation demonstrates the need to use several parameters for evaluating the corrosive potential of buried iron.

Overall Area D soil provides the best preservation, with chloride levels being low, pH values being the most nearly neutral and a consistently high concentration of gravel size particles.

When viewing all parameters, an overall burial condition of stable/low reactivity

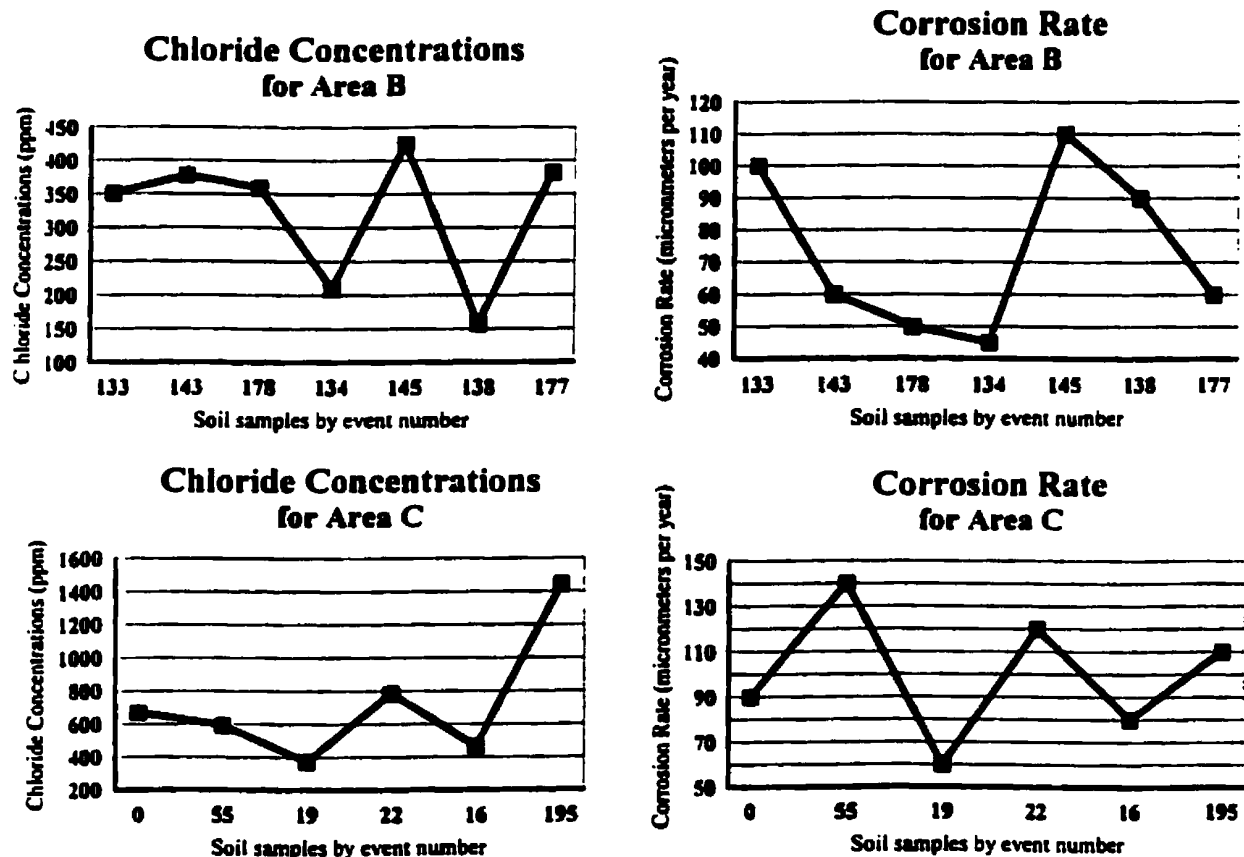


Figure 8.4 Line graphs showing Cl concentration and corrosion rate for soils from Areas B and C.

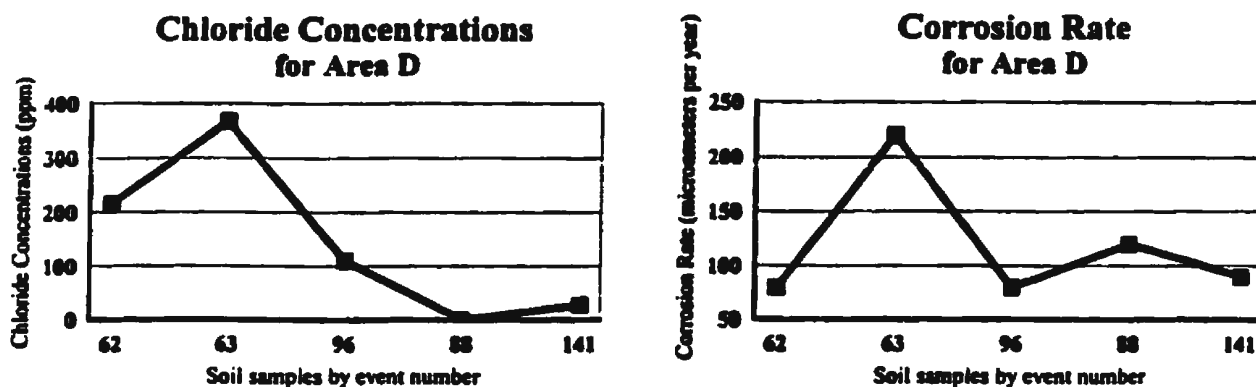


Figure 8.5 Line graph showing Cl concentration and corrosion rate for soil from Area D.

describes the Ferryland site.

8.4 Model for the Corrosion Reaction of the Ferryland Iron Nail Samples

Table 8.4a summarizes the averaged chemical composition for Fe, Cl, P, Si and O in corrosion halos and at iron/corrosion interfaces on iron nails excavated from the Ferryland site. The corrosion halo composition of Fe, Cl and P is similar for nails from Areas C and D. Nails from Area D have a greater concentration of Si in their corrosion halos than those of Area C. Nails from Area B have the highest Cl and Si concentration and lowest Fe concentration in their corrosion halos.

Table 8.4a
Chemical Composition at Corrosion Halo and Iron/Corrosion Interface

Chemical Composition for Corrosion Halos (%)					
Area	Fe	Cl	P	Si	O
B	27.39±0.29	0.65±0.01	1.23±0.05	7.69±0.07	
C	39.92±0.33	0.10±0.01	2.73±0.06	0.20±0.02	
D	48.89±0.29	0.10±0.01	2.14±0.06	4.95±0.07	
Chemical Composition for Iron/Corrosion Halo Interface					
B	44.70±0.36	0.02±0.01	1.07±0.05	0.41±0.04	15.57
C	33.45±0.32	0.64±0.03	3.45±0.07	7.84±0.08	26.94
D	56.55±0.40	1.23±0.03	0.23±0.04	2.90±0.05	20.27

The chemical composition at the iron/corrosion interface differs for nails from Areas B, C and D. Nails from Area B have the lowest Cl and Si concentration at the interface. Iron concentration at the interface is lowest for nails from Area C. Iron nails from Area C have the highest concentrations of P and Si at the interface. Iron nails from Area D have the highest Cl and Fe concentration at the interface. Nails from Area D have the greatest iron loss probably because of high Cl levels at the metal surface. This is supported by the observed iron nail condition summarized in Table 8.4a indicating that an estimated total iron loss of 40 - 79% exists for 86% of the Area D nail samples.

Figure 8.6 is a schematic drawing showing iron and chlorine distribution for nails from the Ferryland site. Figure 8.7 provides an example using nail 128193. The icon

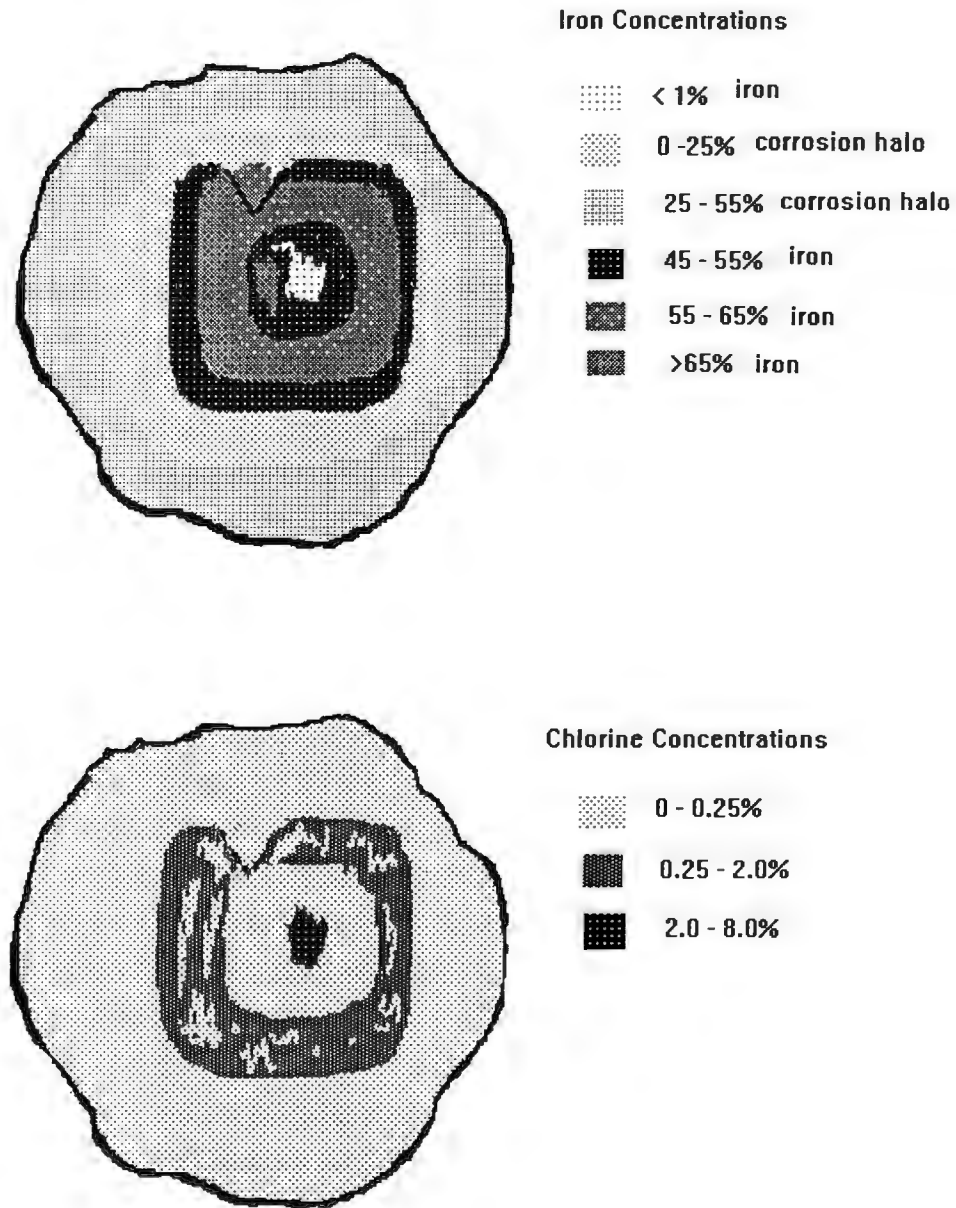
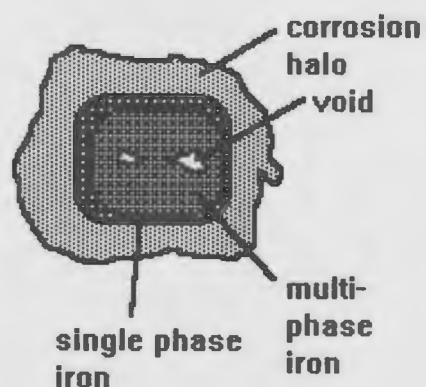


Figure 8.6 Schematic drawing showing iron and chlorine distribution for nails from the Ferryland site.



Sketch of nail (128193) shaft cross-section.



Figure 8.7 Iron/corrosion halo interface for nail sample 128193 (x 10). Note that the crack in the iron meets the corrosion halo probably facilitating the deterioration at the interface. Evidence of deterioration is the multi-phase composition at the interface.

shows the overall pattern of nail deterioration. The photograph shows the iron/corrosion halo interface for nail 128193. Note that the crack in the iron extends to the corrosion halo and probably facilitated Cl enriched soil solution movement to nail interior. Also note the multi-phase nature of the interface indicating a reactive location. Based on Figure 8.6 and Table 8.2a, Cl generally concentrates at the nail interior and iron/corrosion interface with some Cl being concentrated in the corrosion halo. Iron concentrations are low at the nail centre and exterior nail surface. Concentration of iron occurs just below the corroding nail surface. Nails excavated at Ferryland corrode at the centre outwards and at the exterior surface inwards. There is also a migration of carbon resulting in a multi-phase iron texture.

Figure 8.8 shows a possible mechanism for the course of deterioration of the Ferryland iron nails. The porous corrosion halo allows chloride-rich solutions to penetrate to the metal surface. The solutions continue to travel along cracks in the object. The poor condition of the nail interior indicates that the corrosion rate was greater here than at the exterior surface. The carbon enrichment of the metal phase is not likely to have occurred during the manufacture of the nail. Thus the presence of multiple phase(s) of iron is probably the result of some kinetic effect. From the survey of artifacts (Chapter 7) it appears that akaganeite crystallizes in the post-excavation environment. Thus a fourth stage could be added to Figure 8.8 indicating the appearance of akaganeite after the artifact has been stored.

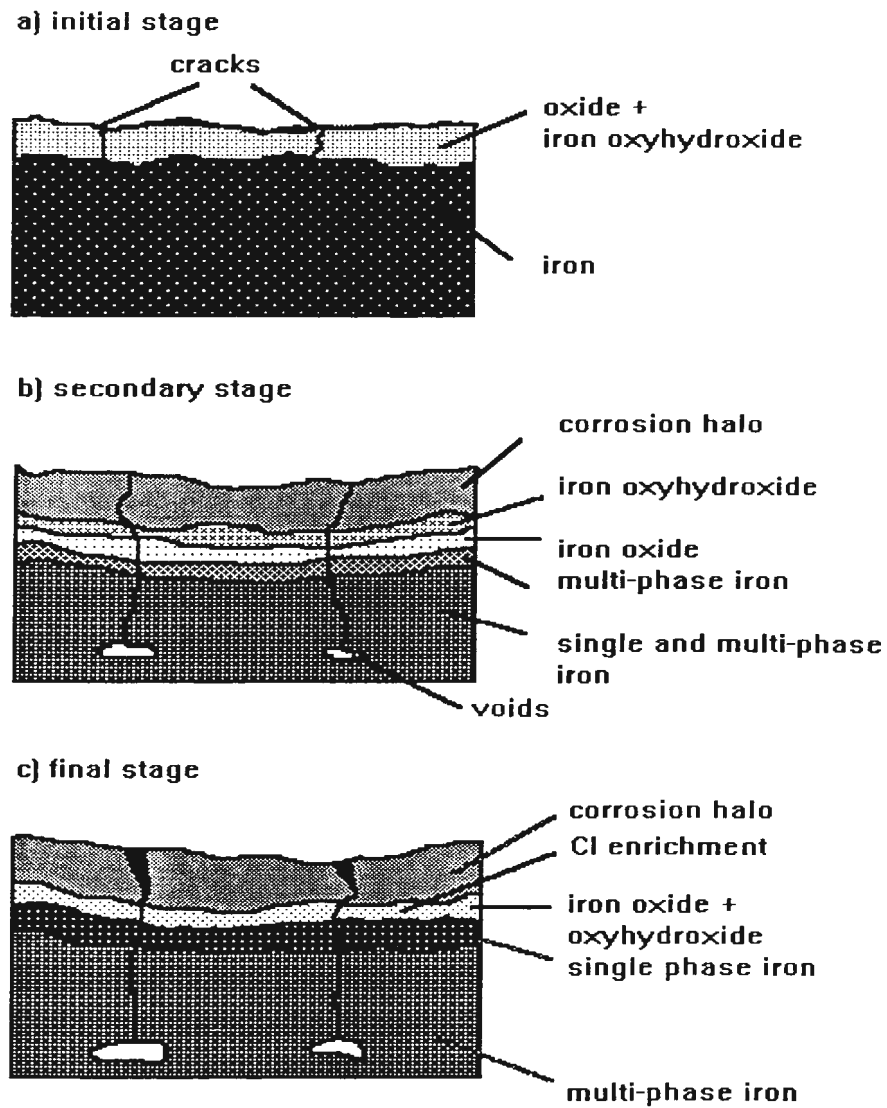


Figure 8.8 Possible mechanism for the course of deterioration of Ferryland iron nails.

Table 8.4b summarizes the metallographic observations for the iron nails. Nails from Areas B and D have the highest proportion of interior metal loss versus exterior metal loss (64:36 ratio). Nails from Areas B and D have high Cl concentration in the corrosion halo at the iron/corrosion interface, respectively. Area C has an even distribution of nails with both corroded interiors and exteriors. The pattern of corrosion is uniform for nails from Areas B and D but varies for nails from Area C.

Table 8.4c summarizes the mineral identification in the corrosion halo. The nails from Area C differ in corrosion halo mineralogy from those of Areas B and D. The corrosion halos of nails from Area C differ by the presence of cacoxenite, goethite and

Table 8.4b
% Distribution of Condition Classifications for Nail Thin-sections

Area	Group 1(G-1) centre void >20% of nail surrounded by multi-phase iron + corrosion halo	Group 2(G-2) centre void <25% of nail surrounded by single phase and multi-phase iron + corrosion halo	Group 3(G-3) single phase iron (10-30%), multi-phase iron (90-70%) + corrosion halo	Group 4(G-4) single phase iron (30-50%), multi-phase iron (70-50%) + corrosion halo	Group 5(G-5) single phase iron (60-90%), multi-phase iron (40-10%) + corrosion halo	Totals per Area
B	27	37	9	18	9	100
C	29	14	43	0	14	100
D	29	35	12	12	12	100
Event	(G-1)	(G-2)	(G-3)	(G-4)	(G-5)	
occupation/ destruction	26	39	22	4	9	100
fill/building	33	17	8	25	17	100

Table 8.4c
Mineral Identification of Corrosion Halo

Area	Mineral							
	qtz	alb	cac	goe	ak	mg	gr	sep
B	X					X		
C	X	X	X	X	X			
D	X	X					X	X

akaganeite in addition to quartz and feldspar. The higher concentration of P in the corrosion halo and at the iron/corrosion interface for nails from Area C is probably from the mineral cacoxenite ($(\text{Fe}_2(\text{PO}_4)_2(\text{OH}) \cdot 12\text{H}_2\text{O})$). Higher concentrations of Cl for nails from Area C is partially from the akaganeite ($\beta\text{-FeOOH}$) mineral which will incorporate Cl in its structure (Turgoose 1985). Table 8.4d summarizes the corrosion halo colour for nails from Areas B, C and D. Separation of samples by corrosion colour correlates with mineralogy. For example, graphite is identified in corrosion halos for nails from Area D. Colour for these samples was a strong brown. Corrosion halo colour for nails from Area C consisting of iron oxyhydroxide in the corrosion halo have a yellow colour. For the nails from Areas B, C and D corrosion halo colour indicates a difference in mineralogy. The nails from Area C consist of iron oxyhydroxides goethite and akaganeite in addition to quartz and feldspar. Corrosion halo colour for the nails from Area C is yellow. This alerts the conservator to the possibility of Cl in the akaganeite structure and that there

Table 8.4d
Summary of Corrosion Halo Colour

Nails from occupation/destruction events		
Area	Events	Colour
B	178,143,133,145	dark yellowish brown to brown
C	19,0,195,	yellowish brown
D	62,96	strong brown
Nails from fill/building events		
B	134,138,177	dark yellowish brown
C	22,55,16	dark yellowish brown to brown
D	63	strong brown

could be extensive iron deterioration. The brown colour for the nails from Area D is produced by the graphite/carbon in the corrosion halo and is indicative of occupation and a burning event. The absence of goethite or akaganeite in the corrosion halos for nails from Areas B and D could indicate that the Cl is concentrated at nail centres. The large percentage of nails with voids at the centre for Areas B and D supports this idea.

8.5 Ferryland Iron Nail Deterioration Model and Turgoose Model : A Comparison

Turgoose (1985, 1992) proposed that the structure of corrosion products at the time of excavation includes a magnetite layer at the metal surface with goethite or an iron oxyhydroxide at the surface of the corrosion and that the soil solution within the pores contains ferrous and chloride ions. After excavation the ferrous ions would oxidize and

akaganeite should crystallize, with chloride ions being incorporated into its structure (Gilbert and Seeley, 1981). Observations presented in Section 8.4 do correlate with the model proposed by Turgoose since an iron oxide and iron oxyhydroxide phase have been identified in the corrosion layers. Cracking and spalling of artifacts in the post-storage environment, as well as chloride concentrations identified by elemental mapping, provide evidence for an akaganeite phase resulting after excavation and further oxidation. One difference is the general lack of goethite identified for the corrosion halos of nails from Areas B and D. Nails with the best fit to the Turgoose model would be those from Area C.

8.6 Methods of Analysis

This thesis incorporates different tools and methods of analysis from different academic disciplines. Samples analysed represent a past material culture and a geological environment spanning approximately 500 million years. Analytical tools of the earth scientist were used to identify artifact conditions of a past culture. For any thesis it is important to understand the relationship between the reason for the analysis and the method applied. The methods used depend on the questions asked and the questions asked depend on the method. Thus, for this thesis, it is not enough simply to understand the analytical techniques and interpretive methodology but also to understand the assumptions of the earth scientist, conservator and archaeologist. Also, this thesis incorporates visual examination, several different analytical methods and archaeological

interpretation, all of which assume different limits for each analysis making application to the question as to extent of impact of the terrestrial burial environment on ferrous metal difficult. Thus part of the aim of this thesis has been to emphasize the fact that when new methods are applied from disciplines different to those for which they were designed one must make sure the new methods are related to the question being asked and take account of the assumptions found in both areas.

The overall method of having both qualitative and quantitative instrumental analysis and visual analysis, though difficult to relate scientifically, was suited to the question asked. To understand the deterioration of the iron nails, a sample of nails from the site was examined to determine density (x-radiography), iron magnetism, visual appearance, metallography, corrosion halo mineralogy, colour, chemical composition and element distribution. The soil surrounding these nails was examined to determine particle size distributions, colour, organic wt%, elemental composition and mineralogy. The soil solution was examined to determine pH, conductivity, corrosion rate and chemical composition. Some of these methods were experimental. For example, the corrosion rate analysis was not designed to use a solution such as soil which has a heterogeneous composition. Also both soil and nail samples represent changes occurring for at least 350 years of burial while the corrosion rates measured represented changes occurring within minutes on a fresh iron surface. The fresh iron surface was, however, exposed to the soil from which the seventeenth-century nails were excavated. Nonetheless, the observed

relative differences between soil samples suggest that a correlation exists between the soil and iron nail. However further work is needed in interpreting the results. For example, soil solution from soil of event 63 had the highest corrosion rate, yet the nail from this event was in good condition. This may represent instrument error or an indication that some component in the corrosion halo is inhibiting the corrosive process. Anomalies such as this indicate that if corrosion rate measurements are to be used with any success a large number of samples must be tested. The elemental mapping of elements in the corroded nail sample probably shows the greatest potential for use in understanding the reactions occurring to buried iron. However, for this thesis the calibration standards for mapping Cl and C were not the best choice for wrought iron. Some work in this area has been done for modern steel but this is a different material from wrought iron. Given that these materials are not commonly studied in earth sciences this is one example where instrumentation should be adapted for the material.

8.7 The Burial Environment as an Alternate Repository for Storage

Can the differences in iron nail condition sufficiently reflect the reactive nature of the soil at the time of excavation? If so can we use excavated archaeological materials as a guide for burial conditions for long term storage of artifacts which have been excavated, researched, stored in dry land facilities and now marked for terrestrial reburial as storage facility. Based on the analyses of this thesis if one was faced with reburial of the Ferryland collection the conditions presented in Table 8.3a would be those to recreate.

The conditions presented in Table 8.3a provided the best preservation for iron and if one is to believe that iron is the most reactive archaeological material then perhaps this would be the storage environment to mimic. However, if organic materials were to be reburied this environment would probably be too dry. Museums and related facilities have for centuries been attempting to create the perfect storage environment for artifacts.

Balancing moisture levels, oxygen and air pollutants has cost millions of dollars within Canada alone with some positive results, however, it is no easy task. The terrestrial burial environment represents a reactive geological environment. Controlling all the parameters that affect this surficial geological environment is probably impossible.

Monitoring such an environment is difficult though some attempts have been made (MacLeod 1996; Corfield 1996; Fry 1996). Based on the results work of this thesis I suggest that archaeologists should be responsible for the storage cost of materials which they excavate and if funding is not available excavation should not proceed. The above system of burial environment analyses could be useful for predicting the condition of buried artifacts which could be used by an archaeologist to assess the cost of conservation and storage.

8.8 Future Work

8.8.1 Samples

Large variation within sample sets for this thesis support the need for large sample groups both in terms of numbers of artifacts and associated soil samples and area of

collection. Also the question of how burial environment affects artifact condition should be approached on a global scale with conservation laboratories affiliated with different archaeological sites participating. Materials being studied should be, where possible, uniform. For archaeological materials pre-dating the industrial revolution such uniformity among individual artifacts is uncommon. However an understanding of the methods of analysis and their limitations can aid in the selection of samples which will be uniform in terms of major compositional components, size, weight and density. In addition, because the terrestrial burial environment is extremely reactive, perhaps some components of the study should be compared to a fossil assemblage in an attempt to identify parameters which may or may not be involved in the fundamental reactions of a burial environment.

8.8.2 Instrumentation

Possibly the greatest impact this thesis has had or will have on the conservation community is that it has demonstrated the variable nature of the archaeological burial environment and the potential value of assessing the corrosion rate for soil solutions to the understanding of kinetic effects of burial and subsequently relating this to element distribution/redistribution for iron objects (Mathias 1994, 1996). However, both instrumentation for corrosion rate and elemental analysis requires further work to adapt them specifically for, in this case, seventeenth-century wrought iron.

In understanding a heterogeneous material and how its differential composition interacts when exposed to different environments it is useful to monitor these changes as they occur. Thus it would be interesting to construct a reaction chamber for use when mapping element distribution with the electron microprobe.

REFERENCES CITED

Alexander, W. and A. Street

1979 *Metals in the Service of Man*. 7th edition. Chaucer, London.

“Archaeological Investigation Permit Regulations” under *The Historic Resources Act* (1985), Newfoundland, pp.888.

Archer, P.J. and B.D. Barker

1987 Phase Changes Associated With the Hydrogen Reduction Conservation Process for Ferrous Artifacts. *Journal of Historical Metallurgy Science*, Vol. 21.

Argo, J.

1981 On the Nature of “Ferrous” Corrosion Products on Marine Iron. *Studies in Conservation*, Vol 26: 42-44.

Argyropoulos, V.

1996 Treatment of Wrought Iron Artifacts from Ferryland and Renews using Sodium Hydroxide and Ethylenediamine. Report on file, Canadian Conservation Institute, Ottawa.

Argyropoulos, V., L.S. Selwyn and J.A. Logan

- 1995 Developing a Conservation Treatment Using Ethylenediamine as a Corrosion Inhibitor for Wrought Iron Objects Found at Terrestrial Archaeological Sites. In *Proceedings of the International Conference on Metals Conservation*, edited by I. MacLeod, S.L. Pennec and L. Robbiola, pp. 153-158. ICOM Committee for Conservation, Paris.

American Society for Testing and Materials

- 1984 ASTM Designation: G 51-77: Standard Test Method for pH of Soil for Use in Corrosion Testing. *Annual Book of ASTM Standards*, pp. 191-192. ASTM, Philadelphia.
- 1996 ASTM Designation: D1125: Electronic Digital Conductivity Meter. *Annual Book of ASTM Standards*, Vol. 11.01: pp. 93-99. ASTM, Philadelphia.
- Barnartt, S.
- 1969 Linear Corrosion Kinetics. *Corrosion Science*, Vol. 9(3): 145-156.
- 1985 Simplified Calculation of pH and Ion Concentrations in High Temperature Phosphate Solutions and Phosphate-Hydroxide Mixtures. *Journal of the Electrochemical Society*, Vol. 132: 2890-2895.

Bealer, A.W.

1976 *The Art of Blacksmithing*. Funk and Wagnalls, New York.

Bell, M.A.

1993 Organic Matter, Soil Properties, and Wheat Production in the High Valley of Mexico. *Soil Science*, Vol. 156(2): 86-93.

Binnie, N.E., L.S. Selwyn and C. Schlichting

1992 Corrosion of Outdoor Iron Artifacts using Rust Conversion Evaluation of New Commercial Products. Paper presented at the 1992 IIC-CG Conference, Ottawa.

Birchenall, C.E. and R.A. Meussner

1977 Principles of Gaseous Reduction of Corrosion Products. In *Corrosion and Metal Artifacts - A Dialogue Between Conservators and Archaeologists and Corrosion Scientists*, edited by B.F. Brown, H.C. Burnett, W.T. Chase, M. Goodway, J. Kruger and M. Pourbaix, pp. 39-57. National Bureau of Standards Special Publication No. 479. Nace, Texas.

Blackshaw, S.M.

- 1982 An Appraisal of Cleaning Methods for Use on Corroded Iron Antiques. In *Conservation of Iron*, pp. 16-20. Maritime Monographs and Reports, No. 53. London.

Brady, J.E.

- 1990 *General Chemistry Principles and Structure*. John Wiley, Toronto.

Brommelle, N.

- 1956 Material for a History of Conservation. *Studies in Conservation*, Vol. 2: 176-184.

Bodey, H.

- 1983 *Nailmaking*. Shire Publications, U.K.

Booth, G.H., A.K. Tiller and F. Wormwell

- 1962 A Laboratory Study of Well Preserved Ancient Iron Nails from Apparently Corrosive Soils. *Corrosion Science*, Vol. 2: 197-202.

Bosch, R.W. and W.F. Bogaerts

- 1996 Instantaneous Corrosion Rate Measurement With Small-Amplitude Potential Intermodulation Techniques. *Corrosion*, Vol. 53(3): 204-212.

Canadian Conservation Institute (CCI)

1974 Interdisciplinary Seminar on Care of Collections. Moncton, New Brunswick.

Carpenter, J.

1986 Conservation of an Anchor from Wrecksite of HMS Sirius (1790). Unpublished report to the Australian Bicentennial Authority, pp. 1-29.

Carpenter, J. and I.D. MacLeod

1993 Conservation of Corroded Iron Cannon and the Influence of Degradation on Treatment Times. In *Preprints, 10th Triennial Meeting, ICOM Committee for Conservation*, Vol. II, Washington, D.C. 22-27 August 1993, edited by J. Bridgland, pp 759-766. ICOM Committee for Conservation, Paris.

Carter, M.

1997 *The Archaeological Investigation of a Seventeenth-Century Blacksmith Shop at Ferryland, Newfoundland*. Unpublished Master's thesis, Department of Anthropology, Memorial University of Newfoundland, St. John's.

Clarke, G.R.

1971 *The Study of Soil in the Field*. 5th edition. Clarendon, Oxford.

Corfield, M.

- 1996 Preventative Conservation for Archaeological Sites. In *Preprints of the Contribution to the Copenhagen Congress, 26-30 August 1996*, pp. 32-37.
- IIC - Archaeological Conservation and its Consequences. Published by The International Institute for Conservation of Historic and Artistic Works.

Costain, C.

- 1985a Storage Solutions for Archaeological Iron. Paper presented at the 11th Annual Conference, International Institute for Conservation - Canadian Group, Halifax, Canada.
- 1985b Measurement of Chlorides in Treatment Solution. *IOCM Committee for Conservation Metals Working Group Newsletter 1*, 1 July: 4-7.

Cox, A. and S.B. Lyon

- 1994 An Electrochemical Study of the Atmospheric Corrosion of Iron-II. Cathodic and Anodic Processes on Uncorroded and Pre-Corroded Iron. *Corrosion Science*, Vol. 36(7): 1177-1192.

Cronyn, J.M.

- 1990 *The Elements of Archaeological Conservation*. Routledge, New York.

Daly Hartin, D.

- 1990 An Historical Introduction to Conservation. In *Shared Responsibility: Proceedings of a Seminar for Curators and Conservators*, edited by B. Ramsay-Jolicoeur and I. Wainwright, pp. 30-38. National Gallery of Canada, Ottawa.

Day, P.R.

- 1965 Particle Formation and Particle-Size Analysis. In *Methods of Soil Analysis*, edited by C.A. Black, pp.545-565. Agronomy No. 9, Part 1. American Society of Agronomy, Madison, Wisconsin.

Deer, W.A., R.A. Howie and J. Zussman

- 1992 *An Introduction to the Rock Forming Minerals*, 2nd edition. John Wiley & Sons, New York.

Deetz, J.

- 1977 *In Small Things Forgotten*. Doubleday, Toronto.

- 1993 *Flowerdew Hundred: The Archaeology of a Virginia Plantation, 1619-1864*. University Press of Virginia, London.

Detournay, J., R. Derie and M. Ghodsi

- 1976 Etude de l'oxydation par aeration de $\text{Fe}(\text{OH})_2$ en milieu chlorure. *Journal of Inorganic Chemistry*, Vol. 15: 265-273.

Dowman, E.

- 1970 *Conservation in Field Archaeology*. Methuen, London.

Eberl, D.D. and T.C. Velde-Bruce McCormick

- 1993 Synthesis of Illite-Smectite from Smectite at Earth Surface Temperatures and High pH. *Clays and Minerals*, Vol. 41(1): 49-60.

Edwards, R.

- 1993 *Cutting Tools*. Institute of Materials, London.

Farrer, T.W., L. Biek and F. Wormwell

- 1953 The Role of Tannates and Phosphates in the Preservation of Ancient Buried Iron Objects. *Journal of Applied Chemistry*, Vol. 3: 80-84.

Furip, D.J., R. Malewicki and D.P Heldman

- 1983 *Colonial Nails from Michilimackinac: Differentiation by Chemical and Statistical Analysis.* Archaeological Completion Report Series, No. 7. Mackinac Island State Park Commission, Mackinac Island, Michigan.

Fry, M.F.

- 1996 Burned but not Forgotten: Sensitivity in Disposing of Major Archaeological Timbers. In *Preprints of the Contribution to the Copenhagen Congress*, 26-30 August 1996, pp. 52-54. IIC - Archaeological Conservation and its Consequences. Published by The International Institute for Conservation of Historic and Artistic Works.

Galster, H.

- 1991 *pH Measurement - Fundamentals, Methods, Applications, Instrumentation.* VCH, New York.

Garrels, R.M. and C.S. Christ

- 1965 *Solutions, Minerals and Equilibria.* Harper and Row, London.

Gaulton, B.

- 1997 *Seventeenth-Century Stone Construction At Ferryland, Newfoundland (Area C)*.
Unpublished Master's thesis, Department of Anthropology, Memorial University
of Newfoundland, St. John's.

Gaynor, J.M.

- 1993 *Tooles of all Sorts to Worke: A Brief Look at Trade Tools in 17th-Century
Virginia*. In *The Archaeology of 17th-Century Virginia*, edited by T.R. Reinhart
and D.J. Pogue, pp. 311-356. The Dietz Press, Virginia.

Gaynor, J.M. and N.L Hagedorn

- 1993 *Tools: Working Wood in Eighteenth-Century America*. Colonial Williamsburg
Foundation, Williamsburg, Virginia.

Gettens, R.J.

- 1963 *Mineral Alteration Products in Ancient Metal Objects*. In *Recent Advances in
Conservation*, edited by G. Thomson, pp. 27-73. Butterworth, Oxford.

Gilberg M.R. and N.J. Seeley

- 1981 *The Identity of Compounds Containing Chloride Ions in Marine Iron Corrosion
Products: A Critical Review*. *Studies in Conservation*, Vol. 26(2): 50-56.

Hansen, J.W., D.E. Canfield and B. Thamdrup

- 1993 The Anaerobic Degradation of Organic Matter in Danish Coastal Sediments; Iron Reduction, Manganese Reduction and Sulfate Reduction. *Geochimica et Cosmochimica Acta*, Vol. 57(16): 3867-3883.

Harris, J.O. and D. Eyre

- 1995 Soil in the Corrosion Process. In *Corrosion I: Metal/Environment Reactions*. 3rd edition. edited by L.L. Shrier, R.A. Jarman and G.T. Butstein, pp. 2:73-86. Butterworth, Oxford.

Heringa, P.K.

- 1981 *Soils of the Avalon Peninsula, Newfoundland*. Newfoundland, Research Branch, Agriculture Canada, Report No. 3. Agriculture Canada, St. John's.

Higgins, R.A.

- 1973 *Engineering Metallurgy 1. Applied Physical Metallurgy*. Hodder and Stoughton, London.

Hjelm-Hansen, N., J. van Lanschot, C.D. Szalkay and S. Turgoose

- 1993 Electrochemical Assessment and Monitoring of Stabilisation of Heavily Corroded Archaeological Iron Artefacts. *Corrosion Science*, Vol. 35: 767-774.

Hodges, H.

1984 *Artifacts*. F.A. Praeger, New York.

Hodych, J.P. and A.F. King

1989 Geology of Newfoundland and Labrador. *Newfoundland Journal of Geological Education*, Vol. 10.

Holstrom, J.G.

1904 *Modern Blacksmithing: rational horse shoeing and wagon making: with rules, tables, recipes, etc., useful to manufacturers, blacksmiths, machinists, well-drivers, engineers, liverymen, horse-shoers, farmers, wagon-makers, mechanics, amateurs and all others who have occasion to perform the work for which this book is primarily intended*. F.J. Drake, Chicago.

Hundal, H.S. and N.S. Pasricha

1993 Nonexchangeable Potassium Release Kinetics in Illitic Soil Profiles. *Soil Science*, Vol. 156(1): 34-41.

International Institute for Conservation-Canadian Group and the Canadian Association of Professional Conservators

- 1989** Code of Ethics and Guidance for Practice for Those Involved in the Conservation of Cultural Property in Canada. Published by the International Institute for Conservation-Canadian Group (IIC-CG) and the Canadian Association of Professional Conservators (CAPC). 2nd edition. Ottawa.

Jackson, M.L.

- 1956** *Soil Chemical Analysis - Advanced Course*. Published by Author. Madison, Wisconsin.
- 1964** Soil Clay Mineralogical Analysis. In *Soil Clay Mineralogy*, edited by C.I. Rich and G.W. Kunze, pp. 245-294. University of North Carolina Press, Chapel Hill, North Carolina.
- 1979** *Soil Chemical Analysis - Advanced Course*. 2nd edition. Published by Author. Department of Soil Science, University of Wisconsin, Madison.

Jade

- 1991 **Jade Search/Match Phase Identification by Profile-Based Search/Matching using ICDD (International Centre for Diffraction Data) and PDF (Powder Diffraction File). Materials Data, Livermore, California.**

Jenner G.A., S.F. Foley, S.E. Jackson, T.H. Green, B.J. Fryer and H.P. Longerich

- 1993 **Determination of Partition Coefficients for Trace Elements in High Pressure-Temperature Experimental Run Product by Laser Ablation Microprobe-Inductively Coupled Plasma-Mass Spectrometry (LAM-ICP-MS). *Geochimica et Cosmochimica Acta*, Vol. 57: 23-24.**

Jones, D.A.

- 1968 **Polarization in High Resistivity Media. *Corrosion Science*, Vol. 1: 19-27.**
- 1992 ***Principles and Prevention of Corrosion*. Maxwell Macmillan, New York.**
- 1996 **Localized Surface Plasticity During Stress Corrosion Cracking. *Corrosion*, Vol. 52(5): 356-362.**

Jordan, D.L.

- 1996 Relative Contributions of Several Cathodic Reactions to the Anodic Dissolution of Electrogalvanized Steel. *Corrosion*, Vol. 52(3): 187-193.

King, A.F.

- 1989 Geological Evolution of the Avalon Peninsula, Newfoundland. In *Geology of Newfoundland and Labrador*, Vol. 10, edited by J.P. Hodych and A.F. King, pp. 17-40. Geological Association of Canada, St. John's, Newfoundland.
- 1990 Geology of the St. John's Area. *Newfoundland: Geological Survey Branch, Department of Mines and Energy, Government of Newfoundland and Labrador*, Report 90-92.

Knight, B.

- 1982 Why Do Some Iron Objects Break Up in Store? In *Conservation of Iron*, edited by R.W. Clarke and S.N. Blackshaw, pp. 50-51. Maritime Monographs and Reports, No. 53. National Maritime Museum, London.

Lehmann, J. and E.M. Nosek

- 1978** Research and Conservation of Iron Objects Discovered in a Shipwreck Lifted from Gdansk Gulf. In *Conservation of Iron Objects Found in Salty Environments*, edited by R.M. Organ, E.M. Nosek and J. Lehmann, pp. 50-64. Historical Monuments Documentation Centre, Warsaw.

Leinonen, H.

- 1996** Stress Corrosion Cracking and Life Prediction Evaluation of Austenitic Stainless Steels in calcium Chloride Solutions. *Corrosion*, Vol. 52(5): 337-346.

Lian, K. and E.I. Meletis

- 1996** Environment-Induced Deformation Localization During Transgranular Stress Corrosion Cracking. *Corrosion*, Vol. 52(5): 347-355.

Light, J.D. and H. Unglik

- 1987** *A Frontier Fur Trade Blacksmith Shop 1796-1812*. Revised edition. Studies in Archaeology, Architecture and History. Minister of Supply and Services Canada, Ottawa.

Limbrey, S.

- 1975** *Soil Science and Archaeology*. Academic Press, New York.

Logan, J.A.

- 1984 An Approach to Handling Large Quantities of Archaeological Iron. In *Conservation on Archaeological Excavations*, edited by S. Price, pp. 14-16. ICCROM Committee for Conservation, 7th Triennial Meeting, Rome.
- 1985 Conservation in the Field: An Example from Red Bay. In *Archaeology in Newfoundland and Labrador - 1985*, edited by J.S. Thomson and C. Thomson, pp. 121-149. Historic Resources Division, Department of Culture, Recreation and Youth. St. John's.
- 1989 The cost of conservation. Paper presented at the Annual Conference, Canadian Archaeological Association, Fredericton, Canada.

Longerich, H.P.

- 1995 *Analysis of Pressed Pellets of Geological Samples Using Wavelength-Dispersive X-Ray Fluorescence Spectrometry*. X-Ray Spectrometry Vol. 24. John Wiley, New York.

Longerich, H.P., S.E. Jackson, J.A. Jenner, J.K Friel, Z. Chen, B.J. Fryer
and A. Frimpong

- 1993 Progress in the Determination of Trace Elements Using Solution Nebulization
ICP-MS. Paper presented at the 1993 European Winter Conference on Plasma
Spectrochemistry, 10-15 January, 1993, Granada, Spain.

Lovelace, D.

- 1673 An Account of the Dutch Raid Upon the Coast of Newfoundland in the Year
1673. Her Majesty's State Paper Office Co. 1/34. Copy on file at the Maritime
History Archive, Memorial University of Newfoundland.

MacKay, A.L.

- 1960 β -ferric oxyhydroxide. *Mineralogy Magazine*, Vol. 32: 545-557.

MacLeod, I.D.

- 1981 Shipwrecks and Applied Electrochemistry. *Journal of Electroanalytical
Chemistry*, Vol. 118: 291-303.
- 1989 Electrochemistry and Conservation of Iron in Sea Water. *Chemistry in Australia*,
Vol. 56: 227-229.

- 1996 In-Situ Conservation of Cannon and Anchors on Shipwreck Sites. In *Preprints of the Contribution to the Copenhagen Congress, 26-30 August 1996*, pp. 111-115. IIC - Archaeological Conservation and its Consequences. Published by The International Institute for Conservation of Historic and Artistic Works.

MacLeod, I.D., P. Mardikian and V.L. Richards

- 1994 Observations on the Extraction of Iron and Chloride Ions from Composite Materials. In *Proceedings of 5th ICOM Group on Wet Organic Archaeological Materials Conference*, edited by P. Hoffman, pp. 199-211. ICOM, Paris.

Mathias, C.

- 1993 Developments in Archaeological Conservation - A Perspective from Newfoundland and Labrador. *Newfoundland Studies*, Vol. 9(2): 311-327.
- 1994 A Conservation Strategy for a Seventeenth Century Archaeological Site at Ferryland, Newfoundland. *Journal of the International Institute for Conservation - Canadian Group*, Vol. 19: 14-23.

- 1996 Assessment of Corrosion Measurements for Soil Samples Excavated at a Seventeenth-Century Colonial Plantation Site. In *Preprints of the Contribution to the Copenhagen Congress, 26-30 August 1996*, pp. 121-126. IIC - Archaeological Conservation and its Consequences. Published by The International Institute for Conservation of Historic and Artistic Works.

McCartney, W.D.

- 1967 *Whitbourne Map Area, Newfoundland*. Geological Survey of Canada, Memoir 341. Ottawa.

- 1969 *Geology of the Avalon Peninsula, Southeast Newfoundland*. American Association of Petroleum Geologists, Memoir 12.

McKeague, J.A. (editor)

- 1978 *Manual on Soil Sampling and Methods of Analysis*. 2nd edition. Canadian Society of Soil Science, Ottawa.

Meilack, D.Z.

- 1977 *Decorative and Sculptured Ironwork*. Crown, New York.

Misawa, T.

1973 The Thermodynamic Consideration for $\text{Fe}^*\text{H}_2\text{O}$ System at 25°C . *Corrosion Science*. Vol. 13: 659-676.

Misawa, T., T. Kyuno, W. Suëtaka and S. Shimodaira

1971 The Mechanism of Atmospheric Rusting and the Effect of Cu and P on the Rust Formation of Low Alloy Steels. *Corrosion Science*, 11(1): 35-48.

Model 352/252 SofiCorr II - Corrosion Measurement and Analysis Software User's Guide. EG&G Instruments Inc. (1992).

Moore, D.M. and R.C. Reynolds Jr.

1989 *X-ray Diffraction and the Identification and Analysis of Clay Minerals*. Oxford University Press, Oxford.

Munsell Soil Colour Charts

1992 Macbeth Division of Kollmorgen Instruments Corp., New York.

Nesic, S., J. Postlethwaite and S. Olsen

1996 An Electrochemical Model for Prediction of Corrosion of Mild Steel in Aqueous Dioxide Solutions. *Corrosion*, Vol. 52(4): 280-306.

Noël Hume, I.

1970 *A Guide to Artifacts of Colonial America*. Random House, New York.

North, N.A.

1982 Corrosion Products on Marine Iron. *Studies in Conservation*, Vol. 27(2): 75-83.

North, N.A. and C. Pearson

1975 Alkaline Sulfite Reduction Treatment of Marine Iron. Paper presented at the 4th Triennial Meeting for the International Committee on Museums, Venice, Italy.

1977 Thermal Decomposition of FeOCl and Marine Cast Iron Corrosion Products. *Studies in Conservation*, Vol. 22: 146-157.

Nosek, E.M.

1978 Research and Conservation of the Iron Objects Currently Displayed at the Salt Mine Museum. In *Conservation of Iron Objects Found in Salty Environments*, edited by R.M. Organ, E.M. Nosek and J. Lehmann, pp. 9-20. Historical Monuments Documentation Centre, Warsaw.

Nriagu, J.O.

1972 Stability of Vivianite and Ion-pair Formation in the System

$\text{Fe}_3(\text{PO}_4)_2 \cdot \text{H}_3\text{PO}_4 \cdot \text{H}_2\text{O}$. *Geochimica and Cosmochimica Acta*, Vol. 36: 459-470.

Oldham K.B. and F. Mansfield

1971 A Modification of the Stern-Geary Linear Polarization Equation. *Corrosion*

Science, Vol. 11: 787-796.

Organ, R.M.

1977 The Current Status of the Treatment of Corroded Metal Artifacts. In *Corrosion*

and Metal Artifacts - A Dialogue Between Conservators and Archaeologists and

Corrosion Scientists, edited by B.F. Brown, H.C. Burnett, W.T. Chase,

M. Goodway, J. Kruger and M. Pourbaix, pp. 107-142. National Bureau of

Standards Special Publication No. 479. Nace, Texas.

Parfitt, R.L. and J.D. Russel

1977 Adsorption on Hydrous Oxides IV: Mechanism of Adsorption of Various Ions on

Goethite. *Journal of Soil Science*, Vol. 28: 297-305.

Parkins, R.N.

- 1996 Mechanistic Aspects of Intergranular Stress Corrosion Cracking of Ferritic Steels. *Corrosion*, Vol. 52(5): 363-395.

Parkinson, K.

- 1967 *Metalwork: Theory and Practice*. Pergamon Press, Oxford, New York.

Pearson, C.

- 1977 On-Site Conservation Requirements for Marine Archaeological Excavations. *International Journal of Nautical Archaeology and Underwater Exploration*, Vol. 6: 37-46.

Phillpotts, A.R.

- 1990 *Principles of Igneous and Metamorphic Petrology*. Prentice Hall, New Jersey.

Pogue, D.J.

- 1993 Standard of Living in the 17th-Century Chesapeake: Patterns of Variability Among Artifact Assemblages. In *The Archaeology of 17th-Century Virginia*, edited by T.R. Reinhart and D.J. Pogue, pp. 371-400. The Dietz Press, Virginia.

Pollastro, R.M.

- 1993 Considerations and Applications of the Illite/Smectite Geothermometer in Hydrocarbon-Bearing Rocks of Miocene to Mississippian Age. *Clays and Minerals*, Vol. 41(2): 119-133.

Pope, P.E.

- 1986 *Ceramics from Seventeenth Century Ferryland, Newfoundland (CgAf-2, Locus B)*. Unpublished Master's thesis, Department of Anthropology, Memorial University of Newfoundland, St. John's.
- 1993 *Documents Relating to Ferryland 1597-1726*. Report on file at the Archaeology Unit, Memorial University. St. John's.

Pourbaix, M.

- 1966 *Atlas of Electrochemical Equilibria in Aqueous Solutions*. Pergamon Press, Oxford.
- 1975 *Proceedings of the 4th European Symposium on Corrosion Inhibitors*. University of Ferrara, Italy.

- 1977 Electrochemical corrosion and reduction. In *Corrosion and Metal Artifacts - A Dialogue Between Conservators and Archaeologists and Corrosion Scientists*, edited by B.F. Brown, H.C. Burnett, W.T. Chase, M. Goodway, J. Kruger and M. Pourbaix, pp.1-16. National Bureau of Standards Special Publication No. 479. Nace, Texas.

Qui, Xing-Chu and Jing-Quan Zhu

- 1993 Rapid Analysis of Cation-Exchange Property in Acidic Soil. *Soil Science*, Vol. 155(4): 301-308.

Refait, P. and J-M.R. Genin

- 1993 The Transformation of Chloride-Containing Green Rust One into Sulphated Green Rust Two by Oxidation in Mixed Cl^- and SO_4^{2-} Aqueous Media. *Corrosion Science*, Vol. 36(1): 55-65.

Rempel, A.W. and B.A. Buffet

- 1997 Formation and Accumulation of Gas Hydrate in Porous Media. *Journal of Geological Research, β , Solid Earth and Planets*, Vol. 102(5): 151-160.

Reynolds Jr., R.C.

- 1989 Diffraction by Small and Disordered Crystals. In *Modern Powder Diffraction, Reviews in Mineralogy, 20*, edited by D.L. Bish and J.E. Post, pp. 145-181. Mineralogical Society of America, Washington, D.C.

Rhoades, J.D.

- 1982 Cation Exchange Capacity. In *Methods of Soil Analysis*, 2nd edition, Part 2, edited by A.L. Page, R.H. Miller and D.R. Keeney, pp. 149-158. Agronomy Monograph No. 9. American Society of Agronomy, Madison, Wisconsin.

Richardson, S.M. and H.Y. McSwen Jr.

- 1980 *Geochemistry, Pathways and Processes*. Prentice-Hall, New Jersey.

Rinuy, A. and F. Schwerzer

- 1982 A Comparative Study of Different Desalination Methods. In *Conservation of Iron*, edited by R.W. Clarke and S.N. Blackshaw, pp. 44-49. Maritime Monographs and Reports, No. 53. National Maritime Museum, London.

Robie, R.A., B.S. Hemingway and J.R. Fisher

- 1978 *Thermodynamic Properties of Minerals and Related Substances*. U.S. Geological Survey Bulletin No. 1452. Reston, Virginia.

Rocchini, G.

- 1994 Corrosion Rate Monitoring of Metallic Materials Using the Linear Response.
Corrosion Science, Vol. 36(6): 1047-1061.

Romanoff, M.

- 1957 *Underground Corrosion*. National Bureau of Standards, Circular No. 579.
Washington, D.C.

Rose, E.R.

- 1952 *Torbay Map Area, Newfoundland*. Geological Survey of Canada, Memoir 165.
Ottawa.

Rostoker, W. and J.R. Dvorak

- 1990 *Interpretation of Metallographic Structures*. 3rd edition. Academic Press,
Toronto.

Schlesinger, W.H.

- 1991 *Biochemistry: An Analysis of Global Change*. Academic Press, Toronto.

Schroder, P.A.

- 1993 A Chemical, XRD and (Super 27) AL MAS NMR Investigation of Miocene Gulf Coast Shales with Application to Understanding Illite/Smectite Crystal-Chemistry. *Clays and Minerals*, Vol. 41(6): 668-679.

Scott, B.

- 1989 The Retrieval of Technological Information From Corrosion Products on Early Wrought Iron Artifacts. In *Evidence Preserved in Corrosion Products: New Fields in Artifact Studies*, edited by R. Janaway and B. Scott, pp. 8-14. Occasional Papers No. 8, The United Kingdom Institute for Conservation, U.K.

Scott, D.A. and N.J. Seeley

- 1987 The Washing of Fragile Iron Artifacts. *Studies in Conservation*, Vol. 32: 73-76.

Selwyn, L.S. and J.A. Logan

- 1993 Stability of Treated Iron: A Comparison of Treatment Methods. In *Preprints, 10th Triennial Meeting, ICOM Committee for Conservation*, Vol. II, Washington, D.C., 22-27 August 1993, edited by J. Bridgland, pp. 803-807. ICOM Committee for Conservation, Paris.

Sheldrick, B.H. and C. Wang

- 1993 Particle Size Distribution. In *Soil Sampling and Methods of Analysis*, edited by M.R. Carter, pp. 499-511. Canadian Society of Soil Science. Lewis, Florida.

Shima, M. and H. Yabuki

- 1979 Studies on the rust for ancient iron implements. *Scientific Papers on Japanese Antiques and Art Crafts*, Vol. 24: 77-82.

Shreir, L.L.

- 1995 Outline of Electrochemistry. In *Corrosion II: Corrosion Control*. 3rd edition. Edited by L.L Shreir, R.A. Jarman and G.T. Butstein, pp. 20:3-55. Butterworth, Oxford.

Shreir L.L., R.A. Jarman and G.T. Butstein (editors)

- 1995a *Corrosion I: Metal/Environment Reactions*. 3rd edition. Butterworth, Oxford.

- 1995b *Corrosion II: Corrosion Control*. 3rd edition. Butterworth, Oxford.

Simmons, E.J.

- 1955 Use of the Pearson Bridge in Corrosion Inhibitor Evaluation. *Corrosion*, Vol. 11: 255-261.

Singley, K.

- 1988 *The Conservation of Archaeological Artifacts from Freshwater Environments.*
Lake Michigan Maritime Museum, Michigan.

Skold, R.V. and T.E. Larsen

- 1957 Measurement of the Instantaneous Corrosion Rate by Means of Polarization Data.
Corrosion, Vol. 13: 139-142.

Skoog, D.A. and D.M. West

- 1982 *Fundamentals of Analytical Chemistry.* 4th edition. Saunders College:
Philadelphia.

Smith, C.S.

- 1977 Some Constructive Corroding. In *Corrosion and Metal Artifacts - A Dialogue
Between Conservators and Archaeologists and Corrosion Scientists*, edited by
B.F. Brown, H.C. Burnett, W.T. Chase, M. Goodway, J. Kruger and M. Pourbaix,
pp. 143-166. National Bureau of Standards Special Publication No. 479. Nace,
Texas.

Stern, M. and A.L. Geary

- 1957 Electrochemical Polarization - A Theoretical Analysis of the Shape of Polarization Curves. *Journal of the Electrochemical Society*, Vol. 104: 56-63.

Stolow, N. (editor)

- 1972 *Progress in Conservation*. The National Gallery of Canada, Ottawa.

Taylor, R.M. and U. Schwertmann

- 1977 Iron oxides. In *Minerals in Soil Environments*, edited by J.B. Dixon and S.B. Weed, pp. 145-180. Soil Science Society of America, Wisconsin.

Tuck, J.A.

- 1985 Looking for the Colony of Avalon. In *Archaeology in Newfoundland and Labrador - 1984*, edited by J.S. Thomson and C. Thomson, pp. 378-397. Historic Resources Division, Department of Culture, Recreation and Youth. St. John's.
- 1989 Excavations at Ferryland, Newfoundland - 1986. In *Archaeology in Newfoundland and Labrador -1986*, edited by J.S. Thomson and C. Thomson, pp. 296-307. Historic Resources Division, Department of Culture, Recreation and Youth. St. John's.

1992 The Ferryland Archaeology Project - 1992. Report on file at the Historic Resources Division, Department of Tourism and Culture, Government of Newfoundland and Labrador. St. John's.

1993 Archaeology at Ferryland, Newfoundland. *Newfoundland Studies*, Vol. 9(2): 294-310.

1996 Archaeology at Ferryland, Newfoundland 1936-1995. *Avalon Chronicles*, Vol. 1:21-41.

Tuck, J.A. and D.T. Robbins

1986 A Glimpse of the Colony of Avalon. In *Archaeology in Newfoundland and Labrador - 1985*, edited by J.S. Thomson and C. Thomson, pp. 237-249. Historic Resources Division, Department of Culture, Recreation and Youth. St. John's.

Turgoose, S.

1982a The Nature of Surviving Iron Objects. In *Conservation of Iron*, edited by R.W. Clarke and S.N. Blackshaw, pp. 1-7. Maritime Monographs and Reports, No. 53. National Maritime Museum, London.

1982b Post Excavation Changes in Iron Antiquities. *Studies in Conservation*, Vol. 27: 97-101.

1985 The Corrosion of Archaeological Iron During Burial and Treatment. *Studies in Conservation*, Vol. 30: 13-18.

1989a Structure, Composition and Deterioration of Unearthed Iron Objects. *International Symposium on the Conservation and Restoration of Cultural Property: Current Problems in the Conservation of Metal Antiquities*. 4-6 October, pp.35-52.

1989b Corrosion and Structure: Modelling the Preservation Mechanisms. In *Evidence Preserved in Corrosion Products: New Fields in Artifact Studies*, edited by R. Janaway and B. Scott, pp. 30-32. Occasional Papers No. 8, The United Kingdom Institute for Conservation, U.K.

Uhlig, H.H.

1963 *Corrosion and Corrosion Control*. J. Wiley, New York.

Varela, C., C. Vazquez, M.V. Gonzalez-Sangnegorio, M.C. Leiros and F. Gil-Sotres

1993 Chemical and Physical Properties of Opencast Lignite Minesoils. *Soil Science*, Vol. 156: 193-204.

Williams, H., S.J. O'Brien, A.F. King and M.M. Anderson

1995 Avalon Zone - Newfoundland. In *Geology of the Appalachian-Caledonian Orogen in Canada and Greenland*, edited by H. Williams, pp. 226-237. *Geology of Canada No. 6*, Geological Survey of Canada.

Williams, H. and R.K. Stevens

1974 The Ancient Continental Margin of Eastern North America. In *The Geology of Continental Margins*, edited by C.A. Burke and C.L. Drake, pp. 781-796. Springer Verlag, New York.

Weygers, A.G.

1974 *The Modern Blacksmith*. Van Nostrand Reinhold, New York.

Wynne, E.

1622 Letter to George Calvert, Ferryland, 28 July 1622. In *Newfoundland Discovered, English Attempts at Colonization, 1610-1630*, edited by G. Cell, pp. 195-198. Hakluyt Society, London (1982).

Yamashita, M., H. Miyuki, Y. Matsuda, H. Nagano and T. Misawa

- 1994** The Long Term Growth of the Protective Rust Layer Formed on Weathering Steel by Atmospheric Corrosion During a Quarter of a Century. *Corrosion Science*, Vol. 36(2): 283-299.

Zuo, J.Y., M. Pourbaix, Y.P. Liu and C.C. Xu

- 1995** Potential-pH Diagrams of Stress Effects on Occluded Cell Corrosion Inside Stress Corrosion Cracks. *Corrosion*, Vol. 51(3): 177-184.

Zucchi, F., G. Morigi and V. Bertolasi

- 1977** Beta Iron Oxide Hydroxide Formation in Localized Active Corrosion of Iron Artifacts. In *Corrosion and Metal Artifacts - A Dialogue Between Conservators and Archaeologists and Corrosion Scientists*, edited by B.F. Brown, H.C. Burnett, W.T. Chase, M. Goodway, J. Kruger and M. Pourbaix, pp. 103-105. National Bureau of Standards Special Publication No. 479. Nace, Texas.

APPENDIX 5a

Procedure used to Process Samples for Organic Weight Percent Analysis

- 1) Weigh out 5g of soil which has had the greater than 2mm particle size removed.
- 2) To sample add 5ml NaOAc, 10ml 30% hydrogen peroxide, 10ml H₂O.
- 3) Heat solution at 100°C for 15 minutes.
- 4) Remove from oven and leave for 5 days.
- 5) Rinse sample with water.
- 6) Remove water by centrifuge (Diamon/IEC Division IEC HT centrifuge) at 7000rpm for 20 minutes.
- 7) Oven dry sample (approximately 20°C).

APPENDIX 5b

Procedure for Clay Mineral Separation**Adapted from Jackson (1964) and Moore and Reynolds (1989)****centrifuge = DAMON/IEC Division IEC HT centrifuge**

- 1) Weigh out 20g of soil of particle size $<1.25\text{mm}$. Cover the 20g sample with distilled water (10:1 water:sample) and let sit for 12 hours.
- 2) Place sample in plastic beaker and disaggregate sample using an ultrasonic probe for 30 seconds using 70 watts of power.
- 3) Centrifuge sample at 2,000 rpm (rotation per minute) for 30 minutes.
- 4) Add 250ml of deionized water to sample and stir for 1 minute. Centrifuge sample at 15,000 rpm for 1 hour.
- 5) To remove organic matter, add 5ml NaOAc and 10ml of 30% hydrogen peroxide to sample. Heat mixture at 50°C for 20 minutes with regular stirring. After 20 minutes remove sample and allow to cool. Centrifuge sample at 800 rpm for 10 minutes discarding supernatant after centrifuge. Repeat #5 process three times.
- 6) Wash sample with 1M NaCl. Allow sample to sit in NaCl solution for 1 hour and repeat three times. Centrifuge between washing at 2,000 rpm for 20 minutes.
- 7) Wash sample four times with 200ml of deionized water. Centrifuge between first and second washing at 2,000 rpm for 20 minutes. Centrifuge at 15,000 rpm between other washing. Test that Cl is removed from sample using a silver nitrate test. Add (drop-wise) silver nitrate to last supernatant. If Cl is present, solution becomes clouded - continue washing until solution is clear.
- 8) Add 200ml of deionized water to sample. Add a pinch of sodium pyrophosphate to the solution and stir for a few minutes. The sodium pyrophosphate acts as a dispersing agent.
- 9) Centrifuge sample at 750 rpm for 6 minutes. Collect the top 5cm suspension. Repeat 4 times.
- 10) Centrifuge sample collected in #9 at 15,000 rpm for 20 minutes. Discard supernatant. The remaining soil will represent the clay component.

APPENDIX 6a

Figure 6.1. Map of Area B showing soil sample locations.

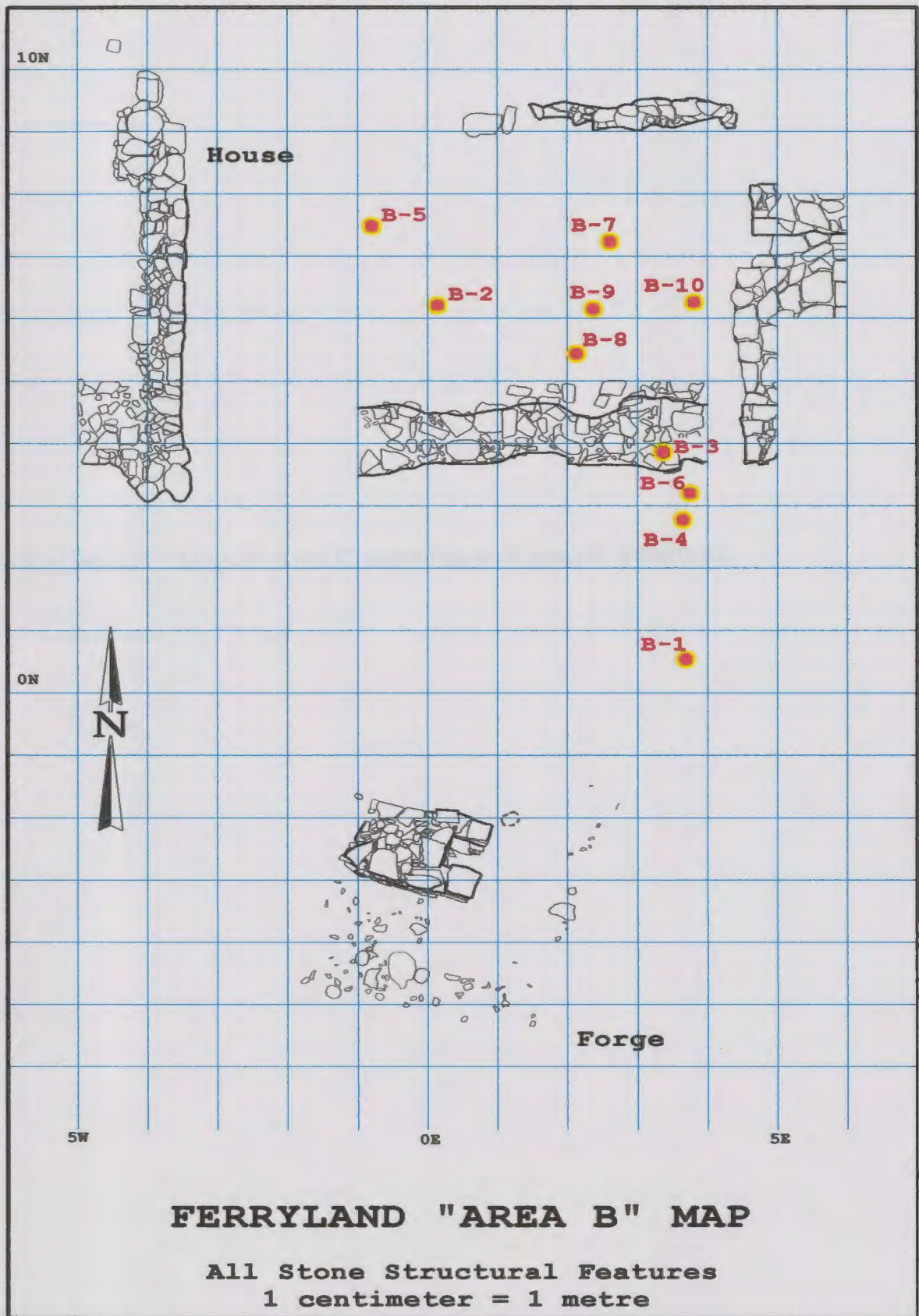


Figure 6.2. Map of Area C showing soil sample locations.

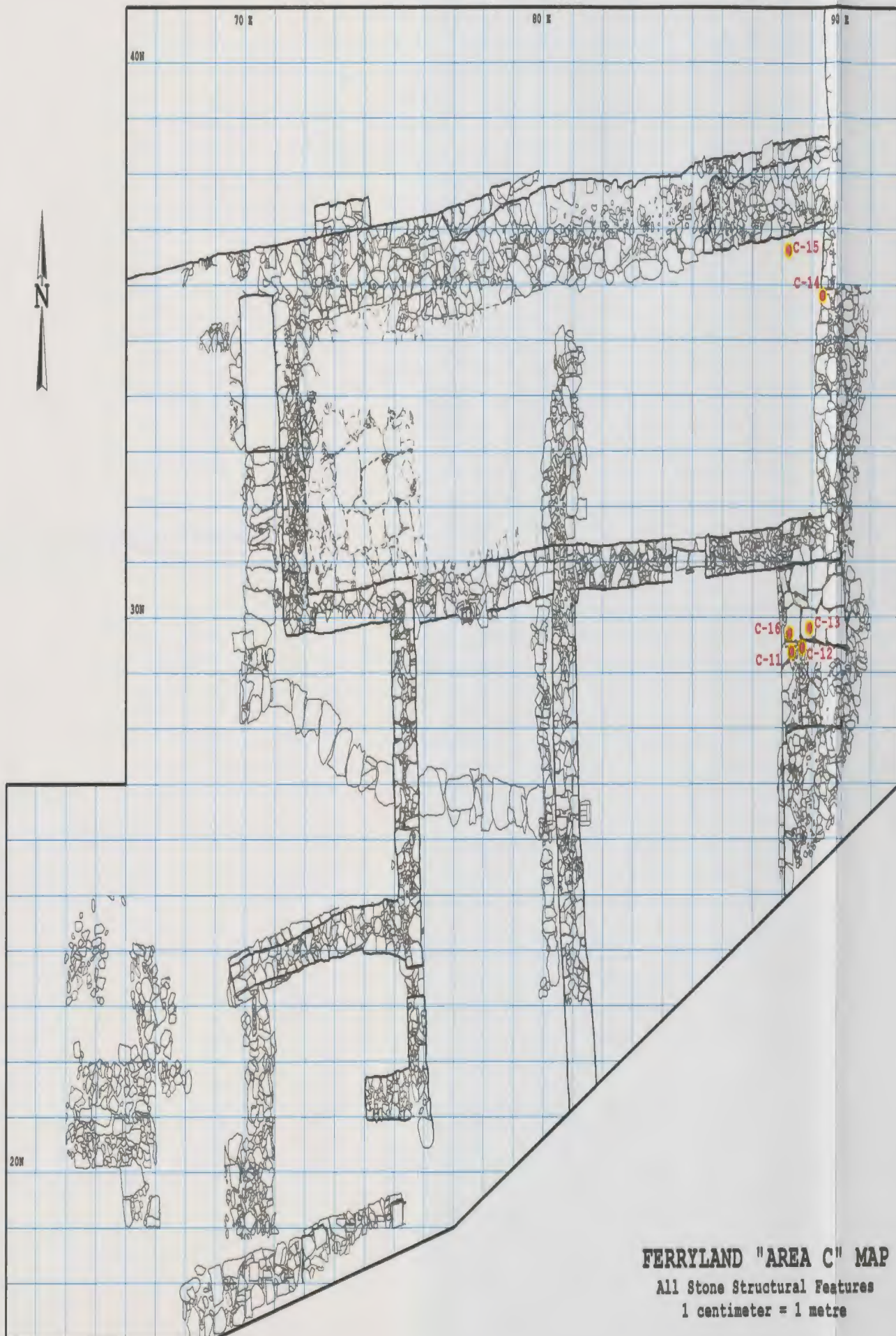
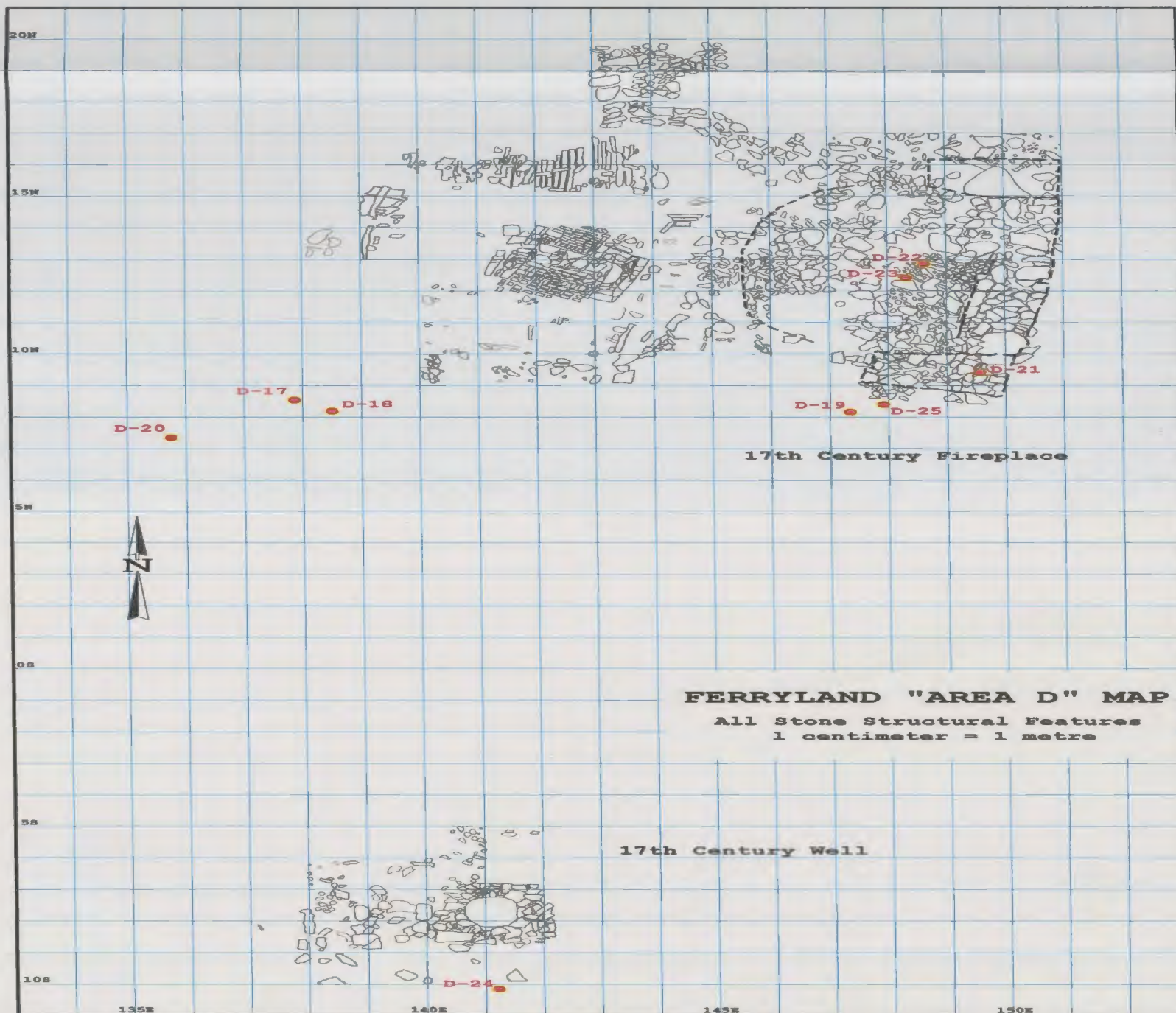


Figure 6.3 Map of Area D Showing soil sample locations.



APPENDIX 6b

Table 6.4a
Element Concentration for Soil Samples
from occupation/destruction events

Sample	Na ₂ O (wt%)	MgO (wt%)	Al ₂ O ₃ (wt%)	SiO ₂ (wt%)	P ₂ O ₅ (wt%)	S (ppm)	Cl (ppm)	K ₂ O (wt%)	CaO (wt%)	Sc (ppm)	TiO ₂ (wt%)	V (ppm)	Cr (ppm)	MnO (wt%)	Fe ₂ O ₃ (wt%)	Ni (ppm)
B-1	1.55	1.14	11.91	54.49	1.69	1316	351	2.19	0.80	16	0.94	113	49	0.11	7.94	6
B-7	1.06	0.85	8.03	39.10	4.72	3718	378	1.56	1.91	12	0.65	93	51	0.37	17.90	21
B-8	1.44	1.25	9.49	43.07	4.49	2737	427	1.78	3.14	12	0.63	100	59	0.45	14.30	19
B-10	1.45	1.29	9.96	44.93	5.50	2901	359	1.76	4.70	13	0.71	113	51	0.31	12.62	22
C-11	1.97	1.33	12.43	53.29	2.13	958	667	2.06	0.68	10	0.63	86	53	0.09	6.99	9
C-13	1.70	1.13	11.45	49.37	3.16	1914	373	1.88	0.74	15	0.76	81	49	0.09	7.82	6
C-16	1.97	1.48	12.56	56.81	1.82	689	1446	2.13	0.64	13	0.82	91	55	0.18	6.63	12
D-17	1.76	1.00	11.37	58.34	1.67	1027	393	1.95	0.91	16	0.81	93	58	0.33	6.16	<LD
D-18	2.25	1.35	13.78	64.28	2.11	946	129	2.12	1.47	14	0.86	88	50	0.30	6.75	9
D-19	2.20	1.25	12.08	57.46	1.54	1348	206	1.85	1.06	16	0.77	77	61	0.21	6.86	5
D-20	2.23	1.33	14.20	64.88	1.79	767	70	2.13	0.85	13	0.85	92	66	0.16	6.01	5
D-21	2.26	1.14	12.59	63.17	1.46	813	282	1.93	0.79	14	0.82	75	42	0.15	5.69	<LD
D-23	2.16	1.30	12.98	61.49	1.65	1729	110	1.98	1.09	14	0.83	88	70	0.16	7.47	12
LD	0.011	0.011	0.008	0.009	0.004	19	33	0.002	0.003	6	0.003	6	7	0.002	0.006	5
Mean	1.85	1.22	11.76	54.67	2.59	1605	399	1.95	1.44	14	0.77	91	55	0.22	8.70	11
standard deviation	0.39	0.26	1.73	8.38	1.40	959	352	0.18	1.20	2	0.10	12	8	0.12	3.78	6
standard error	0.14	0.09	0.72	1.83	0.33	176	67	0.12	0.14	0.6	0.06	7	2.5	0.05	0.79	1

Table 6.4b
Element Concentration for Soil Samples
from occupation/destruction events

Sample	Cu (ppm)	Zn (ppm)	Ga (ppm)	As (ppm)	Rb (ppm)	Sr (ppm)	Y (ppm)	Zr (ppm)	Nb (ppm)	Ba (ppm)	Ce (ppm)	Pb (ppm)	Th (ppm)	U (ppm)	Total (wt%)
B-1	147	65	21	16	80.7	108.4	19.6	197.7	12.5	639	111	655	4	<LD	83.40
B-7	606	286	28	19	69.9	225.7	20.3	153.5	10.2	928	127	2526	<LD	<LD	77.71
B-8	187	270	30	19	82.2	218.1	25.0	191.1	11.4	924	145	1986	<LD	<LD	81.27
B-10	469	349	23	27	68.7	333.1	20.6	157.0	9.7	786	88	1418	<LD	<LD	84.46
C-11	30	58	16	<LD	77.9	117.6	24.2	219.6	13.3	657	111	145	6	<LD	82.29
C-13	70	76	23	<LD	78.6	114.4	23.4	206.9	12.2	659	139	1248	4	<LD	78.94
C-16	35	55	22	<LD	83.4	116.3	25.0	212.7	12.9	563	121	762	5	<LD	85.62
D-17	74	73	25	<LD	87.5	140.9	20.7	208.8	12.3	822	133	1249	<LD	<LD	84.96
D-18	116	147	25	14	90.5	185.3	25.2	233.6	14.1	731	70	1050	6	<LD	95.86
D-19	47	149	17	20	68.5	138.8	23.1	194.6	12.1	1041	107	695	6	<LD	85.96
D-20	56	86	24	<LD	93.3	142.4	24.3	243.9	14.1	629	65	829	6	<LD	94.91
D-21	44	74	19	<LD	72.5	129.3	21.7	217.6	12.8	701	75	467	4	<LD	90.47
D-23	80	307	27	46	84.1	143.6	25.4	220.5	13.6	929	113	1407	6	<LD	91.96
LD	4	4	3	14	0.7	1.2	0.7	1.2	0.7	22	44	4	3	4	-----
Mean	151	153	23	23	79.8	162.6	23.0	204.4	12.4	770	108	1110	5	nil	85.99
standard deviation	180	109	4	11	8.2	63.9	2.1	26.3	1.3	148	26	640	1	nil	5.75
standard error	50	30	1	3	2.3	17.7	0.6	7.3	0.4	41	7	177	0.3		1.59

Table 6.4c
Element Concentration for Soil Samples
from fill/building events and subsoil

Sample	Na ₂ O (wt%)	MgO (wt%)	Al ₂ O ₃ (wt%)	SiO ₂ (wt%)	P ₂ O ₅ (wt%)	S (ppm)	Cl (ppm)	K ₂ O (wt%)	CaO (wt%)	Sc (ppm)	TiO ₂ (wt%)	V (ppm)	Cr (ppm)	MnO (wt%)	Fe ₂ O ₃ (wt%)	Ni (ppm)
B-2	1.73	1.19	11.07	52.56	2.39	1642	217	2.06	1.23	14	0.75	94	65	0.14	7.94	1
B-3	1.94	1.48	13.50	60.79	1.59	788	209	2.38	0.63	12	0.96	108	49	0.15	7.25	0
B-4	1.71	1.37	12.33	56.34	1.85	1108	313	2.19	0.58	12	0.88	101	47	0.16	7.48	<LD
B-5	0.69	0.80	5.69	67.92	1.62	601	100	1.08	0.47	<LD	0.25	29	33	0.19	2.14	<LD
B-6	2.23	1.50	13.21	58.28	0.91	560	157	2.30	0.69	14	0.82	85	48	0.14	6.94	7
B-9	1.47	1.02	10.40	46.83	3.89	2333	382	1.83	1.44	15	0.73	101	51	0.60	12.54	5
C-12	2.08	1.45	13.24	55.17	1.95	817	593	2.12	0.66	<LD	0.86	90	47	0.13	6.84	7
C-14	2.02	1.57	11.81	53.64	2.23	1171	784	2.15	1.39	10	0.77	88	56	0.20	7.34	8
C-15	1.97	1.49	12.71	50.95	4.20	896	462	2.11	1.76	15	0.81	92	48	0.43	8.42	15
D-22	2.00	1.71	11.68	57.72	1.54	1597	368	1.85	0.91	17	0.78	89	46	0.23	6.61	6
LD	0.011	0.011	0.008	0.009	0.004	19	33	0.002	0.003	6	0.003	6	7	0.002	0.006	5
Mean	1.78	1.36	11.56	56.02	2.22	1151	358	2.01	0.98	14	0.76	88	49	0.24	7.35	8
standard deviation	0.44	0.28	2.29	5.78	1.05	558	211	0.37	0.44	2	0.19	22	8	0.15	2.51	4
standard error	0.14	0.09	0.72	1.83	0.33	176	67	0.12	0.14	0.6	0.06	7	2.5	0.05	0.79	1
Subsoil																
D-24	2.13	1.15	14.87	70.76	0.36	225	<LD	2.25	0.31	15	0.98	107	44	0.03	3.10	<LD
D-25	2.64	1.42	13.33	62.22	1.02	311	28	2.05	0.89	15	0.77	69	38	0.13	6.04	10

Table 6.4d
Element Concentration for Soil Samples
from fill/building events and subsoil

Sample	Cu (ppm)	Zn (ppm)	Ga (ppm)	As (ppm)	Rb (ppm)	Sr (ppm)	Y (ppm)	Zr (ppm)	Nb (ppm)	Ba (ppm)	Ce (ppm)	Pb (ppm)	Th (ppm)	U (ppm)	Total (wt%)
B-2	64	103	22	9	81.7	129.2	23.1	200.4	12.3	1125	98	763	5	1	81.82
B-3	75	112	25	11	90.7	122.3	21.5	226.6	14.0	597	72	749	5	4	91.18
B-4	120	56	21	<LD	84.7	102.9	21.2	207.7	13.1	660	86	574	4	<LD	85.45
B-5	19	23	3	<LD	27.2	38.1	6.5	60.0	2.6	398	<LD	97	<LD	<LD	81.10
B-6	132	62	18	13	81.3	121.6	26.8	223.2	13.6	598	116	164	6	4	87.40
B-9	284	203	34	10	78.2	154.7	22.6	180.1	11.3	924	162	2492	<LD	<LD	81.91
C-12	32	65	16	13	77.8	118.0	26.1	217.7	13.7	661	115	136	7	3	84.98
C-14	44	184	18	14	85.3	180.5	24.2	203.0	12.3	1240	77	440	7	<LD	83.81
C-15	98	244	27	16	82.2	199.4	28.7	209.8	12.8	1178	166	1905	3	<LD	85.63
D-22	44	127	21	<LD	73.1	123.8	22.4	205.0	11.7	1002	85	817	5	<LD	85.77
LD	4	4	3	14	0.7	1.2	0.7	1.2	0.7	22	44	4	3	4	
Mean	91	118	20	12	76.2	129.0	22.3	193.3	11.7	838	109	814	5	nil	84.91
standard deviation	77	72	8	2	17.9	44.0	6.1	48.6	3.3	292	35	789	1.4	nil	3.01
standard error	24	23	2	0.6	5.7	13.9	1.9	15.4	1.0	92	11	249	0.4		0.95
Subsoil															
D-24	5	12	22	<LD	118.1	102.2	19.5	251.8	15.3	459	<LD	89	10	<LD	96.16
D-25	23	73	16	<LD	74.0	144.8	28.3	226.5	14.1	555	74	48	8	<LD	90.76

Table 6.4f
Elements probably Derived from Artifacts for Soil Samples
from occupation/destruction events

Sample	Event	Depth (cm)	S (ppm)	Cr (ppm)	Fe ₂ O ₃ (wt%)	Cu (ppm)	Zn (ppm)	As (ppm)	Pb (ppm)
B-1	133	54	1316	49	7.94	147	65	16	655
B-7	143	72-80	3718	51	17.90	606	286	19	2526
B-8	145	75-97	2737	59	14.30	187	270	19	1986
B-10	178	95-110	2901	51	12.62	469	349	27	1418
C-11	0	0-30	958	53	6.99	30	58	<LD	145
C-13	19	53-57	1914	49	7.82	70	76	<LD	1248
C-16	195	89-121	689	55	6.63	35	55	<LD	762
D-17	62	28-40	1027	58	6.16	74	73	<LD	1249
D-18	62	28-40	946	50	6.75	116	147	14	1050
D-19	62	28-40	1348	61	6.86	47	149	20	695
D-20	62	30	767	66	6.01	56	86	<LD	829
D-21	62	34-38	813	42	5.69	44	74	<LD	467
D-23	96	53	1729	70	7.47	80	307	46	1407
Mean			1605	55	8.70	151	153	23	1110
Standard Deviation			959	8	3.78	180	109	11	640

Table 6.4g
Elements probably Derived from Artifacts for Soil Samples
from fill/building events

244

Sample	Event	Depth (cm)	S (ppm)	Cr (ppm)	Fe ₂ O ₃ (wt%)	Cu (ppm)	Zn (ppm)	As (ppm)	Pb (ppm)
B-2	134	38-69	1642	65	7.94	64	103	9	763
B-3	134	55	788	49	7.25	75	112	11	749
B-4	134	57-68	1108	47	7.48	120	56	<LD	574
B-5	134	59	601	33	2.14	19	23	<LD	97
B-6	138	85-120	560	48	6.94	132	62	13	164
B-9	177	80-85	2333	51	12.54	284	203	10	2492
C-12	55	46-53	817	47	6.84	32	65	13	136
C-14	22	57	1171	56	7.34	44	184	14	440
C-15	16	85	896	48	8.42	98	244	16	1905
D-22	63	16-26	1597	46	6.61	44	127	<LD	817
Mean			1151	49	7.35	91	118	12	814
Standard Deviation			558	8	2.51	77	72	2	789

Table 6.4h
Elements Derived from Artifact vs Environment
for soils from occupation/destruction and fill/building events and subsoils

245

Element	occupation/destruction events (mean concentration)	fill/building events (mean concentration)	subsoil D-24	subsoil D-25
Elements derived from the artifacts				
S (ppm)	1605.00	1151.00	225.00	311.00
Cr (ppm)	55.00	49.00	44.00	38.00
Fe ₂ O ₃ (wt%)	8.70	7.35	3.10	6.04
Cu (ppm)	151.00	91.00	5.00	23.00
Zn (ppm)	153.00	118.00	12.00	73.00
As (ppm)	23.00	12.00	<LD	<LD
Pb (ppm)	1110.00	814.00	89.00	48.00
Elements derived from the environment				
SiO ₂ (wt%)	54.67	56.02	70.76	62.22
P ₂ O ₅ (wt%)	2.56	2.22	0.36	1.02
Cl (ppm)	399.00	358.00	<LD	28.00
CaO (wt%)	1.44	0.98	0.31	0.89
Rb (ppm)	79.80	76.20	118.10	74.00
Sr (ppm)	162.60	129.00	102.20	144.80
Ba (ppm)	770.00	838.00	459.00	555.00
Ce (ppm)	108.00	109.00	<LD	74.00

Table 6.4i
Soil Samples with Anomalous Element Concentrations
From Areas B, C and D

Sample	Event	Depth (cm)	Element	Concentration	Deviation from the mean
occupation/destruction events					
B-7	143	72-80	S (ppm)	3718.00	+2133.00
B-7	143	72-80	Fe ₂ O ₃ (wt%)	17.90	+9.20
B-7	143	72-80	Cu (ppm)	606.00	+455.00
B-7	143	72-80	Pb (ppm)	2526.00	+1416.00
B-10	178	95-110	P ₂ O ₅ (wt%)	5.50	+2.91
B-10	178	95-110	CaO (wt%)	4.70	+3.26
B-10	178	95-110	Sr (ppm)	333.10	+170.00
B-10	178	95-110	Nb (ppm)	9.70	-2.70
C-16	195	89-121	Cl (ppm)	1446.00	+1047.00
fill/building events					
B-5	134	59	SiO ₂ (wt%)	67.92	+11.90
B-5	134	59	Fe ₂ O ₃ (wt%)	2.14	-5.21
B-5	134	59	Rb (ppm)	27.20	-49.00
B-5	134	59	Sr (ppm)	38.10	-90.90
B-5	134	59	Y (ppm)	6.50	-15.80
B-5	134	59	Zr (ppm)	60.00	-133.30
B-5	134	59	Nb (ppm)	2.60	-9.10
B-5	134	59	Ga (ppm)	3.00	-17.00
B-9	177	80-85	MnO (wt%)	0.60	+0.36
B-9	177	80-85	Fe ₂ O ₃ (wt%)	12.54	+5.19
B-9	177	80-85	Cu (ppm)	284.00	+193.00
B-9	177	80-85	Pb (ppm)	2492.00	+1678.00
C-14	22	57	Cl (ppm)	784.00	+426.00
C-15	16	85	Zn	244.00	+56.00
C-15	16	85	Pb	1905.00	+1091.00

APPENDIX 6c

Table 6.5a
Chemical Analysis for Soil Solutions
from occupation/destruction events

Sample	Event	Li ppb	Be ppb	B ppb	C cps	N cps	Mg ppb	Al ppb	Si ppb	P ppb	S ppb	Cl ppb	Ca ⁴²	Ca ⁴¹
B-1	133	< 25	< 30	<12 95	2669	9875	1870 9	123 7	169	721	<1602	2952	2129	1960
B-7	143	0 83	< 30	<12 95	2151	9560	1141 0	79 2	436	1225	2495	2348	3770	3458
B-8	145	0 28	< 30	<12 95	2265	9427	371 6	61 2	235	1092	<1602	1038	1559	1442
B-10	178	0 36	< 30	<12 95	2296	9360	662 8	56 8	306	1316	<1602	1063	2107	2057
C-11	0	< 25	< 30	<12 95	1979	9163	41 1	115 9	96	1331	<1602	4939	<1250	<338
C-13	19	0 26	< 30	<12 95	1594	8345	138 8	76 4	186	1416	<1602	5066	<1250	<338
C-16	195	< 25	< 30	<12 95	1825	9770	1130 8	61 7	112	507	<1602	16432	2456	2086
D-17	62	< 25	< 30	<12 95	2446	11156	3679 9	69 2	270	536	1615	1056	6930	6626
D-18	62	< 25	< 30	<12 95	2612	10285	281 8	104 6	166	776	<1602	514	<1250	782
D-19	62	< 25	< 30	<12 95	3046	9613	346 3	126 3	196	841	<1602	618	1905	1663
D-20	62	< 25	< 30	<12 95	2870	9904	705 8	112 5	133	523	< 1602	957	<1250	1272
D-21	62													
D-23	96	0 57	< 30	<12 95	2921	10360	4679 5	158 5	272	322	2148	1040	13436	13483
SD														
SE														
LD - blank		0 25	0 30	12 95	1517	12935	7 05	1 25	66 83	26 07	1601 97	275 17	1250 28	338 267

LD=limit of detection

SD=standard deviation

SE=standard error

Table 6.5b
Chemical Analysis for Soil Solutions
from occupation/destruction events

Sample	Event	Ti ppb	V ppb	Cr ^{VI} ppb	Cr ^{III} ppb	Fe ^{III} ppb	Mn ppb	Fe ^{II} ppb	Fe ^{II} ppb	Co ppb	Ni ppb	Cu ppb	Zn ppb	As ppb
B-1	133	3.63	0.53	0.34	<0.44	55	105.04	116	91	0.85	1.58	7.31	16.83	0.51
B-7	143	3.12	1.11	0.31	<0.44	213	46.90	280	260	0.25	2.90	38.07	33.31	1.11
B-8	145	2.94	0.71	0.30	<0.42	112	44.00	176	158	0.19	0.99	10.20	11.06	1.00
B-10	178	2.95	0.98	0.35	<0.42	75	30.89	130	117	0.29	1.17	20.00	10.67	1.17
C-11	0	1.77	0.76	0.24	<0.47	23	13.89	77	68	0.20	<.75	<6.20	<7.32	0.80
C-13	19	0.94	0.99	<.22	<0.47	<14	4.43	76	53	0.15	<.75	6.49	7.96	1.05
C-16	195	<.82	0.35	<.22	<0.60	<14	354.44	<38	<23	3.88	0.89	<6.20	18.93	0.37
D-17	62	1.66	0.24	0.28	<0.42	<14	304.08	68	<46	0.75	2.39	<6.20	50.27	0.61
D-18	62	3.64	0.46	0.39	<0.41	70	44.62	118	105	0.16	1.57	18.30	9.21	0.90
D-19	62	3.00	0.52	0.73	0.68	45	105.65	106	92	0.24	1.09	10.66	24.15	4.56
D-20	62	1.92	0.30	0.38	<0.42	65	248.30	95	86	1.07	1.49	7.73	22.24	0.46
D-21	62													
D-23	96	1.21	0.11	0.41	<0.42	<14	886.46	48	<78	3.37	4.16	9.76	659.38	7.61
SD														
SE														
LD - blank		338.27	0.82	0.08	0.22	0.41	13.95	0.15	36.44	11.24	0.02	6.20	7.32	0.07

Table 6.5c
Chemical Analysis for Soil Solutions
from occupation/destruction events

Sample	Event	Br ppb	Se ppb	Rb ppb	Sr ppb	Mo ppb	Ag ppb	Cd ppb	Sn ppb	Sb ppb	I ppb	Cs ppb	Ba ppb	La ppb
B-1	133	111.38	<0.75	0.23	17.12	0.14	0.01	<0.02	0.57	0.31	3.53	<0.00	1.38	0.03
B-7	143	21.80	<0.68	1.68	39.22	0.49	0.03	0.03	1.12	0.27	5.86	0.01	1.94	0.03
B-8	145	29.90	<0.68	0.27	13.21	0.28	0.02	0.02	0.75	0.25	7.41	<0.00	1.27	0.02
B-10	178	40.42	<0.69	0.27	19.14	0.24	0.02	<0.02	0.68	0.24	7.58	0.01	0.70	0.02
C-11	0	14.32	<0.67	<0.20	0.99	1.30	0.01	<0.02	<0.31	0.14	3.76	<0.00	0.31	0.06
C-13	19	11.64	<0.67	0.20	2.45	0.200	0.02	<0.02	0.56	0.21	3.24	<0.00	0.43	0.07
C-16	195	21.05	<0.67	0.42	16.59	0.07	0.01	<0.02	0.76	0.11	1.82	<0.00	0.90	0.09
D-17	62	25.22	<0.68	0.25	94.09	0.06	0.01	0.06	<0.31	0.15	4.67	<0.00	19.73	0.02
D-18	62	24.84	<0.68	<0.20	10.14	0.16	0.01	<0.02	<0.31	0.19	8.06	<0.00	1.94	0.04
D-19	62	40.11	<0.69	<0.20	20.41	0.15	<0.01	0.07	<0.31	0.26	5.92	<0.00	12.52	0.09
D-20	62	66.64	<0.71	<0.20	19.16	0.06	<0.01	0.02	<0.31	0.14	6.19	<0.00	6.34	0.05
D-21	62													
D-23	96	51.82	1.29	0.36	145.19	0.04	0.01	2.39	<0.31	0.21	4.69	<0.00	192.88	0.08
SD														
SE														
LD - blank		8.94	0.66	0.20	0.05	0.01	0.01	0.02	0.31	0.01	0.06	0.01	0.10	0.00

Table 6.5d
Chemical Analysis for Soil Solutions
from occupation/destruction events

Sample	Event	Ce ppb	Hg ppb	Tl ppb	Pb ppb	Bi ppb	U ppb
B-1	133	0.08	<0.12	<0.02	2.20	<0.01	0.02
B-7	143	0.07	<0.12	<0.02	15.00	<0.01	0.01
B-8	145	0.06	<0.12	<0.02	16.95	<0.01	0.01
B-10	178	0.07	<0.12	<0.02	4.81	<0.01	0.01
C-11	0	0.22	<0.12	<0.02	0.50	<0.01	0.03
C-13	19	0.29	<0.12	0.02	4.51	<0.01	0.01
C-16	195	0.31	<0.12	0.03	1.96	<0.01	<0.00
D-17	62	0.05	<0.12	<0.02	2.86	<0.01	0.01
D-18	62	0.08	<0.12	<0.02	3.20	<0.01	0.02
D-19	62	0.18	<0.12	<0.02	3.78	<0.01	0.03
D-20	62	0.13	<0.12	<0.02	2.67	<0.01	0.03
D-21	62						
D-23	96	0.15	0.18	<0.02	14.05	<0.01	0.02
SD							
SE							
LD - blank		0.00	0.12	0.02	0.13	0.01	0.01

Table 6.5e
Chemical Analysis for Soil Solutions
from fill/building events and subsoil

Sample	Event	Li 7 ppb	Be ppb	B ppb	C cps	N cps	Mg ppb	Al ppb	Si ppb	P ppb	S ppb	Cl ppb	Ca ⁴¹ ppb	Ca ⁴¹ ppb
B-2	134	<25	<30	<12.95	2826	10080	2193.5	133.8	153	642	<1602	1780	4806	4662
B-3	134	<25	<30	<12.95	2305	9849	905.0	92.2	172	971	<1602	1691	1910	1835
B-4	134	<25	<30	<12.95	2019	9844	886.4	74.6	72	303	<1602	1074	<1250	1190
B-5	134	<25	<30	<12.05	1969	9327	350.7	64.2	<67	538	<1602	635	<1250	964
B-6	138	<25	<30	<12.95	2096	9642	251.3	92.8	126	426	<1602	1871	<1250	415
B-9	177	<25	<30	<12.95	2410	9082	372.1	92.7	165	1092	<1602	2240	<1250	877
C-12	55	<25	<30	<12.95	1807	9279	148.5	66.6	69	653	3147	6788	<1250	<338
C-14	22	<25	<30	<12.95	2065	8945	148.9	64.0	161	792	<1602	33109	<1250	388
C-15	16	<25	<30	<12.95	1933	9171	41.8	94.3	300	1686	<1602	10049	<1250	<338
D-22	63	0.49	<30	<12.95	4021	8630	2475.1	269.7	167	1080	1797	5630	3451	3419
Mean					2345	9385	777	105	154	818		6487		1719
SD					658	458	873	62	68	405		9834		1540
SE														
Subsoils														
D-24	88	0.78	0.30	<12.95	2441	8742	295.0	185.8	155	530	<1602	773	<1250	497
D-25	141	<25	<30	<12.95	2241	9916	189.1	193.0	257	948	<1602	476	<1250	874
LD - blank		0.25	0.30	12.95	1517	12935	7.05	1.25	66.83	26.07	1601.97	275.17	1250.28	338.27

Table 6.5f
Chemical Analysis for Soil Solutions
from fill/building events and subsoil

Sample	Event	Ti ppb	V ppb	Cr ^{VI} ppb	Cr ^{III} ppb	Fe ^{III} ppb	Mn ppb	Fe ^{II} ppb	Fe ^I ppb	Co ppb	Ni ppb	Cu ppb	Zn ppb	As ppb
B-2	134	2.47	0.57	0.42	<0.43	30	559.67	77	72	3.57	2.14	7.33	83.26	0.51
B-3	134	4.15	0.38	0.29	<0.43	43	160.48	92	89	0.62	1.75	8.93	20.40	0.52
B-4	134	1.88	0.20	<.22	<0.42	<14	176.03	47	42	0.78	1.58	7.80	27.15	0.20
B-5	134	1.63	0.34	<.22	<0.42	25	430.56	77	73	1.03	0.88	7.58	14.64	0.37
B-6	138	3.02	0.57	0.31	<0.43	36	31.70	92	74	0.52	<.75	20.07	9.85	0.34
B-9	177	3.17	0.78	0.33	<0.43	85	262.70	139	130	0.67	2.32	28.31	16.96	0.81
C-12	55	1.36	0.44	<.22	<0.49	<14	64.15	46	41	0.88	<.75	<6.20	11.89	0.40
C-14	22	1.92	0.84	0.28	1.37	<14	55.12	64	56	0.25	<.75	<6.20	14.27	0.93
C-15	16	3.99	1.20	0.33	0.70	49	11.67	108	94	0.17	<.75	6.58	<7.32	2.32
D-22	63	2.04	0.43	0.71	<0.47	50	1212.21	82	86	2.50	2.08	11.33	90.62	0.96
Mean		2.56	0.57	0.38		45	296	82	76	1.10	1.79	12.24	32.12	0.74
SD		0.98	0.29	0.15		20	369	28	26	1.08	0.52	7.83	31.54	0.61
SE														
Subsoils														
D-24	88	8.86	0.59	0.47	<0.42	78	9.30	143	125	0.34	<.75	<6.20	8.04	0.45
D-25	141	6.08	0.65	0.40	<0.41	96	14.62	150	130	0.18	<.75	6.63	<7.32	1.35
I.D - blank		338.27	0.82	0.82	0.22	0.41	13.95	0.15	36.44	11.24	0.02	6.20	7.32	0.07

Table 6.5g
Chemical Analysis for Soil Solutions
from fill/building events and subsoil

Sample	Event	Br ppb	Se ppb	Rb ppb	Sr ppb	Mo ppb	Ag ppb	Cd ppb	Sn ppb	Sb ppb	I ppb	Cs ppb	Ba ppb	La ppb
B-2	134	39.28	<0.69	0.34	57.64	0.14	<0.01	0.09	0.38	0.13	3.11	<0.00	31.32	0.04
B-3	134	19.54	<0.67	<0.20	24.50	0.15	<0.01	<0.02	<0.31	0.16	5.88	<0.00	0.69	0.04
B-4	134	9.13	<0.66	<0.20	12.02	0.07	<0.01	0.03	<0.31	0.09	2.04	<0.00	2.31	0.04
B-5	134	15.51	<0.67	0.41	8.78	0.09	0.01	0.04	<0.31	0.13	2.36	<0.00	2.81	0.05
B-6	138	53.78	<0.70	0.20	3.87	0.29	<0.01	<0.02	<0.31	0.15	4.86	<0.00	0.26	0.06
B-9	177	60.55	<0.71	0.24	11.04	0.20	0.01	0.02	0.70	0.25	8.27	<0.00	2.07	0.04
C-12	55	<9	<0.68	<0.20	3.45	0.09	0.01	<0.02	1.05	0.10	2.17	<0.00	0.54	0.07
C-14	22	33.52	<0.68	<0.20	9.01	0.23	<0.01	<0.02	0.84	0.16	7.18	<0.00	8.41	0.03
C-15	16	31.05	<0.68	0.67	2.21	0.61	0.02	<0.02	1.14	0.24	16.39	<0.00	1.38	0.07
D-22	63	65.31	1.22	0.38	41.18	0.16	0.02	0.22	<0.31	0.16	6.69	<0.00	78.44	0.17
Mean		36.40		0.37	17.37	0.20	0.01	0.04	0.82	0.16	5.89		12.82	0.06
SD		20.09		0.17	18.43	0.16	0.01	0.07	0.30	0.05	4.32		24.90	0.04
SE														
Subsoils														
D-24	88	59.10	<0.71	0.22	6.45	0.11	0.01	<0.02	<0.31	0.09	4.98	<0.00	1.25	0.10
D-25	141	36.68	<0.69	<0.20	7.45	0.22	0.02	<0.02	0.45	0.16	5.04	<0.00	0.41	0.09
L.D. - blank		8.94	0.66	0.20	0.05	0.01	0.01	0.02	0.31	0.01	0.06	0.01	0.10	0.00

Table 6.5h
Chemical Analysis for Soil Solutions
from fill/building events and subsoil

Sample	Event	Ce ppb	Hg ppb	Tl ppb	Pb ppb	Bi ppb	U ppb
B-2	134	0.10	<0.12	<0.02	7.45	<0.01	0.03
B-3	134	0.12	0.14	<0.02	3.87	<0.01	0.01
B-4	134	0.09	<0.12	<0.02	1.74	<0.01	0.01
B-5	134	0.12	<0.12	<0.02	1.32	<0.01	0.02
B-6	138	0.29	<0.12	<0.02	1.22	<0.01	0.01
B-9	177	0.11	<0.12	<0.02	12.75	<0.01	0.02
C-12	55	0.27	<0.12	<0.02	0.34	<0.01	0.01
C-14	22	0.08	<0.12	0.06	0.77	<0.01	0.02
C-15	16	0.21	<0.12	0.03	8.25	<0.01	0.03
D-22	63	0.36	<0.12	<0.02	10.56	<0.01	0.05
Mean		0.17			4.83		0.02
SD		0.10			4.55		0.01
SE							
Subsoils							
D-24	88	0.31	<0.12	<0.02	1.62	<0.01	0.04
D-25	141	0.44	<0.12	<0.02	0.68	<0.01	0.02
LD - blank		0.00	0.12	0.02	0.13	0.01	0.01

APPENDIX 7a

Figure 7.2a. Location of iron nail samples from Area B.

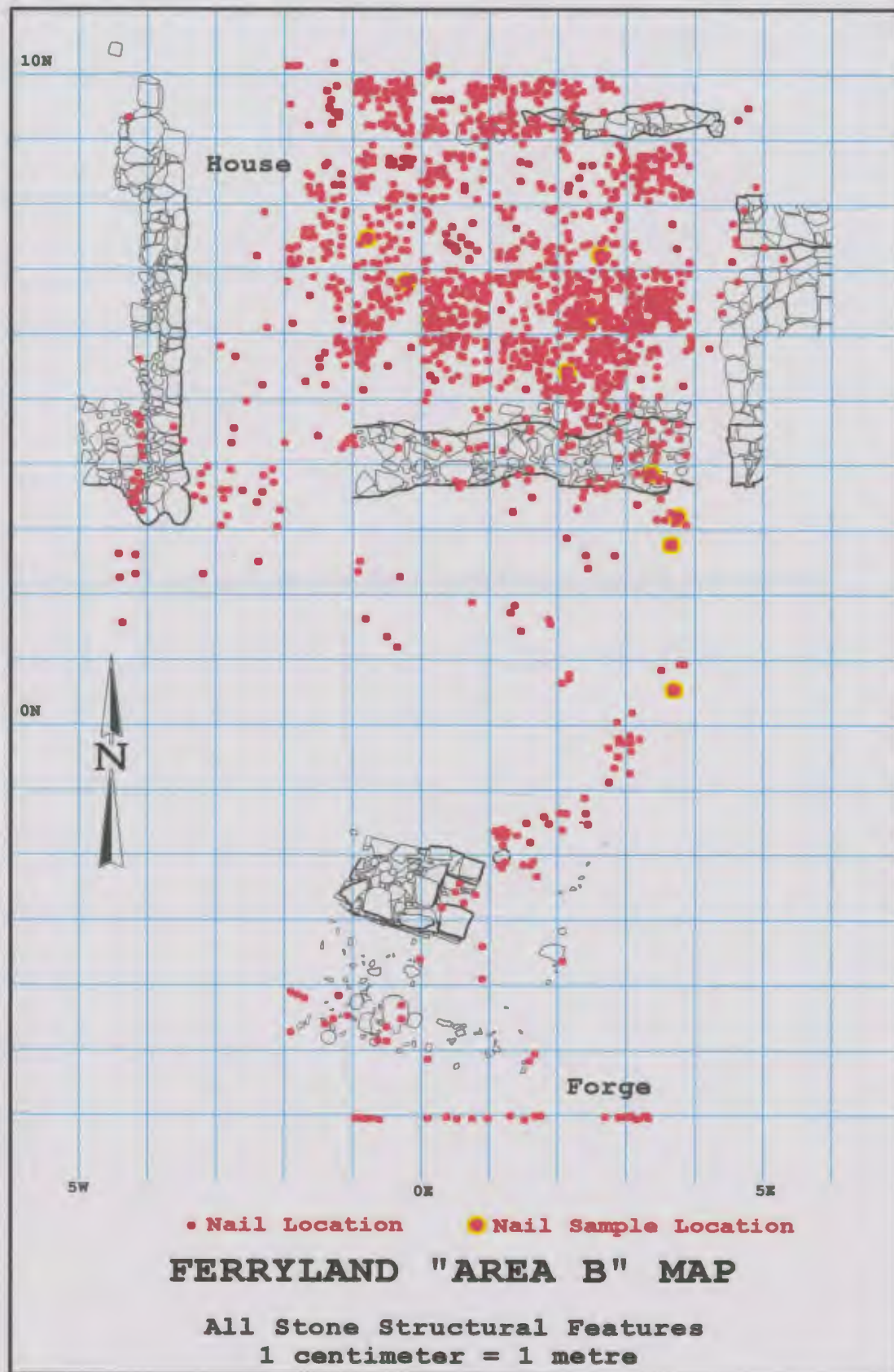


Figure 7.2b. Location of iron nail samples from Area B used for detailed analysis.

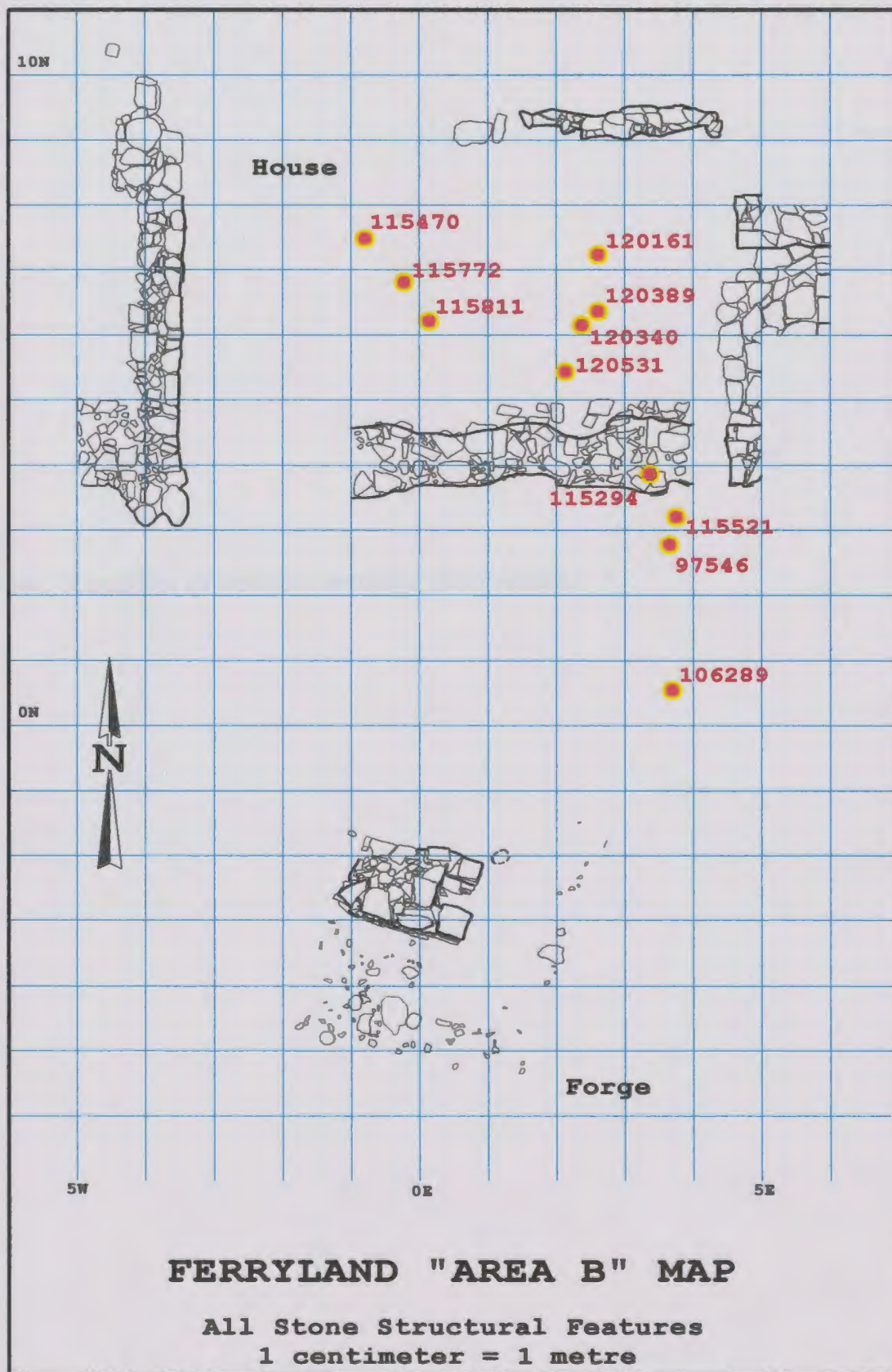


Figure 7.3a. Location of iron nail samples from Area C.



Figure 7.3b. Location of iron nail samples from Area C used for detailed analysis.



Figure 7.4a. Location of iron nail samples from Area D.

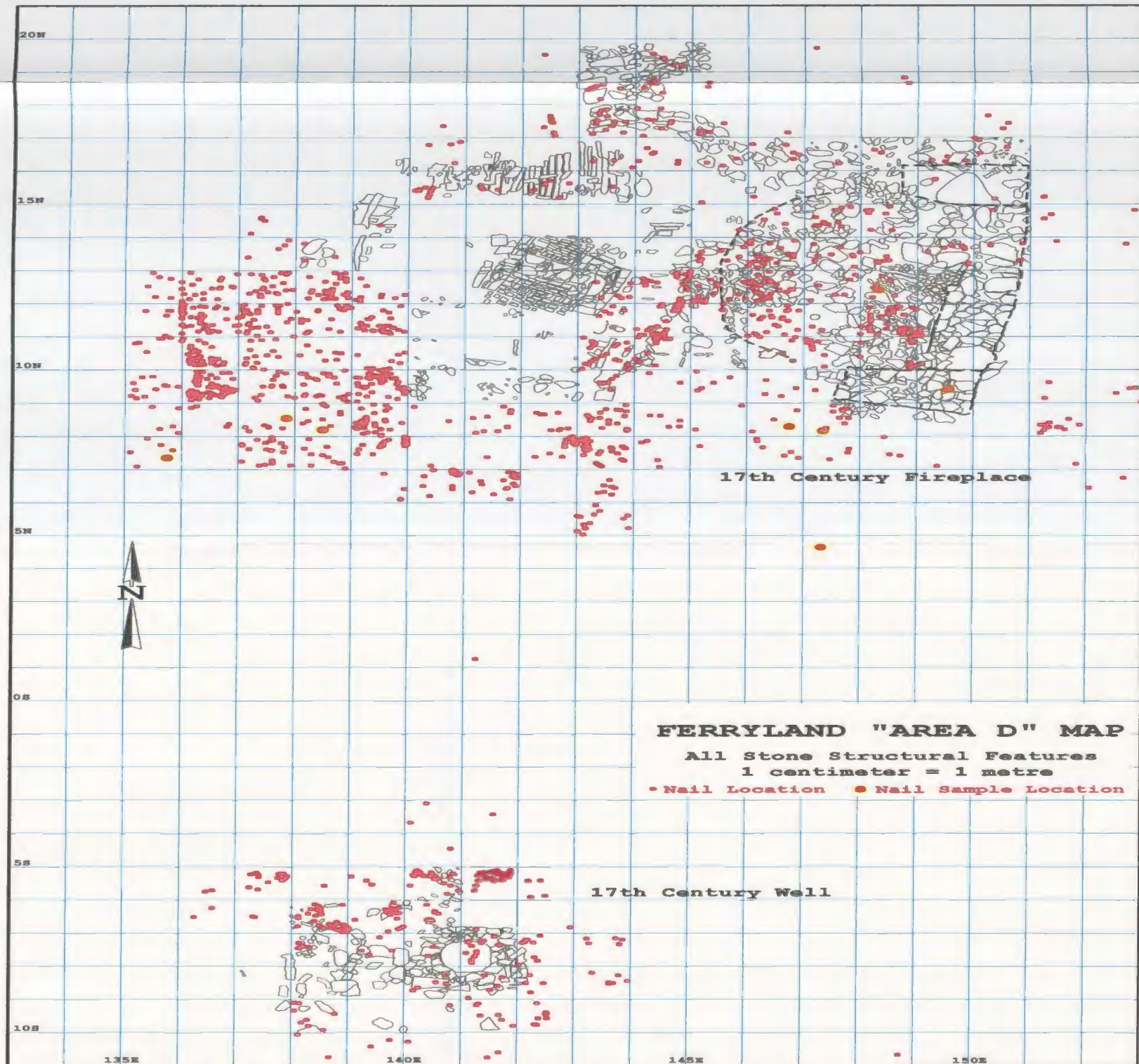
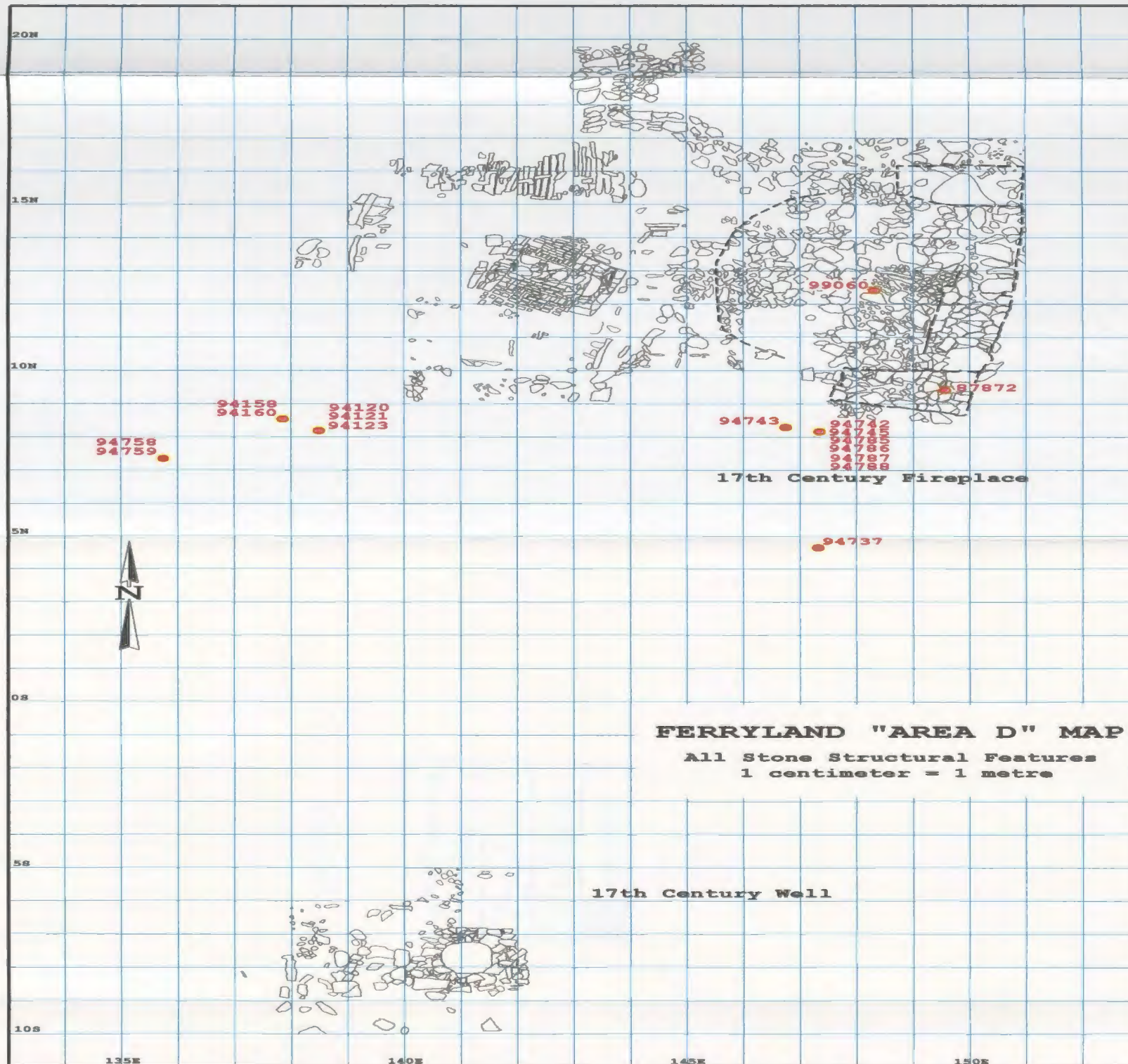





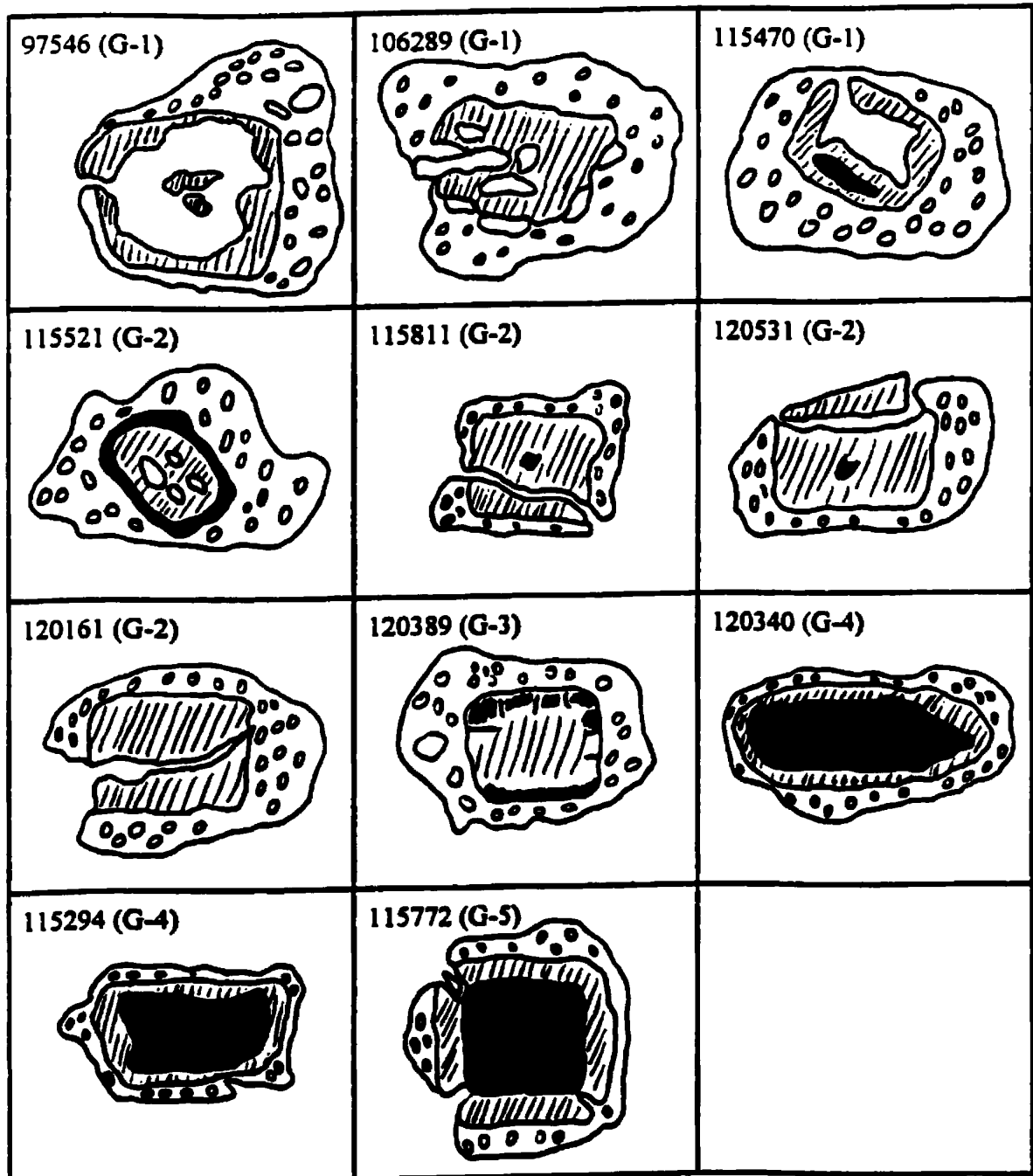
Figure 7.4b. Location of iron nail samples from Area D used for detailed analysis.



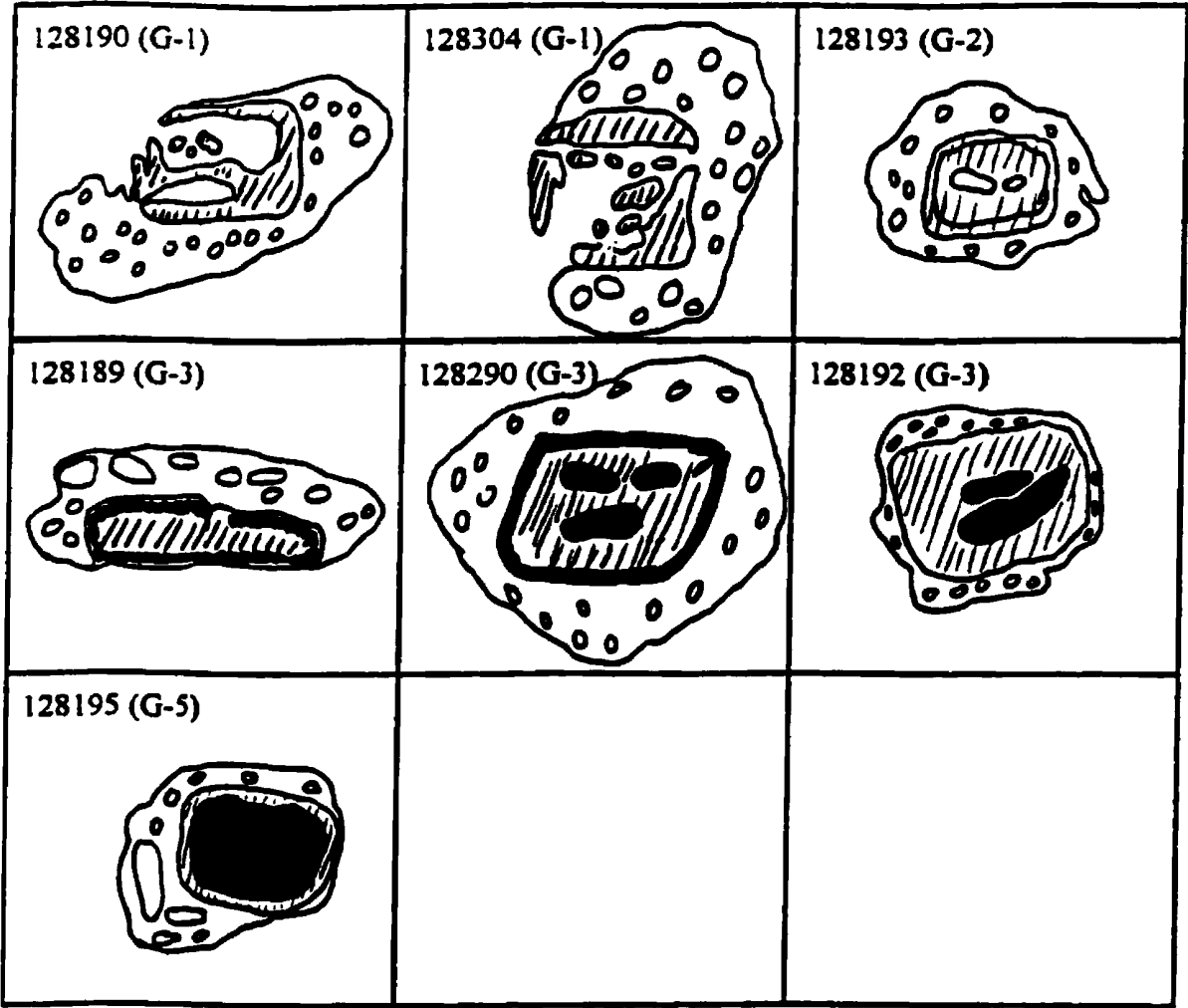
APPENDIX 7b

Key for nail cross section sketches	
	corrosion halo
	multi-phase iron
	single phase iron

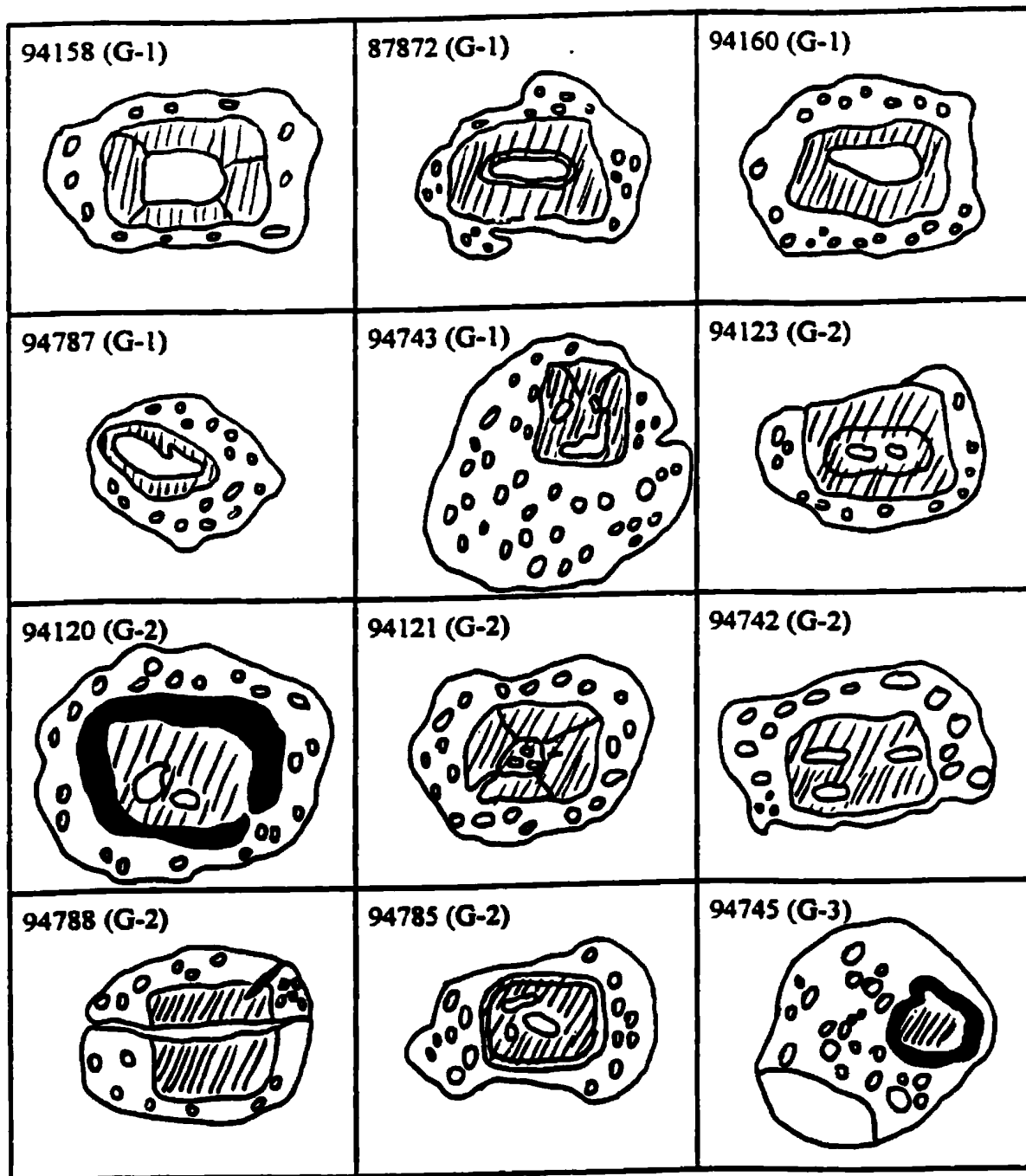
Area B
Sketches of Nail Shaft Cross Sections

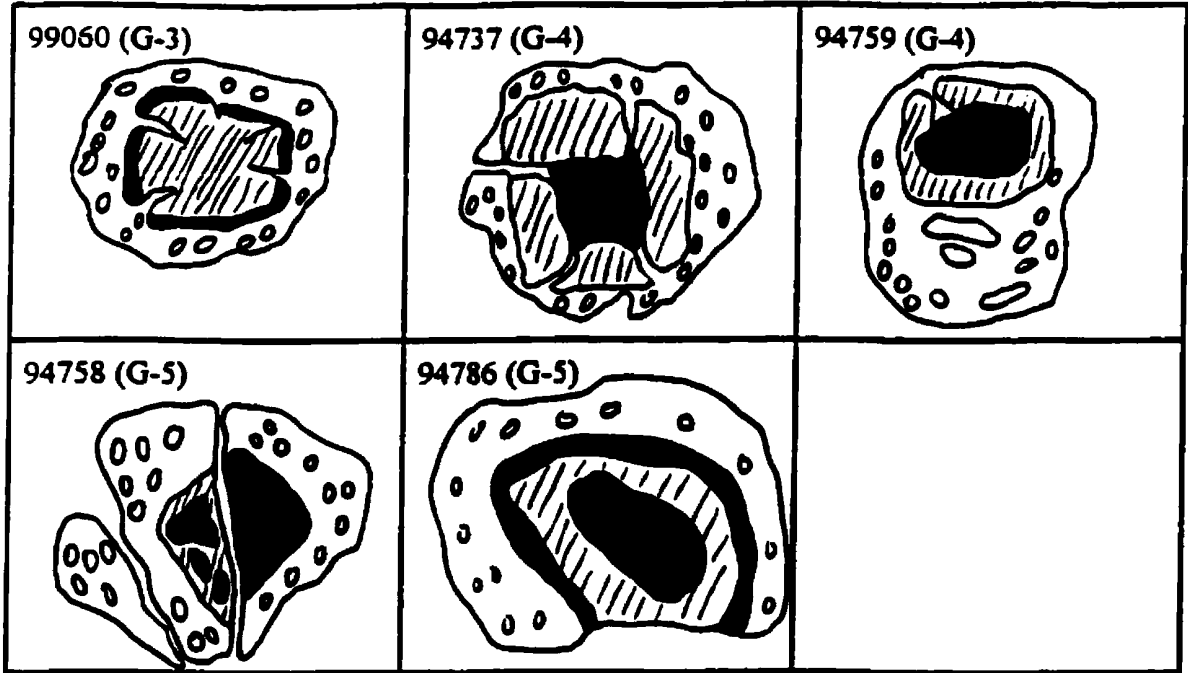


Area C
Sketches of Nail Shaft Cross Sections



Area D
Sketches of Nail Shaft Cross Sections





APPENDIX 7c

Table 7.3.3b
Identification of Mineral Inclusions in Corrosion Halo for Nail 97546

Point location on nail cross-section	S (wt%)	P(wt%)	Al(wt%)	Si(wt%)	Fe(wt%)	Ca(wt%)	K(wt%)	Mg(wt%)	Mn(wt%)	Na (wt%)	O(wt%)	Total	Identification
b-grain	0.00	0.00	9.92	30.54	2.70	0.15	0.23	0.10	0.00	7.94	47.26	98.73	albite
c-grain	0.01	0.00	10.43	31.86	0.69	0.12	0.01	0.15	0.01	8.46	48.76	100.32	albite
d-grain	0.08	0.01	0.28	0.58	7.05	0.17	0.02	0.21	0.02	0.00	3.13	11.41	w/i
e-grain	0.01	0.00	9.48	29.94	0.26	0.07	13.80	0.11	0.03	0.11	45.40	98.73	alkali feldspar
f-grain	0.01	0.00	0.32	42.63	4.56	0.00	0.00	0.02	0.00	0.00	50.16	97.67	quartz
g-grain	0.18	0.00	0.25	0.75	8.82	0.07	0.04	0.06	0.00	0.00	3.70	13.70	w/i
h-grain	0.01	0.00	1.08	43.77	2.37	0.00	0.00	0.40	0.00	0.03	51.77	99.40	quartz

Table 7.3.3c
Chemical Analysis of Iron Core and Corrosion Halo for Nail 128193

Point location on nail cross-section	S(wt%)	P(wt%)	Al(wt%)	Si(wt%)	Fe(wt%)	Ca(wt%)	K(wt%)	Mg(wt%)	Mn(wt%)	Na(wt%)	Cl(wt%)	O(wt%)	Total
a- corrosion halo matrix	0.04	5.13	1.31	0.00	13.09	0.12	0.10	0.14	0.00	0.00	0.15	11.59	31.39
b- same as above	0.04	2.22	0.33	0.25	54.18	0.02	0.02	0.08	0.00	0.00	0.07	18.96	76.00
c- same as above	0.09	0.84	0.36	0.35	52.48	0.00	0.03	0.09	0.00	0.00	0.08	16.83	70.94
d- feldspar	0.04	0.00	9.67	31.61	1.75	0.12	0.22	0.31	0.00	7.47	0.02	47.97	99.00
e- iron	0.09	0.25	0.03	0.22	65.84	0.00	0.09	0.02	0.00	0.00	0.17	19.43	85.91
f- iron near centre void	0.30	0.47	0.06	0.08	51.51	0.00	0.05	0.02	0.00	0.00	2.21	15.52	70.00
g- iron near centre void	0.10	0.25	0.05	0.05	52.93	0.01	0.00	0.04	0.02	0.00	7.33	15.48	75.99
h- iron	0.13	0.01	0.20	0.05	52.47	0.03	0.00	0.06	0.00	0.00	1.56	15.28	69.64
i- iron	0.11	0.45	0.05	1.49	60.21	0.85	0.04	0.10	0.22	0.00	0.15	19.53	81.84
j- iron/ corrosion interface	0.43	3.44	3.31	7.84	33.45	0.07	0.91	0.16	0.00	1.78	0.64	26.94	78.74
k- feldspar	0.01	0.00	4.91	27.48	1.78	0.00	1.24	0.45	0.04	2.19	0.21	37.50	75.76
m- feldspar	0.05	0.05	6.60	36.32	1.71	0.06	0.25	0.16	0.01	5.21	0.12	49.60	99.80
n- feldspar	0.01	0.000	5.94	35.63	2.27	0.00	1.49	0.47	0.12	2.20	0.20	47.90	96.09

Table 7.3.3d
Chemical Analysis of Iron Core and Corrosion Halo for Nail 120389

Point location on nail cross-section	S(wt%)	P(wt%)	Al(wt%)	Si(wt%)	Fe(wt%)	Ca(wt%)	K(wt%)	Mg(wt%)	Mn(wt%)	Na(wt%)	Cl(wt%)	O(wt%)	Total
a- corrosion halo matrix	0.13	2.99	1.79	4.54	33.63	0.75	0.49	0.37	0.06	0.09	0.07	21.00	65.84
c- corrosion halo matrix	0.07	1.92	0.73	3.85	38.12	0.24	0.12	0.13	0.14	0.00	0.06	18.55	63.59
d- iron/corrosion interface	0.03	0.30	0.01	0.12	43.22	2.08	0.03	0.05	0.42	0.00	0.02	13.85	59.99
e- iron	0.07	0.32	0.00	0.29	68.40	0.02	0.03	0.04	0.00	0.00	0.00	20.34	89.34
f- iron	0.18	0.53	0.14	0.48	60.50	0.10	0.00	0.00	0.00	0.00	0.04	18.77	80.60
g- iron	0.09	0.33	0.00	0.24	64.00	0.03	0.00	0.00	0.00	0.00	0.03	19.03	83.59
h- iron	0.18	0.56	0.14	0.15	59.03	0.00	0.00	0.00	0.16	0.00	0.09	18.02	78.18
i- iron	0.04	0.01	0.18	0.28	54.69	0.00	0.00	0.00	0.07	0.00	0.02	16.15	71.30
j- iron	0.03	0.02	0.04	0.40	69.60	0.02	0.02	0.02	0.00	0.00	0.00	20.39	90.38
k- iron	0.10	3.43	1.30	3.61	48.67	0.37	0.07	0.13	0.13	0.00	0.03	23.79	81.17
l- feldspar	0.02	0.35	5.39	30.21	11.58	0.06	1.93	0.54	0.05	1.74	0.02	44.34	96.08

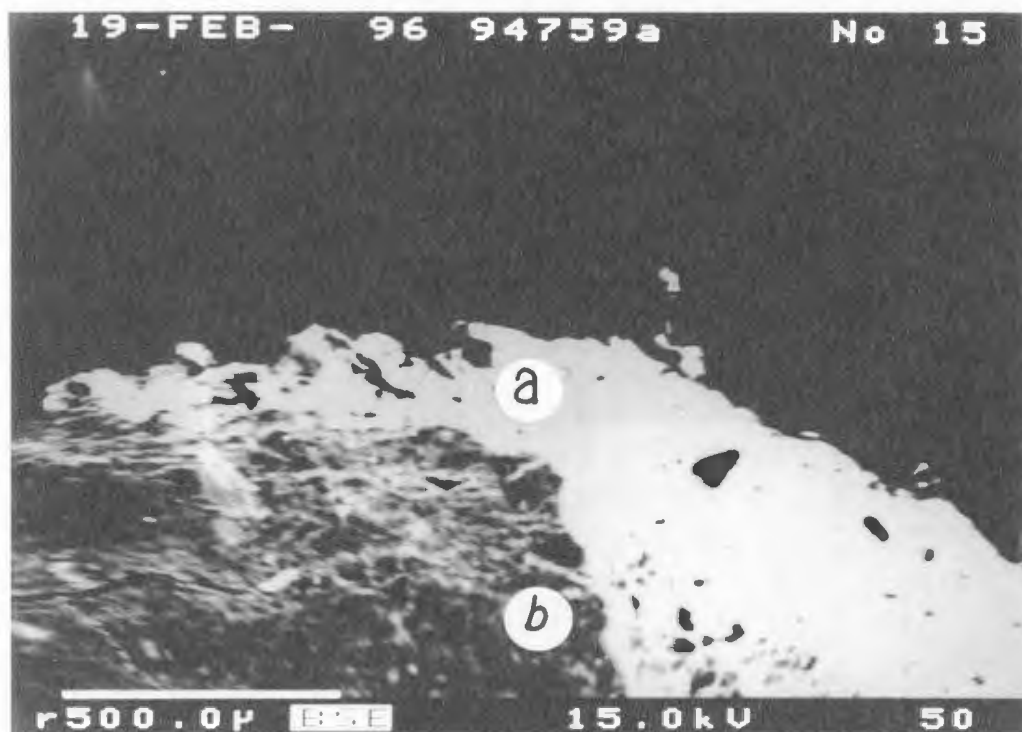
Table 7.3.3e
Identification of Mineral Inclusions in Corrosion Halo for Nail 115470

Point location on nail cross-section	S wt%	P wt%	Al wt%	Si wt%	Fe wt%	Ca wt%	K wt%	Mg wt%	Mn wt%	Na wt%	O wt%	Total	Identification
a-grain	0.03	0.00	10.59	31.66	0.15	0.29	0.00	0.11	0.09	8.34	48.51	99.39	albite
b-grain	0.33	0.00	4.58	40.40	0.44	0.00	0.63	0.13	0.00	2.97	51.39	100.41	feldspar
c-grain	0.04	0.00	0.50	45.42	0.17	0.00	0.00	0.05	0.00	0.04	52.20	98.16	quartz
d-grain	0.00	0.00	10.35	30.75	2.10	0.22	0.06	0.16	0.00	8.10	47.73	92.24	feldspar
e-grain	0.02	0.00	0.14	46.36	0.48	0.00	0.00	0.00	0.00	0.00	53.07	100.04	quartz
f-corrosion halo matrix	0.09	1.46	1.97	7.74	22.73	0.01	0.40	0.15	0.00	0.66	19.28	54.24	w/ iron corrosion
g-corrosion halo matrix	0.10	1.35	5.71	9.77	19.82	0.05	2.01	0.68	0.03	1.89	24.55	64.06	w/ iron corrosion
h-grain	0.00	0.00	0.35	46.19	0.29	0.00	0.00	0.06	0.07	0.00	53.02	99.84	quartz
i-corrosion halo matrix	0.12	0.71	4.45	14.17	24.61	0.12	0.64	0.09	0.01	3.02	29.36	77.19	w/ iron corrosion
j-same as above	0.20	1.34	2.51	12.53	35.30	0.14	0.38	0.18	0.01	0.46	28.86	81.90	w/ iron corrosion
k-same as above	0.24	1.15	3.42	8.31	36.51	0.18	0.91	0.41	0.00	0.03	25.11	76.25	w/ iron corrosion
l-same as above	0.26	0.60	0.73	2.30	27.57	0.15	0.04	0.12	0.00	0.00	12.13	43.74	w/
m-same as above	0.07	0.03	2.81	6.57	1.66	0.01	1.12	0.39	0.00	0.27	11.04	23.85	w/
n-same as above	0.39	0.77	3.87	7.10	33.95	0.13	1.12	0.30	0.05	0.51	23.09	71.23	w/ iron corrosion
p-iron/corrosion interface	0.09	2.12	0.54	0.67	46.17	0.22	0.08	0.02	0.03	0.00	17.29	67.00	w/ iron corrosion
q-grain	0.02	0.00	0.51	46.20	0.29	0.00	0.00	0.00	0.00	0.00	53.17	100.17	quartz
r-grain	0.01	0.00	0.19	46.79	0.32	0.00	0.00	0.01	0.00	0.00	53.56	100.86	quartz
s-grain	0.06	0.06	11.25	23.63	8.70	0.02	4.22	1.78	0.05	1.56	41.99	93.12	feldspar
t-grain	0.05	0.01	7.58	32.20	4.81	0.06	1.45	1.24	0.04	2.65	46.83	96.76	feldspar
u-grain	0.05	8.24	2.44	9.55	23.89	0.26	0.83	0.22	0.05	0.00	30.95	76.37	feldspar

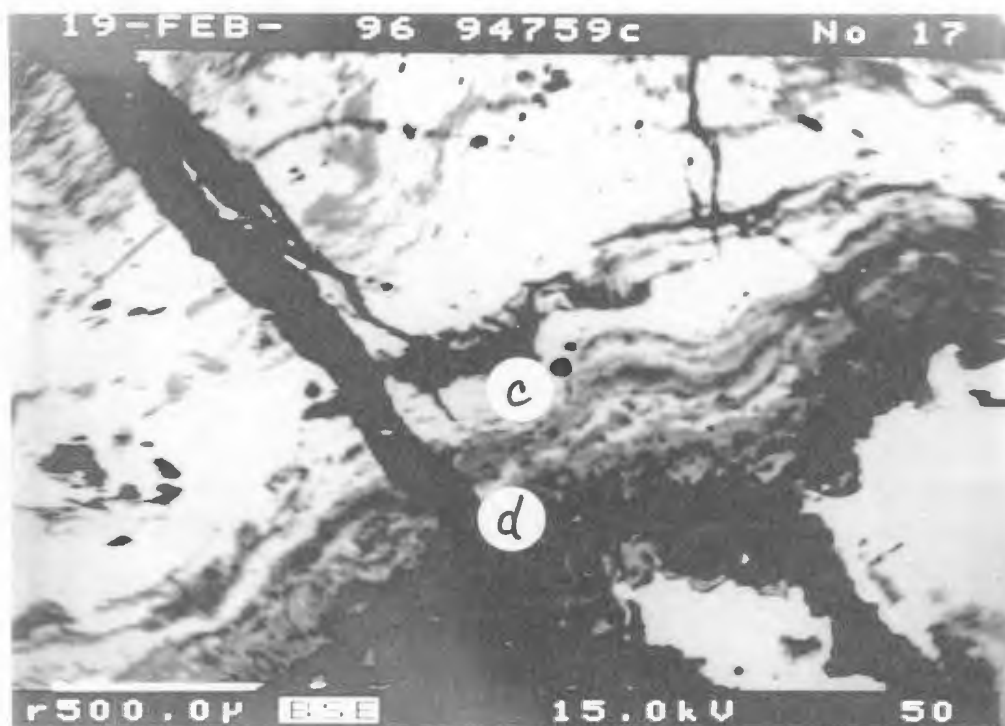
Table 7.3.3f
Chemical Analysis of Iron Core and Corrosion Halo for Nail 94759

273

Point location on nail cross-section	S wt%	P wt%	Al wt%	Si wt%	Fe wt%	Ca wt%	K wt%	Mg wt%	Mn wt%	Na wt%	Cl wt%	O wt%	Total
a- corrosion halo matrix	0.06	3.02	1.57	2.53	52.00	0.09	0.41	0.19	0.02	0.00	0.04	23.29	83.01
b-feldspar	0.06	0.00	3.07	36.38	4.86	0.00	0.14	0.71	0.07	0.48	0.00	46.23	91.87
c-iron /corrosion interface	0.16	0.00	0.01	0.11	67.79	0.00	0.02	0.00	0.00	0.00	0.00	19.50	87.59
d-iron /corrosion interface	0.49	0.00	0.24	0.02	53.75	0.00	0.00	0.06	0.00	0.00	4.70	15.86	75.03
f- iron	0.00	0.00	1.02	0.03	0.60	0.00	0.01	0.02	0.00	0.01	2.43	1.08	5.14
g- iron	0.08	0.00	0.02	0.67	61.05	0.03	0.01	0.00	0.02	0.00	0.09	18.26	80.08
h-iron/ corrosion interface	0.21	0.77	1.19	10.46	43.93	0.03	0.19	0.02	0.08	0.57	0.03	26.90	84.21
i- iron/ corrosion interface	0.20	0.14	0.05	1.00	60.75	0.00	0.01	0.01	0.00	0.00	0.06	18.83	80.97
j- quartz	0.04	0.00	0.16	46.65	0.93	0.00	0.00	0.03	0.00	0.00	0.00	53.56	101.30
k- corrosion halo matrix	0.18	1.83	2.77	4.85	51.49	0.01	0.91	0.31	0.06	0.08	0.06	25.62	88.17
m- corrosion halo matrix	0.26	1.56	4.18	7.47	43.18	0.04	1.21	0.40	0.06	0.00	0.20	27.25	85.71
n- feldspar	0.00	0.00	10.77	33.01	0.83	0.03	0.02	0.02	0.02	7.17	0.02	49.92	101.70



Nail 94759
point a - iron oxide in corrosion halo
point b - feldspar grain



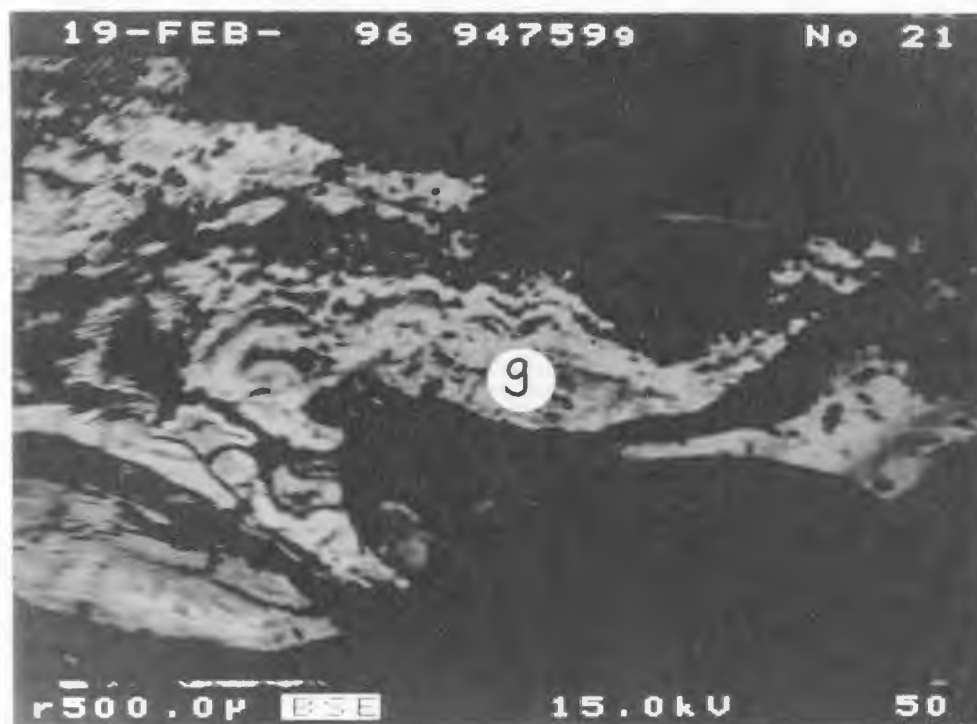
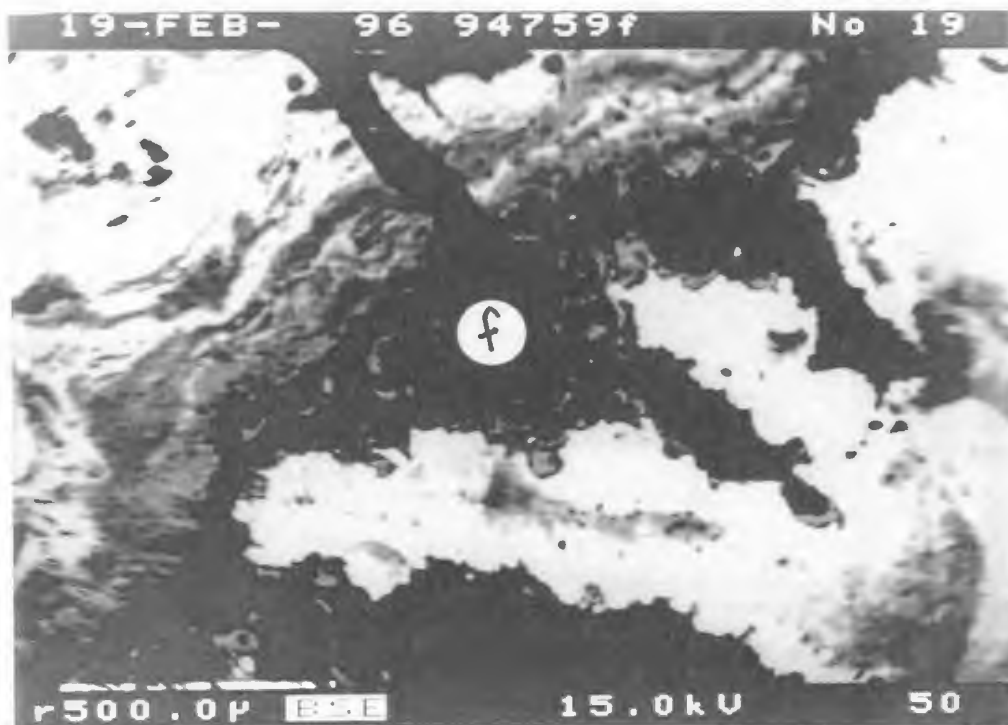
Nail 94759

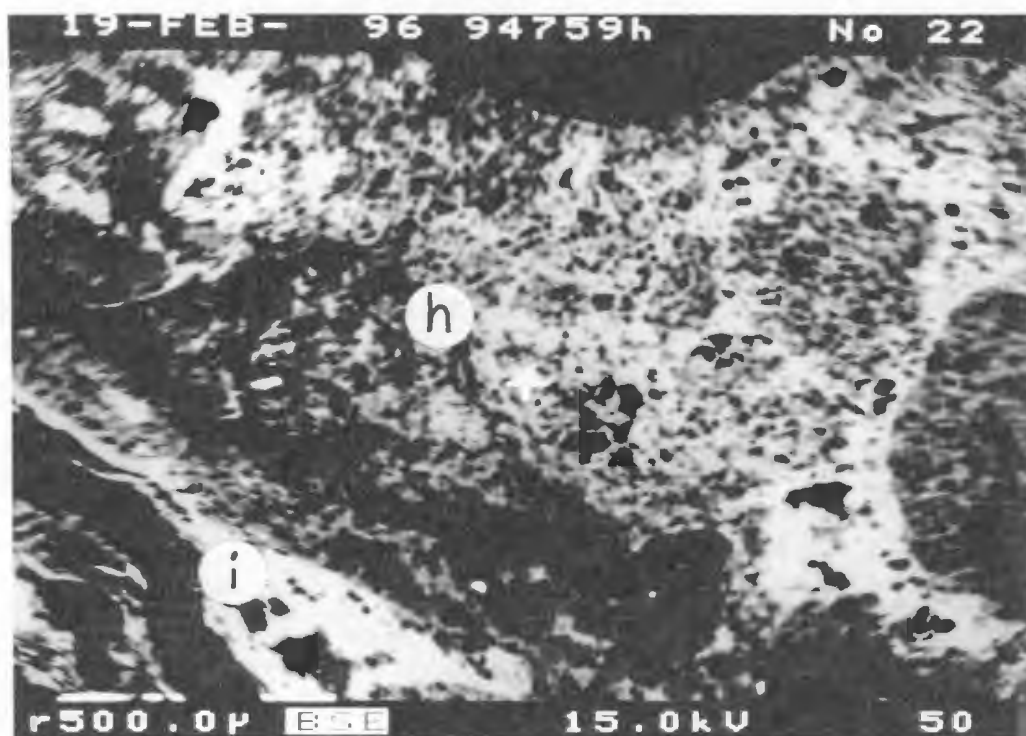
point c - iron/corrosion interface

point d - iron/corrosion interface

Nail 94759
point f
area of high chlorine concentration in
nail centre

Nail 94759
point g
iron



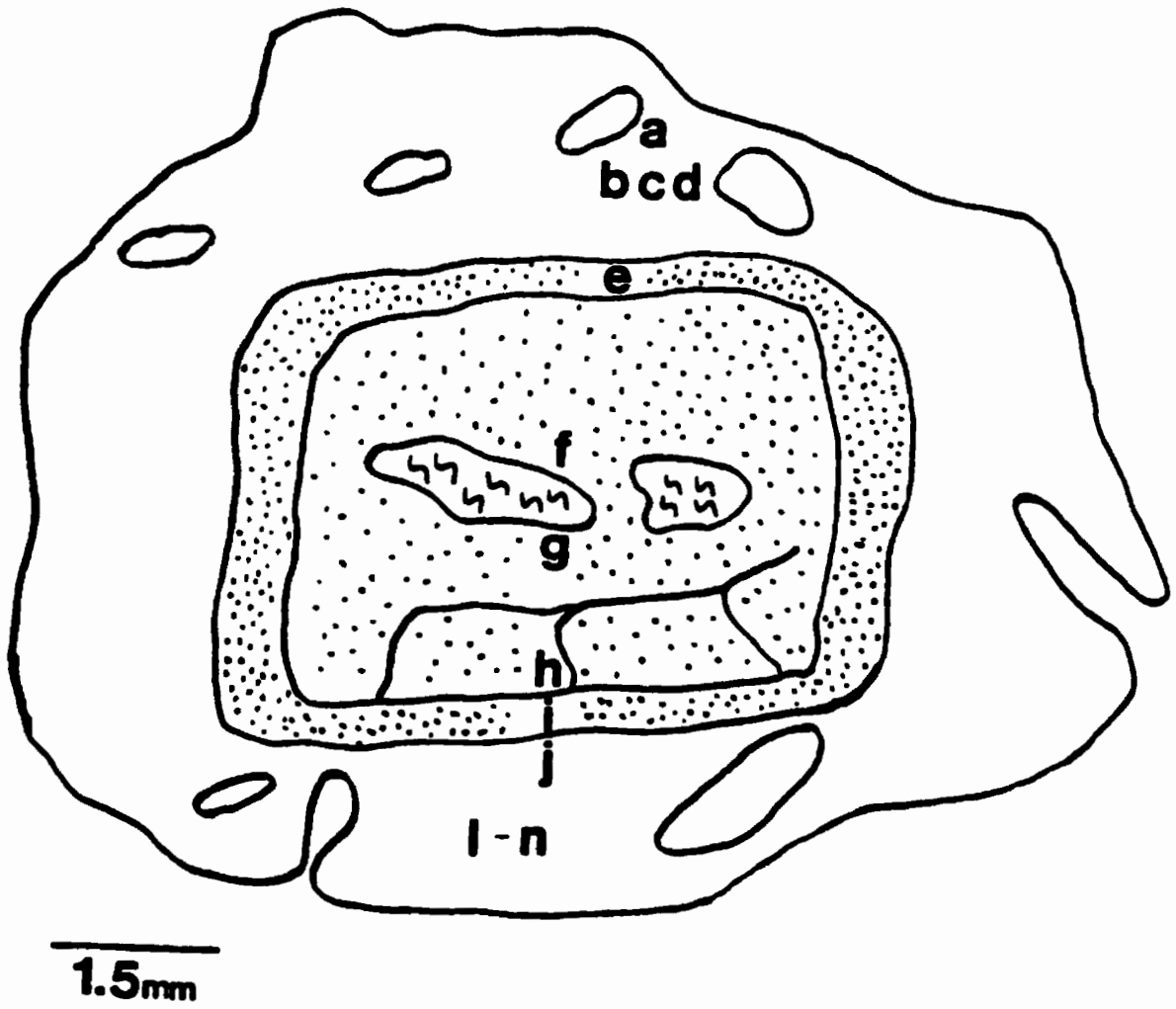


Nail 94759

point h - iron/corrosion interface

point i - iron/corrosion interface

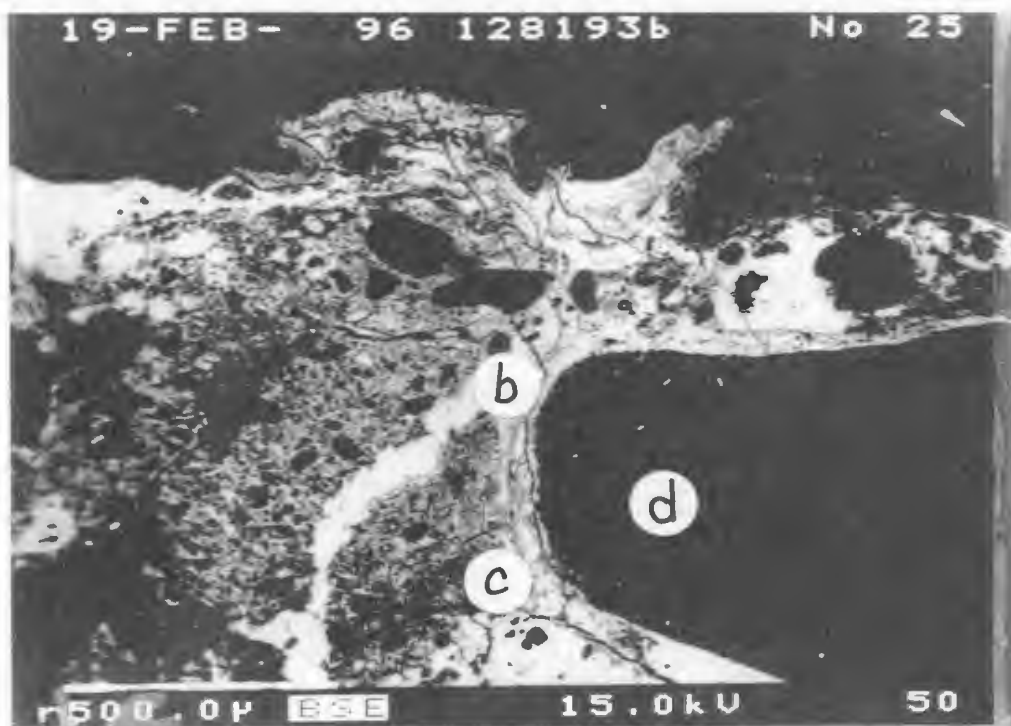
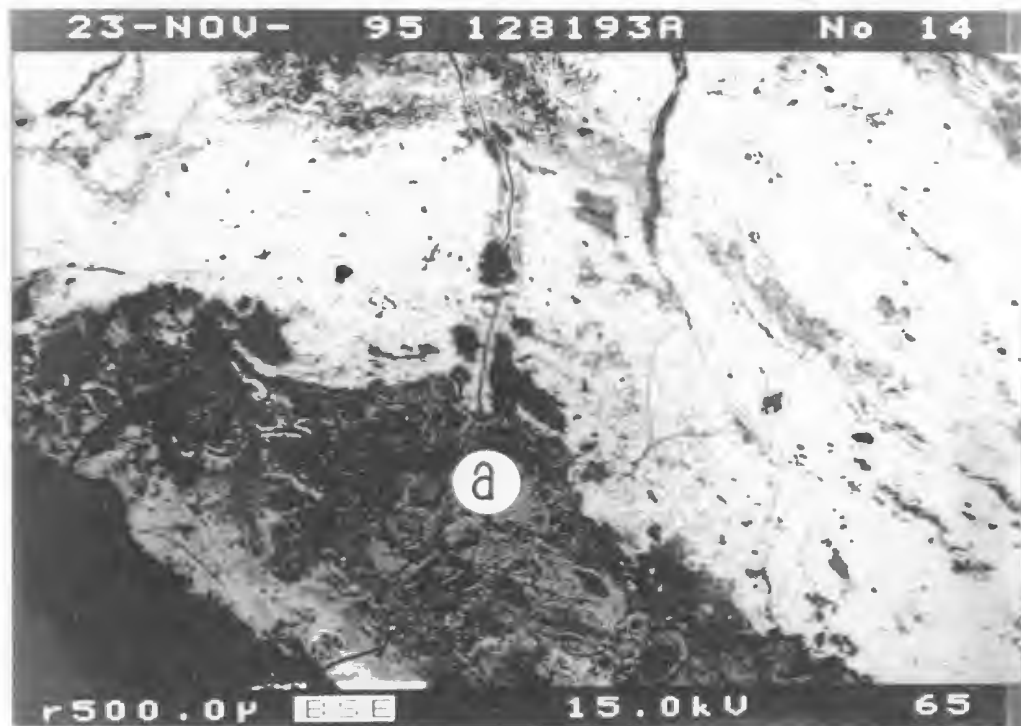
128193
Area C
Event 0
Metallographic Group G-1
occupation/destruction classification



Nail 128193
 point locations
 multi-phase iron
 void

Nail 128193
point a
corrosion halo matrix

Nail 128193
point b - iron in corrosion halo
point c - iron next to grain in corrosion halo
point d - feldspar grain



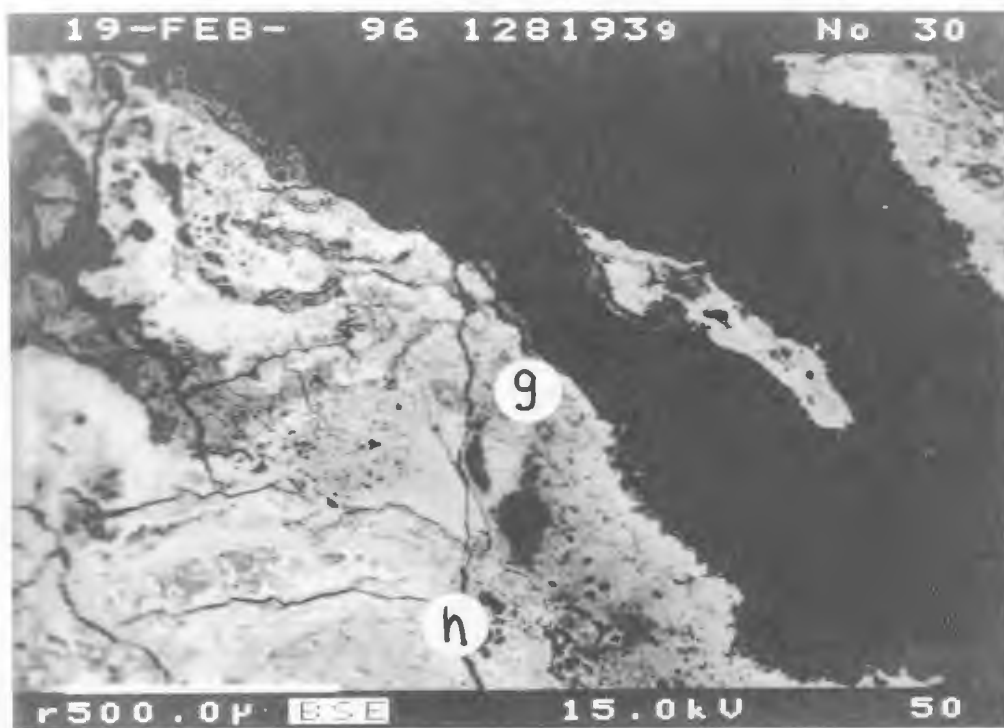
Nail 128193
point e
iron

Nail 128193
point f
iron near centre void



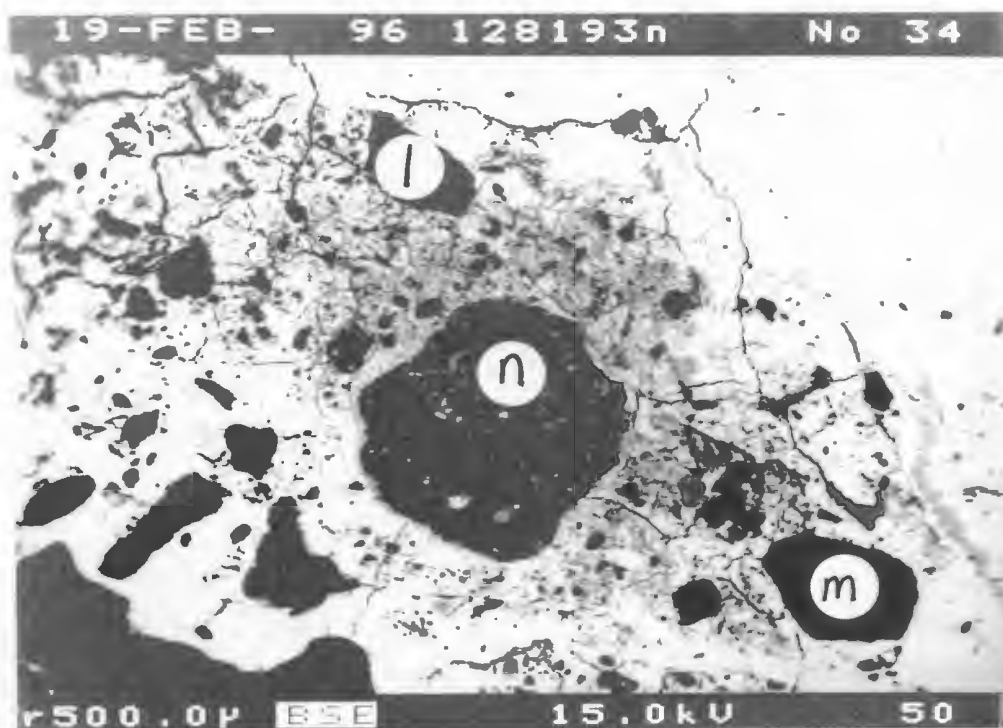
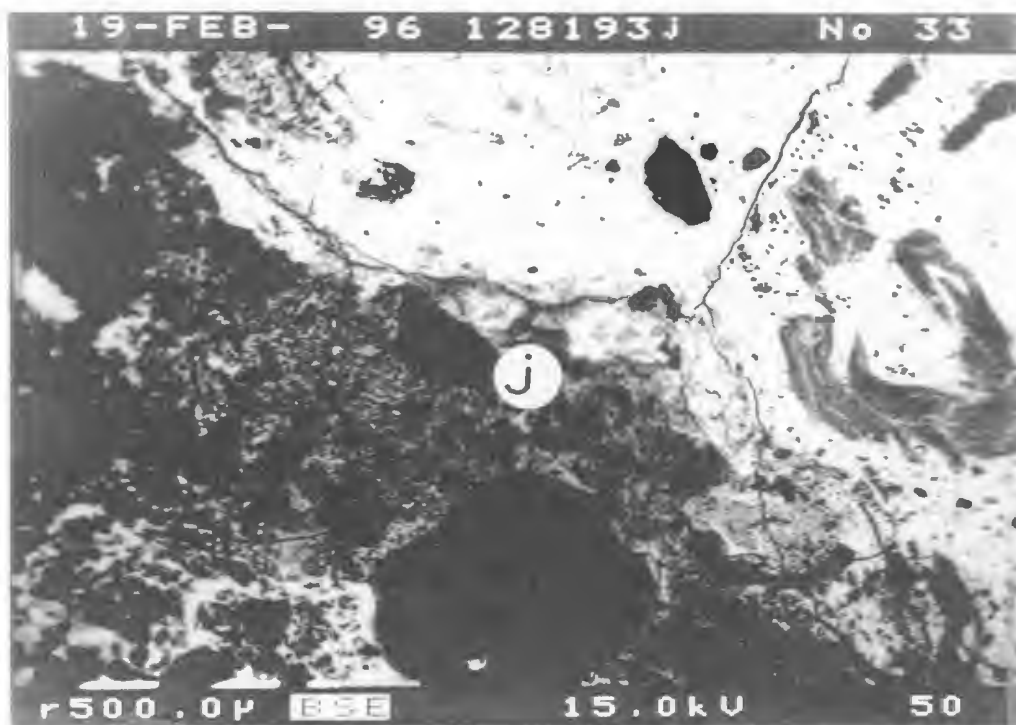
Nail 128193
point g - iron near centre void
point h - iron

Nail 128193
point i
iron at edge of nail

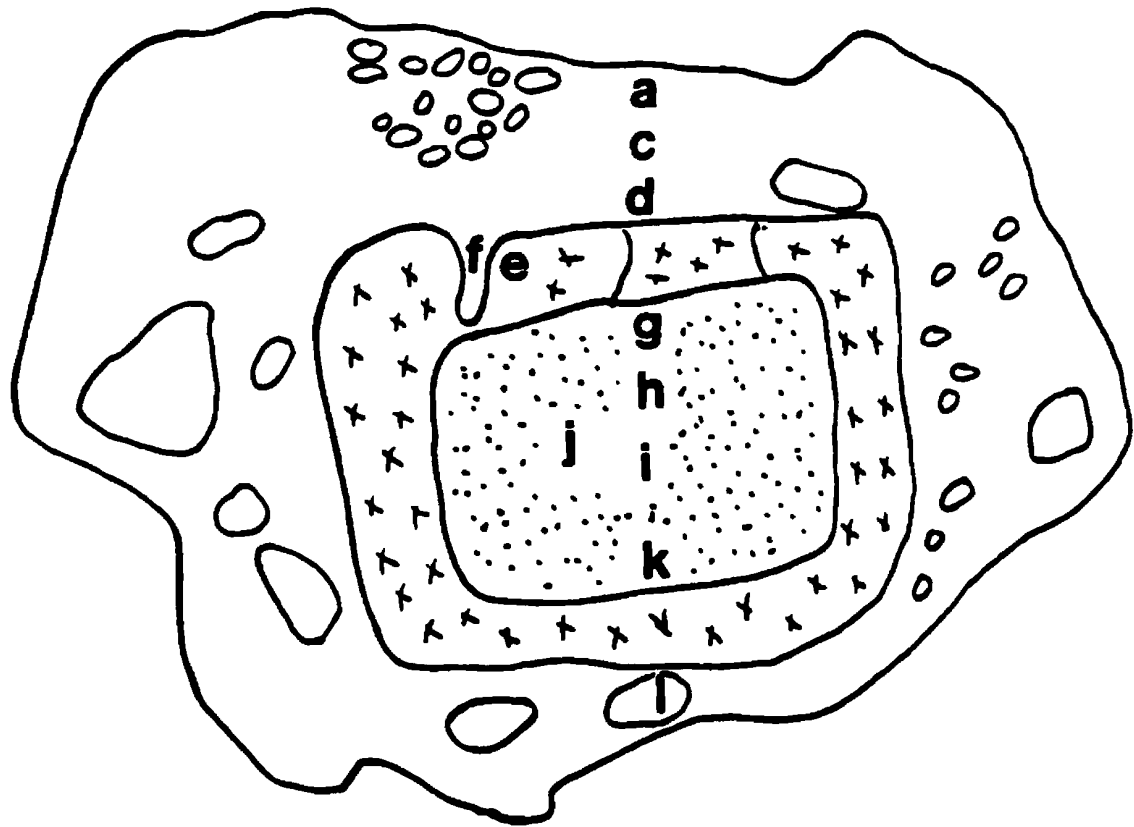


**Nail 128193
point j**



**Nail 128193
points l, m and n
grains in corrosion halo**



120389
Area B
Event 178
Metallographic Group G-1
occupation/destruction



2mm

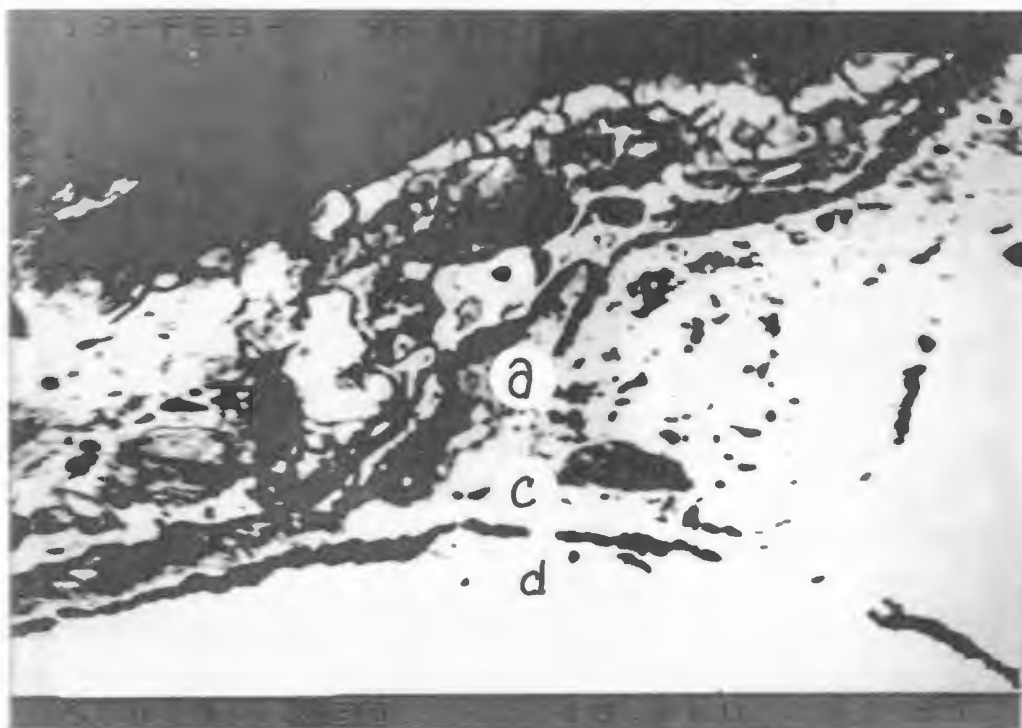
Nail 120389
point locations
single phase iron 
multi-phase iron 

Nail 120389

points a and c - edge of corrosion halo
point d - iron/corrosion halo interface

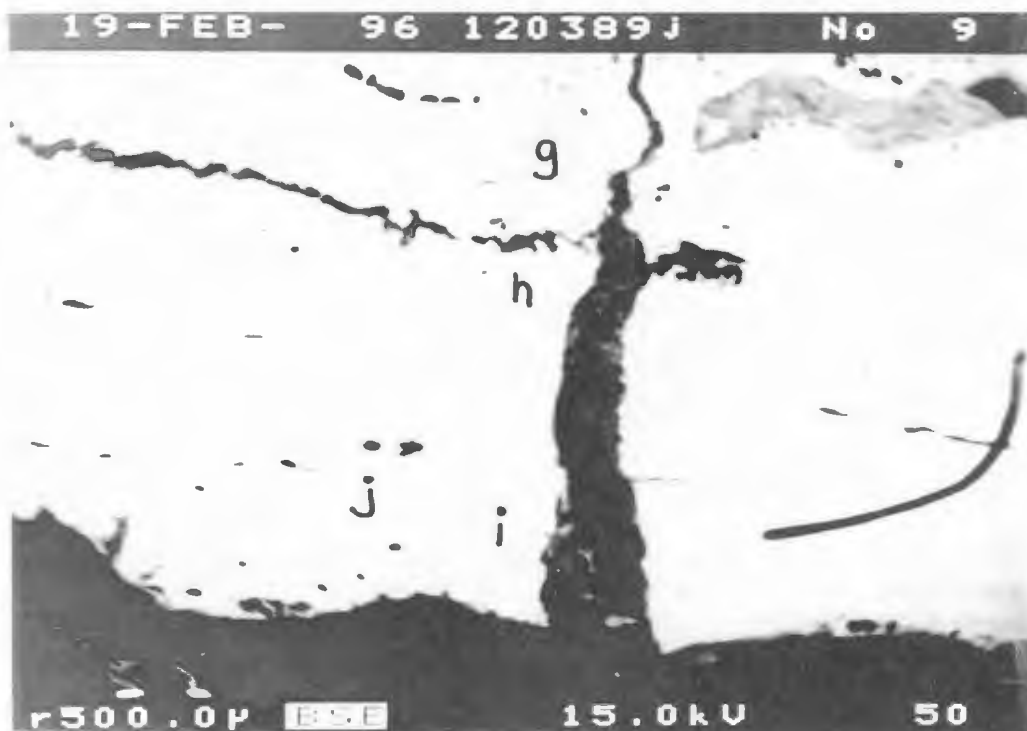
Nail 120389

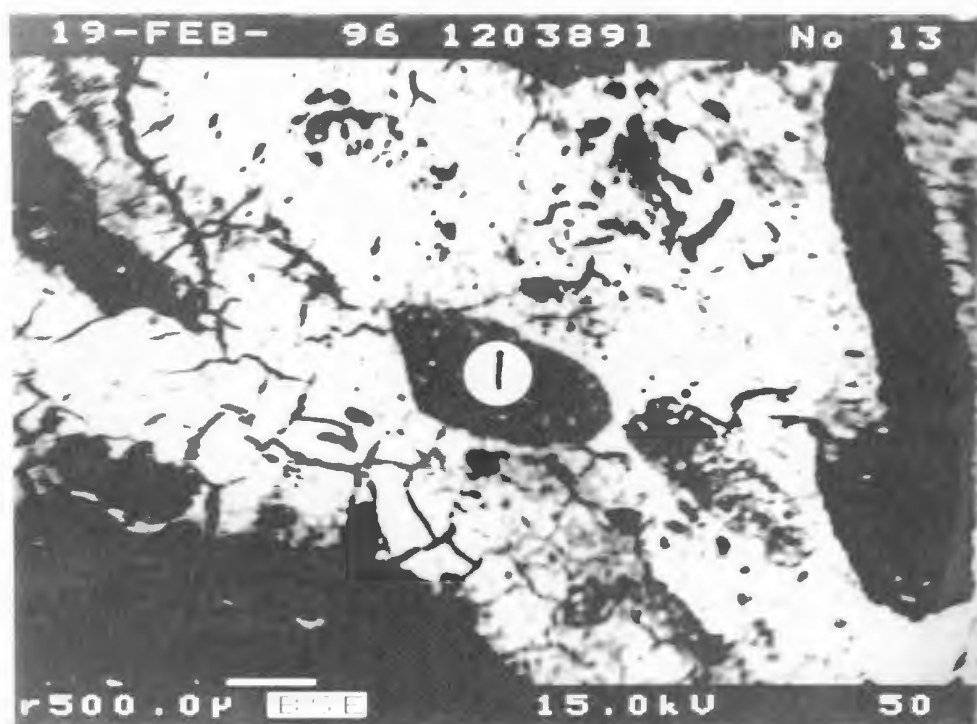
point e - iron in crack
point f - iron next to crack



Nail 120389
points g, h, i and j
iron

Nail 120389
point k
iron

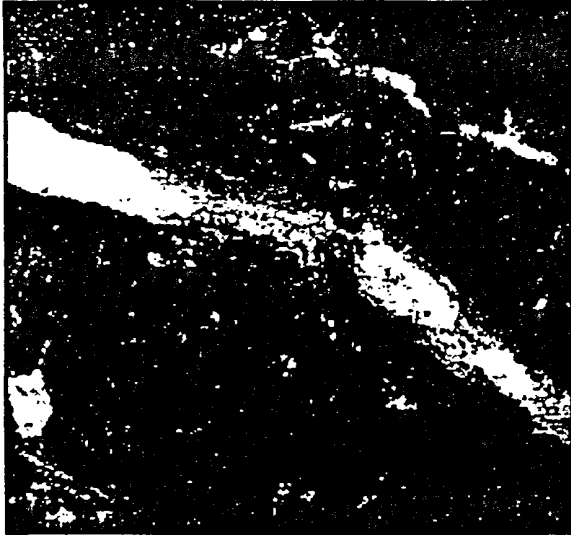




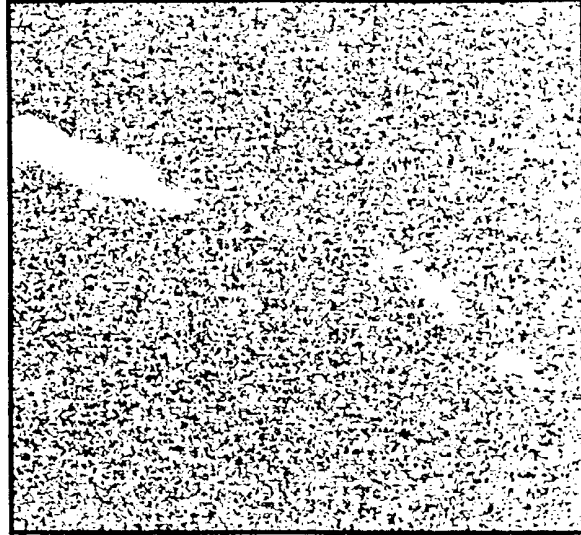
Nail 120389
point 1
feldspar grain

APPENDIX 7d

**ELEMENT MAPS
FOR NAILS
FROM
OCCUPATION/DESTRUCTION
EVENTS**

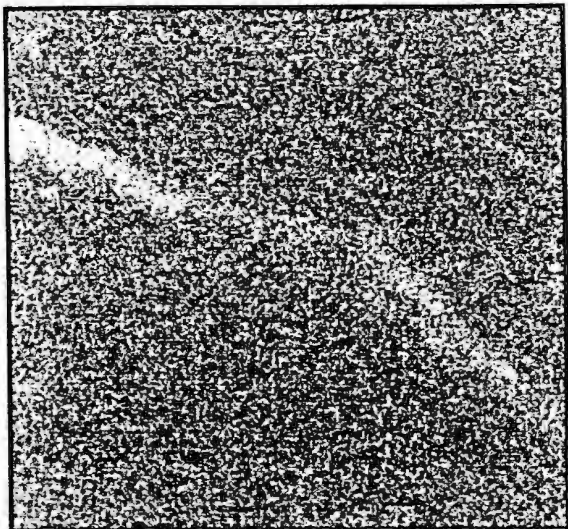


120161 BSE (444 X mag.)



120161 - chlorine by ed

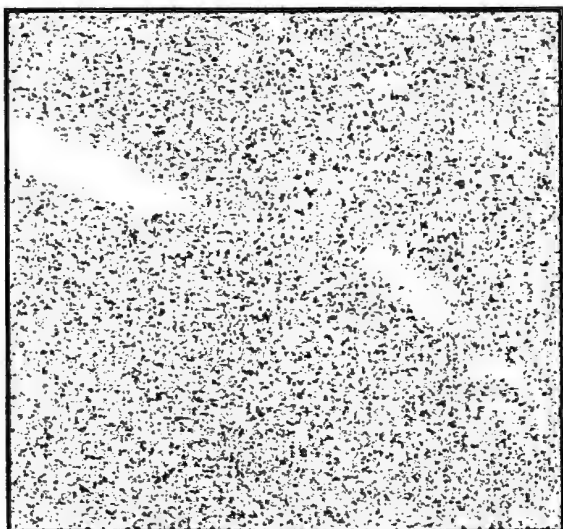
CRACK IN IRON AT CENTRE OF NAIL.



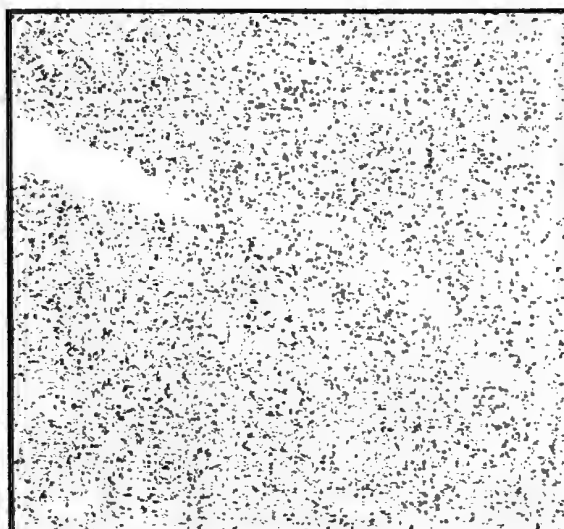
120161 - iron



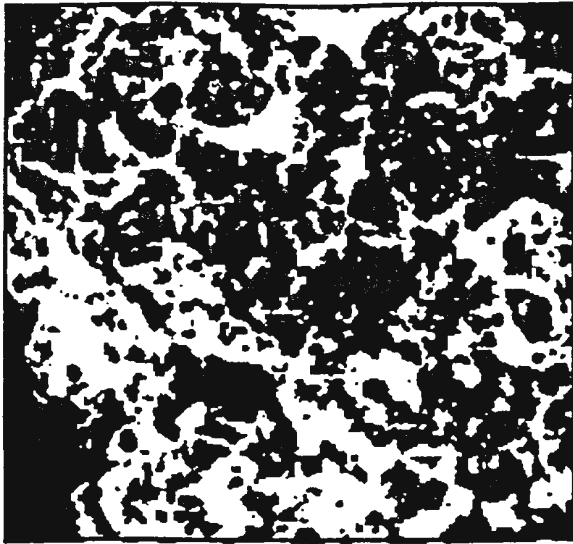
120161 - silicon



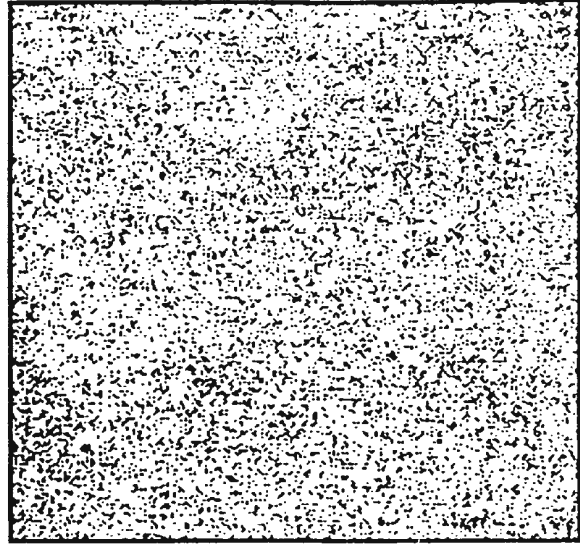
120161 - phosphorus



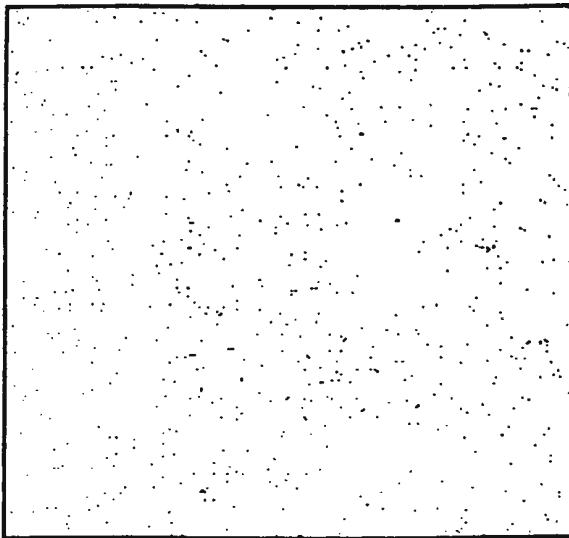
120161 - sulfur



94787 BSE (1500 X mag.)



94787 - chlorine by ed

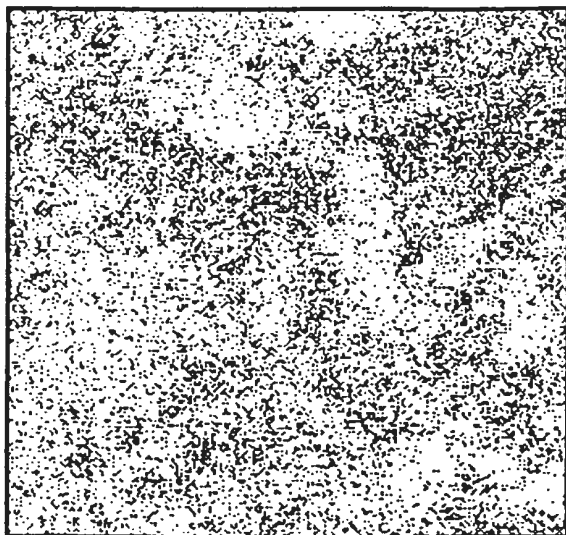


94787 - chlorine by wd

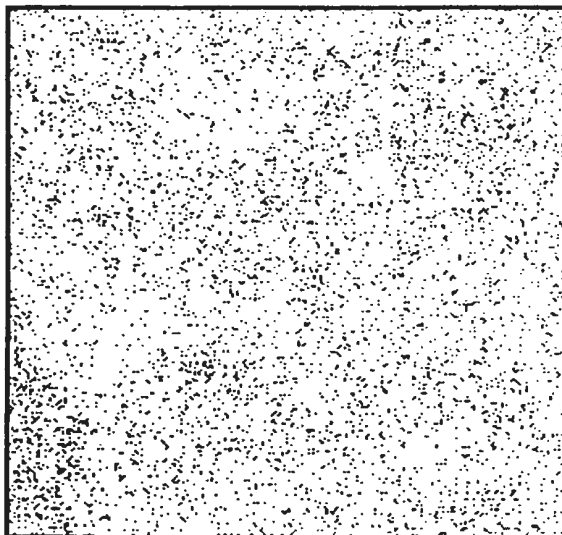


94787 - iron

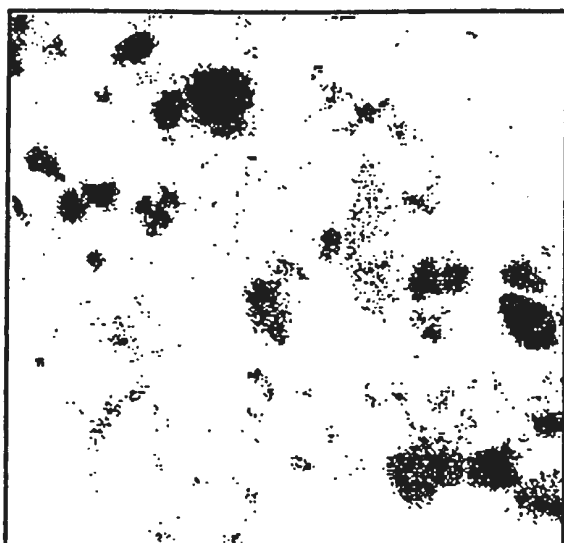
IRON NEAR VOID AT CENTRE OF NAIL.



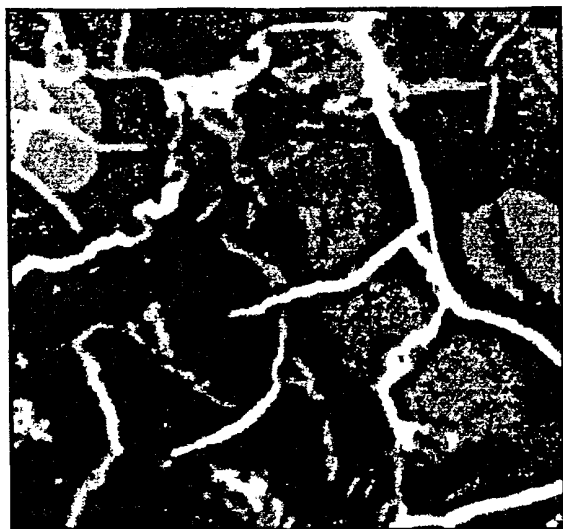
94787 - phosphorus



94787 - sulfur



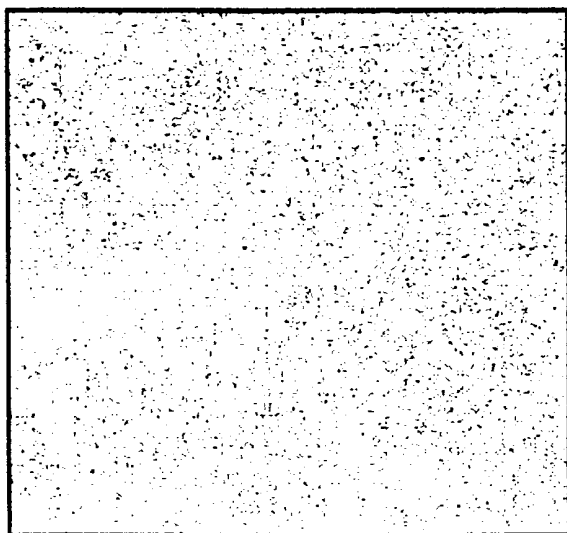
94787 - silicon



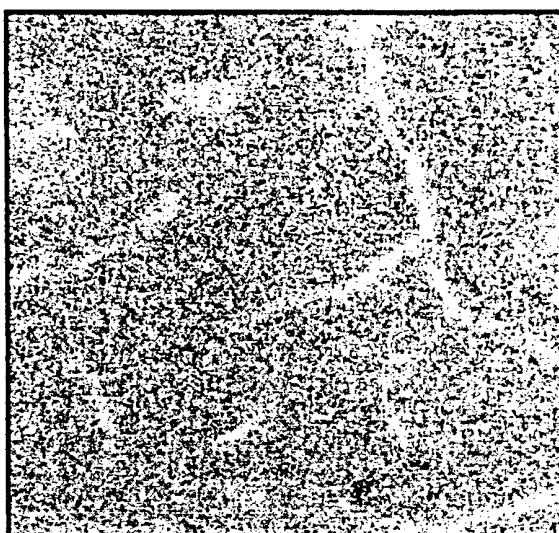
94123 BSE (1500 X mag.)



94123 - sulfur

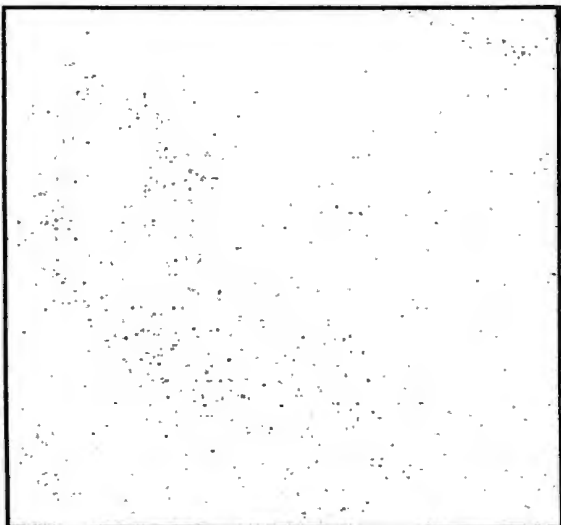


94123 - chlorine by ed

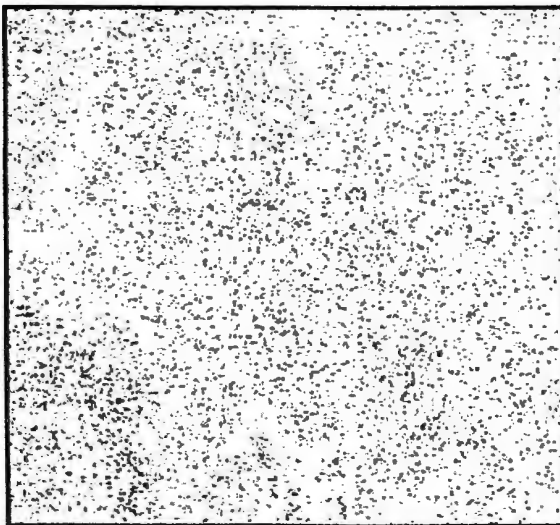


94123 - iron

IRON CONCENTRATED AT GRAIN BOUNDARIES.



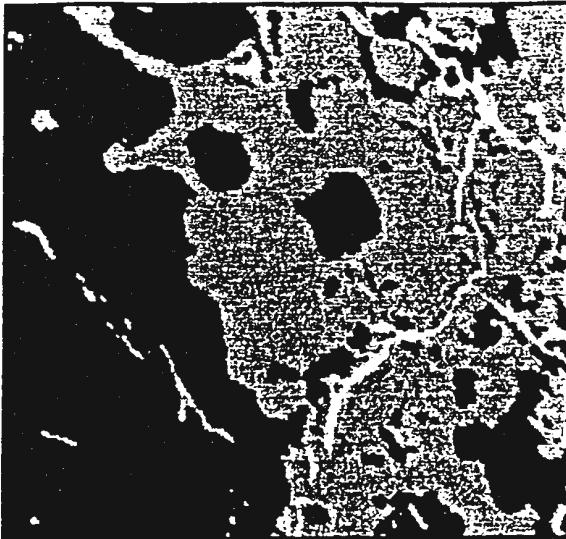
94123 - chlorine by wd



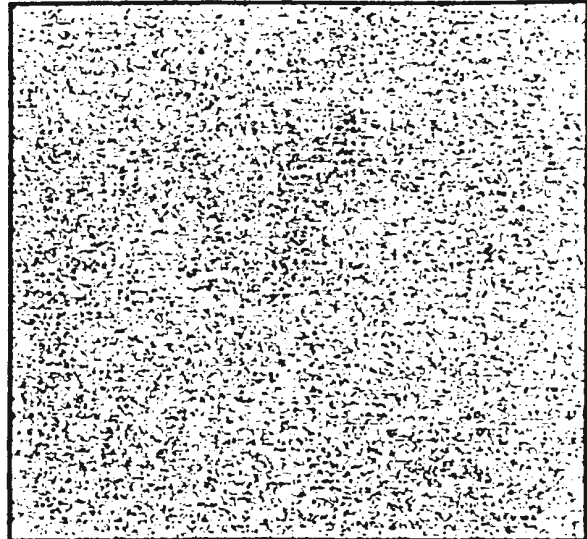
94123 - phosphorus



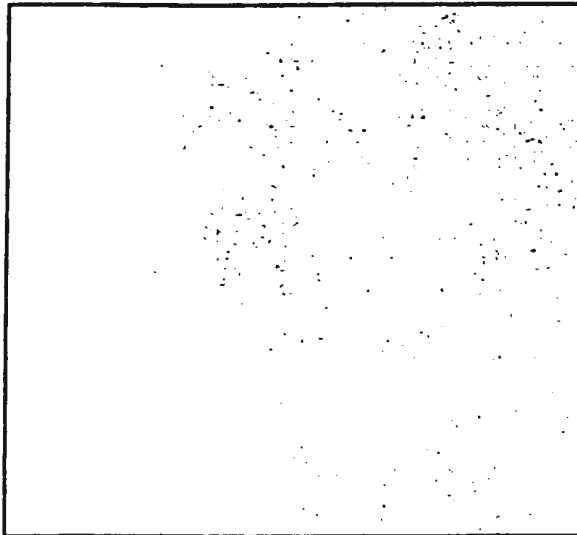
94123 - silicon



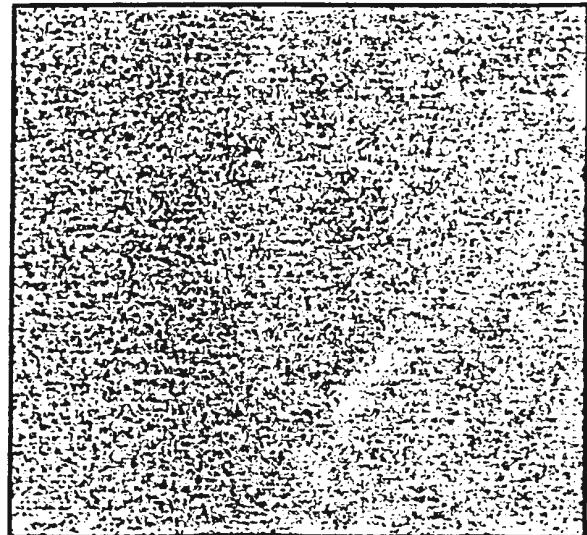
94123 BSE (1500 X mag.)



94123 - chlorine by ed

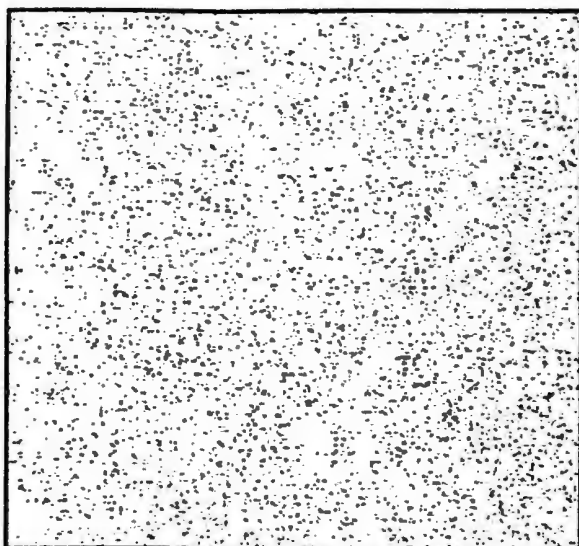


94123 - chlorine by wd

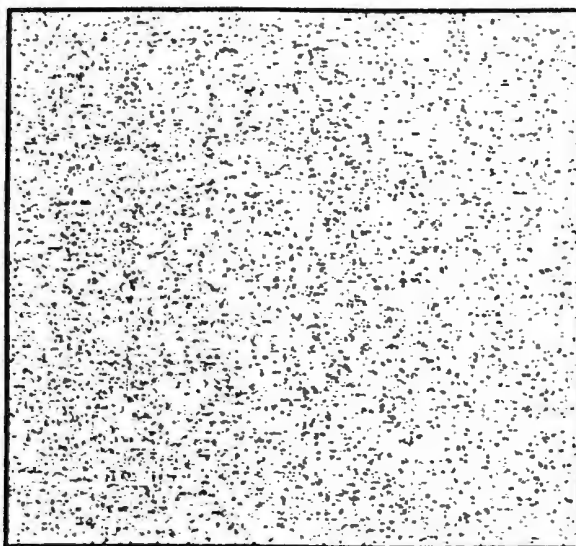


94123 - iron

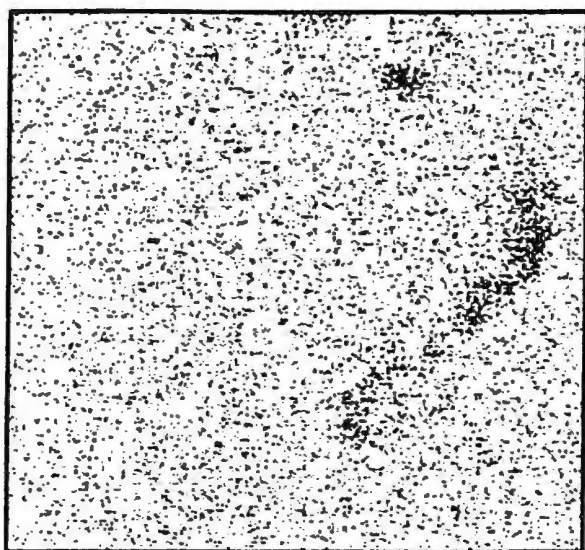
MULTI-PHASE IRON.



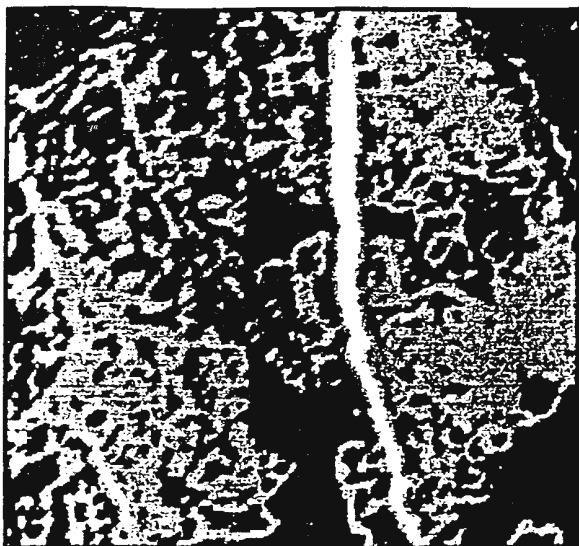
94123 - phosphorus



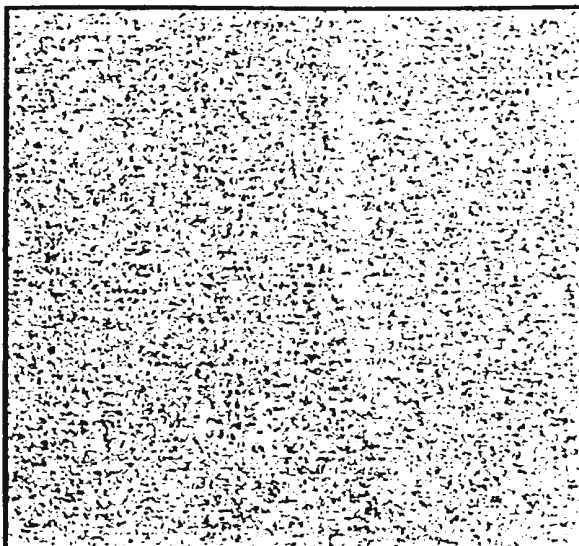
94123 - sulfur



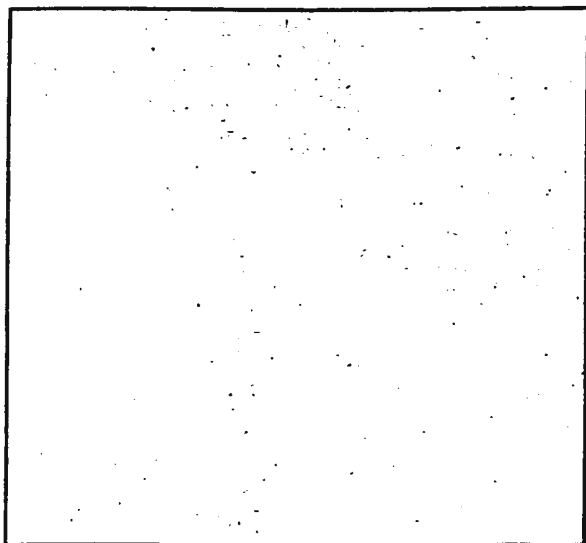
94123 - silicon



94123 BSE (1500 X mag.)

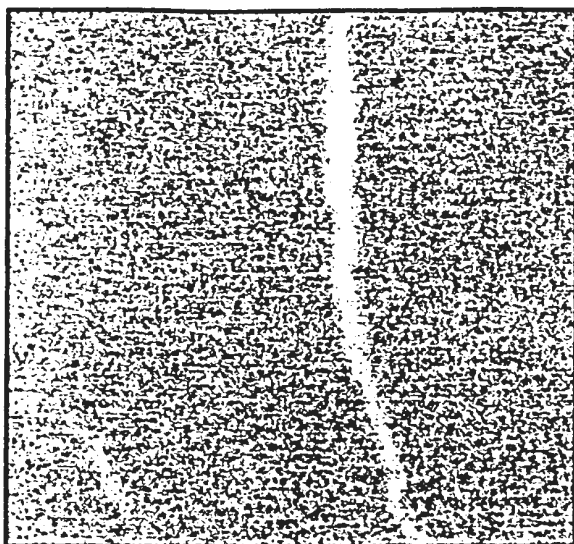
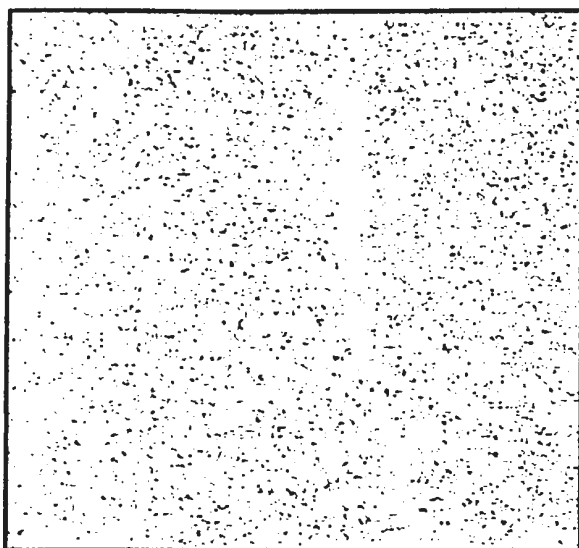
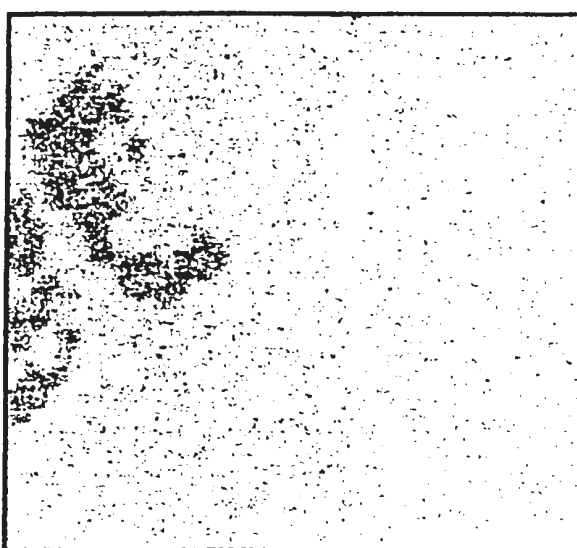


94123 - chlorine by ed



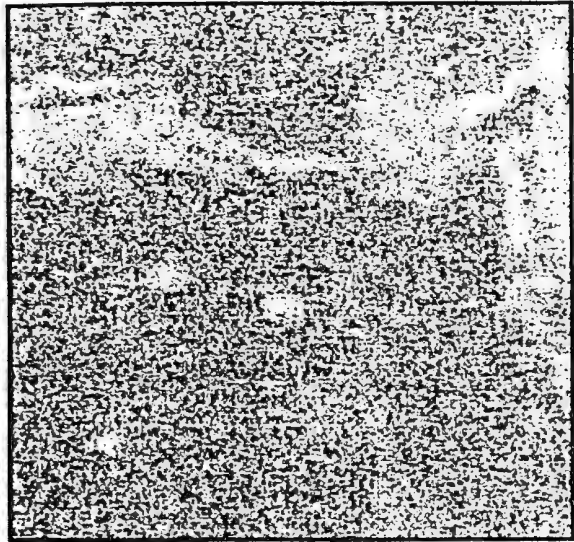
94123 - chlorine by wd

CRACK IN MULTI-PHASE IRON.

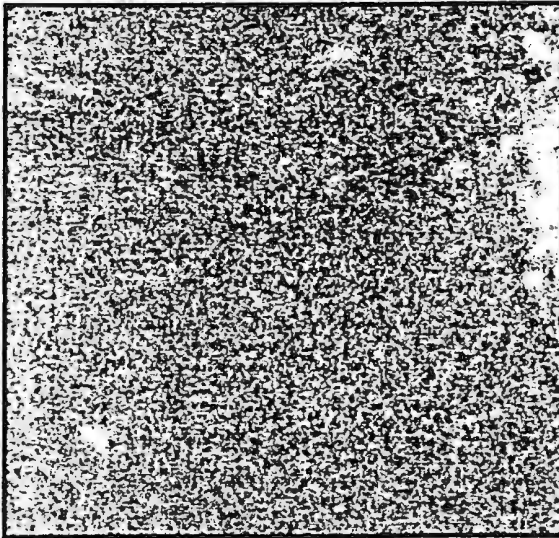
**94123 - iron****94123 - phosphorus****94123 - sulfur****94123 - silicon**



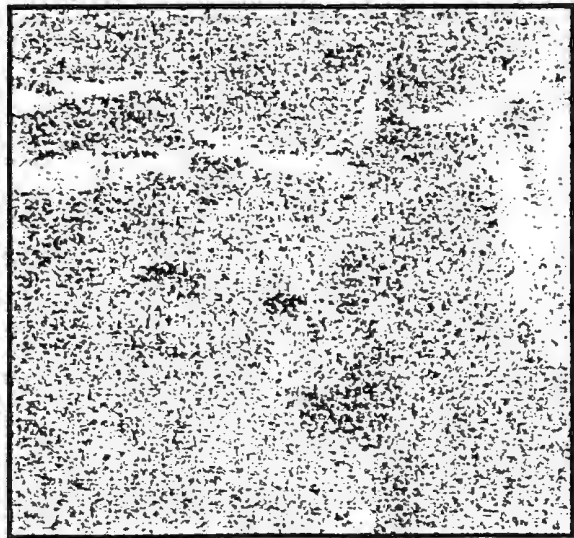
94785 BSE (1500 X mag.)



94785 - chlorine



94785 - iron



94785 - phosphorus

IRON NEAR A CRACK.



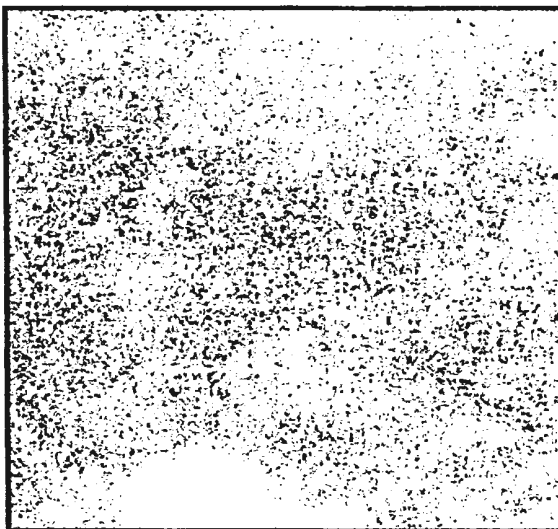
94785 - sulfur



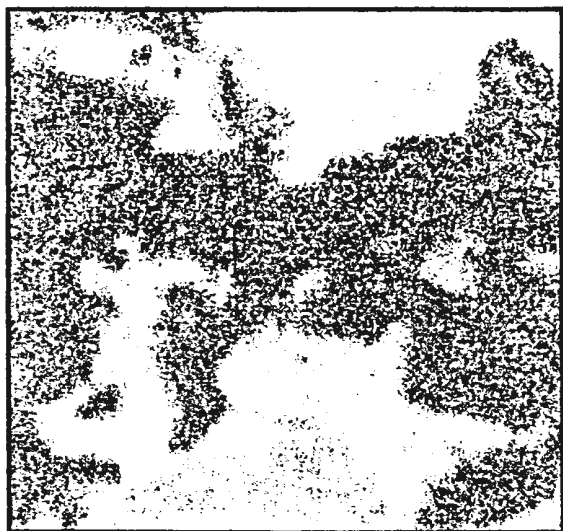
94785 - silicon



94785 BSE (1500 X mag.)



94785 - chlorine

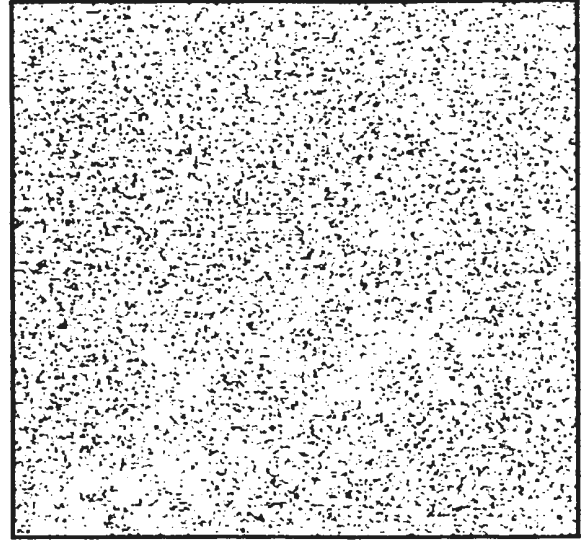


94785 - iron

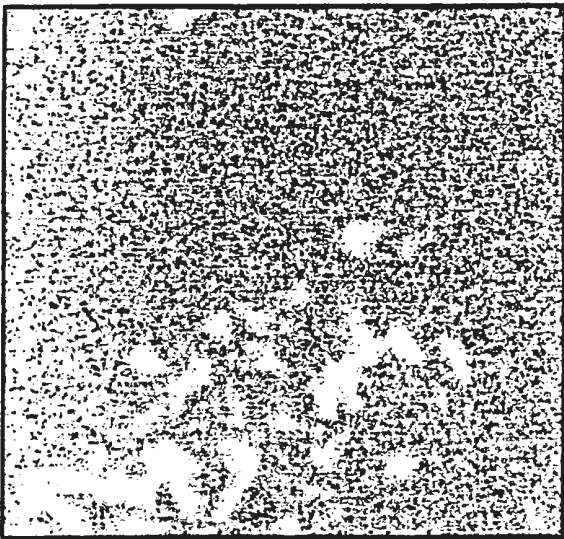
MULTI-PHASE IRON.



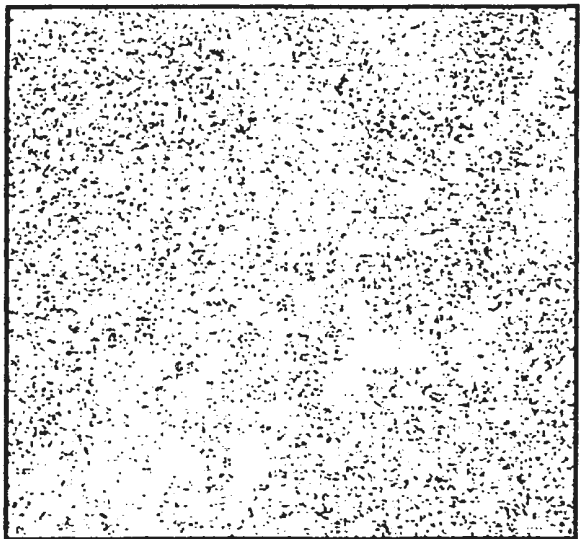
87872 BSE (1500 X mag.)



87872 - chlorine

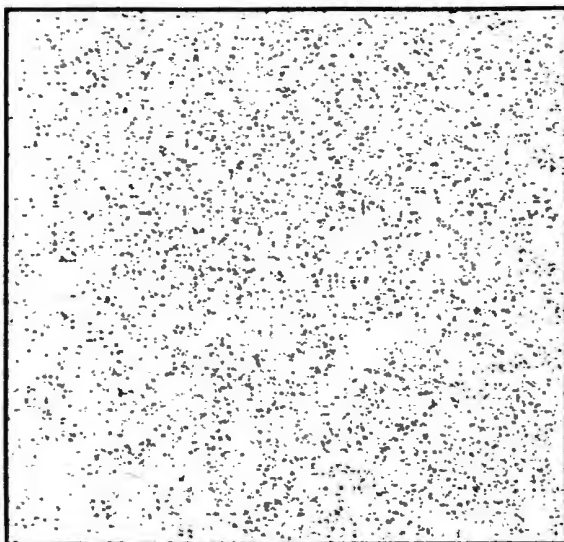


87872 - iron

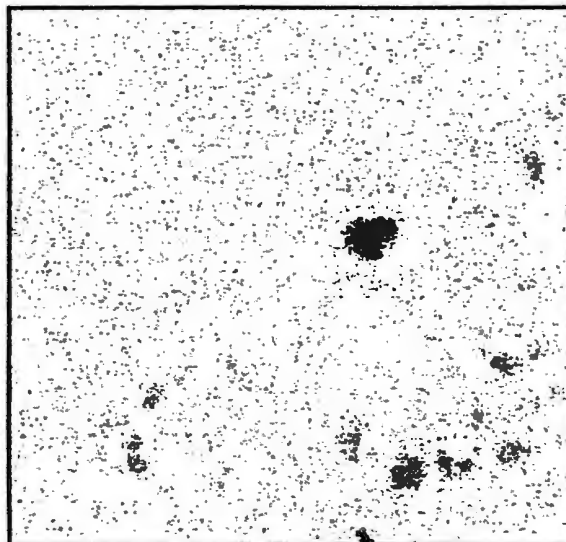


87872 - phosphorus

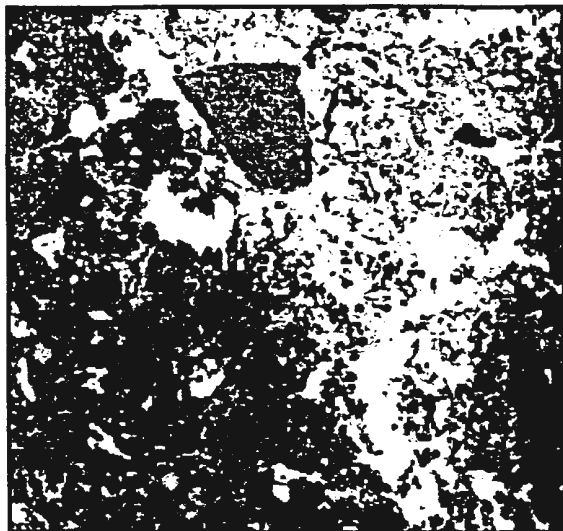
MULTI-PHASE IRON.



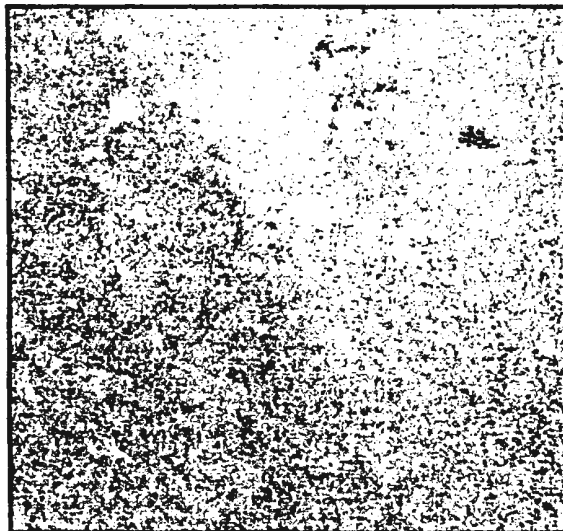
87872 - sulfur



87872 - silicon



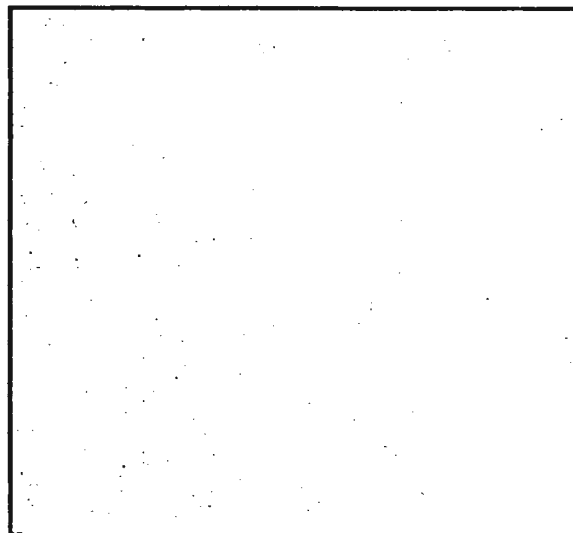
120161 BSE (500 X mag.)



120161 - iron

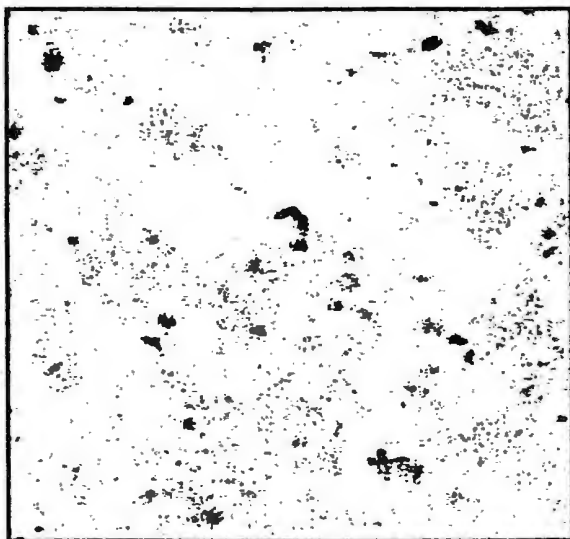


120161 - chlorine by ed

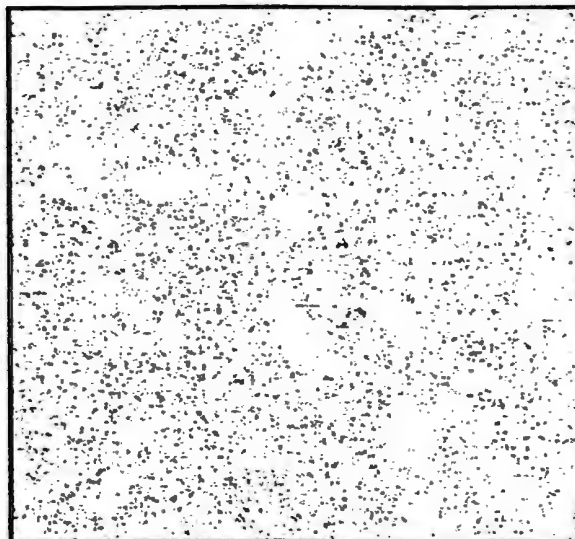


120161 - chlorine by wd

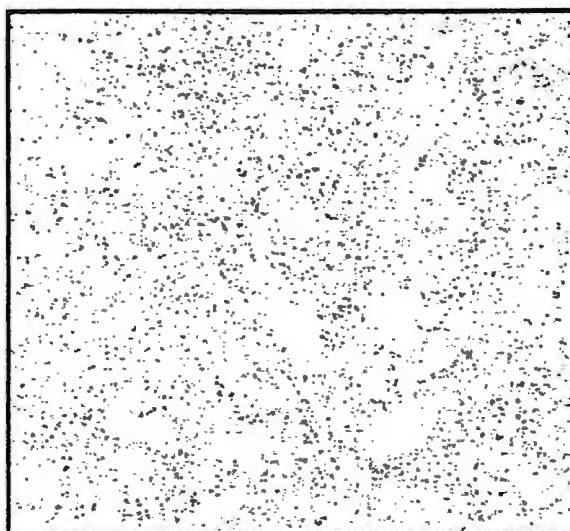
IRON AT EDGE OF NAIL.



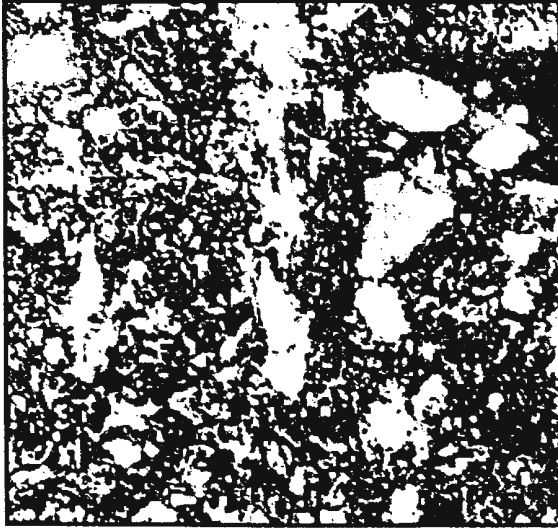
120161 - silicon



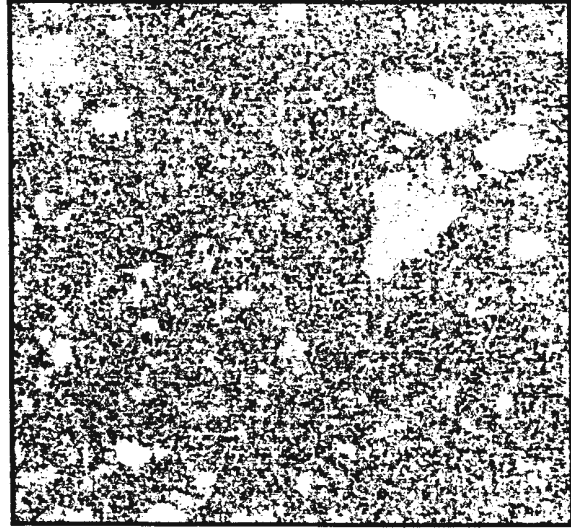
120161 - phosphorus



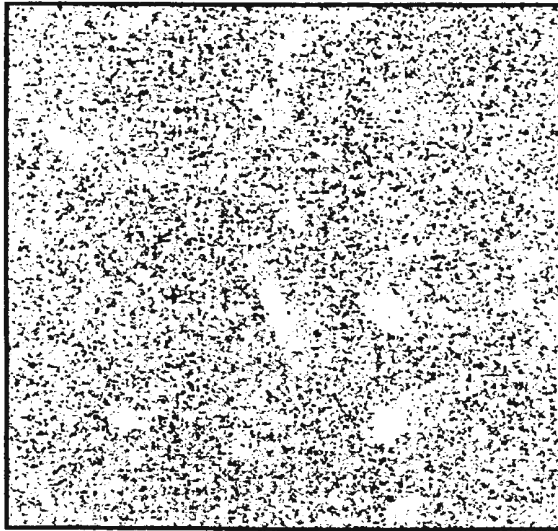
120161 - sulfur



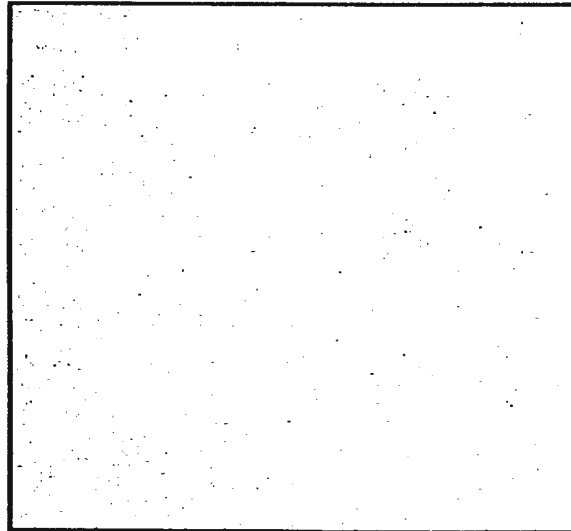
120161 BSE (1000 X mag.)



120161 - iron

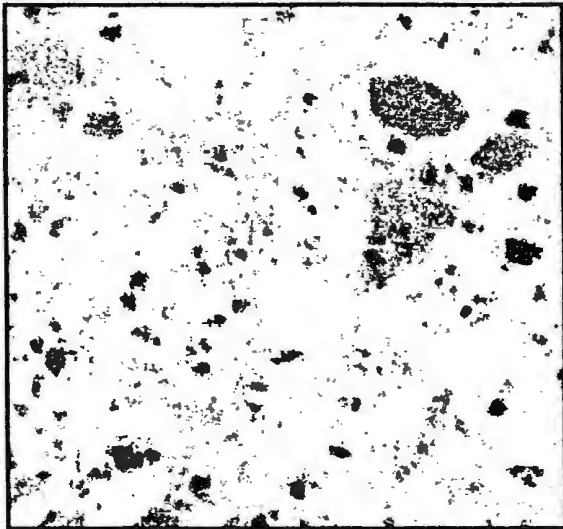


120161 - phosphorus

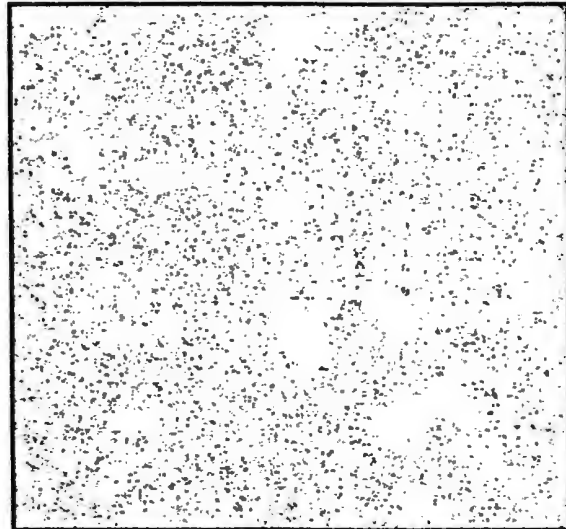


120161 - chlorine by wd

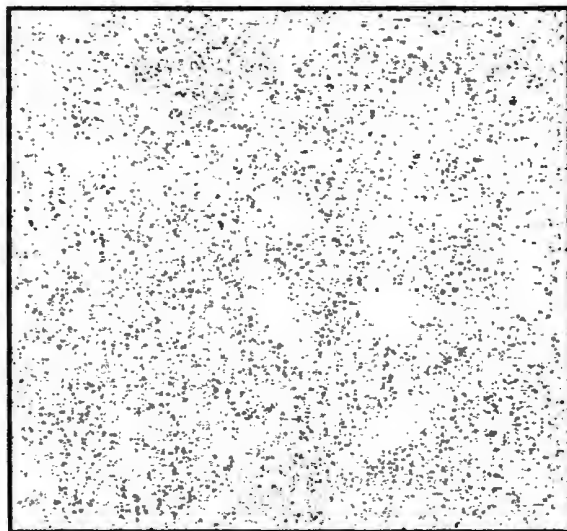
CRACK AT EDGE OF NAIL.



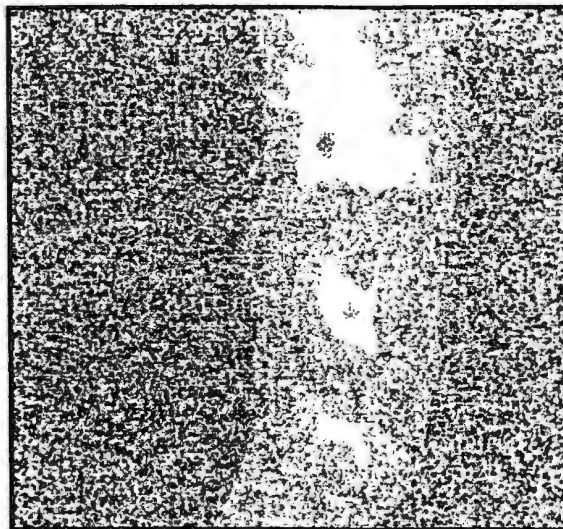
120161 - silicon



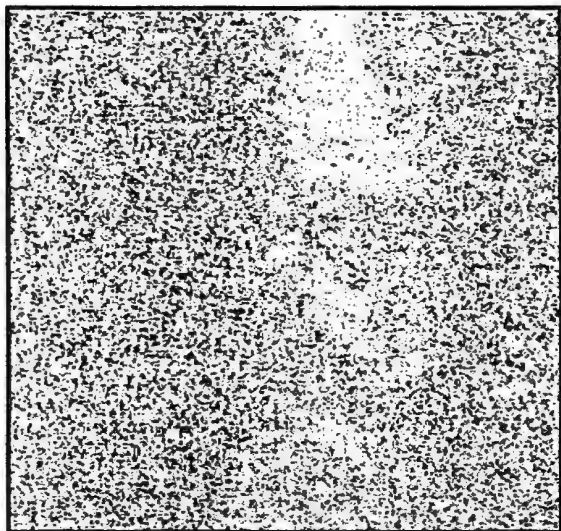
120161 - phosphorus



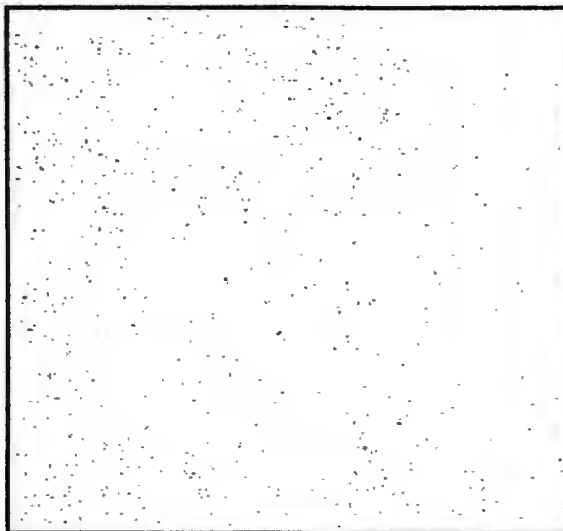
120161 - sulfur



120389 - iron

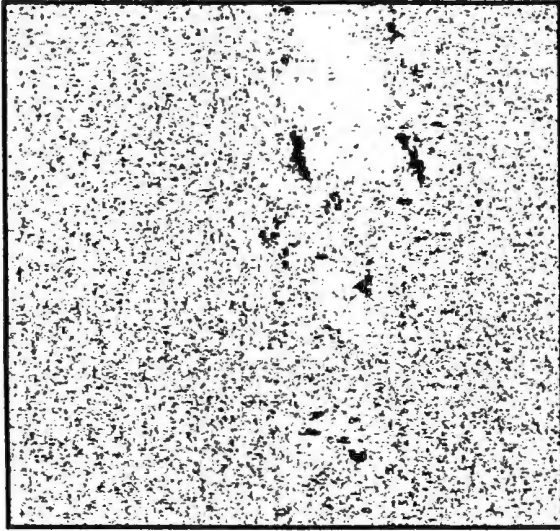


120389 - chlorine by ed

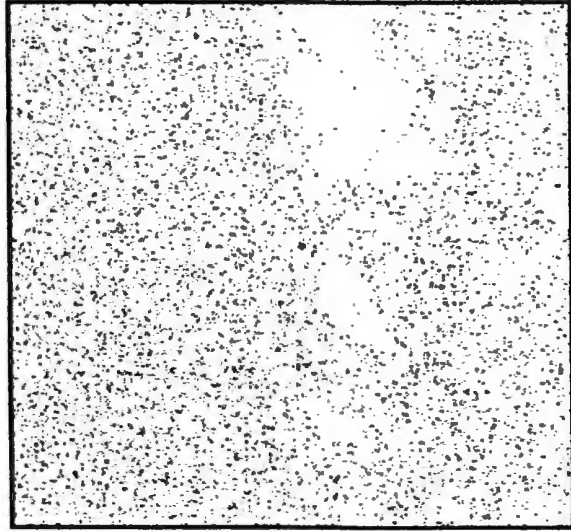


120389 - chlorine by wd

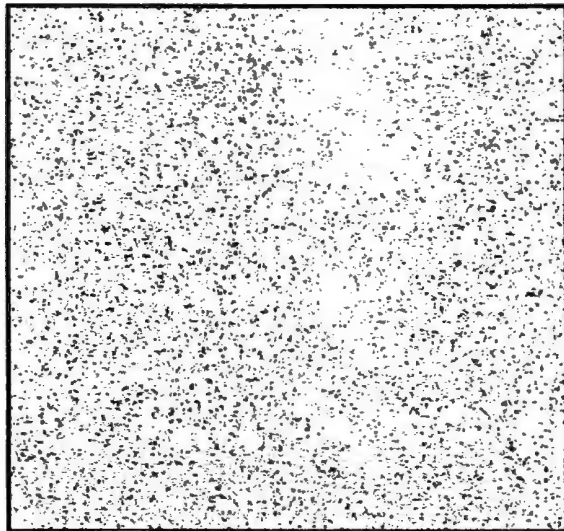
CRACK IN IRON AT EDGE OF NAIL (216 X mag.).



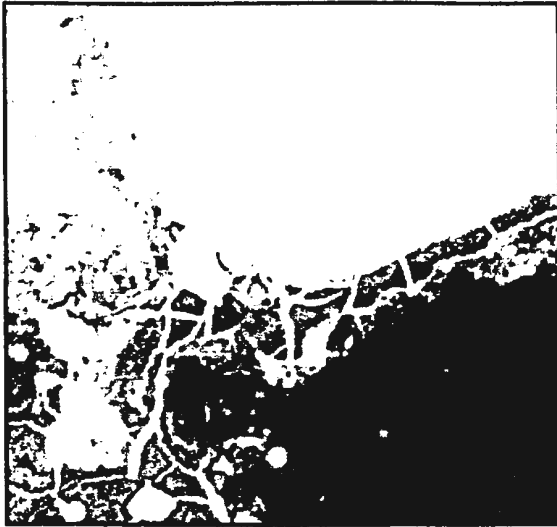
120389 - silicon



120389 - phosphorus



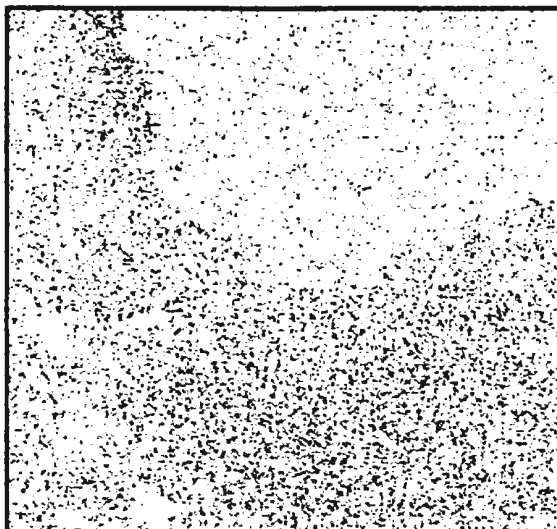
120389 - sulfur



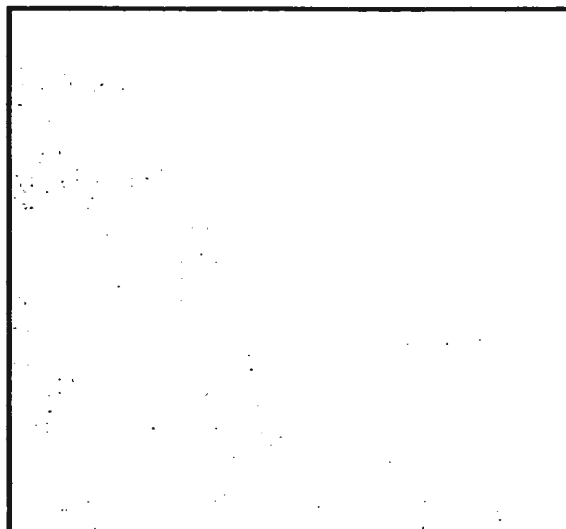
120161 BSE (400 X mag.)



120161 - iron

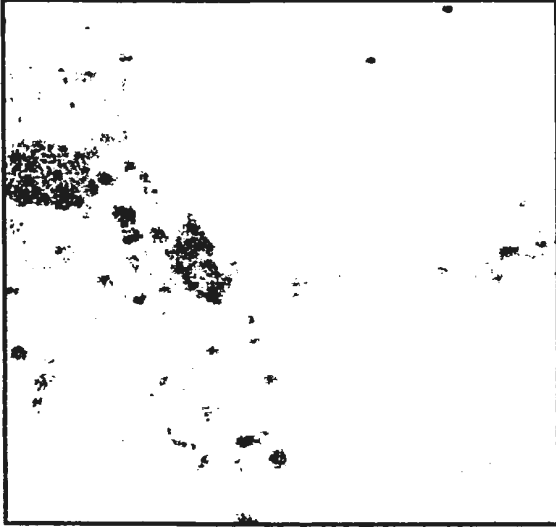


120161 - chlorine by ed



120161 - chlorine by wd

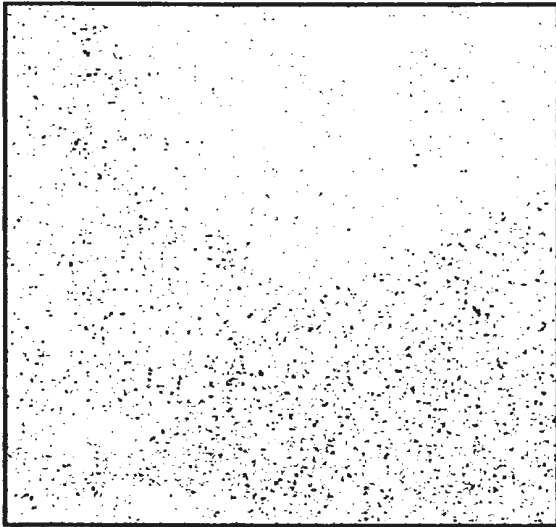
IRON/CORROSION HALO INTERFACE.



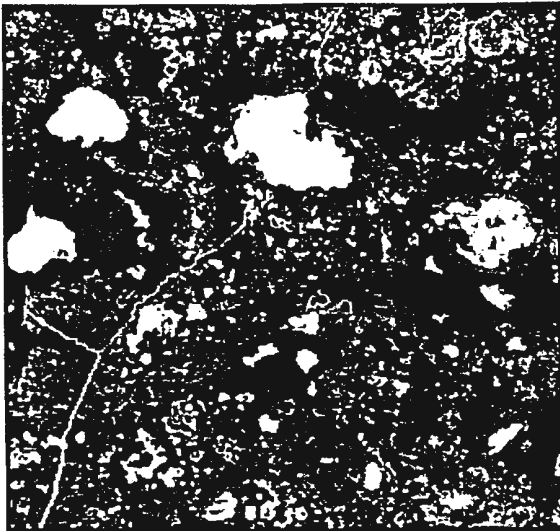
120161 - silicon



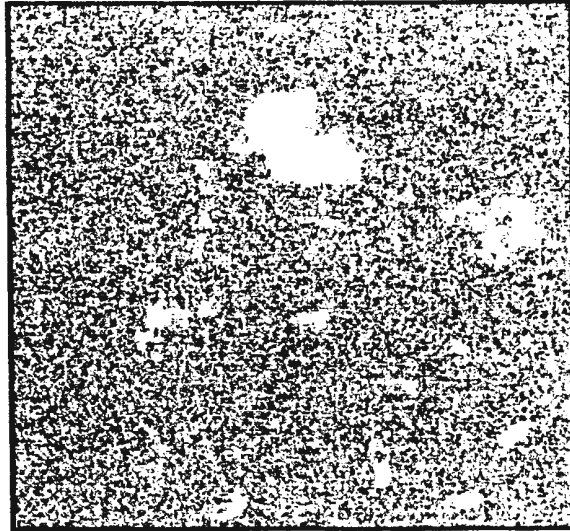
120161 - phosphorus



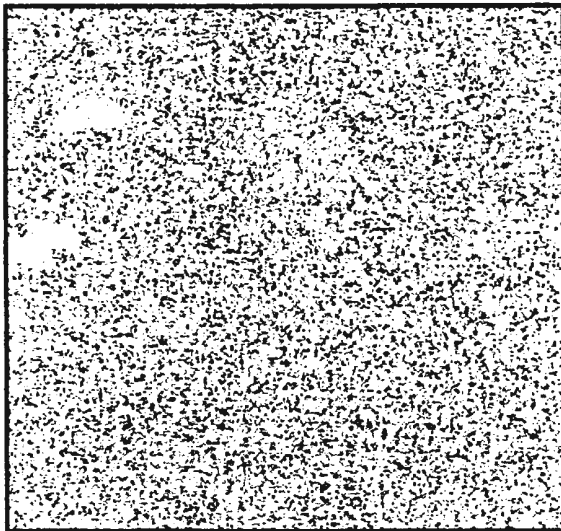
120161 - sulfur



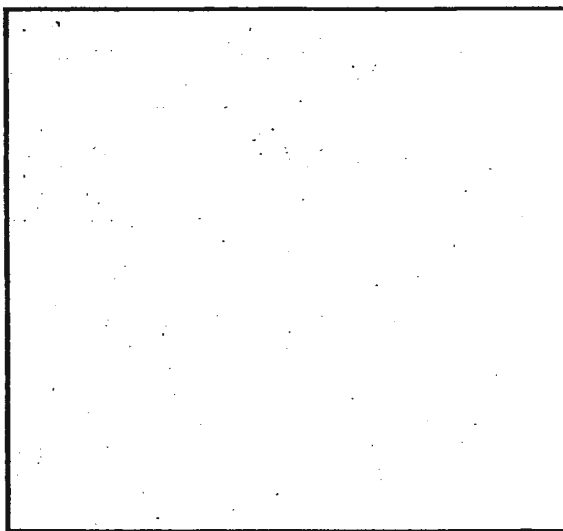
120161 BSE (400 X mag.)



120161 - iron

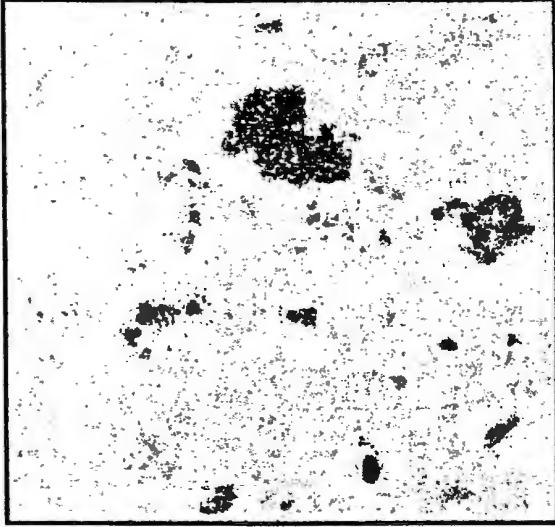


120161 - chlorine by ed

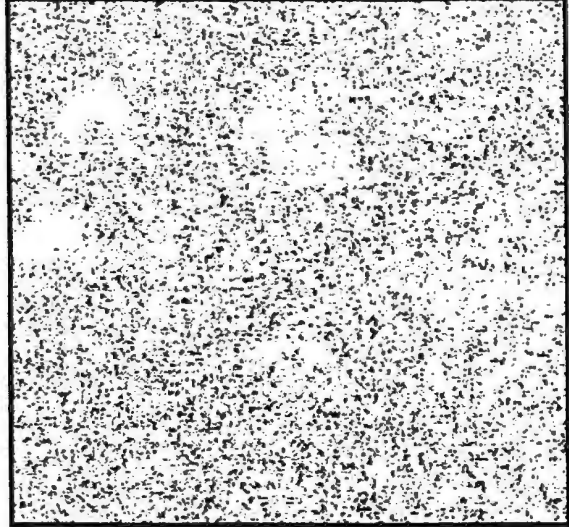


120161 - chlorine by wd

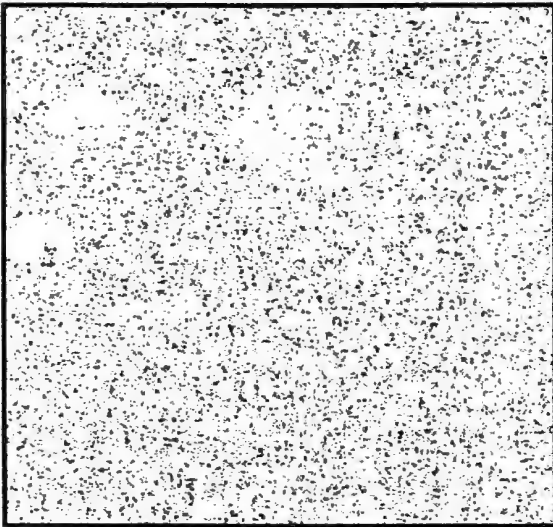
IRON/CORROSION HALO INTERFACE.



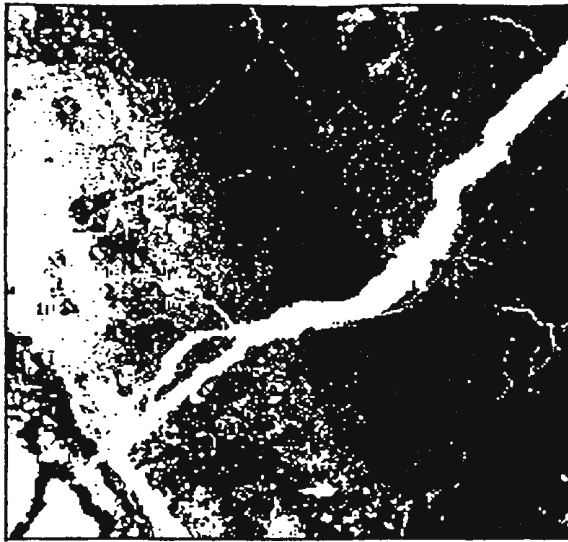
120161 - silicon



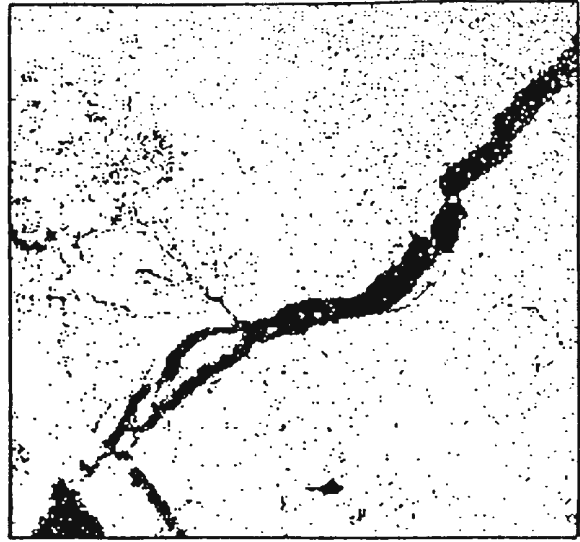
120161 - phosphorus



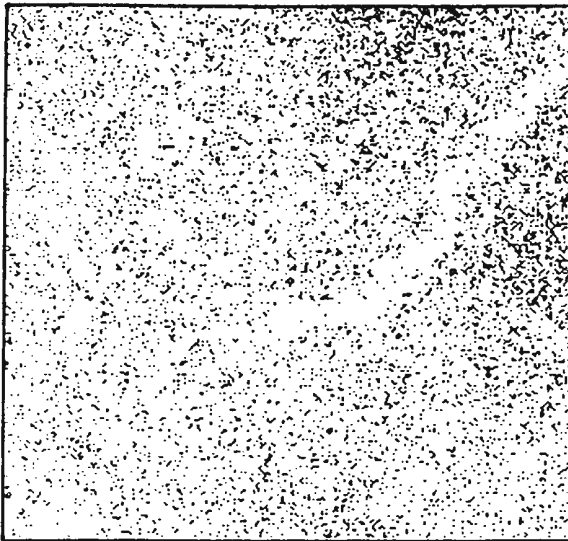
120161 - sulfur



99060 BSE (50 X mag.)



99060 - carbon

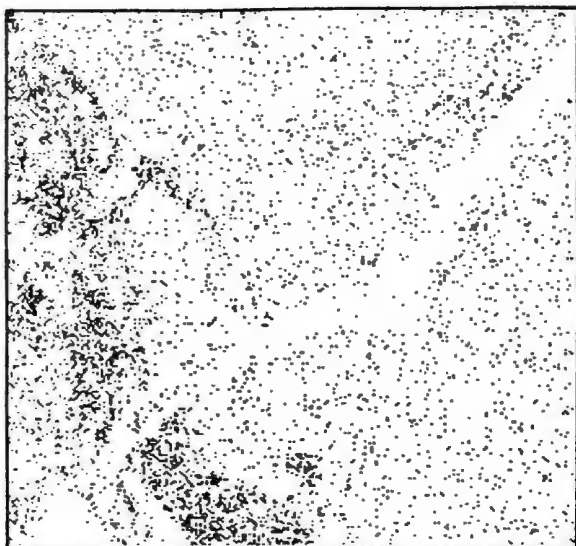


99060 - chlorine

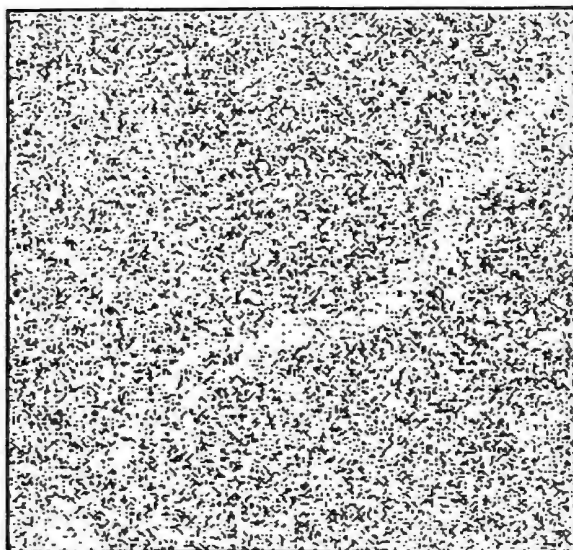


99060 - iron

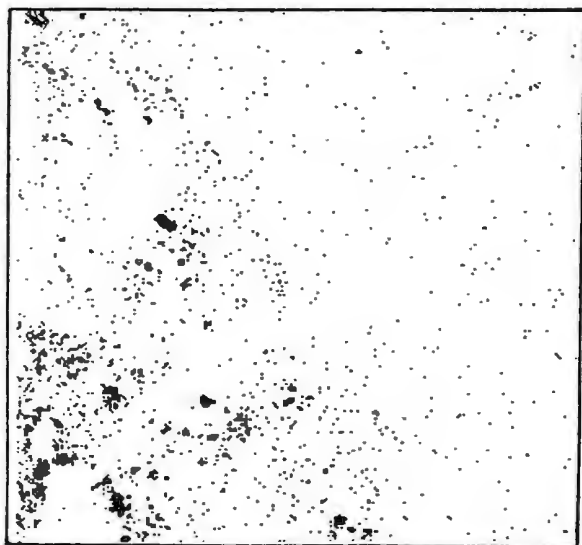
IRON/CORROSION HALO INTERFACE.



99060 - phosphorus



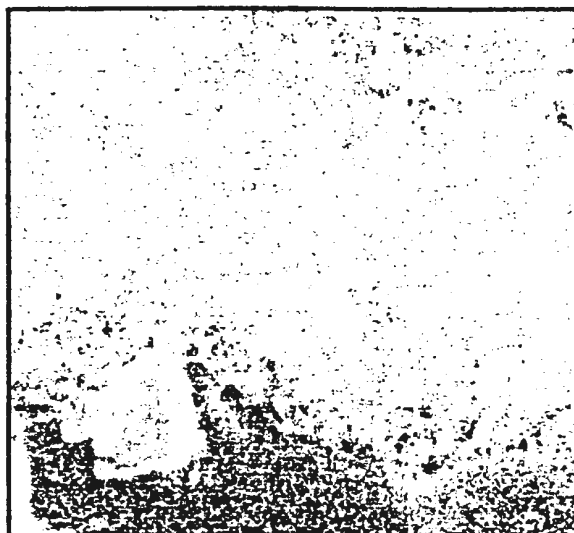
99060 - sulfur



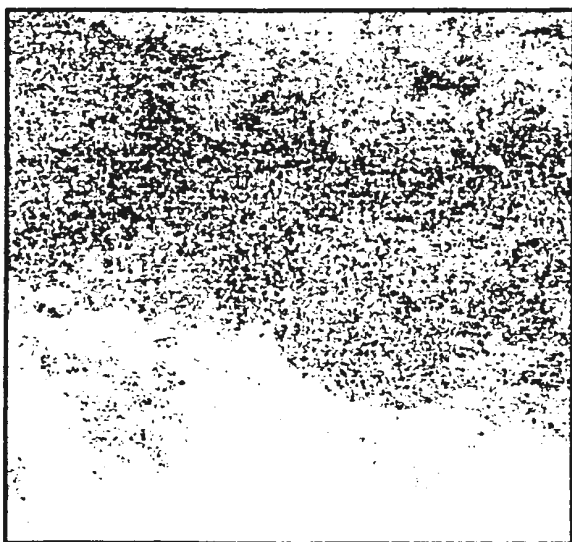
99060 - silicon



94759 BSE (50 X mag.)



94759 - carbon



94759 - iron



94759 - chlorine

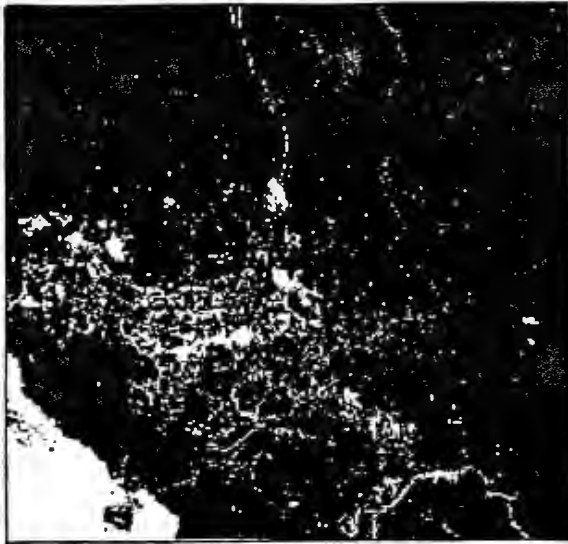
IRON/CORROSION HALO INTERFACE.



94759 - phosphorus



94759 - sulfur



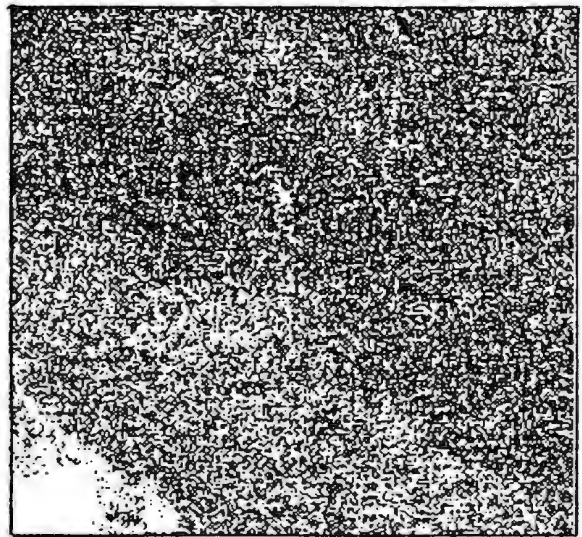
128193 BSE (65 X mag.)



128193 - carbon

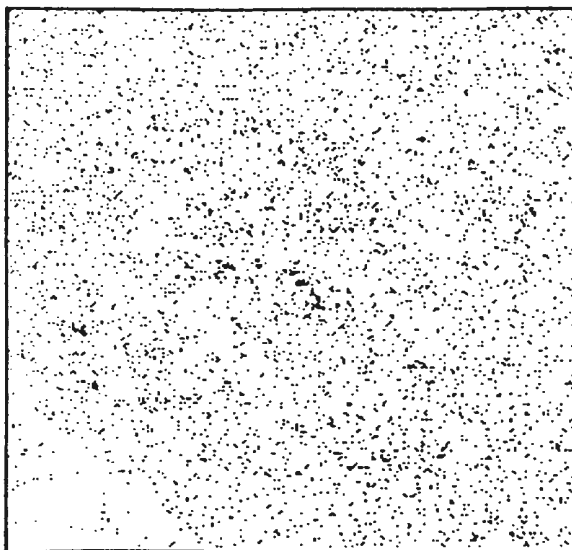


128193 - chlorine

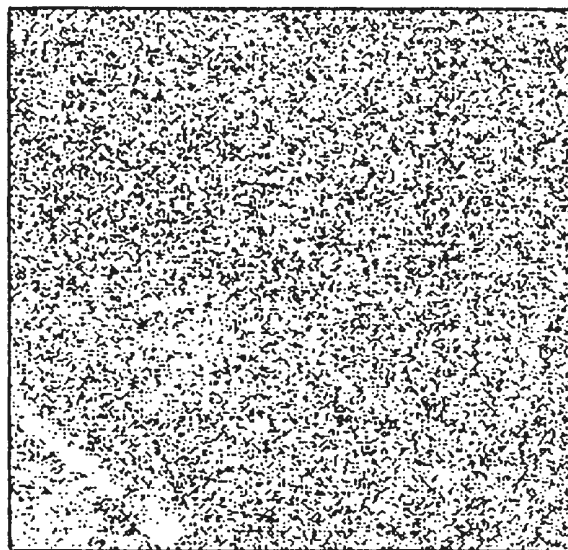


128193 - iron

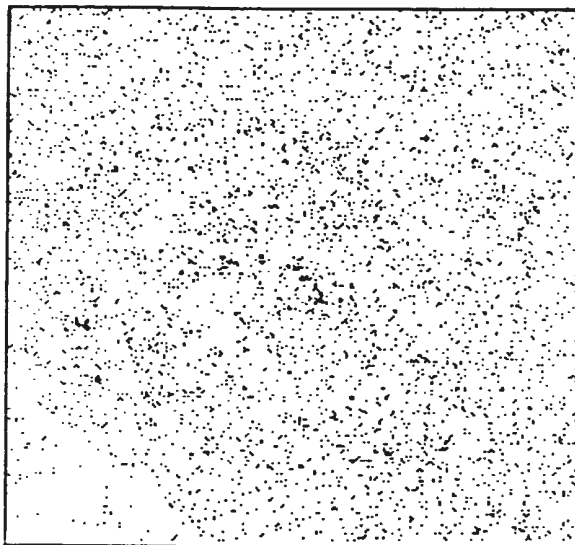
IRON/CORROSION HALO INTERFACE.



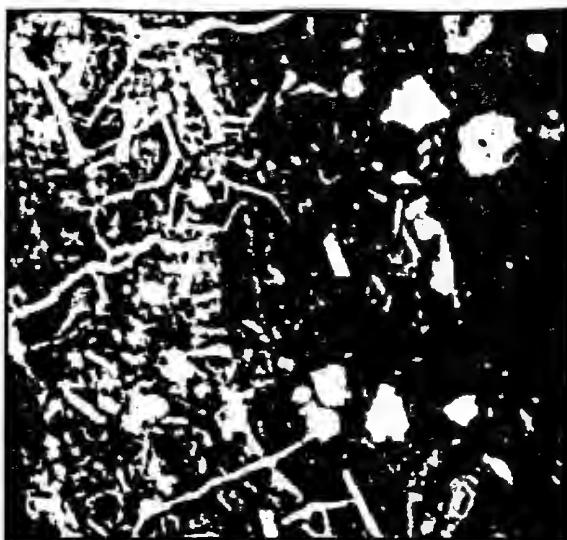
128193 - phosphorus



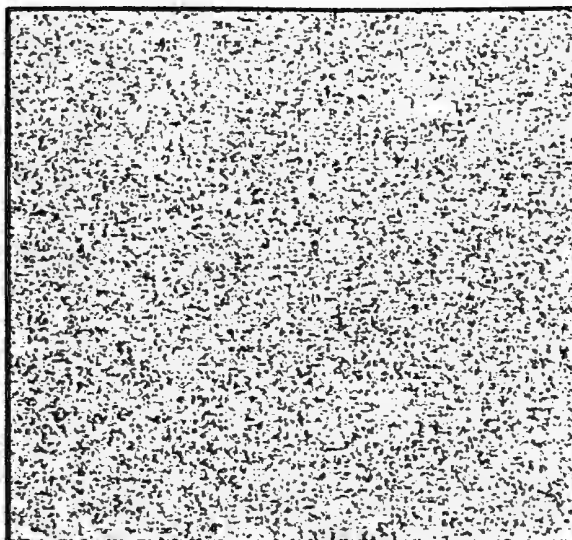
128193 - sulfur



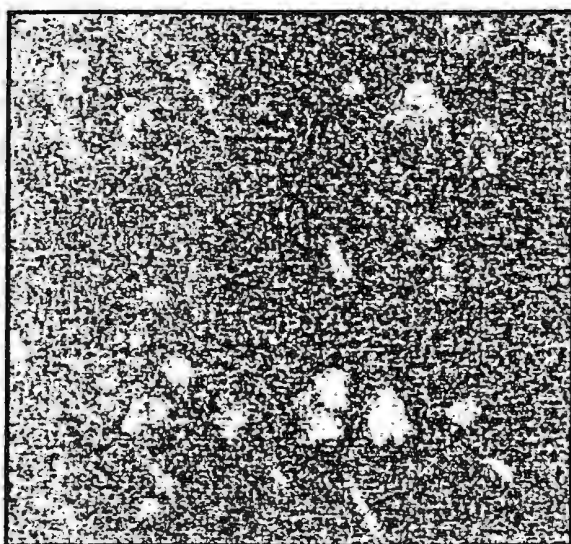
128193 - silicon



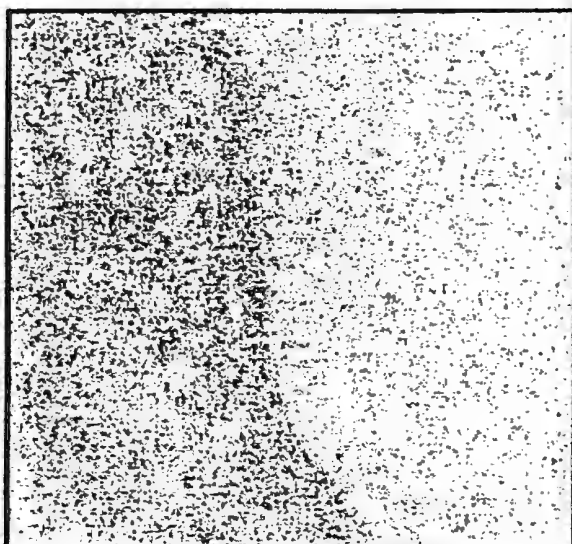
87872 BSE (1500 X mag.)



87872 - chlorine

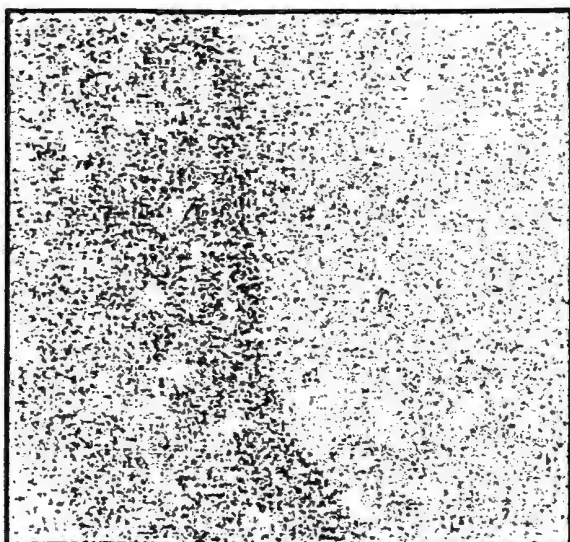


87872 - iron



87872 - phosphorus

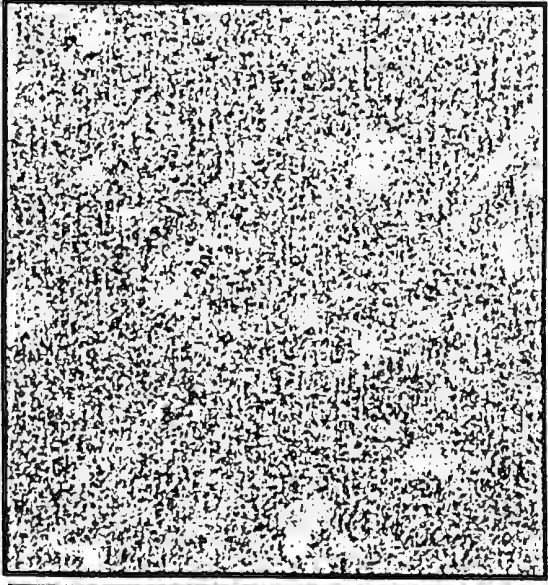
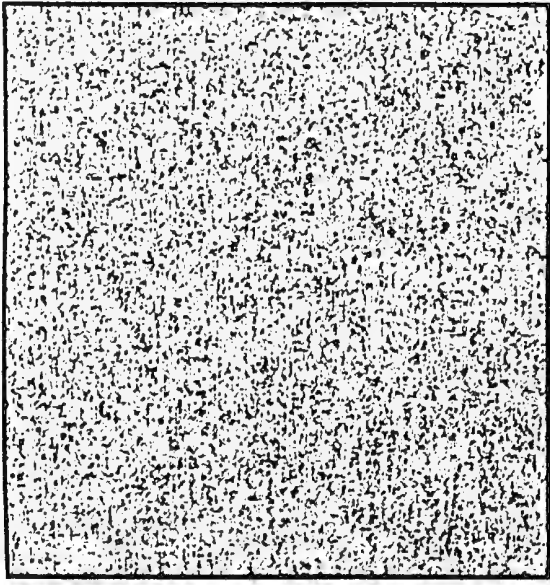
CORROSION HALO.



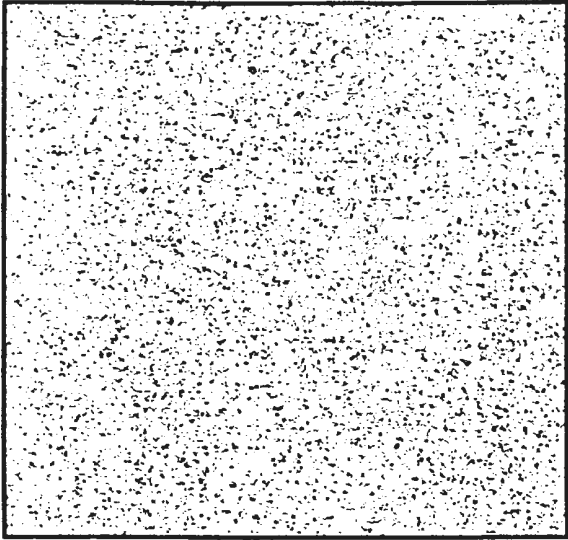
87872 - sulfur



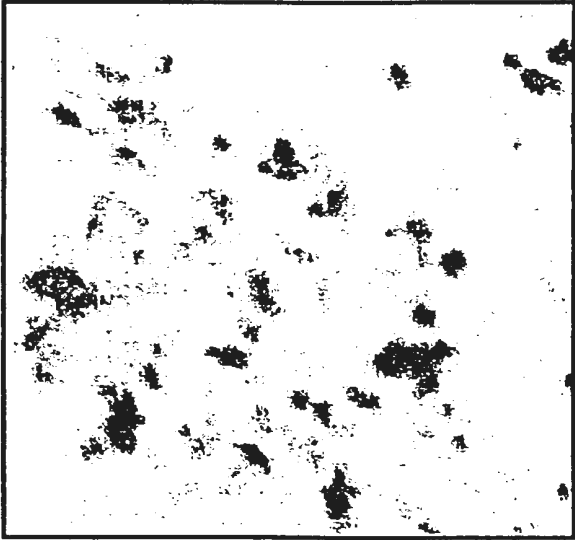
87872 - silicon



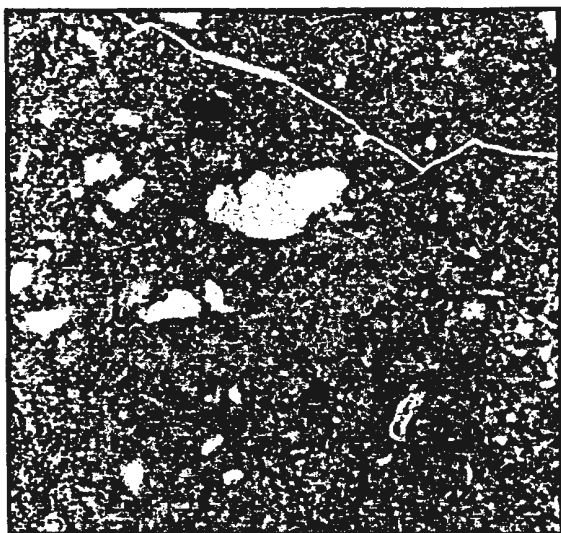
CORROSION HALO.



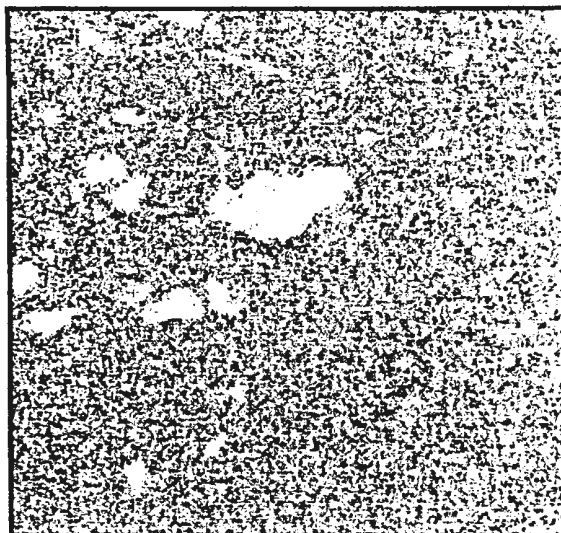
94158 - sulphur



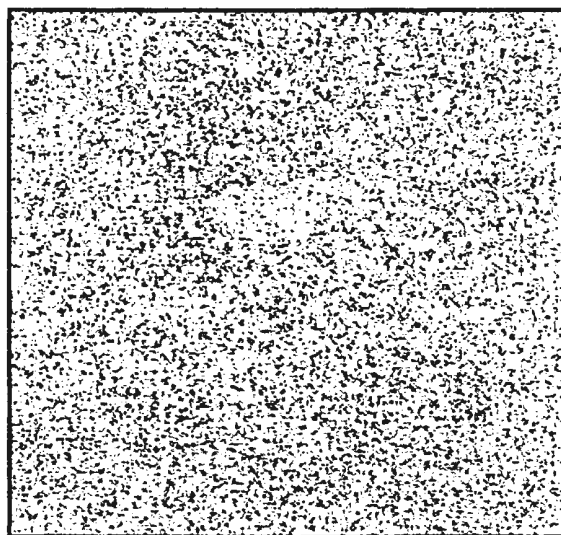
94158 - silicon



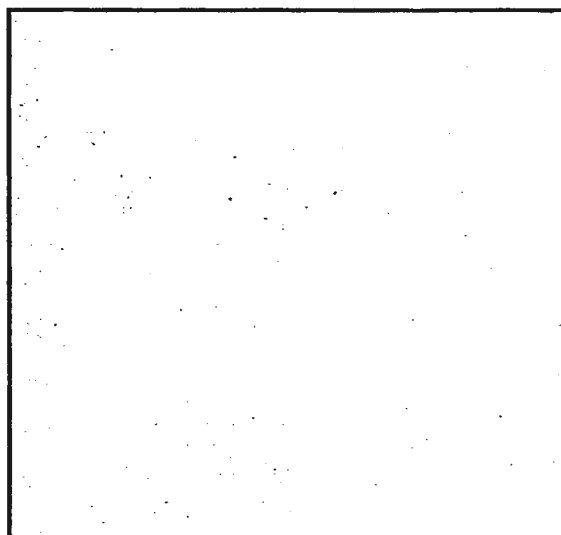
120161 BSE (400 X mag.)



120161 - iron

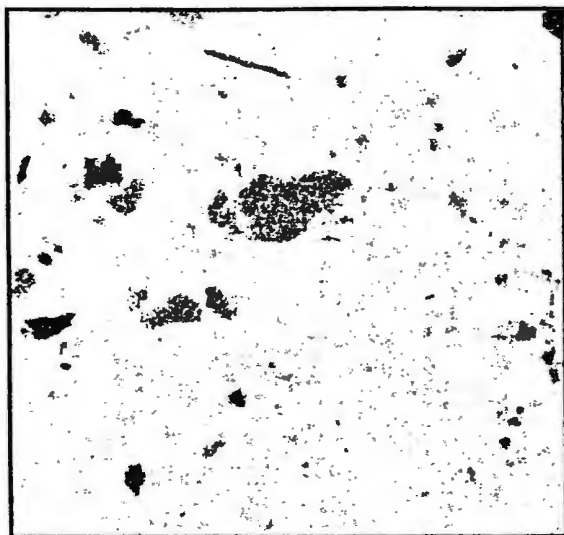


120161 - chlorine by ed



120161 - chlorine by wd

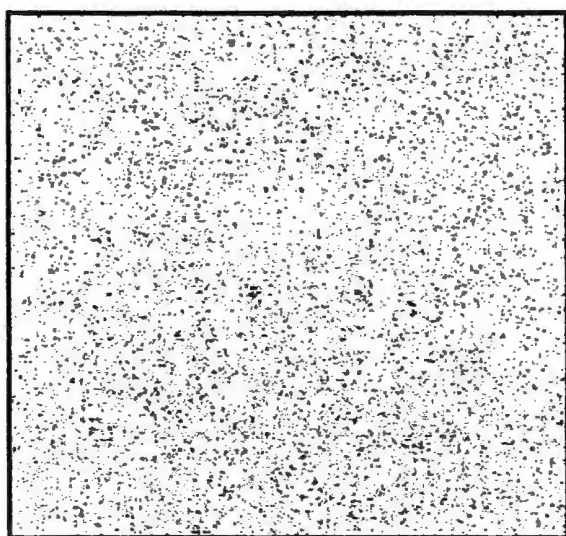
EDGE OF CORROSION HALO.



120161 - silicon



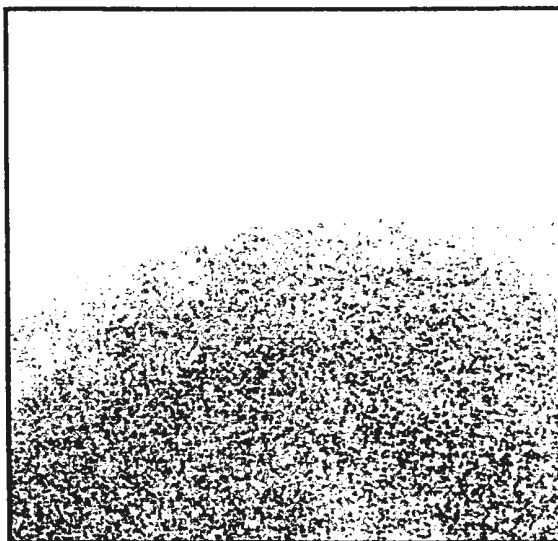
120161 - phosphorus



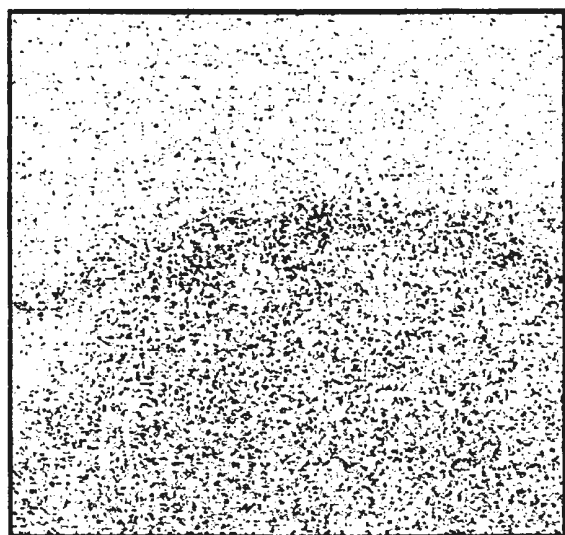
120161 - sulfur



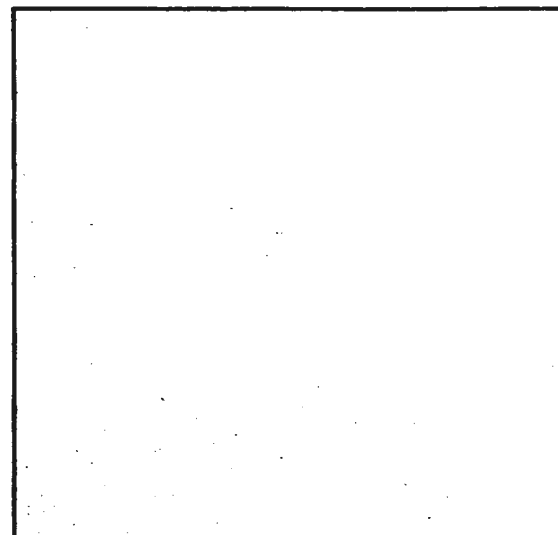
120161 BSE (519 X mag.)



120161 - iron



120161 - chlorine by ed



120161 - chlorine by wd

EDGE OF CORROSION HALO.



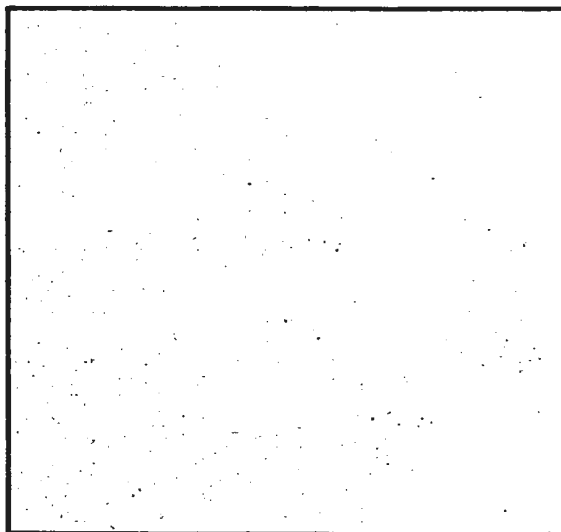
120161 BSE (70 X mag.)



120161 - iron

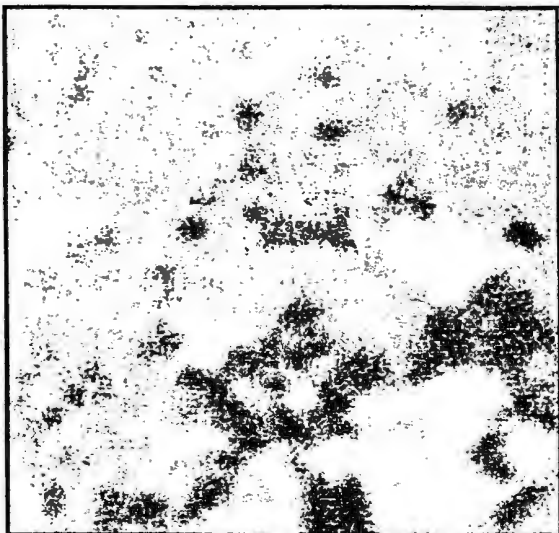


120161 - chlorine by ed



120161 - chlorine by wd

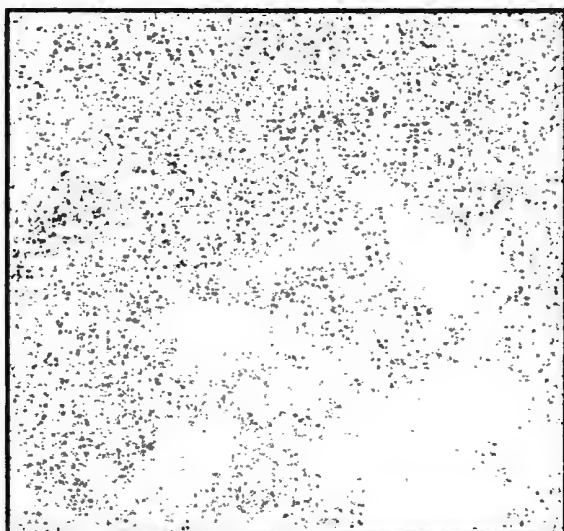
CORROSION HALO.



120161 - silicon

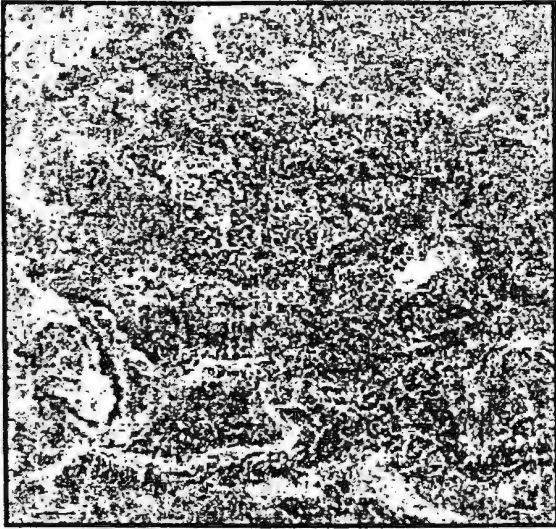


120161 - phosphorus

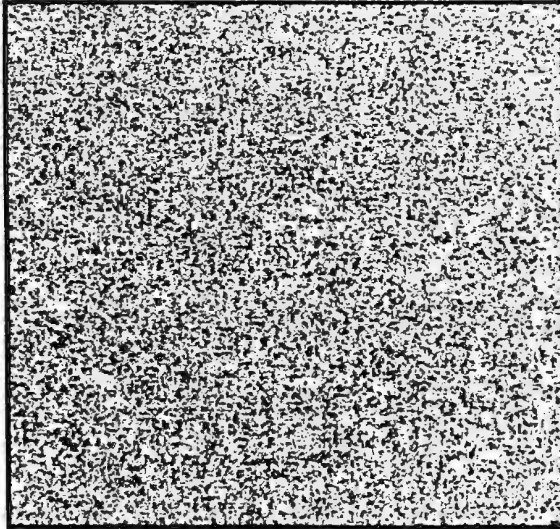


120161 - sulfur

**ELEMENT MAPS
FOR NAILS
FROM
FILL/BUILDING
EVENTS**

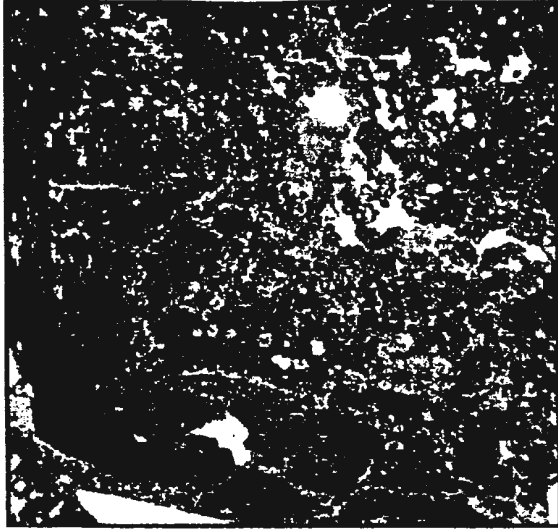


115811 BSE (75 X mag.)

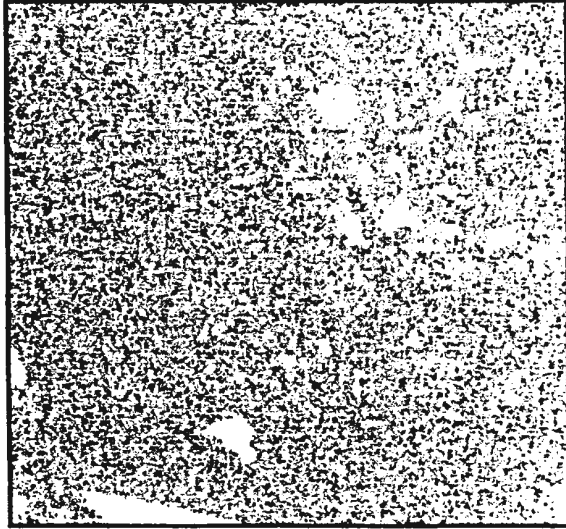


115811 - iron

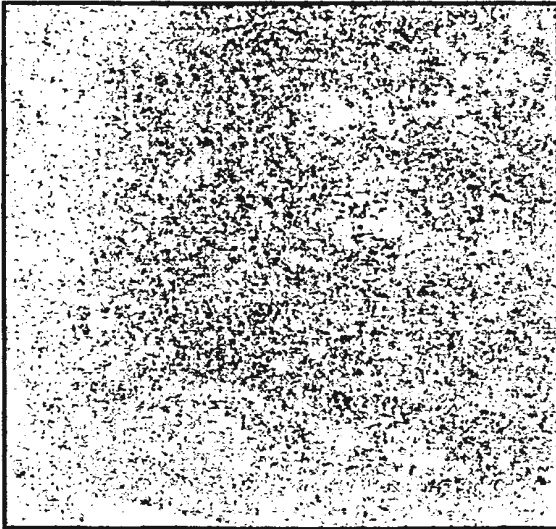
CENTRE OF NAIL.



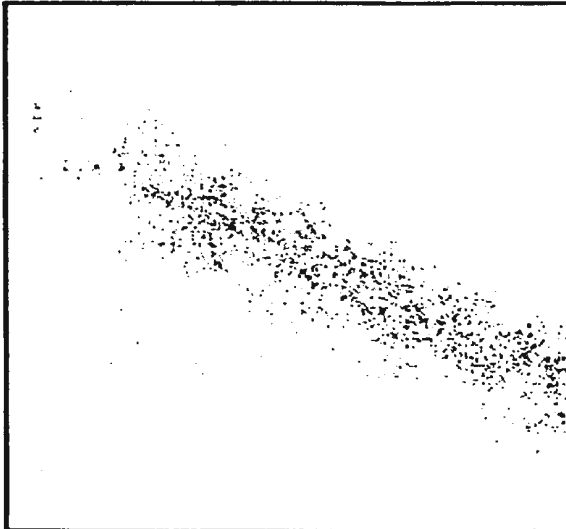
97546 BSE (1000 X mag.)



97546 - iron



97546 - chlorine by ed



97546 - chlorine by wd

EDGE OF VOID AT CENTRE OF NAIL.



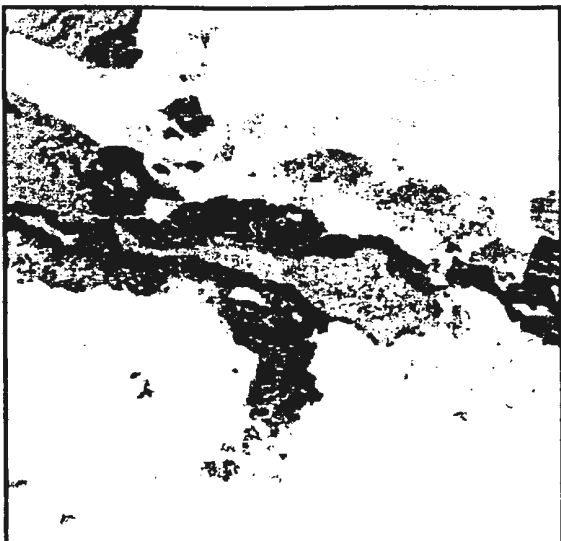
97546 - silicon



97546 - phosphorus



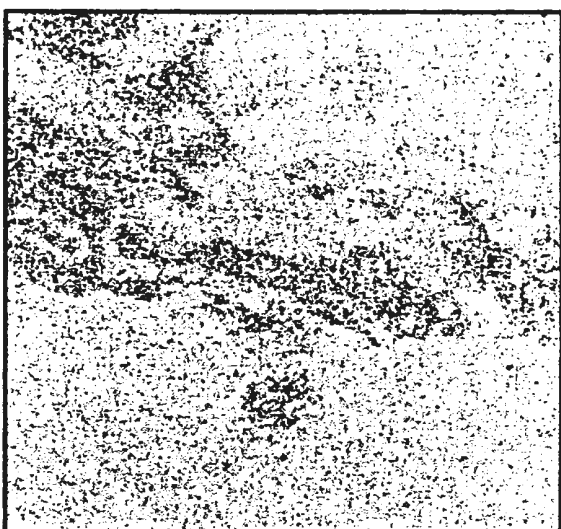
97546 - sulfur



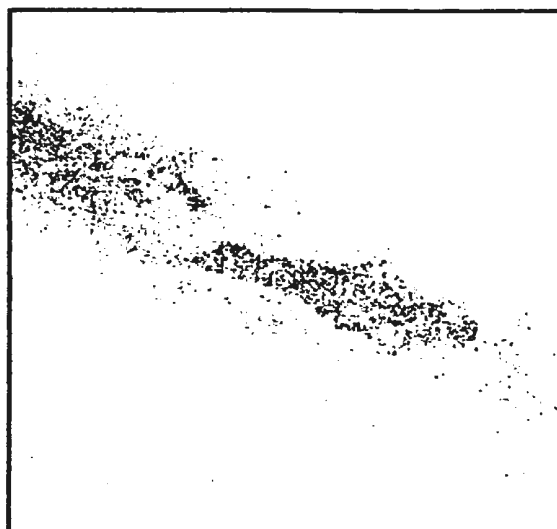
97546 BSE (50 X mag.)



97546 - iron

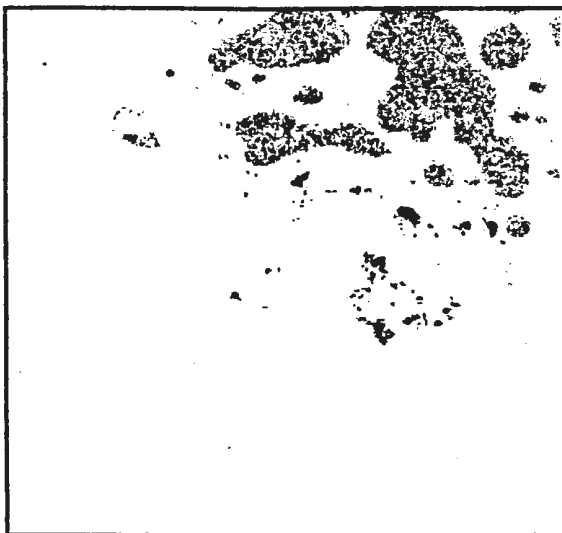


97546 - chlorine by ed

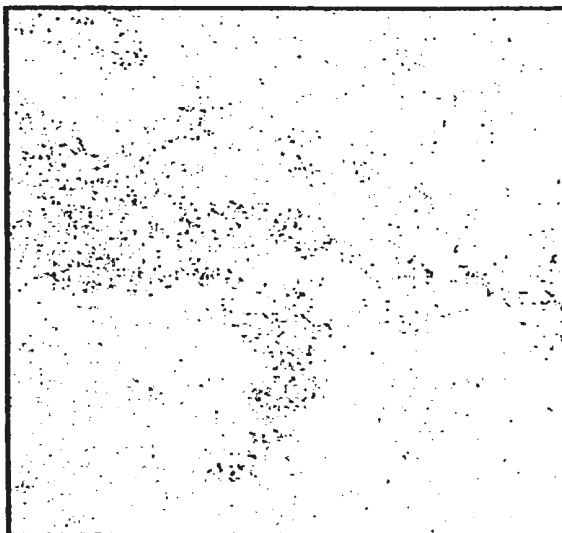


97546 - chlorine by wd

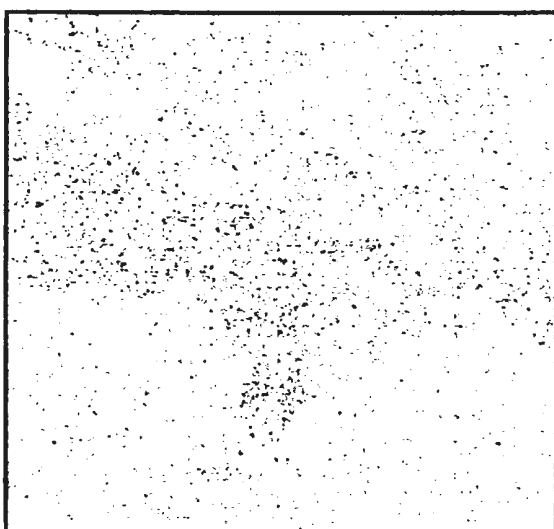
EDGE OF VOID AT NAIL CENTRE.



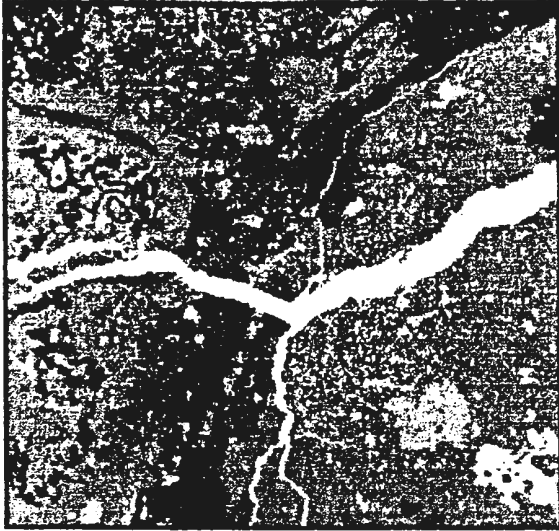
97546 - silicon



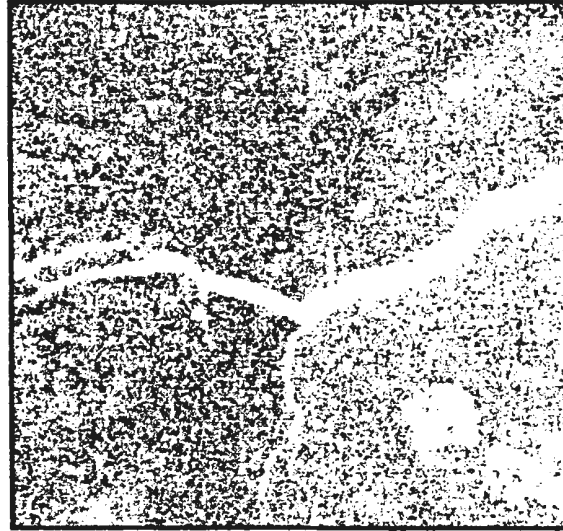
97546 - phosphorus



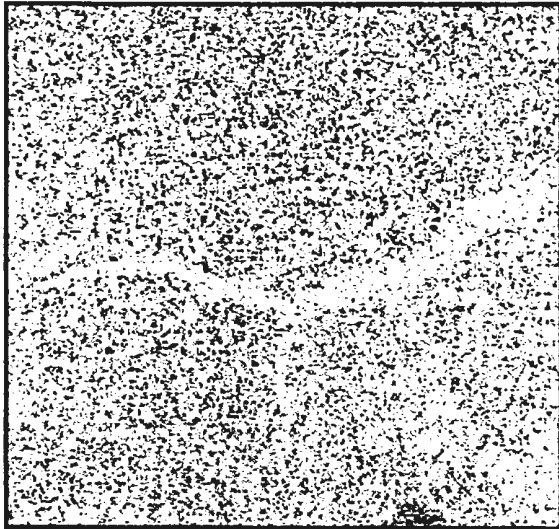
97546 - sulfur



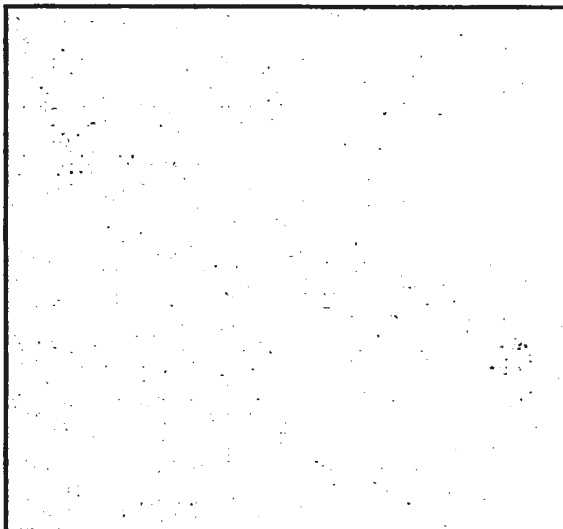
97546 BSE (50 X mag.)



97546 - iron

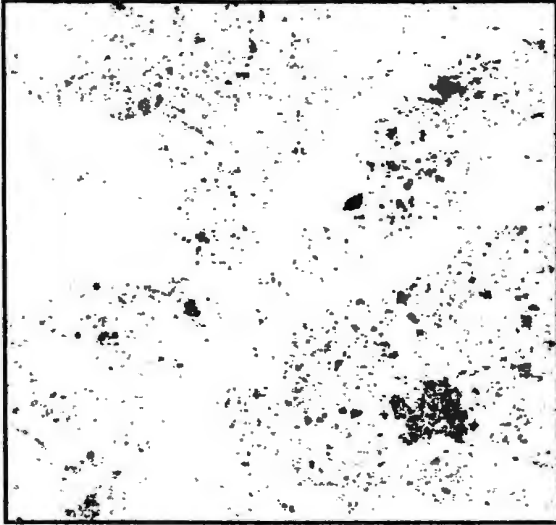


97546 - chlorine by ed



97546 - chlorine by wd

CRACK IN IRON.



97546 - silicon



97546 - phosphorus



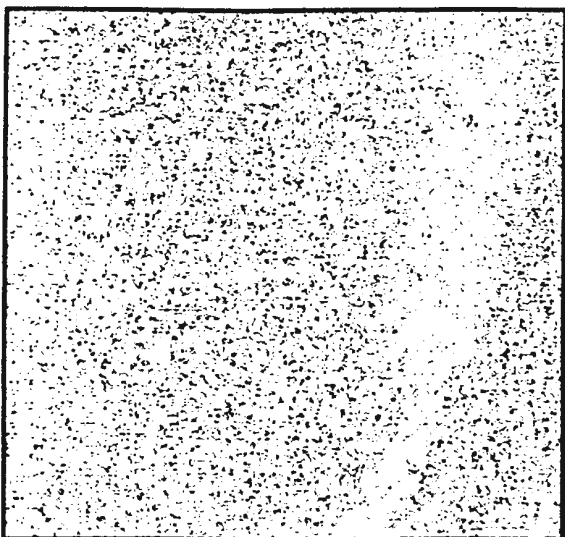
97546 - sulfur



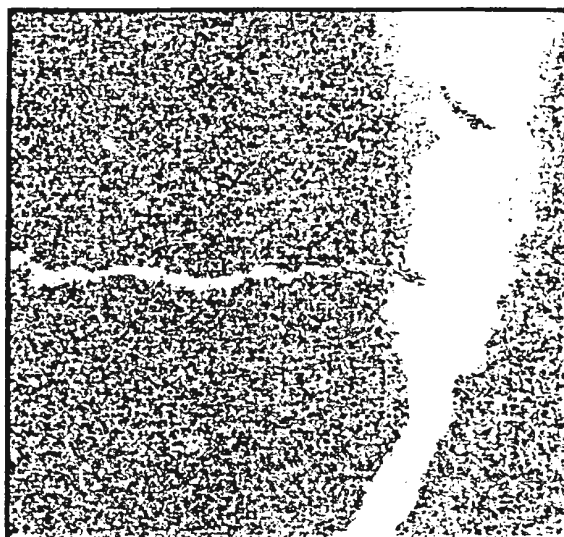
94737 BSE (50 X mag.)



94737 - carbon

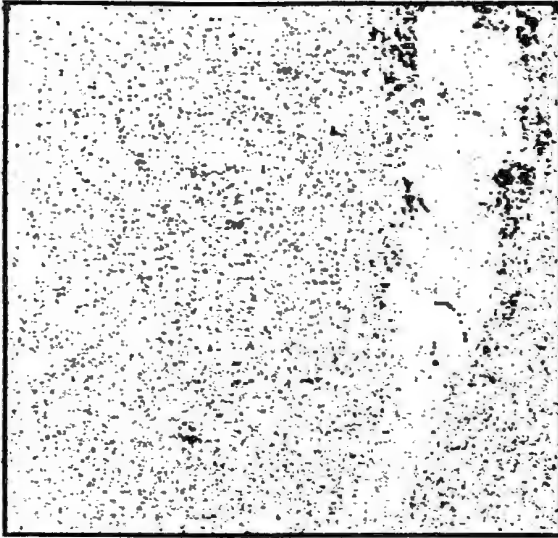


94737 - chlorine

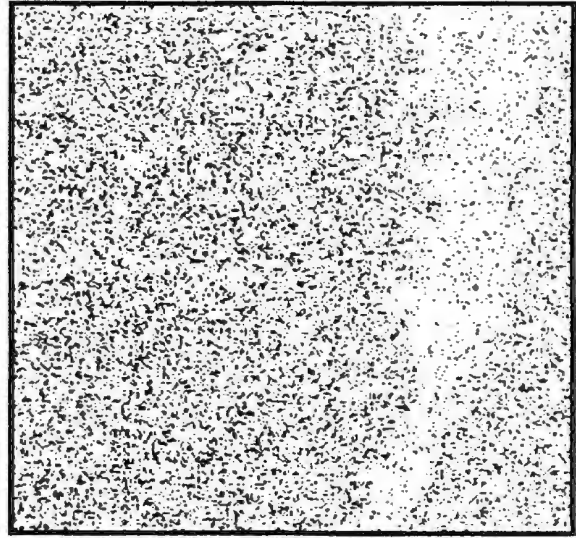


94737 - iron

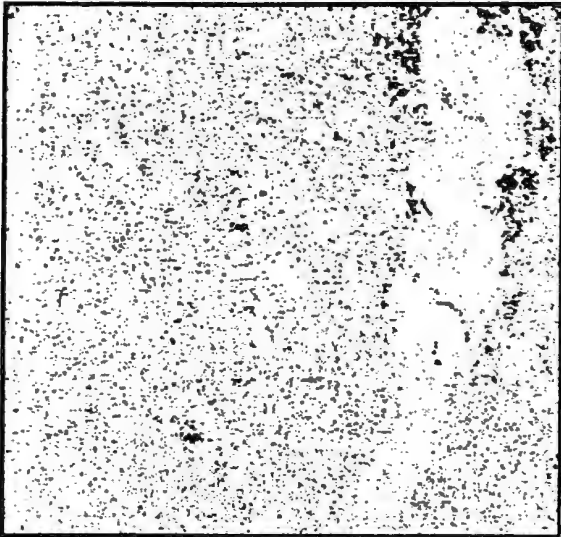
CRACK IN IRON.



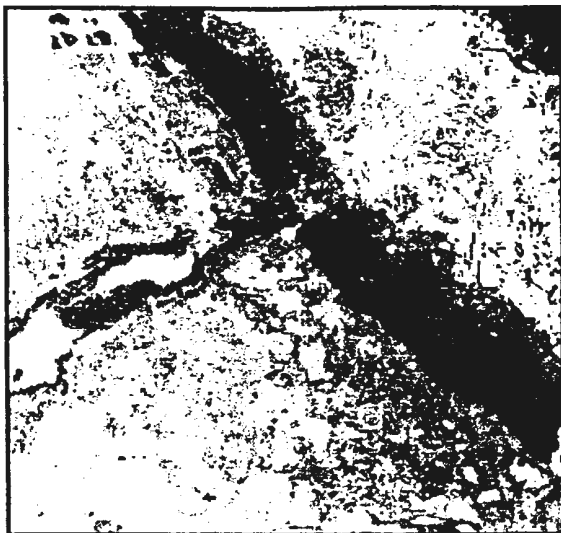
94737 - phosphorus



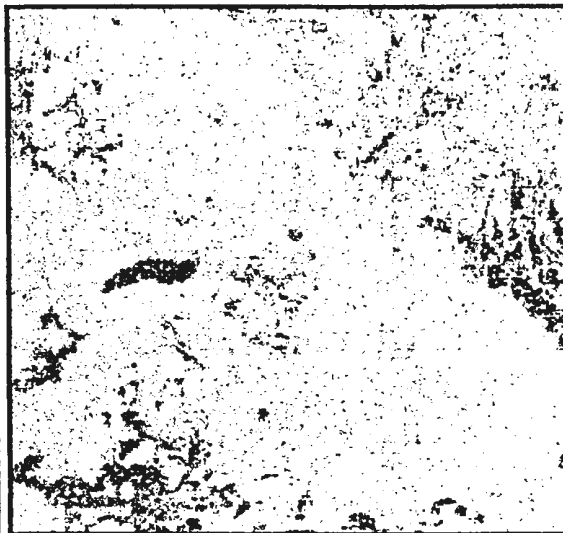
94737 - sulphur



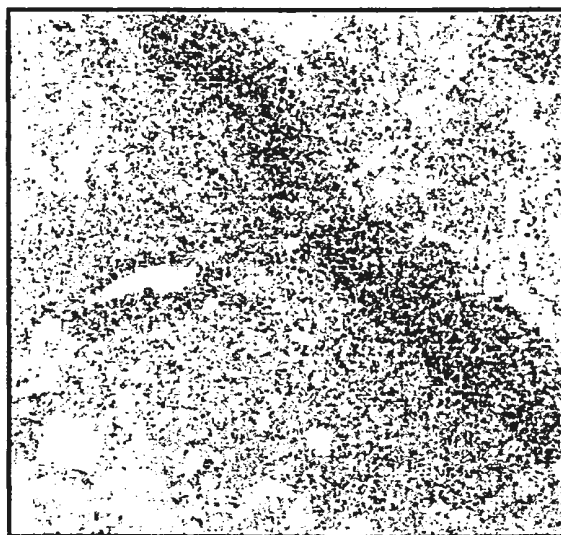
94737 - silicon



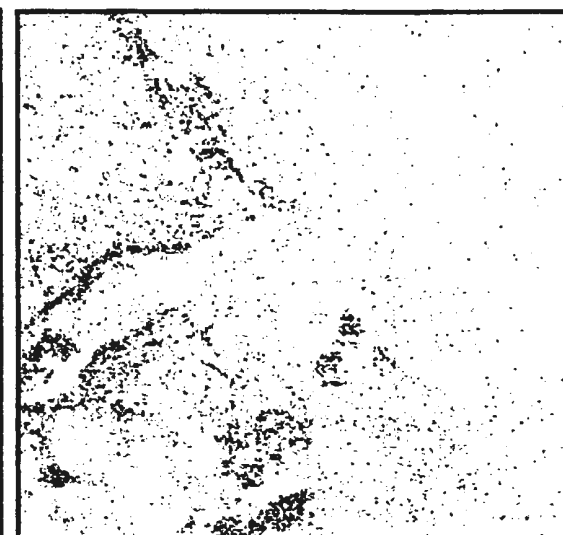
115521 BSE [60 X mag.]



115521 - carbon

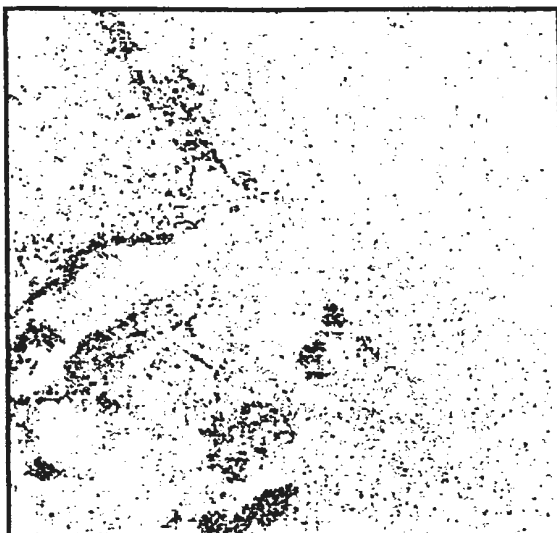


115521 - iron

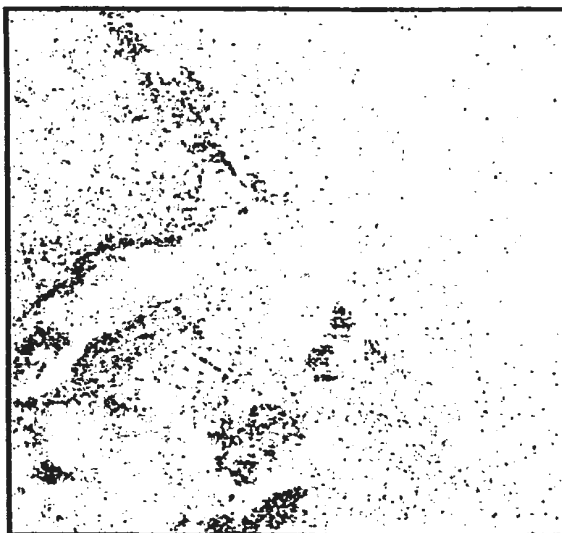


115521 - phosphorus

IRON/CORROSION HALO INTERFACE.



115521 - sulfur



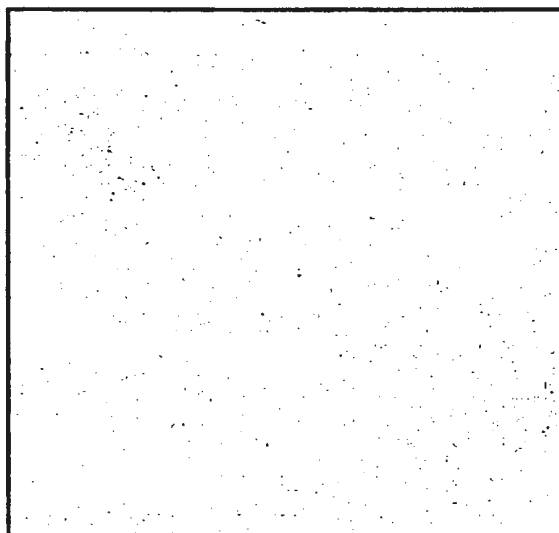
115521 - silicon



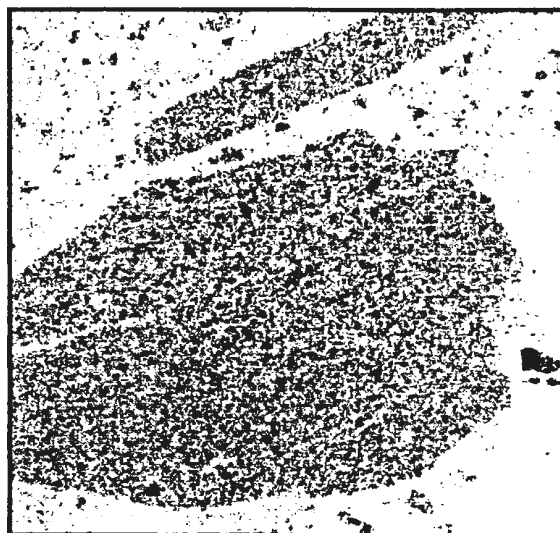
97546 BSE (1000 X mag.)



97546 - iron

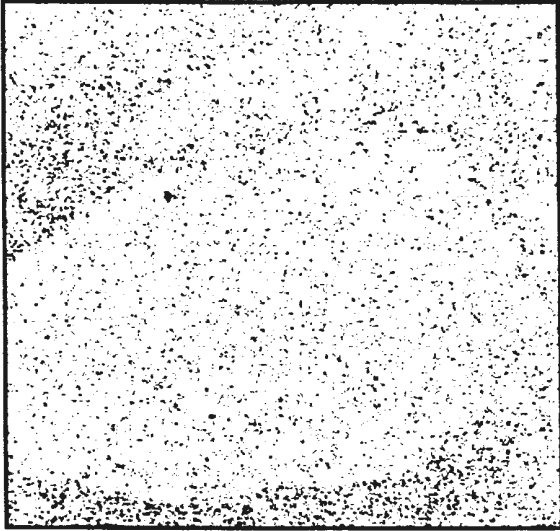


97546 - chlorine by wd

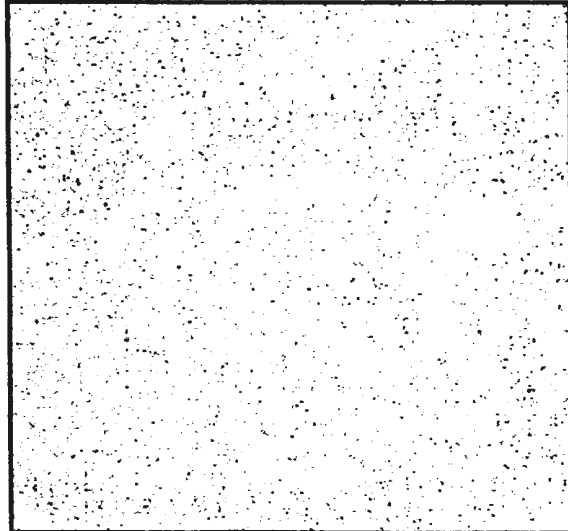


97546 - silicon

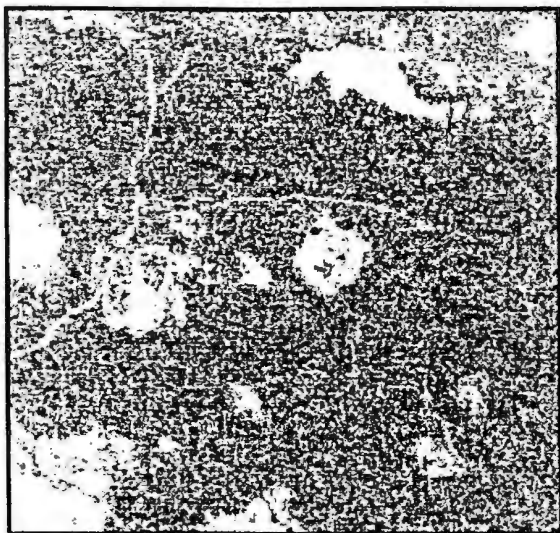
GRAIN IN CORROSION HALO.



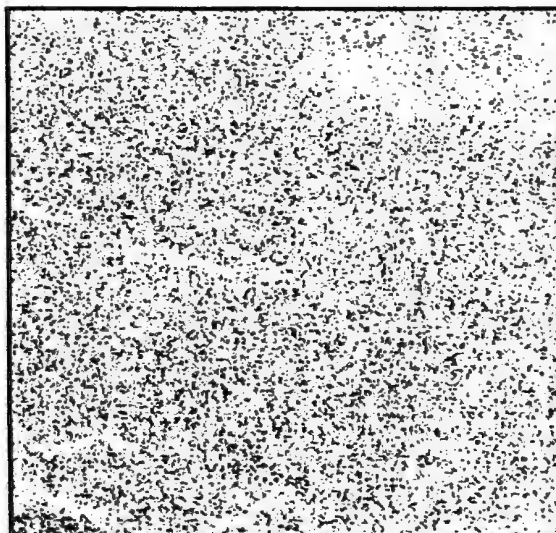
97546 - phosphorus



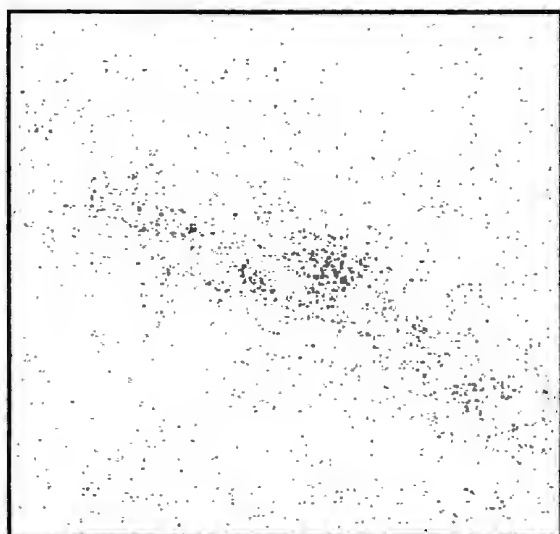
97546 - sulfur



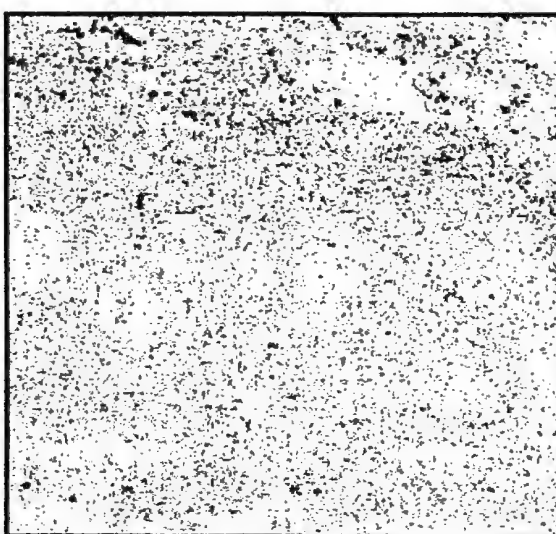
115470 (1000 X mag.) - iron



115470 - chlorine by ed

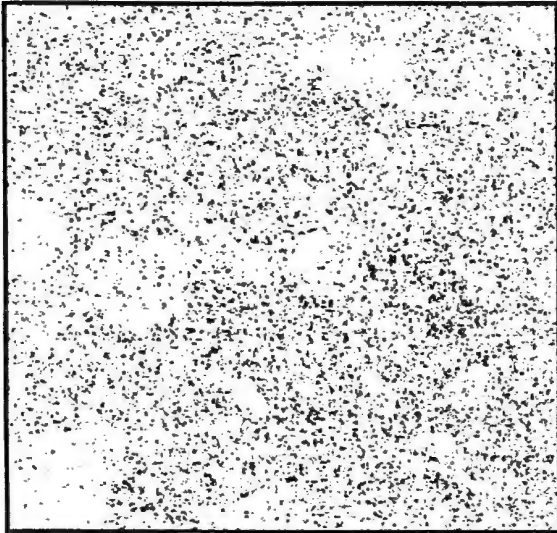


115470 - chlorine by wd



115470 - silicon

CRACK IN CORROSION HALO.



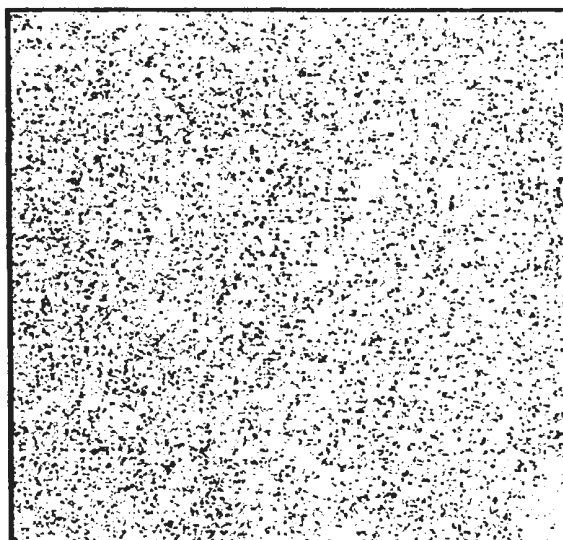
115470 - phosphorus



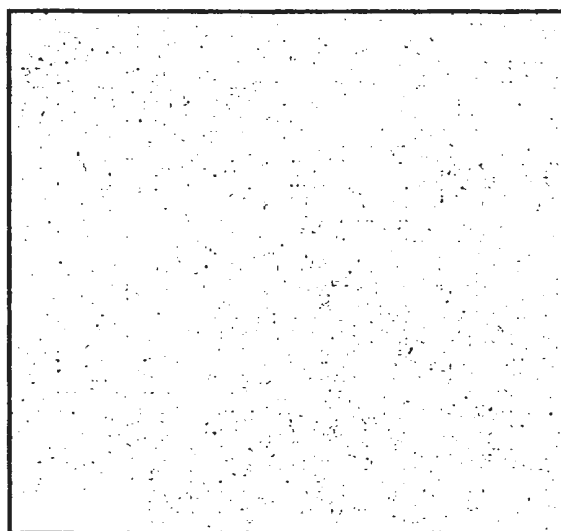
115470 - sulfur



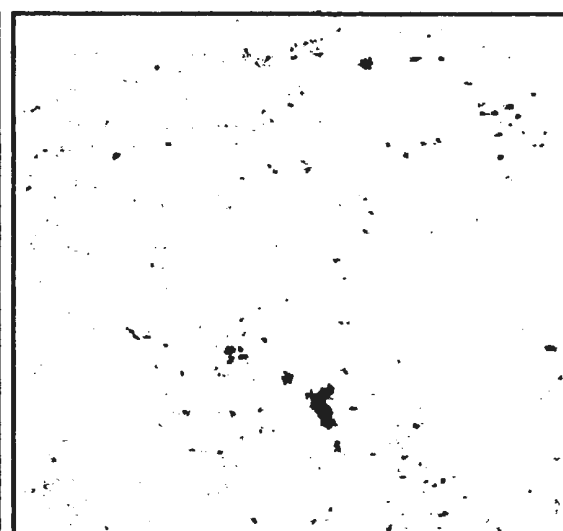
115470 (1000 X mag.) - iron



115470 - chlorine by ed

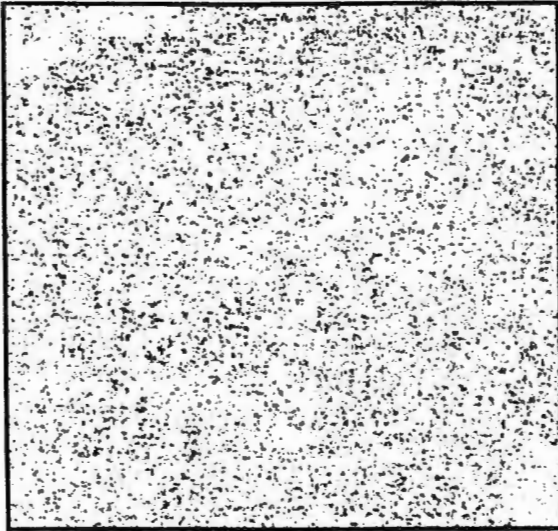


115470 - chlorine by wd



115470 - silicon

WOOD IN CORROSION HALO.



115470 - phosphorus



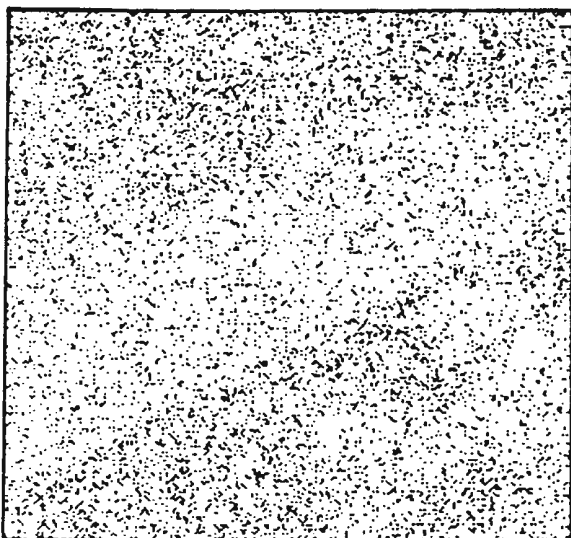
115470 - sulfur



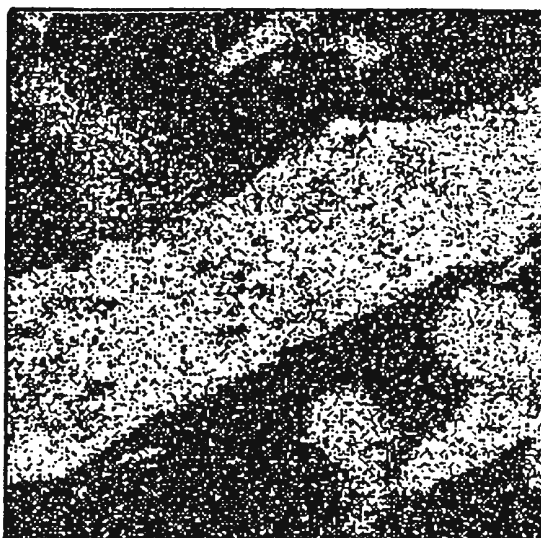
115294 slag BSE (800X mag.)



115294 slag - carbon



115294 slag - chlorine

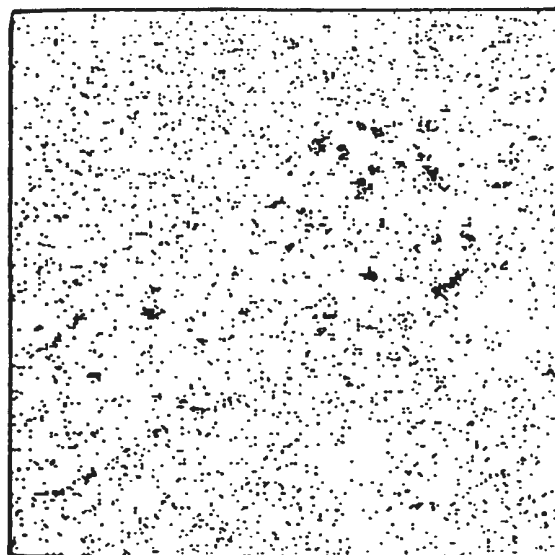


115294 slag - iron

SLAG IN IRON.



115294 slag - silicon



115294 slag - sulfur

APPENDIX 7e

Area B Nails
Instrument setting of 55kV/5mA

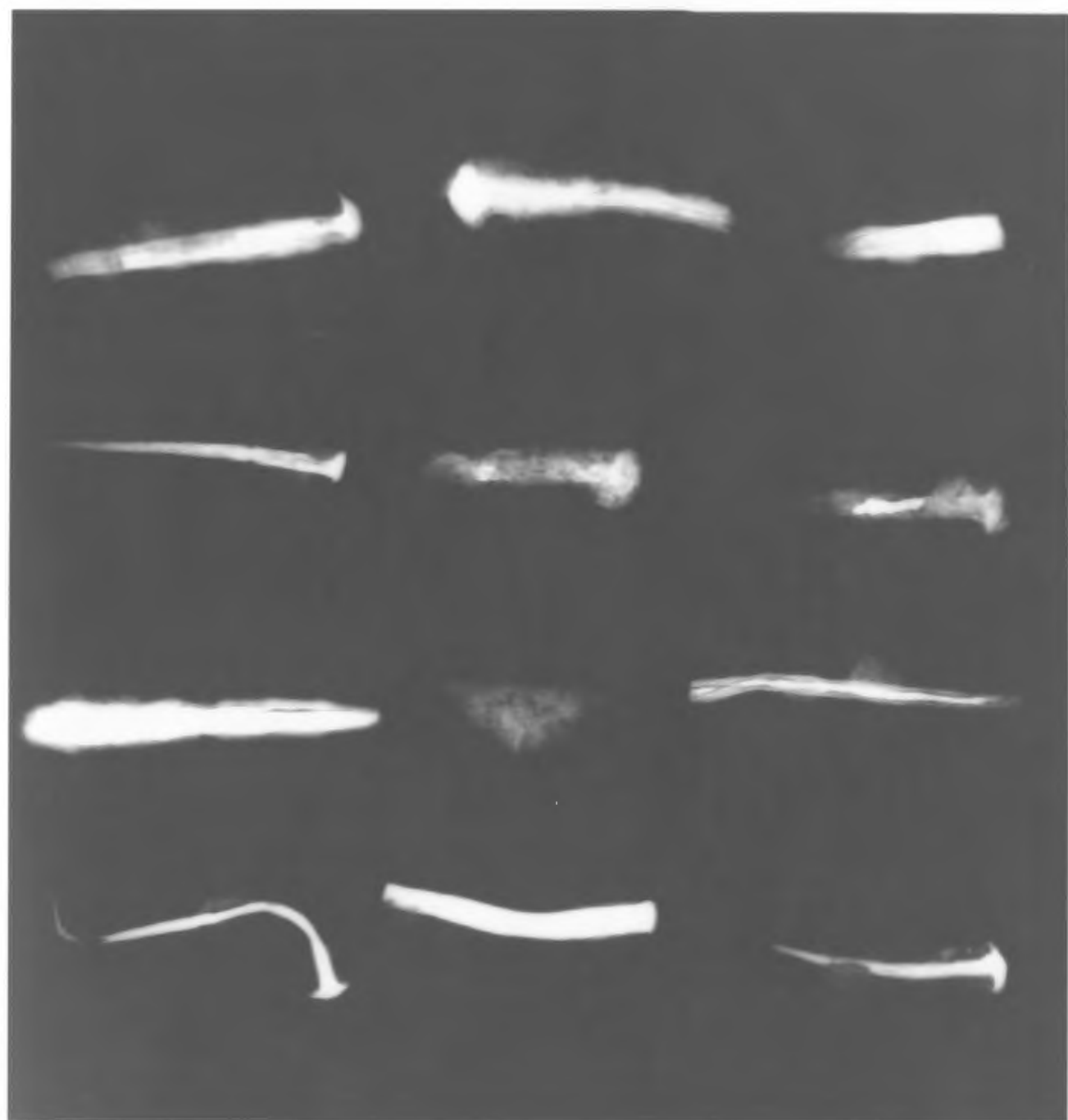
352

115772		



Area B Nails
Instrument setting of 80kV/5mA

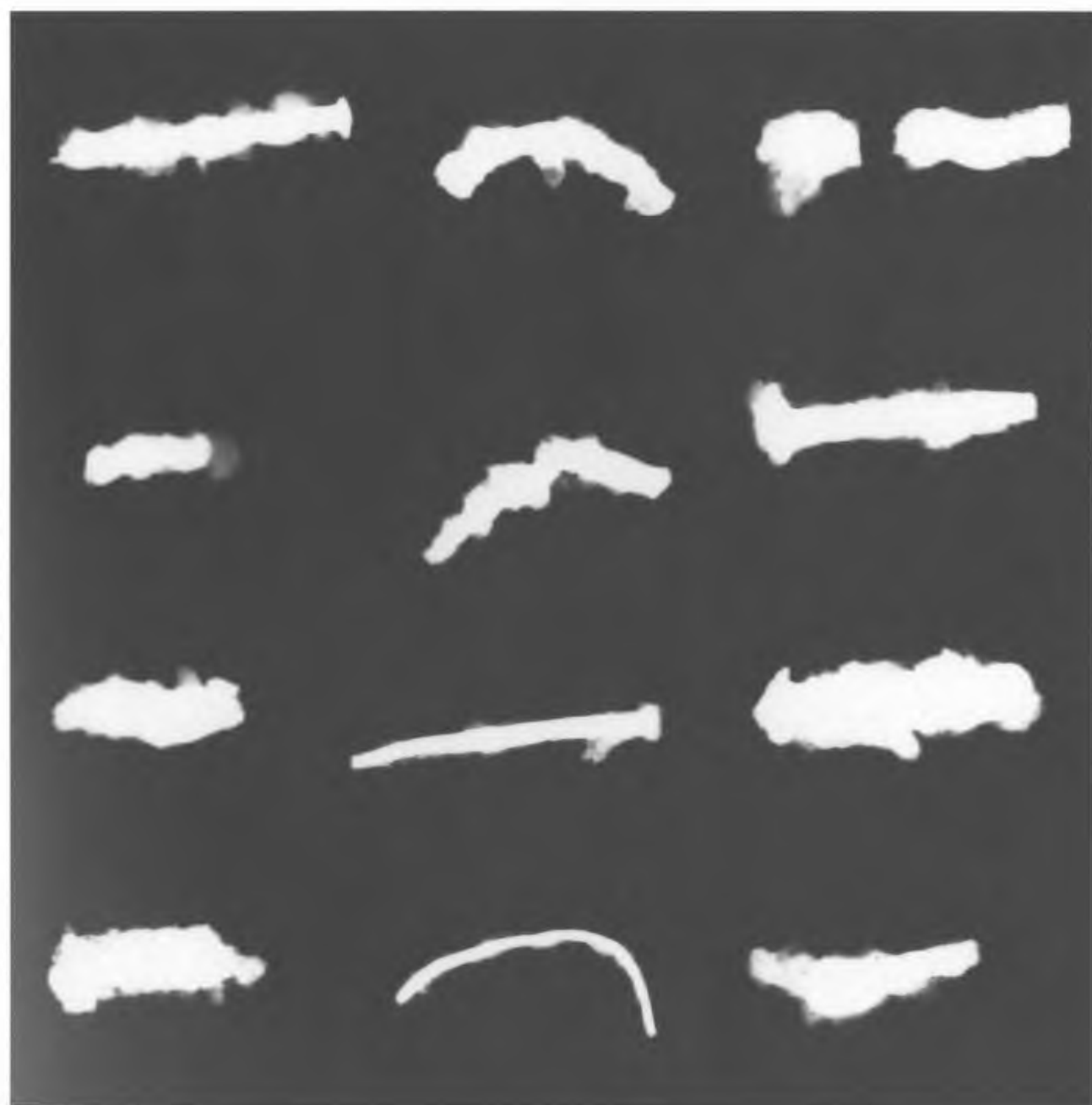
115772		



Area B Nails
Instrument setting of 55kV/5mA

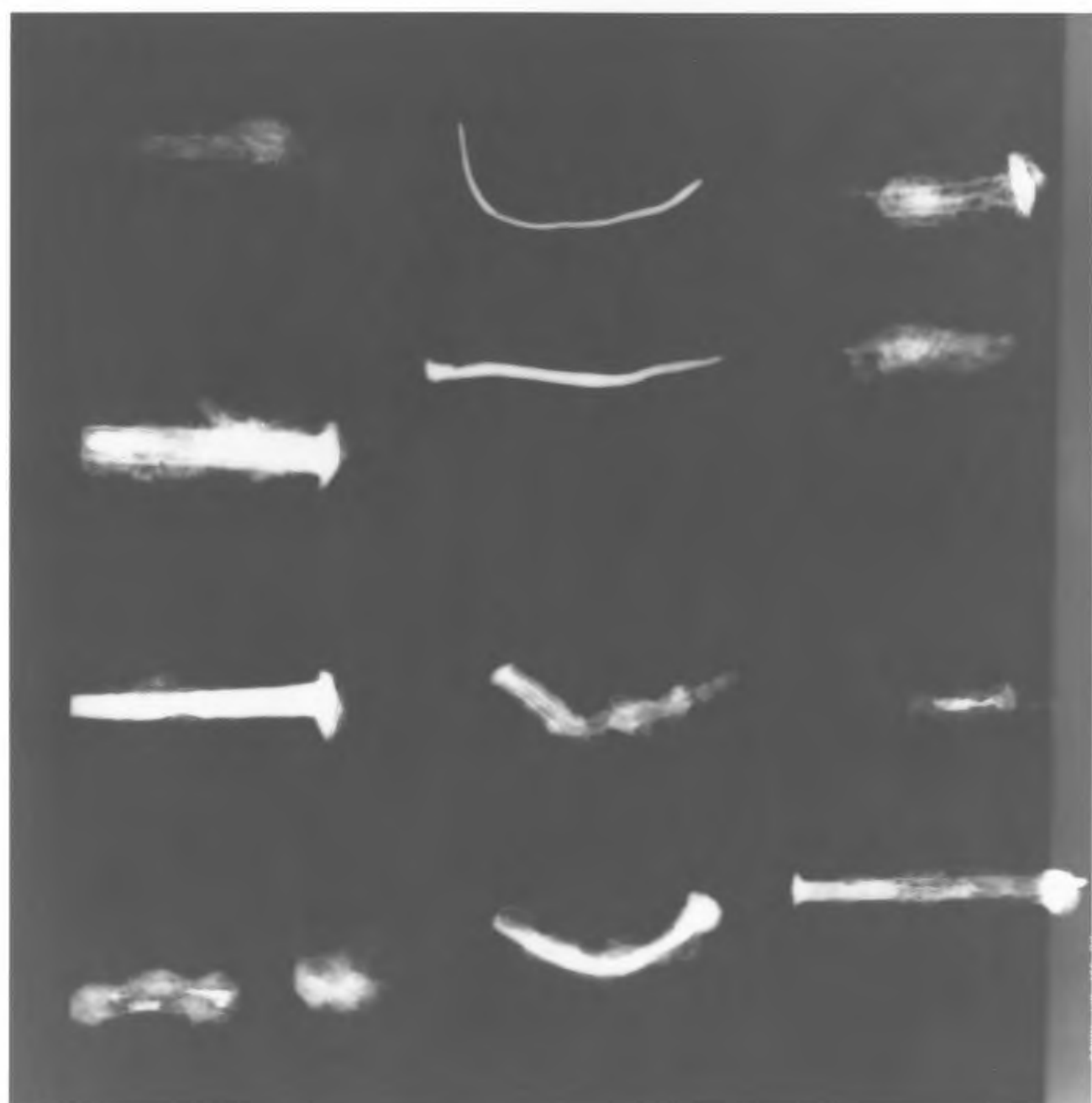
354

115470		
	115521	120531
	115294	120161
	120340	106289



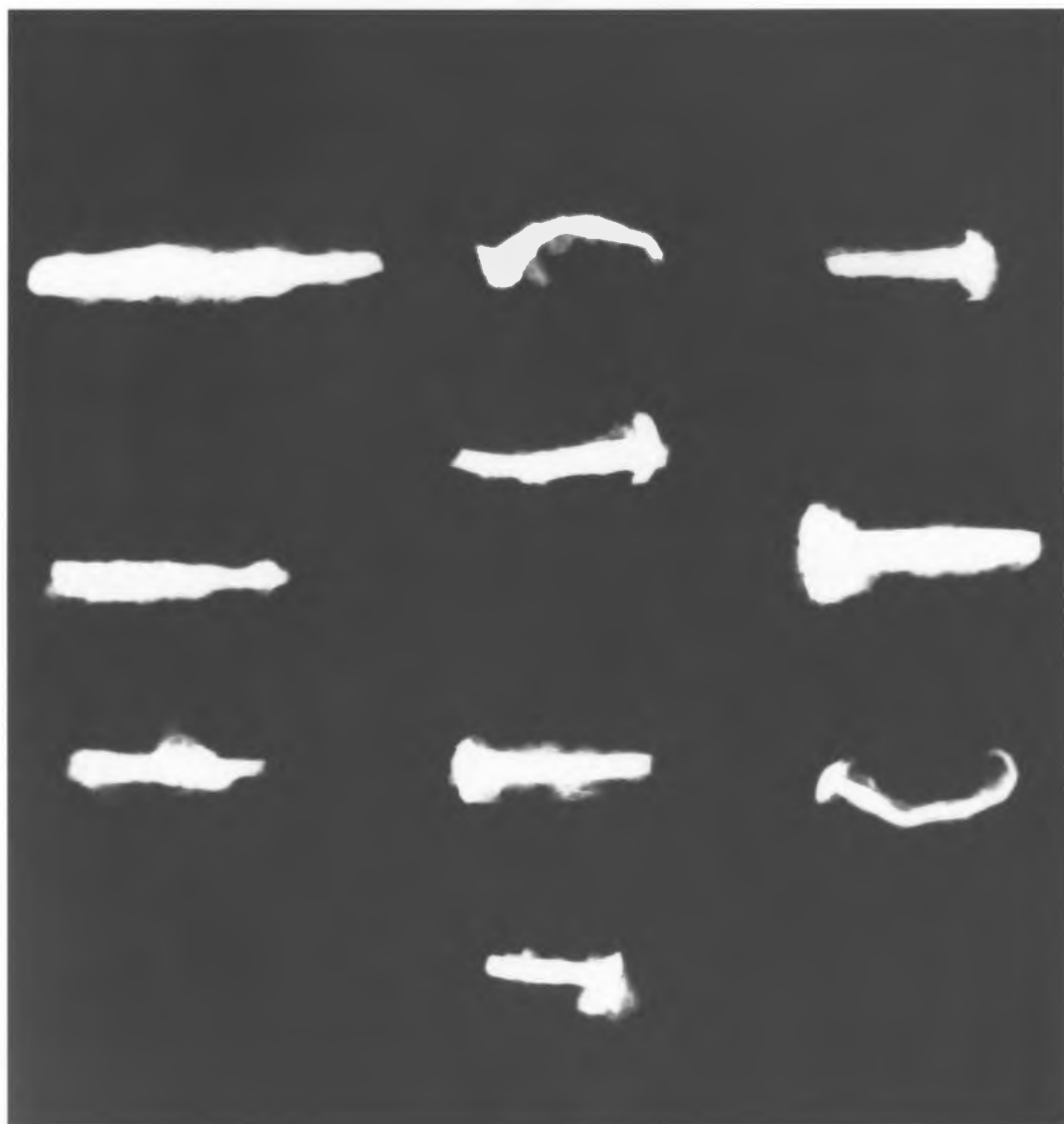
Area B Nails
Instrument setting of 80kV/5mA

106289	120340	
120161	115294	
120531	115521	
97546		115470



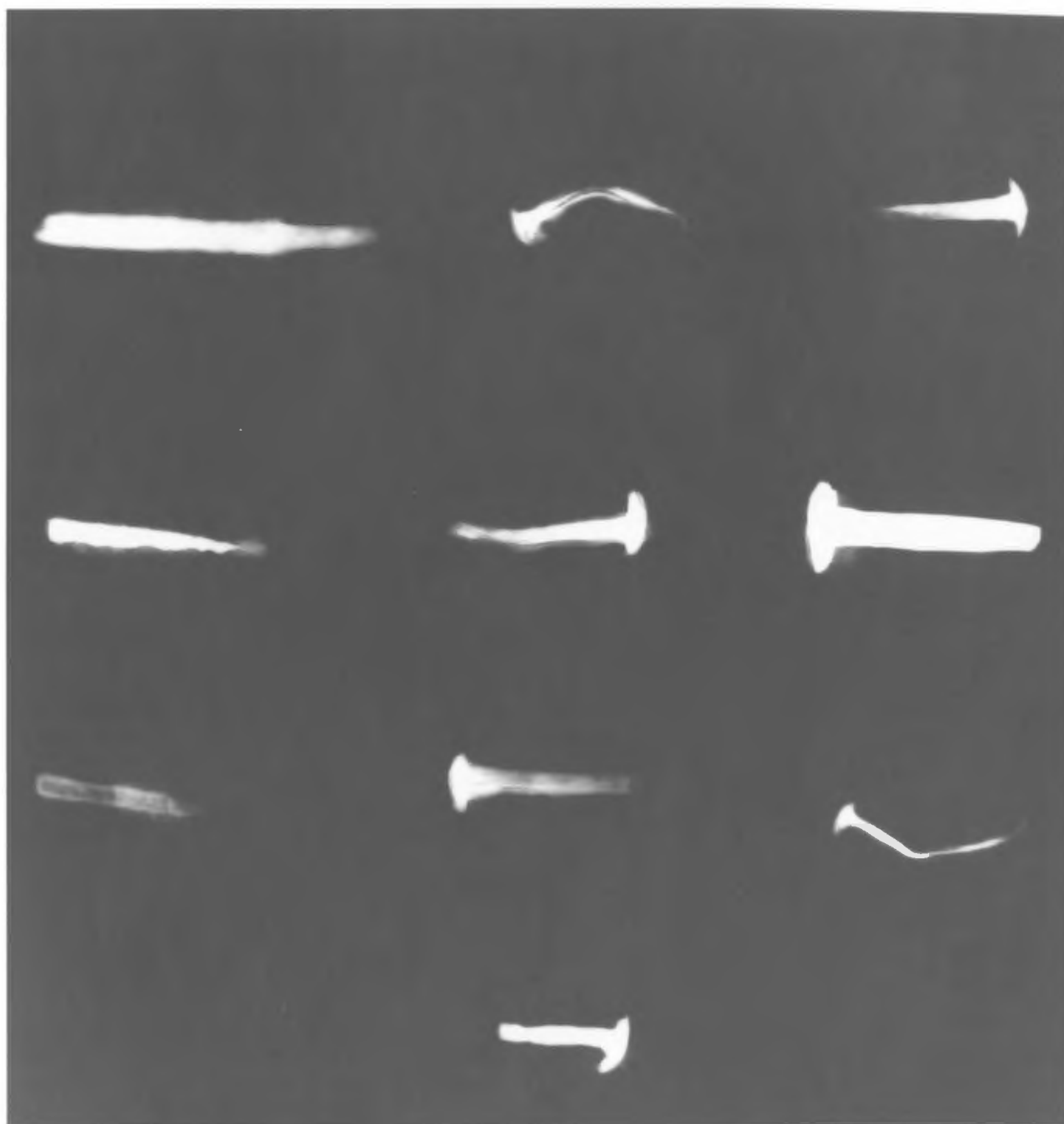
Area B Nails
Instrument setting of 55kV/5mA

115811		
	120389	



Area B Nails
Instrument setting of 80kV/5mA

115811		
	120389	



Area C Nails
Instrument setting of 55 kV/5mA

128193	128195	128190
128192	128189	128304
128290		



Area C Nails
Instrument setting of 80kV/5mA

		128290
128304	128195	128192
128190	128189	128193



Area D Nails
Instrument setting of 55kV/5mA

94759		94121
94120		94123
94743		



Area D Nails
Instrument setting of 80kV/5mA

94759		94121
94120		94123
94743		



Area D Nails
Instrument setting of 55kV/5mA

		87872
99060		



Area D Nails
Instrument setting of 80kV/5mA

		87872
99060		



Area D Nails
Instrument setting of 55kV/5mA

94742	94787 (x-rayed after thin-section removed)	
94745	94785	94737
94788	94786	
94158	94160	94758



Area D Nails
Instrument setting of 80kV/5mA

94742	94787 (x-rayed after thin-section removed)	
94745	94785	94737
94788	94786	
94158	94160	94758



Table 7.3.5a
Nail Type vs Deterioration (length and width)
for occupation/destruction events

366

Sample	Event	Nail type in pennyweight (d)	Normal length (mm)	Actual length (mm)	% decrease in length	Normal Width (mm)	Actual Width (mm)	% decrease in width
94160	62	8d	64	53	17	12	16	0
128193	0	8d	64	53	17	11	19	0
94785	62	8d	64	55	14	9	-----	100
94745	62	8d	64	55	14	9	9	0
94120	62	10d	76	46	40	11	12	0
106289	133	10d	76	50	34	11	-----	100
94787	62	10d	76	54	29	11	-----	100
94786	62	10d	76	60	21	11	14	0
94788	62	10d	76	62	18	12	14	0
128290	195	10d	76	65	15	15	18	0
94742	62	10d	76	70	8	11	-----	75
120389	178	16d	90	45	50	11	15	0
87872	62	16d	90	51	43	11	-----	100
94743	62	16d	90	65	28	11	19	0
99060	96	16d	90	65	28	11	14	0
94759	62	16d	90	66	27	12	19	0
120531	145	20d	102	61	40	17	18	0
120161	143	20d	102	61	40	17	18	0
94758	62	30d	115	57	50	16	17	0
94158	62	30d	115	65	44	16	16	0
94121	62	30d	115	65	44	16	-----	90
94123	62	30d	115	66	48	16	18	0
128189	19	40d	127	47	63	25	-----	100

Table 7.3.5b
Nail Type vs Deterioration (length and width)
for fill/building events

367

Sample	Event	Nail type in pennyweight (d)	Normal length (mm)	Actual length (mm)	% decrease in length	Normal width (mm)	Actual width (mm)	% decrease in width
128195	22	8d	64	50	22	12	21	0
128190	55	10d	76	35	54	9	-----	100
128192	55	10d	76	32	58	12	15	0
128304	16	10d	76	45	41	10	-----	70
115521	138	10d	76	56	26	9	-----	100
115294	134	10d	76	67	12	8	10	0
115470	134	16d	90	62	31	10	9	10
115811	134	16d	90	75	17	11	-----	100
97546	134	20d	102	61	40	17	-----	100
94737	63	20d	102	71	30	17	-----	100
115772	134	30d	115	83	28	18	-----	100
120340	177	?	75	66	12	•	•	12

*no indication that a nail head was part of initial manufacture

Table 7.3.5c
Nail Type vs Deterioration (thickness)
for nails from occupation/destruction events

368

Sample	Nail type in penny-weight (d)	Normal size	Actual size		% decrease in core diameter
		thickness (mm)	iron core (mm)	corrosion halo (mm)	
94160	8d	6	4	4	33
128193	8d	7	6	9	14
94785	8d	6	5	9	17
94745	8d	7	5	6	29
94120	10d	9	5	3	44
106289	10d	7	6	8	14
94787	10d	7	6	3	14
94786	10d	7	4	4	43
94788	10d	9	5	6	44
128290	10d	7	5	7	29
94742	10d	7	5	7	29
120389	16d	9	5	11	44
87872	16d	9	6	10	33
94743	16d	9	5	6	44
99060	16d	8	6	8	25
94759	16d	9	5	13	44
120531	20d	10	8	4	20
120161	20d	9	6	12	33
94758	30d	10	6	2	40
94158	30d	11	8	6	27
94121	30d	10	7	10	30
94123	30d	10	8	5	20
128189	40d	12	10	12	17

Table 7.3.5d
Nail Type vs Deterioration (thickness)
for nails from fill/building events

369

Sample	Nail type in penny-weight (d)	Normal Size	Actual size		% decrease in core diameter
		thickness (mm)	iron core (mm)	corrosion halo (mm)	
128195	8d	7	4	4	44
128190	10d	7	4	11	43
128192	10d	9	4	5	55
128304	10d	8	6	7	25
115521	10d	7	5	7	29
115294	10d	6	4	2	33
115470	16d	6	5	8	17
115811	16d	9	6	6	33
97546	20d	10	8	5	20
94737	20d	10	7	3	30
115772	30d	10	7	6	30
120340	*	3	2	1	33

*object identification of nail is probably incorrect

Table 7.3.5e

[illegible]

Table 7.3.5f
Internal Nail Condition (metallographic) vs Decrease in Core Diameter
for G-3, G-4 and G-5 Metallographic Groups

[illegible]

APPENDIX 7f

Table 7.4.3a
Corrosion Halo Mineralogy
Sorted by Colour for 7.5YR hue
Areas B, C and D

373

Nail	alb	san	cac	ll	hm	goe	ak	mg	mf	chr	mh	gr	sep	phl	metallo graphic Group	Area	Event Group
7.5YR 3/4																	
94787		✓		✓	✓			✓		✓		✓	✓	✓	G-1	D	a/d
94786		✓						✓		✓		✓	✓	?	G-5	D	a/d
7.5YR 4/4																	
120340						?		✓							G-4	B	7b
115470	✓												?	?	G-1	B	7b
99060	✓							??				??	✓		G-2	D	a/d
115521					✓			✓		✓		✓			G-2	B	7b
128304			✓		✓	✓									G-1	C	7b
7.5YR 4/6																	
94737	✓			??								??	?		G-4	D	7b
94745	✓											✓	✓		G-1	D	a/d
94742		✓										✓	?		G-2	D	a/d
94160	✓												?		G-1	D	a/d
94158	✓						??						?		G-1	D	a/d
7.5YR 5/6																	
94120						?	??					✓	?		G-2	D	a/d
94785	✓											✓	✓		G-2	D	a/d
87872	✓			?			??						?	?	G-1	D	a/d
94759	✓			??									??		G-4	D	a/d
94758	✓												??		G-5	D	a/d

Table 7.4.3b
Corrosion Halo Mineralogy
Sorted by Colour for 10YR hue
Areas B, C and D

374

Natl	alb	san	cac	ll	hm	goe	ak	mg	mf	chr	mh	gr	sep	phl	metallo graphic Group	Area	Even Group
10YR 4/4																	
120161								✓	✓						G-2	B	o/d
128190	✓		✓			??	??								G-1	C	o/b
128192	✓		✓			?	?								G-3	C	o/b
97546	✓					?	?	?					?	?	G-1	B	o/b
115294					✓	?		✓		✓		✓	?	?	G-4	B	o/b
115811						?	?	✓		✓	✓				G-2	B	o/b
120389		✓	✓			✓	✓	✓							G-3	B	o/d
10YR 5/6																	
128290			✓			?	✓								G-3	C	o/d
94123				??			??					✓	?		G-2	D	o/d
10YR 5/8																	
94121	✓			?		?	??					✓	?		G-2	D	o/d
10YR 3/6																	
115772	✓		✓			✓	✓	✓				✓			G-3	B	o/b
10YR 6/4																	
128195	✓		✓				✓						✓	✓	G-5	C	o/b
128189	✓		✓			??	??								G-3	C	o/b
10YR 4/6																	
94788	?											✓	✓		G-2	D	o/d
94743	✓					✓							??		G-1	D	o/d
10YR 5/3																	
120531															G-1	D	o/d
106289													?		G-1	B	o/d
10YR 5/4																	
128193	✓		?				?								G-2	C	o/d

APPENDIX 7g

Table 7.6a
Area B Chemical Analysis of Slag

Sample Number	Na ₂ O wt%	MgO wt%	Al ₂ O ₃ wt%	SiO ₂ wt%	P ₂ O ₅ wt%	S (ppm)	Cl (ppm)	K ₂ O wt%	CaO wt%	Sc (ppm)
Sample 1	0.55	0.43	4.99	11.93	1.04	16986.59	1326	0.66	1.32	13
Sample 2	1.23	1.29	14.66	30.00	0.66	6349.3	397	2.53	1.11	20
Sample 3	1.10	0.72	12.72	23.97	1.40	8665.04	613	2.42	1.57	17
Sample 4	1.16	0.58	10.08	22.73	1.01	12197.37	1740	1.76	1.29	16
Sample 5	0.98	1.10	15.39	25.80	0.54	8062.53	262	2.64	0.91	23
Sample 6	0.62	0.23	7.42	17.00	0.93	19173.21	579	1.02	1.30	20
Sample 7	0.29	0.22	3.05	9.06	0.97	9780.85	1412	0.34	0.58	15
Sample 8	0.72	0.73	7.12	16.53	1.29	12550.54	755	0.95	2.61	13
Sample 9	0.77	0.49	9.21	19.95	0.91	10322.49	1033	1.98	1.23	21
Sample 10	0.70	0.33	7.89	15.64	0.89	7860.13	942	1.63	0.95	13
Sample 11	1.34	1.54	13.90	30.84	0.60	5456.86	339	2.47	1.09	19
Sample 12	0.32	0.12	3.69	8.16	1.22	8079.17	636	0.70	0.40	6
Sample 13	0.60	0.27	6.65	13.71	1.03	13595.29	2008	1.41	0.93	14
Sample 14	0.65	0.44	10.66	17.12	1.29	10982.20	762	1.65	1.03	20
Sample 15	0.92	0.65	11.13	22.88	0.67	8607.52	1886	2.26	0.97	12
Sample 16	0.32	0.17	6.22	12.76	1.26	9054.47	980	0.68	0.81	12
Sample 17	0.57	0.55	8.56	17.40	0.96	11531.38	1299	1.66	0.74	6
Sample 18	0.70	0.38	9.26	23.35	0.59	9775.84	724	1.89	0.78	14
Sample 19	1.20	2.05	13.82	22.70	0.70	7148.82	5392	2.01	3.63	38
Sample 20	0.65	0.48	7.51	16.42	1.55	10311.77	493	1.40	0.75	1
Sample 21	0.71	0.36	8.18	16.59	0.83	12212.33	610	1.64	1.34	12
Sample 22	0.78	0.34	8.55	18.44	0.47	10027.5	1091	1.37	1.20	17
Sample 23	0.87	0.56	7.90	20.07	1.21	9145.49	845	1.53	1.13	9
Sample 24	0.38	0.16	4.77	9.24	1.08	8621.11	1827	0.58	0.72	12
Sample 25	0.49	0.21	5.21	11.55	1.43	6585.37	885	0.84	0.90	7
Sample 26	0.97	1.02	10.39	31.07	0.60	8036.46	228	2.01	3.58	19
Sample 27	0.45	0.27	8.03	17.22	1.22	25893.61	1096	1.51	0.68	19
Sample 28	1.07	0.96	12.05	33.79	0.51	6709.08	140	2.11	3.92	14
Sample 29	1.08	0.74	13.38	23.14	0.82	6025.83	664	2.33	1.25	27
Sample 30	0.88	0.77	7.85	22.48	1.04	5208	1682	1.29	2.38	13
Mean	0.77	0.61	9.01	19.38	0.96	10165.23	1088.20	1.58	1.37	15.4
L.D.	0.010	0.11	0.008	0.011	0.003	12	25	0.003	0.003	9

L.D. = limit of detection

Table 7.6b
Area B Chemical Analysis of Slag (continued)

Sample Number	TiO ₂ wt%	V (ppm)	Cr (ppm)	MnO wt%	Fe ₂ O ₃ T wt%	Ni (ppm)	Cu (ppm)	Zn (ppm)	Ga (ppm)	As (ppm)
Sample 1	0.19	87	42	0.20	48.75	21.58	200.72	7.04	0.25	17.92
Sample 2	0.50	168	131	0.08	20.77	39.83	70.50	<LD	4.53	23.47
Sample 3	0.42	201	129	0.08	24.56	23.72	128.83	<LD	3.21	21.39
Sample 4	0.40	373	90	0.09	29.15	39.12	187.75	6.04	12.73	29.17
Sample 5	0.47	182	144	0.06	21.39	50.91	83.03	<LD	3.04	8.50
Sample 6	0.19	337	108	0.04	36.16	54.44	165.45	<LD	8.52	39.37
Sample 7	0.17	81	48	0.09	54.74	87.65	258.02	<LD	11.71	95.34
Sample 8	0.29	119	74	0.23	39.58	36.54	185.93	<LD	6.52	30.96
Sample 9	0.37	155	123	0.06	31.14	18.92	210.36	<LD	4.96	31.35
Sample 10	0.29	132	84	0.05	41.29	16.14	178.52	<LD	5.96	26.20
Sample 11	0.48	160	112	0.11	17.94	28.64	55.25	<LD	1.86	11.60
Sample 12	0.16	67	32	0.10	52.81	9.81	411.84	0.20	4.85	60.46
Sample 13	0.28	133	98	0.09	37.83	37.78	133.40	6.29	7.19	8.63
Sample 14	0.38	234	124	0.07	31.44	39.37	199.05	24.80	11.54	20.44
Sample 15	0.38	159	116	0.04	26.67	20.92	171.69	<LD	6.27	23.32
Sample 16	0.30	280	85	0.06	43.21	87.80	427.23	54.93	13.90	20.63
Sample 17	0.35	122	106	0.06	34.49	17.29	91.06	<LD	3.04	18.20
Sample 18	0.37	437	161	0.05	25.04	74.03	247.31	8.20	14.91	7.99
Sample 19	0.52	199	150	0.14	14.98	79.37	27889.92	1101.08	18.48	140.48
Sample 20	0.28	225	74	0.07	39.28	53.83	514.92	8.11	13.95	40.38
Sample 21	0.30	151	86	0.07	37.46	20.51	169.40	<LD	8.54	8.00
Sample 22	0.36	202	104	0.05	35.65	22.74	207.82	<LD	4.90	12.27
Sample 23	0.33	111	96	0.12	30.22	22.74	207.82	23.06	12.58	40.29
Sample 24	0.21	86	61	0.12	49.01	44.41	320.46	<LD	5.05	30.89
Sample 25	0.21	101	76	0.04	43.43	11.03	150.35	50.63	13.44	19.91
Sample 26	0.37	196	93	0.05	18.75	49.34	153.39	35.33	7.59	21.21
Sample 27	0.35	412	116	0.03	34.98	73.54	279.97	7.38	13.65	37.23
Sample 28	0.39	195	111	0.04	15.27	47.65	135.99	0.00	6.28	20.03
Sample 29	0.42	188	144	0.06	25.34	37.80	106.38	0.00	5.92	24.85
Sample 30	0.44	139	102	0.20	48.23	15.32	138.34	7.53	4.90	23.91
Mean	0.35	187.73	100.67	0.085	33.65	39.43	1122.69	44.69	8.01	31.81
L.D.	0.004	6	8	0.002	0.006	6	4	4	3	16

Table 7.6c
Area B Chemical Analysis of Slag (continued)

378

Sample Number	Rb (ppm)	Sr (ppm)	Y (ppm)	Zr (ppm)	Nb (ppm)	Ba (ppm)	Ce (ppm)	Pb (ppm)	Th (ppm)	U (ppm)	Total wt%
Sample 1	28.12	351.39	17.79	73.33	7.37	2065.99	-2.10	20.71	7.97	4.77	96.48
Sample 2	130.06	383.30	29.62	172.78	16.19	1641.74	82.63	308.54	14.30	5.72	94.07
Sample 3	121.47	715.16	33.03	152.75	13.25	2772.92	150.04	13.52	15.74	5.01	89.68
Sample 4	79.08	184.76	31.14	178.03	12.83	607.34	75.28	23.68	12.91	7.11	90.64
Sample 5	137.43	380.47	30.27	154.77	15.24	1767.22	119.30	12.67	17.59	4.76	89.30
Sample 6	43.45	253.95	37.24	147.16	15.69	765.97	83.89	21.93	14.32	5.40	88.82
Sample 7	15.95	167.41	10.13	63.97	6.79	1392.60	36.75	25.55	7.93	<LD	95.97
Sample 8	43.17	603.87	25.41	116.47	10.97	2610.61	21.72	43.12	10.24	3.78	94.18
Sample 9	1110.60	498.29	27.40	153.66	12.13	1955.13	59.94	18.75	14.51	3.77	87.94
Sample 10	83.88	443.11	23.81	111.59	10.55	1770.71	52.71	20.30	12.47	6.29	93.29
Sample 11	119.83	303.83	28.39	168.11	15.13	1574.92	116.76	10.15	13.71	4.73	90.61
Sample 12	34.86	87.19	9.40	49.70	4.94	1034.27	45.58	47.58	7.53	<LD	92.64
Sample 13	73.37	343.52	19.98	107.00	9.45	1707.92	69.67	21.94	8.95	1.02	85.79
Sample 14	99.37	306.45	32.92	145.23	13.95	1467.85	125.85	38.60	18.52	7.20	86.18
Sample 15	121.52	401.52	26.67	163.59	12.60	1729.54	99.84	30.32	11.11	3.79	88.38
Sample 16	33.81	94.48	23.72	117.25	14.53	544.08	70.42	31.34	8.75	4.33	89.62
Sample 17	95.26	281.47	21.94	125.97	13.07	1444.31	78.85	20.73	11.68	2.93	88.19
Sample 18	95.17	223.59	48.38	179.55	16.33	1836.55	148.53	197.36	12.20	10.74	83.92
Sample 19	110.22	487.78	34.85	144.99	14.63	2206.06	125.14	542.11	12.83	2.49	82.95
Sample 20	67.44	239.44	23.99	108.09	10.11	770.34	25.29	26.13	7.47	9.18	92.32
Sample 21	92.90	315.22	30.38	128.35	10.46	1334.34	102.15	21.64	13.89	2.49	91.17
Sample 22	71.11	351.00	31.01	161.92	13.43	1334.57	40.24	16.52	12.45	6.40	90.75
Sample 23	74.85	258.40	20.94	123.92	10.76	1085.91	63.72	28.54	10.34	3.09	85.79
Sample 24	27.43	281.89	25.11	78.77	7.85	698.56	65.90	28.48	5.21	8.13	90.87
Sample 25	41.85	259.41	18.18	87.52	8.14	1106.98	34.72	88.86	8.28	4.74	87.01
Sample 26	96.68	865.73	33.65	163.61	14.09	1855.21	62.83	30.20	12.22	5.75	90.86
Sample 27	76.83	301.48	42.82	164.36	14.47	1660.14	89.41	48.29	11.27	13.28	89.83
Sample 28	102.74	1012.10	33.01	158.94	13.79	1934.59	75.11	25.30	17.24	3.94	91.79
Sample 29	124.62	532.13	31.82	163.61	13.40	2306.67	110.84	15.99	18.02	5.45	89.55
Sample 30	65.14	610.84	30.65	123.32	11.46	2808.50	92.42	17.44	11.50	<LD	87.53
Mean	113.94	384.64	27.78	132.94	12.12	1593.05	77.52	59.88	12.04	4.86	89.87
L.D.	0.8	1.4	0.8	1.3	0.8	29	48	4	3	4	n/a

Table 7.6d
Area C Chemical Analysis of Slag

Sample Number	Na ₂ O wt%	MgO wt%	Al ₂ O ₃ wt%	SiO ₂ wt%	P ₂ O ₅ wt%	S (ppm)	Cl (ppm)	K ₂ O wt%	CaO wt%	Sc (ppm)
Sample 31	1.47	1.42	16.83	26.79	0.72	3516.45	274	2.73	1.11	27
Sample 32	0.90	0.57	10.94	22.15	1.07	7399.31	840	2.13	1.25	12
Sample 33	0.77	0.29	7.53	15.95	0.77	10063.39	1088	1.57	1.60	10
Sample 34	0.71	0.28	7.40	14.94	0.71	10084.78	879	1.39	0.81	16
Sample 35	0.58	0.46	9.28	15.92	1.42	8600.73	556	1.76	0.86	14
Sample 36	0.49	0.27	6.06	14.19	0.85	7367.88	1714	1.17	0.74	8
Sample 37	1.03	0.43	8.64	16.07	1.19	9109.49	893	1.40	1.21	11
Sample 38	0.80	0.66	11.85	24.23	1.29	10277.81	280	2.27	1.24	19
Sample 39	1.27	1.01	10.34	23.68	1.04	5129.06	653	1.94	1.12	7
Sample 40	0.94	0.49	9.91	20.82	0.98	6853.75	1064	2.15	1.12	8
Sample 41	0.44	0.19	5.35	10.91	1.26	8482.54	1702	1.19	0.84	16
Sample 42	1.01	0.68	10.60	22.46	0.75	6980.77	379	2.19	1.20	16
Sample 43	0.94	0.61	11.49	24.01	1.11	6596.37	428	2.09	1.06	13
Sample 44	0.37	0.26	9.19	16.86	1.10	19425.06	679	1.79	0.56	20
Sample 45	0.67	0.95	20.15	31.09	0.44	7215.14	161	2.09	0.69	35
Sample 46	2.00	1.19	14.65	29.11	0.86	4357.35	375	2.21	2.12	16
Mean	0.90	0.61	10.64	20.57	0.97	8216.24	747.81	1.88	1.10	15.5
L.D.	0.010	0.11	0.008	0.011	0.003	12	25	0.003	0.003	9

Table 7.6e
Area C Chemical Analysis (continued)

380

Sample Number	TiO ₂ wt%	V (ppm)	Cr (ppm)	MnO wt%	Fe ₂ O ₃ T wt%	Ni (ppm)	Cu (ppm)	Zn (ppm)	Ca (ppm)	As (ppm)
Sample 31	0.44	206	156	0.24	19.95	61.63	93.69	<LD	9.67	22.06
Sample 32	0.39	171	124	0.05	29.09	39.64	146.43	<LD	8.40	18.30
Sample 33	0.29	117	74	0.05	39.34	29.99	144.87	<LD	7.02	37.31
Sample 34	0.26	122	71	0.07	44.68	5.05	138.71	<LD	4.61	24.90
Sample 35	0.36	155	106	0.04	31.64	20.41	221.04	10.85	1.36	79.95
Sample 36	0.23	105	75	0.05	42.54	17.03	235.75	<LD	5.79	25.04
Sample 37	0.28	116	78	0.05	37.63	32.28	160.10	4.11	7.41	22.55
Sample 38	0.40	163	128	0.05	23.17	19.25	96.85	<LD	5.85	16.96
Sample 39	0.39	130	89	0.06	28.05	29.65	266.91	17.32	10.56	10.81
Sample 40	0.36	152	126	0.10	30.08	15.42	151.97	<LD	9.66	12.20
Sample 41	0.24	108	80	0.04	41.53	22.78	185.48	15.31	6.23	35.47
Sample 42	0.40	170	131	0.06	26.33	6.90	235.39	<LD	5.17	18.37
Sample 43	0.36	156	120	0.04	28.37	32.64	202.17	<LD	7.97	44.29
Sample 44	0.41	493	118	0.04	31.87	38.02	141.84	4.61	11.97	40.69
Sample 45	0.72	776	202	0.03	14.19	94.26	227.65	<LD	13.27	24.56
Sample 46	0.47	176	123	0.14	18.37	41.25	85.73	<LD	7.09	1.73
Mean	0.38	207.25	112.56	0.07	30.43	31.64	170.91	3.26	7.63	27.20
L.D.	0.004	6	8	0.002	0.006	6	4	4	3	16

Table 7.6f
Area C Chemical Analysis of Slag

Sample Number	Rb (ppm)	Sr (ppm)	Y (ppm)	Zr (ppm)	Nb (ppm)	Ba (ppm)	Ce (ppm)	Pb (ppm)	Th (ppm)	U (ppm)	Total wt%
Sample 31	141.43	268.58	38.18	138.34	13.02	1381.09	105.48	15.95	18.07	3.90	90.91
Sample 32	113.28	513.70	29.36	161.31	13.21	2137.02	96.19	16.07	13.97	5.00	90.04
Sample 33	82.98	402.37	23.58	122.51	10.99	1651.69	31.45	19.45	12.38	3.94	91.49
Sample 34	65.69	335.60	20.07	95.10	9.04	1437.42	48.74	30.76	11.33	<LD	96.16
Sample 35	103.68	364.57	22.14	123.98	10.20	1717.08	85.28	27.63	12.44	7.90	82.97
Sample 36	62.82	271.53	16.43	85.49	7.93	1283.24	38.60	25.05	9.92	4.34	90.60
Sample 37	69.42	317.37	20.35	95.33	8.98	1370.14	110.74	38.25	11.21	5.21	91.89
Sample 38	119.00	462.89	28.72	168.04	12.89	1993.44	92.65	36.84	13.74	6.38	87.02
Sample 39	93.90	362.28	24.22	150.05	13.05	1485.46	71.87	37.59	14.05	4.46	90.91
Sample 40	109.42	403.03	23.94	139.03	11.90	1650.72	54.62	18.72	15.34	7.68	88.13
Sample 41	66.38	321.81	17.57	89.53	8.54	1571.01	50.73	35.90	12.19	4.46	84.43
Sample 42	114.37	456.24	29.10	157.21	13.41	1969.05	115.63	15.15	14.35	3.90	86.06
Sample 43	112.19	432.98	25.50	135.75	11.90	1720.20	86.46	22.56	13.10	4.30	91.67
Sample 44	93.75	196.39	37.11	135.13	14.04	609.56	118.39	17.05	11.87	13.34	84.53
Sample 45	97.51	219.27	69.19	257.68	23.32	674.44	194.49	28.27	20.55	15.02	89.95
Sample 46	106.69	566.16	33.91	182.46	13.82	2348.54	84.98	15.71	19.39	3.90	90.61
Mean	97.03	368.42	28.71	139.81	12.27	1562.51	86.64	25.06	14.00	5.86	89.21
L.D.	0.8	1.4	0.8	1.3	0.8	29	48	4	3	4	N/A

Table 7.6g
Area B Statistical Analysis of Slag Chemistry
(after rejecting outlying values)

Species and Units	Mean	Median	Standard Deviation	% Standard Deviation	Spread
TiO ₂ (wt %)	0.35	0.37	0.1	27.7	0.36
V (ppm)	151.72	155	47.24	31	167
Cr (ppm)	100.67	103	31.55	31.3	129
MnO (wt%)	0.07	0.06	0.03	42.9	0.11
Fe ₂ O ₃ (wt%)	33.65	34.73	11.19	33.2	39.76
Ni (ppm)	31.21	28.64	14.05	45	44.63
Cu (ppm)	170.65	170.54	63.92	37.5	265.21
Zn (ppm)	8.25	0	15.00	182.8	54.93
Ga (ppm)	7.65	6.28	4.2	54.9	14.66
As (ppm)	24.37	23.67	10.51	43.1	32.39
Na ₂ O (wt%)	0.77	0.71	0.29	37.7	1.05
MgO (wt%)	0.52	0.46	0.31	59.6	1.17
Al ₂ O ₃ (wt%)	9.01	8.36	3.28	36.4	12.34
SiO ₂ (wt%)	19.38	17.92	6.73	34.7	25.63
P ₂ O ₅ (wt%)	0.96	0.96	0.3	31.2	1.00
S (ppm)	9622.87	9054.47	3207.51	33.3	13965.21
Cl (ppm)	939.79	845	523.48	55.7	1060
K ₂ O (ppm)	1.50	1.63	0.64	40.5	2.3
CaO (wt%)	1	0.97	0.28	28	1.17
Se (ppm)	14.62	14	5.62	38.4	26
Rb (ppm)	79.57	79.00	34.83	43.8	121.40
Sr (ppm)	304.64	329.37	210.72	54.8	924.91
Y (ppm)	27.78	29	8.33	30	38.90
Zr (ppm)	132.94	145.11	35.67	26.8	129.85
Nb (ppm)	12.12	12.92	2.97	24.5	11.39
Be (ppm)	1093.05	1650.94	600.52	30.2	2264.42
Ce (ppm)	77.52	75.19	37.22	48	190.04
Pb (ppm)	25.37	24.49	10.04	39.6	37.94
Th (ppm)	12.04	12.31	3.41	28.3	13.31
U (ppm)	4.00	4.75	3	61.5	13.20

Table 7.6h
Area C Statistical Analysis of Slag Chemistry
(after rejecting outlying values)

Species and Units	Mean	Median	Standard Deviation	% Standard Deviation	Spread
TiO ₂ (wt %)	8.35	8.36	0.07	21	0.24
V (ppm)	146.21	153.5	30.26	20.7	101
Cr (ppm)	106.6	118	26.61	25	85
MnO (wt%)	0.06	0.05	0.03	50	0.11
Fe ₂ O ₃ (wt%)	30.43	29.58	8.97	29.5	30.49
Ni (ppm)	28.2	29.82	9.03	32	25.83
Cu (ppm)	170.91	156.03	55.88	32.7	181.18
Zn (ppm)	nil	nil	nil	nil	nil
Ga (ppm)	7.63	7.25	2.97	38.9	11.91
As (ppm)	23.68	22.55	11.74	49.6	42.56
Na ₂ O (wt%)	0.9	0.85	0.41	45.5	1.63
MgO (wt%)	0.61	0.53	0.36	59	1.23
Al ₂ O ₃ (wt%)	10.64	10.12	3.88	36.5	14.8
SiO ₂ (wt%)	28.57	21.48	5.01	28.2	20.18
P ₂ O ₅ (wt%)	0.97	1.01	0.26	26.8	0.98
S (ppm)	7468.99	7367.88	2047.65	27.4	6761.36
Cl (ppm)	747.81	666	470.6	62.9	1553
K ₂ O (ppm)	1.88	2.01	0.44	23.4	1.56
CaO (wt%)	1.1	1.11	0.38	34.5	1.56
Sc (ppm)	15.5	15	7.31	47.2	28
Rb (ppm)	97.03	100.99	22.53	23.2	70.61
Sr (ppm)	368.42	362.58	103.43	28.1	369.77
Y (ppm)	26.01	24.23	6.66	25.6	21.75
Zr (ppm)	131.95	125.75	30.01	22.7	96.97
Nb (ppm)	11.53	11.9	2.09	18.1	6.11
Ba (ppm)	1562.51	1610.26	464.02	29.7	1730.98
Ce (ppm)	79.48	85.28	28.62	36	86.94
Pb (ppm)	25.06	23.0	8.67	34.6	23.1
Th (ppm)	13.99	13.42	3	21.4	10.63
U (ppm)	5.06	4.66	3.71	63.3	15.02



